HZDR-025

MODELLING AND ANALYSIS OF SEVERE ACCIDENTS FOR VVER-1000 REACTORS

Polina Tusheva

Wissenschaftlich-Technische Berichte
HZDR-025 · ISSN 2191-8708

WISSENSCHAFTLICH-
TECHNISCHE BERICHTE

HZDR
HELMHOLTZ
ZENTRUM DRESDEN
ROSSENDORF

Wissenschaftlich-Technische Berichte
HZDR-025

Polina Tusheva

MODELLING AND ANALYSIS OF SEVERE ACCIDENTS FOR VVER-1000 REACTORS

HZDR

HELMHOLTZ
ZENTRUM DRESDEN
ROSSENDORF

Druckausgabe: ISSN 2191-8708

Elektronische Ausgabe: ISSN 2191-8716

Qucosa: http://fzd.qucosa.de/startseite/

Die vorliegende Arbeit wurde sowohl als Dissertation an der Fakultät Maschinenwesen der Technischen Universität Dresden, sowie als Wissenschaftlich-Technischer Bericht des Helmholtz-Zentrum Dresden-Rossendorf mit der Berichtsnummer **HZDR-025** veröffentlicht.

2012

Herausgegeben vom

Helmholtz-Zentrum Dresden-Rossendorf e.V.

Postfach 51 01 19

D-01314 Dresden

Bundesrepublik Deutschland/Germany

Technische Universität Dresden

Fakultät Maschinenwesen

MODELLING AND ANALYSIS OF SEVERE ACCIDENTS FOR VVER-1000 REACTORS

Doctoral Thesis

Polina Tusheva, MSc.

Dresden 2011

Examining committee

Chair of the committee: Prof. Dr.-Ing. habil. Jochen Fröhlich

Thesis supervisor: Prof. Dr. rer. nat. Frank-Peter Weiß
Dr.-Ing. Eberhard Altstadt, Dr.-Ing. Frank Schäfer

Reviewers:
1. Prof. Dr. rer. nat. Frank-Peter Weiß
2. Prof. Dr.-Ing. habil. Antonio Hurtado
3. Associate Prof. PhD. habil. Boris Kalchev

Members:
1. Prof. Dr.-Ing. habil. Jochen Fröhlich
2. Prof. Dr. rer. nat. Frank-Peter Weiß
3. Prof. Dr.-Ing. habil. Antonio Hurtado
4. Associate Prof. PhD. habil. Boris Kalchev
5. Prof. Dr.-Ing. Clemens Felsmann

Day of the defense: March 9th, 2012

To the memory of Prof. Lakov

HARI OM TAT SAT

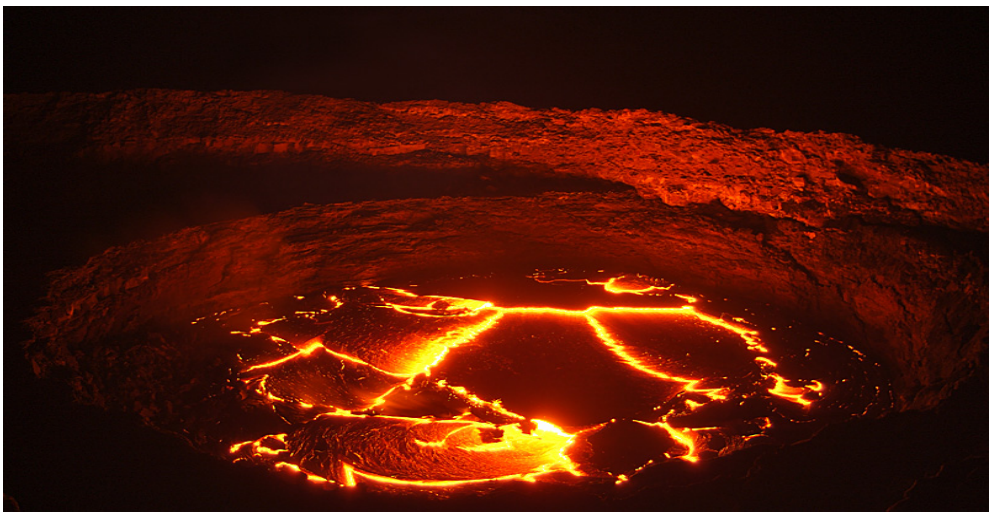

Erta Ale Volcano
Source: Dr. Marco Fulle – Stromboli Online
www.swisseduc.ch

Abstract

Accident conditions involving significant core degradation are termed severe accidents /IAEA: NS-G-2.15/. Despite the low probability of occurrence of such events, the investigation of severe accident scenarios is an important part of the nuclear safety research. Considering a hypothetical core melt down scenario in a VVER-1000 light water reactor, the early in-vessel phase focusing on the thermal-hydraulic phenomena, and the late in-vessel phase focusing on the melt relocation into the reactor pressure vessel (RPV) lower head, are investigated.

The objective of this work is the assessment of severe accident management procedures for VVER-1000 reactors, i.e. the estimation of the maximum period of time available for taking appropriate measures and particular decisions by the plant personnel. During high pressure severe accident sequences it is of prime importance to depressurize the primary circuit in order to allow for effective injection from the emergency core cooling systems and to avoid reactor pressure vessel failure at high pressure that could cause direct containment heating and subsequent challenge to the containment structure. Therefore different accident management measures were investigated for the in-vessel phase of a hypothetical station blackout accident using the severe accident code ASTEC, the mechanistic code ATHLET and the multi-purpose code system ANSYS.

The analyses performed on the PHEBUS ISP-46 experiment, as well as simulations of small break loss of coolant accident and station blackout scenarios were used to contribute to the validation and improvement of the integral severe accident code ASTEC. Investigations on the applicability and the effectiveness of accident management procedures in the preventive domain, as well as detailed analyses on the thermal-hydraulic phenomena during the early in-vessel phase of a station blackout accident have been performed with the mechanistic code ATHLET. The results of the simulations show, that the effectiveness of the procedures strongly depends on the ability of the passive safety systems to inject as much water as possible into the reactor coolant system.

The results on the early in-vessel phase have shown potentially delayed RPV failure by depressurization of the primary side, as slowing the core damage gives more time and different possibilities for operator interventions to recover systems and to mitigate or terminate the accident. The ANSYS model for the description of the molten pool behaviour in the RPV lower plenum has been extended by a model considering a stratified molten pool configuration. Two different pool configurations were analysed: homogeneous and segregated. The possible failure modes of the RPV and the time to failure were investigated to assess the possible loadings on the containment. The main treated issues are: the temperature field within the corium pool and the RPV and the structure-mechanical behaviour of the vessel wall.

The results of the ASTEC calculations of the melt pool configuration were applied as initial conditions for the ANSYS simulations, allowing a more detailed and more accurate modelling of the thermal and mechanical behaviour of the core melt and the RPV wall.

Moreover, for the late in-vessel phase, retention of the corium in the RPV was investigated presuming external cooling of the vessel wall as mitigative severe accident management measure. The study was based on the finite element computer code ANSYS. The highest thermo-mechanical loads are observed in the transition zone between the elliptical and the vertical vessel wall for homogeneous pool and in the vertical part of the vessel wall, which is in contact with the molten metal in case of sub-oxidized pool. Assuming external flooding will retain the corium within the RPV. Without flooding, the vessel wall will fail, as the necessary temperature for a balanced heat release from the external surface via radiation is near to or above the melting point of the steel.

Kurzfassung

Störfälle in einem Kernkraftwerk, die eine Kernzerstörung zur Folge haben, werden als schwere Störfälle bezeichnet /IAEA: NS-G-2.15/. Trotz der geringen Eintrittswahrscheinlichkeit derartiger Störfälle ist die Untersuchung von schweren Störfallszenarien ein wichtiger Bestandteil der nuklearen Sicherheitsforschung. Für ein hypothetisches Kernschmelzszenario in einem VVER-1000 Leichtwasserreaktor wurden sowohl die frühe als auch die späte Störfallphase mit Beschränkung auf den Zeitraum vor Versagen des Reaktordruckbehälters ("In-Vessel Phase") untersucht. Der Schwerpunkt der Untersuchungen zur frühen Störfallphase lag auf den thermohydraulischen Phänomenen und für die späte Störfallphase wurde die Verlagerung der Kernschmelze in das untere Plenum des Reaktordruckbehälters (RDB) untersucht.

Das Ziel dieser Arbeit war die Bewertung von Notfallmaßnahmen für VVER-1000 Reaktoren und hierbei insbesondere die Abschätzung der maximalen Zeitspanne für die Einleitung geeigneter Maßnahmen sowie das Fällen spezifischer Entscheidungen des Bedienpersonals. Bei schweren Störfallszenarien auf hohem Druckniveau (Hochdruckpfad) ist es von vorrangiger Bedeutung, den Druck im Primärkreislauf zu reduzieren und dadurch die Notkühleinspeisung zu ermöglichen. Des Weiteren sollen durch die primärseitige Druckabsenkung ein RDB-Versagen unter hohem Druck mit direkter Aufheizung des Containments und die daraus folgenden Belastungen für die Containmentstruktur vermieden werden. Daher wurden verschiedene Notfallmaßnahmen während der Früh- und Spätphase eines hypothetischen Störfalls mit Totalausfall der Stromversorgung (Station Blackout) unter Anwendung der Rechenprogramme ASTEC, ATHLET und ANSYS untersucht.

Der Integralcode ASTEC für die Simulation schwerer Störfalle wurde für Analysen zum PHEBUS ISP-46 Experiment sowie für Simulationen zu einem Kühlmittelverluststörfall mit kleinem Leck und zum Totalausfall der Stromversorgung eingesetzt. Diese Simulationsrechnungen sind ebenfalls wesentlicher Bestandteil der vorgelegten Arbeit und leisten einen wichtigen Beitrag zur Validierung und Verbesserung von ASTEC. Mit dem Systemcode ATHLET wurden Untersuchungen zur Anwendbarkeit und zur Effektivität von Notfallmaßnahmen in der Frühphase eines Station Blackout Störfalls sowie zu den hierbei auftretenden thermohydraulischen Phänomenen durchgeführt. Die Ergebnisse der Simulationsrechnungen zeigen, dass die Effektivität der Notfallmaßnahmen in starkem Maß von der aus den passiven Systemen in den Reaktorkühlkreislauf eingespeisten Wassermenge abhängt.

Die Berechnungen zur Frühphase des Störfalls Totalausfall der Stromversorgung haben gezeigt, dass das Versagen des RDB bei Anwendung der primärseitigen Druckentlastung zeitlich verzögert wird. Durch die Verlangsamung der Kernschädigung stehen dem Bedienpersonal mehr Zeit und Möglichkeiten für Interventionen zur Verfügung, um Systeme wieder in Betrieb zu nehmen und alternative Notfallmaßnahmen zu planen und umzusetzen, wodurch die Störfallfolgen begrenzt oder Kernschäden sogar vermieden werden können. Das ANSYS Modell für die Beschreibung des Schmelzepools im unteren Plenum des RDB wurde um ein Modell für einen geschichteten Schmelzepool erweitert. Zwei verschiedene Poolkonfigurationen wurden analysiert: homogen und geschichtet. Die möglichen Versagensmechanismen des RDB und die

Zeit bis zum Versagen wurden untersucht, um mögliche Beanspruchungen für das Containment abzuschätzen. Das Temperaturfeld im Inneren des Schmelzepools und des RDB sowie das strukturmechanische Verhalten der RDB-Wand standen dabei im Zentrum der Untersuchungen.

Die Ergebnisse der ASTEC-Simulationen für die Zusammensetzung des Schmelzepools wurden als Anfangs- und Randbedingungen für die ANSYS-Simulationen genutzt. Diese Vorgehensweise ermöglicht eine detailliertere Modellierung und eine genauere Berechnung des thermischen und mechanischen Verhaltens der Kernschmelze und der RDB-Wand.

Mit dem Finite Elemente Code ANSYS wurde die späte Störfallphase unter Annahme einer RDB-Außenkühlung als Notfallmaßnahme mit dem Ziel untersucht, die Schmelze im RDB zurückzuhalten. Für den homogenen Schmelzepool wurden die höchsten thermo-mechanischen Belastungen in der Übergangszone zwischen der elliptischen und der vertikalen Druckbehälterwand beobachtet. Im Fall der segregierten Schmelze traten die höchsten Belastungen im vertikalen Teil der Druckbehälterwand auf, welcher in Kontakt mit geschmolzenem Metall steht.

Bei Anwendung der RDB-Außenkühlung wird die Kernschmelze im Inneren des RDB zurückgehalten. Ohne externe Flutung wird die RDB-Wand versagen, da die notwendige Temperatur für eine ausgeglichene Wärmeabgabe durch Wärmestrahlung von der RDB-Außenseite nahe oder über dem Schmelzpunkt des Stahles liegt.

Резюме

Аварийни състояния характеризиращи се със значително разрушаване на активната зона на реактора се дефинират като тежки аварии /IAEA: NS-G-2.15/. Независимо от ниската честота на възникване на такива събития, изследването на тежки аварии е важна част от областта на ядрената безопасност. Анализирана е хипотетична авария със стопяване на зоната на реактор с лека вода тип ВВЕР-1000. Разгледани са двете под-фази на вътрешнокорпусна тежката авария: ранна вътрешнокорпусна фаза - с фокус върху термо-хидравличните явления и късна вътрешнокорпусна фаза - с фокус върху придвижването и позиционирането на стопилката в долната част на корпуса на реактора.

Цел на настоящата работа е анализ и оценка на процедури за управление на тежки аварии за реактори тип ВВЕР-1000 като например определяне на максималния период от време за предприемане на подходящи действия и решения от страна на персонала на ядрената централа. По време на събитие тежка авария под високо налягане изключително важно е намаляване на налягането по първи контур, като по този начин може да се осъществи подаване на вода в контура от системите за безопасност на реактора и в същото време се предотвратява разкъсване на корпуса на реактора под високо налягане, което би довело до директно загряване и опасност за структурата на контейнмента. Анализирани са различни мерки за управление на тежки аварии по време на вътрешнокорпусната фаза за хипотетично инициращо събитие “пълно обезточване на централата“ (загуба на външно и вътрешно електрозахранване) с помоща на интегралния код за тежки аварии ASTEC, механичния код ATHLET и комерсиалния код ANSYS.

Анализи направени на базата на експеримента PHEBUS ISP-46 както и компютърно моделиране на аварии “малък теч от първи контур” (SBLOCA) и “пълно обезточване“ (SBO) са принос към верифицирането и валидирането на интегралния код за тежки аварии ASTEC. Направени са изследвания за приложимостта и ефективността на мерките за аварийни процедури в частта предпазни мерки, както и детайлни анализи на термо-хидравличните явления и ефекти по време на ранната фаза на авария “Пълно обезточване на блока“ са проведени с помоща на механичния код ATHLET. Получените резултати показват, че ефективносста на аварийните процедури зависи силно от способността на пасивните системи за доставяне на вода до реактора.

Резулатите от анализите на ранната вътрешнокорпусна фаза показват, че при мярка “намаляване на налягането по първи контур“ времето до пропукване на корпуса на реактора се удължава, както и забавянето на процеса на разрушаване на активната зона на реактора би довело до повече време за възстановяване на системите за безопасност, което от своя страна би спомогнало спиране на аварията или смекчаване на последствията от аварията. По този начин операторите на централа биха имали повече време за и различни възможности за действие.

За описание на поведението на стопилката в долната част на корпуса на реактора е приложен модел разработен въз основата на комютърния код ANSYS. Този модел е

допълнен чрез новоразработен модел отчитащ възможното разделяне на стопилката. Анализирани са две конфигурации: хомогенна стопилка и разделена стопилка. Изследвани са различните режими на спукване на корпуса на реактора както и времето до разрушаване на корпуса на реактора за оценка на последствията върху структурата на контейнмента. Основно са разгледани температурното поле в стопилката и реактора както и структурно-механичното поведение на стената на корпуса на реактора.

Резултатите, получени въз основа на компютърния код ASTEC при моделирането на конфигурацията на стопилката в дъното на корпуса на реактора са приложени като входни данни при моделирането с ANSYS. По този начин е осигурено по-точно моделиране на термичното и механичното поведение на стопилката и стената на корпуса на реактора.

По време на късната фаза, като мярка за намаляване на последствията от тежка авария, е изследвана възможността за задържане на стопилката в корпуса на реактора чрез външно охлаждане на реактора. Анализите се основават на кода ANSYS по метода на крайните елементи. Най-високото термо-механично натоварване се наблюдава в преходната зона между елиптичната и вертикалната част от стената на корпуса на реактора в случай на хомогенна стопилка и във вертикалната част от стената на реактора в случай на сегрегирана стопилка. Прилагането на мярка външно охлаждане на реактора би спомогнало задържането на стопилката в корпуса на реактора. Без външно охлаждане целостта на стената на корпуса на реактора ще се наруши (скъсване на стената на корпуса на реактора), тъй като необходимата температура за балансирано отвеждане на топлината на външната стена чрез радиационно излъчване е приблизително равна или по-висока от точката на топене на корпусната стомана.

Contents

List of figures

List of tables

Formulas

Latin Symbols

A	[m^2]	Area
c	[-]	Constant
c_p	[J/kgK]	Specific thermal capacity
Da	[-]	Damköhler-number
E	[Pa]	Young modulus, modulus of elasticity
g	[m/s^2]	Gravitational acceleration (g=9.81 m/s^2)
Gr	[-]	Grashoff-number
h	[W/m^2K]	Heat transfer coefficient
H	[m]	Height
L	[m]	Length, Distance
m	[kg]	Mass
Nu	[-]	Nusselt-number
p	[Pa]; [bar]	Pressure
P	[W]	Power
Pr	[-]	Prandtl-number
q	[W/m^2]	Heat flux
q_V	[W/m^3]	Volumetrical heat
Q	[W]	Power
R	[m]	Radius
Ra	[-]	Rayleigh-number
s	[m]	Thickness
t	[s]; [min]; [h]	Time
Δt	[s]	Time difference
T	[°C]; [K]	Temperature
ΔT	[K]	Temperature difference
v	[m/s]	Velocity
V	[m^3]	Volume
x	[m]	Horizontal coordinate
y	[m]	Vertical coordinate

Greek Symbols

α	[1/K]	Linear thermal expansion coefficient
α	[m^2/s]	Thermal diffusivity
α	[W/m^2 K]	Heat transfer coefficient
β	[1/K]	Volumetric thermal expansion coefficient
ε	[-]	Emissivity
η	[Pa s]	Dynamic viscosity
λ	[W/mK]	Thermal conductivity
ϑ	[-]	Dimensionless temperature
ξ	[-]	Dimensionless thickness coordinate
ν	[m^2/s]	Kinematic viscosity
ψ	[-]	Dimensionless velocity profile
ρ	[kg/m^3]	Density
σ	[Pa]	Stress
σ_{eqv}	[Pa]	Von-Mises equivalent stress
σ_{SB}	[$W/m^2 K^4$]	Stefan-Boltzmann constant ($5.67 \cdot 10^{-8}$ W/m^2K^4)

Indices

A	area
allow	allowable
ax	axial
amb	ambient
b, bulk	bulk
bdu	boundary layer, upper
bdw	boundary layer, wall
con	conduction
conv	convection
cr(u)	crust
crit	critical
cyl	cylinder/cylindrical
dn	down
e, ext	external
eff	effective
el	electrical
eqv	equivalent
fail	failure
gen	generate(d)
hom	homogeneous
i, in	internal
init	initial
l	liquid
liq	liquidus
m	mix(ing)
max	maximal
melt	molten pool, melt
met, metal	metal
nom	nominal
out	outer
ox(ide), ol	oxide (layer)
rad	radiation
rem	remaining
s	surface
SBL	side-boundary layer
sd	side
sol	solidus
STL	stratified layer
tg, tang	tangential
TML	turbulent mixing layer
th	thermal
tot, total	total
tr	true
u	ultimate
up	upper
v	volumetric
w, wall	wall
x	horizontal, radial
y	vertical, axial
0	initial, zero

Abbreviations

AC	Alternating Current
AIC	Silver-Indium-Cadmium (Control Rods Material)
ADE	Automatic Depressurization
AM	Accident Management
AMM	Accident Management Measure
ANSYS	ANalysis SYStems (Engineering Simulation Software)
AP1000	Westinghouse Electric Company's Reactor
APDL	ANSYS Parametric Design Language (Macro-Language)
ASTEC	Accident Source Term Evaluation Code
ATHLET	Analysis of THermal-hydraulics of LEaks and Transients
ATWS	Anticipated Transidents Without SCRAM
BALI	BAin LIquide (Experimental Programme)
BDBA	Beyond Design Basis Accident
BRU-A	Steam Dump to Atmosphere
BRU-K	Steam Dump to Condenser
BWR	Boiling Water Reactor
BZOK	Fast Activated Isolation Valve
CEA	Commissariat à l'Énergie Atomique
CFD	Computational Fluid Dynamics
CHF	Critical Heat Flux
COPO	COrium POol (Experimental Programme)
CSNI	Committee on the Safety of Nuclear Installations
CV	Control Volume, Check Valve
DBA	Design Basis Accident
DC	Downcomer
DCH	Direct Containment Heating
DG	Diesel Generator
ECC	Emergency Core Cooling
ECCM	Effective Convection Conduction Model
ECCS	Emergency Core Cooling System
EDF	Électricité de France
EFWP	Emergency Feedwater Pump
EFWS	Emergency Feedwater System
EPR	European Pressurized Water Reactor
EPRI	Electric Power Research Institute
EVC	External Vessel Cooling
FE	Finite Elements
FEM	Finite Element Method/Model
FOREVER	Failure of Reactor Vessel Retention
FP	Fission Products
FPRD	Framework Programmes for Research and Development
FPT1	Second Test of the PHEBUS Fission Product (FP) programme
FW	Feedwater
FZD	Forschungszentrum Dresden-Rossendorf e.V. (nowadays Helmholtz-Zentrum Dresden-Rossendorf, HZDR)
GCSM	General Control Simulation Module
GRS	Gesellschaft für Anlagen- und Reaktorsicherheit mbH

HA	Hydro-accumulators
HCO	Heat Conduction Object
HECU	Heat conduction module within ATHLET
HEPA	High Efficiency Particulate Airfilter
HPIS	High Pressure Injection System
HPME	High Pressure Melt Ejection
IAEA	International Atomic Energy Agency
IBRAE RAN	Институт проблем безопасного развития атомной энергетики, Российская Академия Наук (Russian Academy of Sciences)
INEEL	Idaho National Engineering and Environmental Laboratory
INSAG	International Nuclear Safety Group
IRSN	Institut de Radioprotection et de Sûreté Nucléaire
ISP	International Standard Problem
IVR	In-Vessel Retention
KTH	Kungliga Tekniska högskolan (Royal Institute of Technology), Stockholm
LBLOCA	Large Break Loss of Coolant Accident
LOCA	Loss of Coolant Accident
LPIP	Low Pressure Injection Pump
LPIS	Low Pressure Injection System
LWR	Light Water Reactor
MASCA	MAterial SCAling Project (Experiment)
MBLOCA	Medium Break Loss of Coolant Accident
MCCI	Molten Core Concrete Interaction
MCP	Main Coolant Pump
MDB	Material Data Bank
MVITA	Melt-Vessel Interaction – Thermal Analysis
NEA	Nuclear Energy Agency
NPO Luch	Научно-Исследовательский Институт Научно-Производственное объединение "Луч" ("Luch"- Scientific-Reasearch Institute)
NPP	Nuclear Power Plant
OECD	Organisation for Economic Co-operation and Development
OKB	Gidropress, Опытно-Конструкторское Бюро (Experiment-Constructional Bureau)
OLHF	OECD Lower Head Failure (Experiment)
PIE	Post-Irradiation Examination
PORV	Pressurizer Power Operated Relief Valve
PSA	Probabilistic Safety Assessment
PSD	Primary Side Depressurization
PRZ	Pressurizer
PWR	Pressurized Water Reactor
RAB	Reactor Application and Benchmarking
RCC KI	Российский Научный Центр Курчатовский институт (Kurchatov Institute)
RIA	Reactivity Initiated Accident
RPV	Reactor Pressure Vessel
SA	Severe Accident
SAM	Severe Accident Management
SAMG	Severe Accident Management Guidelines
SAMM	Severe Accident Management Measures

SARNET	Severe Accident Research Network
SBLOCA	Small-Break Loss of Coolant Accident
SBO	Station Blackout
SCRAM	Emergency Shutdown of Reactor
SG	Steam Generator
SNL	Sandia National Laboratories
SSD	Secondary Side Depressurization
STUK	Radiation and Nuclear Safety Authority Finland
TFD	Thermo-Fluiddynamic
TFO	Thermo-Fluiddynamic Object
TMI	Three Mile Island (A Nuclear power plant in USA)
UCSB	University of California, Santa Barbara
UHS	Ultimate Heat Sink
UP	Upper Plenum
VDI	Verein Deutscher Ingenieure
VVER	Water-Water Energetic Reactor

1 Introduction

It is the main objective of the nuclear safety to maintain the barriers for the retention of radioactivity in order to protect the workers and the public from the hazards of nuclear radiation. The safety functions required to achieve this fundamental protection goal are implemented by the operational and safety systems. All these systems are elements in a staggered safety concept, known as the defence-in-depth concept, which is meant to optimize the interaction of the manifold systems in respect to their effect on the safety of the nuclear power plant. The defence-in-depth concept consists of five levels and these levels are aiming /IAEA: INSAG-10/, /IAEA: INSAG-12/ at:

Level 1: Prevention of abnormal operation and failures using the operational systems. The realization is supported by conservative design, high constructional and operational quality

Level 2: Control of abnormal operation and detection of failures by the operational systems in combination with the limiting and protection systems

Level 3: Control of design basis accidents by the safety systems

Level 4: Control of severe plant conditions, including prevention of severe accidents and mitigation of their consequences by accident management measures

Level 5: Mitigation of the radiological consequences of significant releases of radioactive materials by off-site emergency response.

Methods of deterministic safety analysis /IAEA: SSG-2/ as well as probabilistic safety analysis (PSA) /IAEA: TECDOC-1200/ are applied to provide an evaluation of the balance of the plant design and operation with regard to safety. They deliver a quantification of the risk in terms of core damage frequency and the related radioactive source term. In this way they reveal whether the protection measures and functions are adequate. An important objective is also to avoid, if possible, the damage to the core and the failure of the reactor pressure vessel.

Usually, the safety case has to be demonstrated for design basis accidents (DBAs) and for beyond design basis accidents (BDBAs) /IAEA: 23, IAEA: NS-R-1/. DBAs represent a class of

postulated accidents to, which the safety systems and functions of the nuclear power plant (NPP) had been designed in order to control the event and to exclude the release of harmful amounts of radioactivity. Despite the low probability of occurrence, the investigation of severe accident scenarios is an important part of the nuclear safety research. The probability of occurrence of severe accident in light water reactors lays in the order of $10^{-6} \div 10^{-5}$ per reactor year /IAEA: INSAG-12/. The initiators to severe accidents can be very complex /MAG 2005/, including multiple failures of safety systems, faulted conditions, man-made and natural hazards.

On the one side, it is the aim of the severe accident research to better understand the phenomena, involving thermal-hydraulics, physico-chemical and mechanical processes. On the other side the investigations strive for effective severe accident management measures.

Severe accident progression in light water reactors can be classified in two phases: in-vessel phase (covering core degradation, corium behaviour in the lower head, reactor pressure vessel failure) and ex-vessel phase (covering melt ejection, possibly direct containment heating, molten core-concrete interaction, hydrogen generation and combustion or detonation).

At a postulated accident sequence with loss of all emergency core cooling systems, and if no additional cooling of the reactor core is provided by passive systems, external means and sources, the primary circuit starts to boil off, the core starts to heat-up, because of the residual power, the fuel progressively overheats, the fuel claddings crack, and the reactor core melts down. An additional source of heat is given by the strong exothermal steam-oxidation, arising from the contact of the zirconium in the cladding material and the vapour in the reactor core, resulting in additional generation of heat and substantial production of hydrogen. The interaction of the fuel with the cladding material produces low-melting-point eutectics, resulting in the relocation of material in the core. During the process of corium slumping downwards, and by the contact of hot slumping debris pieces with colder zones of still not melted materials in the reactor, corium pools are formed. With the further core degradation, the molten materials continue relocating downwards. Finally, the molten corium accumulates in the lower plenum of the reactor pressure vessel and causes thermal and mechanical stresses of the reactor pressure vessel wall material, which can lead to the failure of the reactor pressure vessel.

The reactor pressure vessel is the last barrier to keep the corium inside the reactor, and thus to prevent higher loads to the containment. Because of that, it is important to keep this barrier intact as long as possible. A particular aspect is that the load to the vessel exponentially decreases with the decreasing of the decay heat in the corium pool. This means that the longer the corium can be retained in the vessel, the easier it is to keep it there.

To assess the behaviour of a nuclear power plant during transient or accident conditions, proper computer models are needed, which have gone through extended verification and validation. The assessment of the implemented models is generally realized by comparison of the results to experimental data (code-to-experiment comparison), comparison of the results to code data (code-to-code comparison) and application of combination matrix considering complex physical effects and phenomena, applied codes, relevant accident sequences and types of nuclear power plants.

In the framework of this doctoral thesis, the ASTEC code was applied for the investigation of the whole accident progression till failure of the reactor pressure vessel (RPV). For further validation, the ASTEC code capability in simulation of severe accident phenomena has been checked and proved against the PHEBUS ISP46 FPT1 experiment. Detailed investigation on the main phenomena arising during the early in-vessel phase of the severe accident scenario was done with ASTEC and the results were compared to results provided by the validated mechanistic code ATHLET. Moreover, ATHLET was applied for the investigation of applicability, effectiveness and optimization of accident management measures.

The results of the ASTEC code covering the late in-vessel phase of severe accident scenario were used as input data into the finite element code ANSYS, to analyse the thermal and mechanical behaviour of the RPV after core melting. A comparison of the time from fully developed molten pool in ASTEC and ANSYS till failure of the RPV was done. Additionally, external cooling of the RPV was analysed with the help of ANSYS as severe accident management measure for in-vessel melt retention (Appendix D, Appendix F).

This thesis is devoted to the investigation of aspects relevant to the in-vessel phase. Considering a hypothetical core melt down scenario (a station blackout accident) in a VVER-1000 pressurized water reactor (PWR), the early in-vessel phase scrutinizing the thermal-hydraulic phenomena, and the late in-vessel phase focusing on the melt relocation into the reactor pressure vessel lower head, were investigated.

The thesis consists of eight parts. In the first Chapter a brief introduction to the problem of the severe accidents is given.

Based on a literature review in the second Chapter, an overview is given and the status of research is described, concerning severe accidents in pressurized water reactors, and the different strategies for management of a severe accident. A brief description of the Fukushima accident, a station blackout scenario in boiling water reactor (BWR), and a comparison of the sequence of events following a station blackout for both BWR- and PWR-type of reactors are additionally provided.

The third Chapter covers the most commonly used codes for severe accident analyses, the requirements for the simulations and the specifics and the modules of the currently developed integral severe accidents code ASTEC.

Chapter four focuses on the validation of the ASTEC code by performing post-test analyses of the PHEBUS FPT1 ISP-46 test. The calculated code results are compared against experimental data.

Chapter five includes the code modelling of the early in-vessel phase of a severe accident of a VVER-1000 reactor. The main characteristics of a VVER-1000 nuclear power plant and the building of the ASTEC input deck are pointed out. The ASTEC and ATHLET models used for the early in-vessel phase investigations are described.

Chapter six includes the accident sequence analyses accomplished with the computer code ASTEC. Transient analyses up to reactor pressure vessel failure were performed without

application of accident management measures (AMM) and with application of AMM. Code-to-code comparison in predicting the main thermal-hydraulic phenomena was performed with the validated mechanistic code ATHLET. The possible accident management strategies and operator actions were analysed.

The seventh part focuses on the late in-vessel phase of a severe accident, when the molten corium is already relocated into the reactor pressure vessel lower head. The severe accident management procedures related to the late phase, as well as the thermal-hydraulic phenomena important for the late phase and the molten pool behaviour are discussed. The possibility is investigated for in-vessel melt retention by ex-vessel cooling of the reactor pressure vessel of a VVER-1000 reactor. A new mathematical model, describing the molten pool behaviour and heat transfer into the corium pool is implemented in the finite element method (FEM) code ANSYS. The output data of the early in-vessel phase from the ASTEC code serve as initial input data in ANSYS. Two possible molten pool configurations were considered: homogeneous pool and segregated pool. The heat transfer in the molten pool, the thermal and the structural results of the numerical study are discussed. For the segregated pool configuration, a parameter study on the critical thickness of the metal layer is done.

The summary and the main conclusions are presented in the last part of the theses, Chapter eight.

2 Overview and status of the research

This Chapter gives an overview of the severe accident research, focusing on relevant safety aspects of the pressurized water reactors, different measures and strategies for severe accident management, as well as the current status of the ongoing research.

2.1 Severe accidents in pressurized water reactors – classification and safety related aspects

The reactor safety issues are of primary importance for preserving the health of the population and ensuring no release of radioactivity and fission products into the environment. Nowadays the work of many nuclear safety and research organizations in that field is focused on improving the safety of existing nuclear power plants, developing new methods, computer codes and state-of-the-art standards. Many experimental programmes have been launched to support the ongoing theoretical research, to validate physical models, to qualify computer codes and to elaborate or optimize safety related standards, guidelines and accident management procedures. Activities to enhance the safety cover a wide range of topics including siting, design, construction, commissioning, utilization and decommissioning, and at the same time improving the safety analysis and the safety management. Special attention has been given to the assessment of the source term, radionuclide transport within containment, and respectively confinement, and releases to the environment. The reactor safety plays a significant role for all operating nuclear power plants, the plants under construction and also for future plants design and concepts.

The safety of the NPPs is based on the "defence-in-depth" concept, which relies on successive physical barriers /IAEA: INSAG-10/: fuel matrix, cladding, primary system pressure boundary and containment, and other provisions to confine the radioactive materials and on multiple levels of protection against damage to these barriers. Within the design basis of a NPP, a number of initiating events are considered NPP /IAEA: 23/. According to the probability of occurrence and potential consequences, an event may be classified as an anticipated operational occurrence (also called a transient) or a design basis accident (DBA).

An accident exceeding the design basis of the NPP is called a beyond design basis accident (BDBA). Such an accident may or may not involve degradation of the reactor core /IAEA: 23/. An accident involving core degradation, typically with core melting, is also called a severe accident (SA). This group of the events are with low probability of occurrence. They may occur by multiple failures of safety systems. If the safety systems, delivering water to the reactor core, are not restored, significant core degradation may arise and the integrity of the barriers can be lost, involving overheating of the nuclear fuel and leading to release of fission products /IAEA: NS-G-2.15/.

Studies, research and efforts are a continuing process made at improving the safety and reliability of existing and newly developed nuclear power plants at prevention of a core melt accident. Accidents like TMI-2 (March 28th, 1979), Chernobyl (April 26th, 1986) and Fukushima (March 11th, 2011) show that even with a low probability of occurrence, such accidents can not be excluded. The hazard of the core melt accidents to the public, if the containment fails, must be additionally assessed. Therefore, knowledge-base for prevention or mitigation of those accidents is being acquired. According to /IAEA: NS-R-1/, the severe accidents should be taken into account in the design and operation of NPPs. On national level this is determined by the national nuclear regulatory agencies.

Referring to /IAEA: NS-G-2.15/ and /IAEA: 56/, for identification of the severe accidents events, and the respective preventive and mitigative measures, probabilistic safety analysis methods are combined with engineering judgement. The identification of the source events should be based on realistic or best estimate assumptions, methods and analytical criteria /IAEA: NS-R-1/.

The severe accident phenomena include the interactions between the melted core materials with the inner reactor structures, the persisting water inside the reactor pressure vessel, the release, transport and deposition of fission products. Therefore the analysis of these phenomena is very complex /SEH 2001/, /SARNET 2006/, /SARNET 2008/. The interaction of the core melt could lead to ablation of structures, steam explosions, vessel failure, concrete melting and generation of gases, spreading/dispersion of debris /SARNET 2008/. These phenomena involve the thermal-hydraulic behaviour, chemistry processes and phenomena arising at high temperatures, material interactions at high temperatures, physics of aerosols etc.. Investigated is the behaviour of the reactor, the reactor safety systems and the containment. The loads on the containment are determined by the way how an accident would proceed, the level of the fuel damage, maintaining the molten fuel within the reactor pressure vessel or spreading of the corium mass out of the reactor. They are classified into the following basic groups: loads to the containment (1) at which the containment remains intact, (2) which could lead to containment failure early and (3) which could lead to containment failure much later. The "early" versus the "late" distinction is based on the physical loads on the containment (e.g. steam-concrete and corium-concrete interaction, high temperature and pressure loads, chemical reactions and H_2-explosions), as well as on the physical processes that control the concentration of fission product aerosols in the containment atmosphere /SEH 2001/, /SARNET 2006/.

The phenomena and the associated severe accident phases are typically divided into two groups:

- In-vessel phase: covering core heat-up, fuel degradation, release of fission products (the source term), hydrogen production, material relocation, mass and composition of the melt, thermal and mechanical loads on the reactor pressure vessel, failure of the reactor pressure vessel, release of molten corium into the containment building, loads on the containment
- Ex-vessel phase: covering thermal and chemical interaction between core debris and containment structures, and containment behaviour, including transport of radioactive substances, ex-vessel hydrogen production, loads on the containment.

For evaluation of accident management strategies a precise description of the physical processes and the phenomena during the in-vessel accident progression is essential. The early in-vessel phase of an accident should be assessed as correct as possible as it exert an influence on the late in-vessel phase processes, as well as on the ex-vessel phase of a severe accident.

Parallel to the ongoing research and experimental programmes special attention is given on the development of computer codes that simulate the behaviour of the whole nuclear power plant, covering all phenomena from heat generation in the reactor core and heat transfer to the secondary side up to core melting, fission products release and interaction with reactor pressure vessel (RPV) and containment structures. Computer modelling is also used to assess the probabilities and the consequences of hypothetical incidents and accidents in nuclear power plants, and accordingly to that basis to determine the effectiveness of the preventive and mitigative accident management measures and procedures. Nevertheless, research and experimental programmes are needed for obtaining, renewing and updating the data bases taken into consideration in the process of code development, validation, assessment and application.

2.2 Severe accident management measures for pressurized water reactors

The severe accident management is straightforwardly related to the defence-in-depth concept. In accordance with defence in depth, each design level should be protected individually, independently of other levels. The main objectives of severe accident management are /IAEA: 32/:

- Prevention of the accident from leading to core damage
- Termination of core damage
- Maintaining the integrity of the containment for as long as possible
- Minimizing on-site and off-site releases and their adverse consequences
- Achieving a long term stable state.

Two basic ways are followed in the severe accidents research: preventive domain and/or mitigative domain. Plant specific severe accident management guidelines (SAMGs) are developed and implemented. Different countries apply different approaches of severe accident management

measures. Two approaches are usually followed: the so called "Westinghouse approach" and the "French approach". For implementation of the SAMGs, depending on the plant design, each plant is performing procedural, operational as well as equipment changes. Observed is the capability of usage of safety and non-safety systems beyond their originally intended function and anticipated operating conditions /IAEA: NS-G-2.15/.

Main issues in the severe accident management are keeping the primary circuit integrity, keeping the pressurized premises integrity and creating of conditions for cool-down of the reactor core or of the debris after its damage.

Basic SAM actions are /SARNET 2006/, /SARNET 2008/, /IRSN 2007/:

- Cooling a degraded core

This strategy is realized by water injection into the RPV. It is included as a severe accident management strategy in the SAMG of many nuclear power plants. Injecting water to the hot core would accelerate the exothermal steam-zirconium reaction, leading to increased steam and hydrogen production and resulting in higher loads to the containment structures. This action would help in the process of stopping the core degradation and retention of the degraded core materials inside the RPV. The procedure is water delivery to the core as soon as possible.

To make available the water delivery to the core by means of active or passive safety systems, or by external sources, another accident management strategy is applied i.e. "Reactor coolant system depressurization". The different safety systems start to pour water in the RPV at different pressure levels. This strategy can be realized by means of safety valves installed either on the primary side of the reactor coolant system - so called Primary Side Depressurization (PSD) or on the secondary side of the reactor coolant system - so called Secondary Side Depressurization (SSD). The preferred way for PWRs is the SSD by the secondary "Bleed and Feed" procedure - first depressurization and then feeding the steam generators' secondary side and thereby cooling down the primary side and reducing its pressure. If this action is ineffective or not available, depressurization can be accomplished by direct opening of the pressurizer relief- and safety valves - PSD, primary "Bleed and Feed" procedure. The application of this strategy would help the water delivery to the core and in that way high pressure melt ejection and direct containment heating could be avoided. The possible drawbacks at application of this strategy are the high hydrogen production rates and higher possibility of in-vessel energetic fuel-coolant interaction.

Another strategy is flooding of the reactor pressure vessel compartments. Regarding its application there is a considerable variation among the countries. The strategy of in-vessel retention (IVR) by ex-vessel cooling (EVC) is one of the adopted strategies for mitigation of a severe accident. This concept has been already approved by the Finnish Regulatory Agency (STUK) to be a part of the severe accident management procedures for the Loviisa NPP, Finland, with a VVER-440 reactor /KYM 1997/, /BEC 2008/. Besides its feasibility for such small power reactors, the concept is also investigated for some GEN III and advanced light water reactors with higher core powers, such as the Westinghouse AP1000 /KOL 1996/, /KOL 1999/, /SCO 2003/, /ESM 2004/, /REM 2005/. This strategy strongly depends on the design of the reactor cavity. By applying the strategy of in vessel retention of corium, the possible

violent fuel-coolant interaction in the reactor cavity and thus the pressure loads in the cavity and respectively to the containment could be avoided.

- Management of combustible gases

This strategy is applied to reduce the H_2 and the CO inventory in the containment. Depending on the type of the reactor different equipment, which could deal with the combustible gases is used. Generally PWRs operating countries have installed passive autocatalytic recombiners in the containment building. They can reduce the H_2 and CO concentrations to keep the containment pressure at a low level. Some PWRs and also BWRs have applied igniters, to produce intentional H_2 or CO burns. Containment venting is a strategy considered also for the reduction of the combustible gas inventory.

- Management of containment temperature, pressure and integrity

This strategy is realized by the automatic or manual usage of the containment sprays. In that way a condensation of the released steam is realized. Sprays are also used in longer term in conjunction with heat exchangers, which can extract the heat from the containment to avoid pressurization. Fan cooler systems in PWRs can extract heat and avoid late pressurization due to release of non-condensable gases during melt coolant interaction (MCCI). Containment flooding is also considered in PWR NPPs, as it depends on the containment size too.

Many European countries include also the strategy of containment venting, to avoid late failure due to over-pressurization by non-condensable gases released during MCCI.

- Management of the radioactivity releases

This strategy is realized by the containment heat removal system and the venting systems. The purpose here is reduction of the containment pressure. A strategy for reducing the inventory in the containment is the initiation of the containment sprays. They are designed for early operation and steam condensation after loss of coolant accidents (LOCA) and not for long term operation as in case of severe accidents. Sprays could provide effective aerosol deposition due to interception of droplets. The availability of the system strongly depends on the AC power. Applied are also filtering systems (as HEPA filters).

2.3 Status of the research worldwide

Severe accident research programmes are established /IRSN 2007/ in many countries with nuclear power sector i.e. the United States, Japan, France, Germany, Belgium, Canada, South Korea, Switzerland, Sweden and Russia. Basically, each country has focused on one or more particular aspects in the severe accidents research field. Worldwide the nuclear safety research programmes are concentrated from one side on representation of the severe accident phenomena experimentally, and on other side in the development of simulation codes for safety analysis. Joint research programmes supported by the European Commission through its Framework Programmes for Research and Development (FPRD), within the frames of the Organisation for Economic Co-operation and Development (OECD) have been initiated. For optimizing the data

base knowledge in the severe accident research, a part of the Sixth Framework Programme was the Severe Accident Research Network of Excellence (SARNET) project, coordinated by IRSN. The SARNET project has involved 49 participants from 19 different countries, either members of the European Union or new candidates for membership, as well as Switzerland. Basic issue has aimed at improvement of the scientific knowledge. The focus has laid on the development and validation of the integral severe accidents code ASTEC and methodologies for probabilistic safety analysis (PSA) level 2.

A large number of in-pile and out-of-pile experiments have been used to develop models and codes to allow a complete simulation of reactor accidents. In particular, one of those programmes is the PHEBUS FP programme /PHE 2001/ carried out by CEA, France, with international collaboration. This programme has been of the few programmes of a global nature within the severe accident research performing core melt experiments on a prototypic rod bundle with fission products transport through a representative primary system and the containment of a PWR. Through the Committee on the Safety of Nuclear Installations (CSNI), the OECD coordinates research programmes in the field of the severe accidents.

Experimental programmes to quantify the effects from severe accidents have been widely discussed also in Germany. From the latest big experimental facilities are the QUENCH facility /IS 1/ to investigate the physico-chemical processes and to get data on the hydrogen source term, the COMET facility /ALS 1999/to examine the late vessel melt behaviour and the DISCO facility /IS 2/ to study the core melt dispersal.

Experiments covering investigations in the field of the late in-vessel phenomena, behaviour of the molten pool, heat fluxes in case of IVR in the RPV lower plenum include the COPO experiments /KYM 1993/, /HEL 1997/, /HEL 1998/ conducted in Finland, which provide data for heat fluxes as a function of the azimuthal angle for a half scale slice representation of the torospherical (VVER-440 vessel model) and hemispherical lower head. Isothermal upper boundary conditions and crust formation were modelled in some of the experiments. In France was employed the BALI facility /BON 1998/, which is a full-scale slice geometry representation of the spherical lower head of the French PWRs. The UCSB experiments were performed on the mini-ACOPO and ACOPO facilities /THF 1997a/, /THF 1997b/. The facility represents a hemi-spherical half-scale three-dimensional model. The heat fluxes are imposed on the inner surface of the vessel wall by a heat generating fluid.

The SULTAN facility (France, CEA) /ROU 1997/ for large scale vessel coolability investigates the heat transfer during the boiling process on the outer surface of the vessel due to cavity flooding. The impact of the critical heat flux on the ex-vessel cooling has been also investigated.

In the Nuclear Energy Agency of the Organisation for Economic Co-operation and Development (NEA-OECD) the RASPLAV project /IS 3/ have been used molten salts as simulant material as well as in the SIMECO facility at the Royal Institute of Technology, Sweden /IS 4/. The RASPLAV project results have provided data on the behaviour of molten corium pools and the heat load on the lower head of the reactor pressure vessel, as the thermal

conditions affect the lower head failure mode. The project also covers the issue of the accident management strategies during a reactor core meltdown scenario /IS 5/.

A collaborative project called MASCA carried out at the Russian Research Centre "Kurchatov Institute" (RRC KI) /IS 6/, /IS 7/ in co-operation with a number of scientific and research associations of Russia: IBRAE RAN, NPO Luch (Podolsk, Moscow region), NPO ThermIKS sponsored in collaboration with the NEA-OECD has focused on experiments and analysis within the field of the retention of molten corium within the light-water reactor (LWR) lower vessel head. The MASCA and MASCA-2 experimental programmes have followed the RASPLAV project and have been focused on investigation of the in-vessel phenomena during a severe accident. For the case of in-vessel melt retention by external cooling of the RPV a focus should be given if the melt configuration is coolable by the supplied water quantity. Conservative methods are used. In that case the RPV sustainability on thermal and mechanical loads should be proved. Challenging issue for the IVR is the critical thickness of the molten steel layer situated above the oxide pool.

Analytical models and codes are used for analyses of the results derived from different experimental programmes. The conclusions derived from the experiments are adapted to reactor applications and benchmarking.

Concerning the applicability and effectiveness of accident management measures in the preventive domain (early phase of severe accidents), usually system codes like RELAP, CATHARE or ATHLET are widely used to investigate the response of the reactor coolant system until heating up of the core. For VVER-1000 type of reactors several investigations on accident management strategies and possible operator actions have been carried out by using the computer code RELAP-5 /CHE 2008/, /GEN 2005/, /MUE 2007/ and /PAV 2007/.

2.4 The Fukushima accident

On the area of the Fukushima I nuclear power plant on March 11th 2011 a severe accident leading to major consequences on the reactor Units 1-4 and the surrounding area has occurred /GRS 2011/, /US NRC 2011/. The accident was primarily caused by an earthquake and tsunami, resulting in a loss of internal and external power supply, as well as a failure of all diesel generators – a station blackout accident. Additionally loss of ultimate heat sinks (UHS) has led to unavailability of service or house water supply, necessary to cool down the nuclear plant safely after the accident has occurred.

A main objective of the work presented in this thesis is investigation on accident progression, typical phenomena and especially on possible countermeasures during a hypothetical station blackout accident for a VVER-1000 PWR-type of reactor (Chapters 5, 6 and 7). Even though the reactor types are different, the consequences and to some extent also the countermeasures after a station blackout are similar (e.g. loss of residual heat removal, loss of emergency core cooling, mass loss from the reactor coolant system, core uncovery, core heat up and core damage at high or low pressure). Regarding that, a brief description of the Fukushima accident and the applied

countermeasures, as well as a comparison for the general course of events after a station blackout for both reactor types are given.

At the site of Fukushima I six BWRs are installed /TEPCO1 2011/, /GRS 2011/, /NIS 2011/. These reactors are LWRs with a total electric power output of 4.7 GW_{el}. They are enveloped in two containment structures: primary and secondary containment. The emergency power supply is realized by two diesel generators as 1 of 2 are shared with the neighbouring unit. Table 2-1 summarizes the main characteristics for Units 1-6.

Table 2-1: Main characteristics of the Fukushima I boiling water reactors, Units 1-6

	Reactor power	**Reactor type**	**Containment type**	**Operating pressure**
Unit 1	460 MW_{el}	BWR-3	Mark I	7.03 MPa
Unit 2-5	784 MW_{el}	BWR-4	improved Mark I	7.07 MPa
Unit 6	1100 MW_{el}	BWR-5	Mark II	7.07 MPa

In a station blackout accident the increase of the reactor pressure usually is limited or reduced by the operation of the relief and safety valves and the residual heat is removed by the steam dump to the pressure suppression pool. Due to loss of power supply the residual heat removal system, necessary for cooling the pressure suppression pool, is unavailable. As a consequence the temperature in the pressure suppression pool starts to rise.

In accidents with decreasing water inventory different emergency core cooling systems can feed the reactor pressure vessel with water from the pressure suppression pool or from a storage tank. Depending on the working principle and the ability to inject at different reactor pressure, the systems are separated as active/passive and high/low pressure systems. After a station blackout the active systems are unavailable and only the systems working on passive principles can feed the reactor coolant system. The emergency core cooling pumps powered by steam turbines are used to inject water also at higher pressures. The steam produced in the reactor is directly transferred to these turbines and from there it is condensing in the pressure suppression pool (wet-well). The pump is injecting water from the pressure suppression pool (or from a storage tank) back to the reactor. Another system, which was installed at Fukushima I Unit 1, is the so called isolation condenser. It consists of a tube bundle installed in a water pool; the tubes are connected to the reactor pressure vessel. In accident conditions, inside of the tubes the steam is condensed and the condensate flows back to the reactor, thereby establishing a heat removal driven by natural circulation and temperature differences. But these systems are not really passive systems, because they need at least battery power supply to operate (e.g. for pump regulation or valve activation).

For Units 1-3 the earthquake with 9.0 magnitude has caused reactor SCRAM, turbine trip and loss of the house load electric power supply. Caused by the severe damages in the surroundings also the external power supply (off-site power) has been lost. At the moment of the earthquake Units 4, 5 and 6 were in periodic inspection outage. The following description focuses on the

main events observed in Units 1-3. The timings for the events in the three units are different, but the general progression of the accident is similar. It is not within the scope of this work to provide a detailed analysis of the Fukushima accident. For that reason a more general description of the accident progression is given.

Units 1, 2 and 3 were automatically shut down by the reactor protection system (reactor SCRAM), as it should normally be. The turbine stop valves have been closed, the recirculation pumps and feedwater pumps have stopped and the containment has been isolated. After the loss of house load and off-site power the emergency power supply system (diesel generators, DG) of Units 1, 2 and 3 has been automatically activated. Though stop of the fission reaction the decay heat from the reactor core is still a source of heat to be removed (around 6 % from the nominal reactor power after SCRAM, continuously decreasing to less than 0.5 % after some days). After loss of the main heat sink (the turbine and the steam dump to condenser), the increasing reactor pressure is limited by the operation of the relief valves and later on it has been reduced by the automatic depressurization (ADE). The steam produced in the reactor core is released by steam dump to the pressure suppression pool. Caused by the decrease of the reactor level the emergency core cooling system has started water delivery to the reactor core. As long as the pressure suppression pool has not lost its ability to condense steam, the residual heat from the reactor can be removed by steam dump to the pressure suppression pool and feeding from the emergency core cooling system. The plant has been in a stable-state condition.

The emergency diesel generators have been operating for an hour and as a result of following extreme tsunami wave the diesel generators station and the essential service water building for cooling of the diesels have been flooded and totally destroyed (common mode failure). With the loss of house load supply (the turbine) and failure of all diesel generators the plant in-site power has been lost. The loss of in- and off-site power supply has led to a total loss of power supply (station blackout). No active safety systems supplying water to the core have been available, as they are electrically power supplied. Also the batteries have been flooded and as a consequence the safety systems, which need battery power to operate, have been failed. The loss of UHS has led to unavailability of water supply for cooling down the reactor units. Mobile diesel generators have been delivered to the site nine hours later and have been connected to the plant.

Due to the continuous increase of the temperature in the wet-well, the pressure suppression pool as remaining heat sink was lost. More steam in the reactor is produced, which could not be effectively removed from the core. The continuous boil off and further decrease of the reactor level lead to core uncovery and heating up of the reactor core. The decay heat and the absence of heat removal from the core result at increase of the fuel and cladding temperatures. At temperatures above 1100 °C the fuel cladding material zircaloy reacts strongly by the contact with the steam in the core. Due to the oxidation processes in the core, resulting in exothermal steam-zirconium reaction with release of great amount of hydrogen and heat, melting of the core materials is expected. Continuous increase of the core temperature has caused ballooning and partial cracking of the fuel cladding leading to release of fission products. The pressure in the containment has continuously increased. Probably due to venting or due to lifting off the primary containment vessel cap hydrogen has been released to the secondary containment and by the

contact with the air it has deflagrated (Units 1 and 3). This has caused serious challenge to the containment structures. Accident management measures for containment depressurization were performed. For Unit 2 a hydrogen explosion inside of the primary containment occurred.

Mobile diesel generators have been delivered to the units to re-establish the water injection to the reactor core. Additionally to mobile and fire-extinguishing pumps also helicopters, water cannon trucks and concrete pumps have been used to supply water to the units. Besides the most important task to provide sufficient core cooling, the supplied water has also been used for cooling the reactor vessel outer wall (ex-vessel cooling) and to re-establish the cooling of the spent fuel storage pools.

To the time of writing this sub-Chapter, the Fukushima accident is still on-going and it would be premature to draw conclusions on the severity of the current state of the plant, the damages on the reactor core, the release of fission products and the environmental assessment. It is supposed that 2/3 of the fuel elements on Unit 1 are damaged, partial core melt on Unit 2 and partial core damage on Unit 3. On May 15th TEPCO have stated that /TEPCO2 2011/: "*Results of the provisional analysis show that the fuel pellets of Unit 1 were melted and fell down to the bottom of RPV at relatively early stage after the tsunami reached the plant. Although RPV is damaged in this provisional analysis, the actual damage of the RPV is considered to be limited according to the temperatures presently measured around the RPV.*". Contamination of the drinking water and food with elements I-131 and Cs-134/137 above the allowed levels has been detected. The Fukushima accident has been initially rated as level five according to the INES scale as later this rate has been increased to level seven due to the high radioactive releases in the first few days of the accident.

Though the conceptual design and the design parameters differences between the boiling water reactors (BWRs) and the pressurized water reactors (PWRs) a raw comparison of the accident progression caused by a station blackout (SBO) event could be made. A simplified scheme for the accident progression in both reactor types is to be seen in Figure 2-1.

The initiating event (SBO) leads to reactor SCRAM, turbine trip, stop of recirculation pumps (BWR) and main circulation pumps (PWR), as well as to loss of feedwater supply (for the reactor in BWRs and for the steam generators in PWRs) and failure of all active emergency core cooling systems. The increasing pressure in the reactor coolant system is controlled by relief and safety valves. After reaching the corresponding set-points, in the BWRs pressure regulation (limitation) or ADE is actuated and the residual heat is removed by steam dump to the pressure suppression pool. The primary to secondary heat removal in the PWRs is realized with the help of the secondary side steam generator relief and safety valves (steam dump to atmosphere). Due to the failure of the pressure suppression pool cooling systems in the BWRs the wet-well temperature increases. As a consequence the pressure suppression pool as a heat sink for steam dump is lost. In PWRs a similar behaviour can be observed. After steam generators depletion (break down of primary to secondary heat transfer) the remaining heat sink is lost and after that the increasing primary pressure is limited by operation of the pressurizer relief valves.

For both reactor types only passive safety injection systems are available. In comparison to a PWR in the BWRs emergency core cooling starts earlier, depending on the decrease of the

reactor water level (caused by pressure regulation or automatic depressurization). Without depressurization the further accident progression occurs at high reactor pressure, with depressurization at low pressure (Figure 2-1). In most BWRs the passive core cooling systems utilize turbine driven pumps, capable to inject water at high pressure. The remaining passive core cooling systems in PWRs are the hydro-accumulators. To activate their injection, the primary pressure has to be reduced below 5.8 MPa in the VVER-1000 reactor or to even lower values for Western-type PWRs. For the primary side depressurization (PSD) the pressurizer relief and safety valves are fully opened (Chapter 6). Without PSD the further accident progression occurs at high primary pressure, with PSD at low pressure (Figure 2-1). After failure of the passive core cooling systems due to batteries depletion, heat up of the pressure suppression pool or low system pressure in BWRs, and after depletion of the hydro-accumulators in PWRs, the continuously decreasing water mass in the reactor leads to core uncovery. Without depressurization for both reactor types the core will heat up and core damage under high pressure is well to be expected. In case that depressurization has been performed heating up of the core and core damage is expected but at low pressure path scenario (Figure 2-1).

The possibilities to prevent or/and mitigate a severe accident resulting from initial event SBO in BWR reactor types are: restoration of the AC power as soon as possible, at high system pressure depressurization of the reactor pressure vessel, restoration of the water injection to the reactor core, injection of boron B-10 (to preclude re-criticality) and flooding of the containment to retain the core/molten materials in the reactor pressure vessel (ex-vessel cooling). The accident management measures and strategies for PWRs are discussed in Chapters 5 to 7.

The accident progression in the Fukushima nuclear power plant, as well as the studies presented with this thesis show, that it is of primary importance to ensure the heat removal and core cooling by passive means for a time period as long as possible. Passive systems play a very important role during a station blackout accident and the power supply from the batteries must be also available as long as possible. One lesson learned from the Fukushima accident is, that after a station blackout the restoration of the power supply can last for a much longer time than a few hours and how difficult it can be to provide power supply and core cooling under such circumstances. For that reason possible accident management measures and strategies have to be carefully investigated and they must be optimized for a grace period as long as possible, as well as for their effectiveness (Chapter 6).

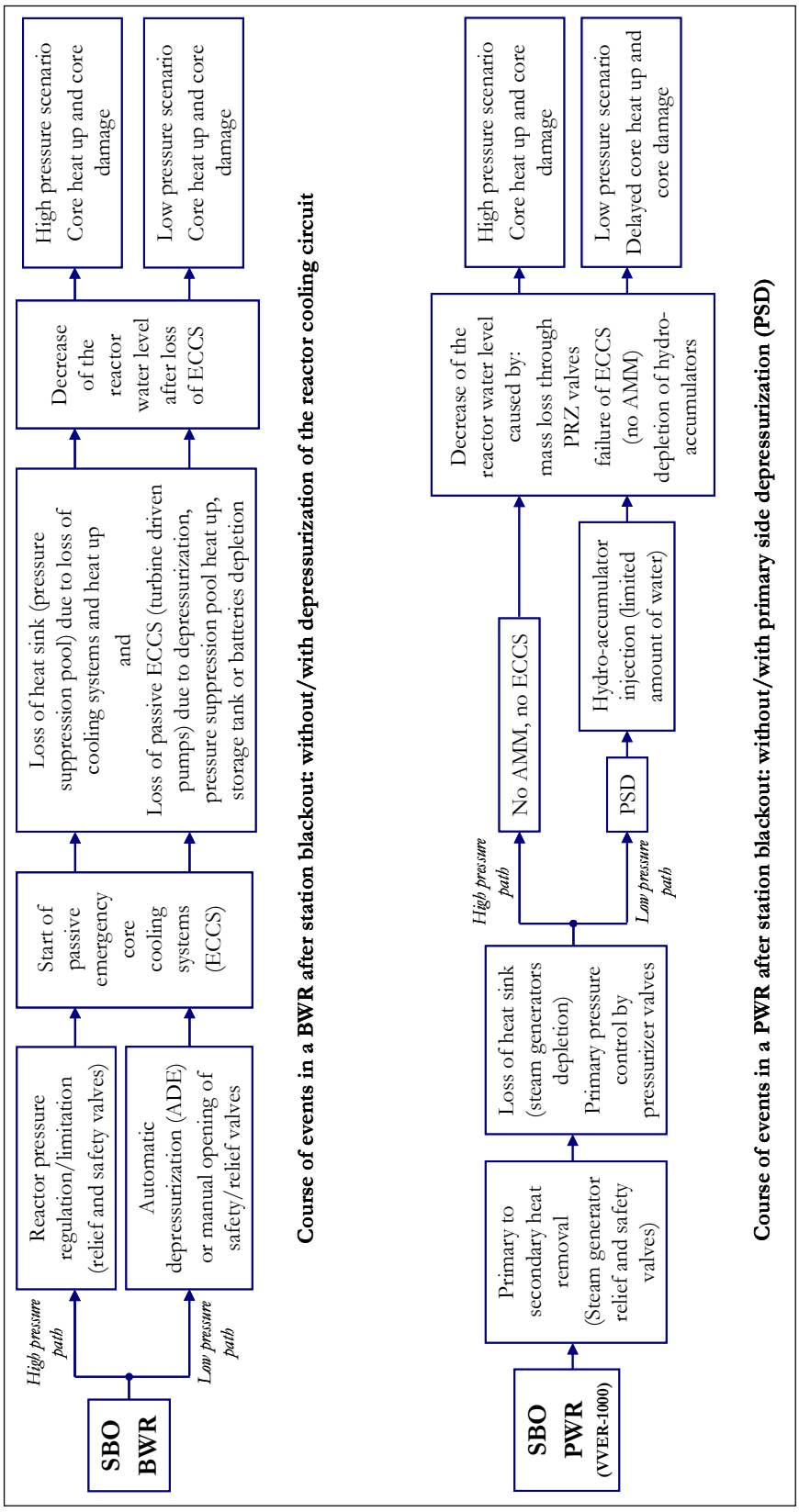

Figure 2-1: Accident progression in a station blackout scenario (without restoration of power supply, only passive safety systems are available)

3 Severe accident analysis and applied codes

In the following Chapter the requirements necessary for the simulations performed with different computer codes, general description of codes for severe accident analysis and particularly the ASTEC code structure are discussed.

3.1 Requirements for the simulations

Basically the assumptions made in accident analyses are related to the reactor design, accident scenarios, which are going to be investigated, specific requirements of national regulatory authorities, international requirements and computer codes. Key issues at performing accident analysis are the selection of computer code relevant for a given accident scenario, selection of the initiating event and acceptance criteria, initial and boundary conditions (input data) for the simulation and assessment of the simulation results. The accident analyses should be done by validated codes /IAEA: 23/.

Two principal methods are applied in the field of safety analysis: probabilistic and deterministic methods. The safety proof for a nuclear power plant is based on deterministic as well as on probabilistic methods.

The probabilistic analyses provide information on the availability of systems, the failure probability of components and safety functions, and finally on the probability of occurrence of accidents as well as on the risk in terms of damage frequency, e.g. for core melt or reactor pressure vessel (RPV) failure.

The deterministic analyses aim at a more realistic simulation of the course of events in accidents, to evaluate the thermal-hydraulics or balance-of-plant behaviour and to derive preventive or mitigative measures for accident management. Different models have to be applied depending on the accident scenarios under investigation, e.g. neutron-kinetics for the heat generation in the reactor core, thermal-hydraulics including heat conduction and heat transfer to account for the primary to secondary heat removal and structural mechanics to model the mechanical response

of components, like piping or the RPV. Two options are widely used with respect to the availability of safety systems and to the initial and boundary conditions:

- Application of best estimate codes with conservative assumptions for the availability of safety systems (e.g. application of single failure criterion and repair) and conservative initial and boundary conditions
- Application of best estimate codes with conservative assumptions for the availability of safety systems and realistic initial and boundary conditions considering uncertainties in the physical models, input and output parameters.

On one hand acceptance criteria are used to assess the accuracy and reliability of the results of safety analysis. On the other hand acceptance criteria based on the defence-in-depth concept are used to evaluate, if a safety proof was successful or not, it means whether an accident can be controlled by the safety systems or not.

Derived from the basic safety goals to protect individuals, the society and the environment against radiological hazard, several acceptance criteria for the different protection goals are formulated like:

- Cladding temperatures and maximum local cladding oxidation must be below certain limits to ensure the core cooling
- Shut-down reactivity must be ensured for control of reactivity
- Limited number of damaged fuel rods and limited amount of oxidized zirconium for retention of radioactivity.

By developing of the input data basis for a computer code, the sources serving as a basis are the documentation on the plant design, the technical specification of the equipment, operational documentation of the plant (limits and conditions, operating instructions and records of the operational regime, set points and function of operational, reactor protection and safety systems) as well as emergency operating procedures and severe accident management guidelines. All the necessary data like geometry, neutron-kinetic and thermal-hydraulic parameters, material properties, characteristics of the systems and drawings, are collected in "Database for safety analysis".

The creation of a plant model for computer codes includes selection of a nodalization scheme and preparation of the code input deck. Depending on the objectives of the analysis, the plant model, or the code input deck, could be accident dependent. Typically for safety proofs different kinds of accidents are investigated, like:

- Reactivity initiated accidents (RIA) and anticipated transients without SCRAM (ATWS)
- Loss of coolant accidents (LOCA), including small, medium sized and large breaks
- Loss of heat sink and loss of power supply.

Verification of the input deck is needed to check its correctness. Validation is performed after the completion of the input deck verification and before starting the accident analysis. The purpose

of validation of the input data is to demonstrate that the model adequately represents the functions of the modelled systems /IAEA: 23/. In that way the limits of the NPP could be assessed.

3.2 Codes for severe accident analysis

The numerical simulation of the severe accident is realized by a two-path approach:

- Integral codes that simulate the entire accident from the initiating event to the possible release of fission products outside the containment and taking into account the main safety systems
- Mechanistic codes that provide more detailed simulation of specific accident phenomena and a more detailed modelling of operational, reactor control and safety systems.

Referring to the severe accident analysis, well known and widely applied severe accident codes are MAAP4, MELCOR, ICARE/CATHARE, SCDAP/RELAP5 and ASTEC.

Objective of the MAAP4 code /IS 8/, /IRSN 2007/, developed for the Electric Power Research Institute (EPRI), is to predict core meltdown sequences, using simple models. MAAP is a modular nodal code, representing the reactor cooling primary system, the secondary system, the engineered safeguard systems, and the containment and auxiliary buildings. The solver matrix is based on the mass and internal energy conservation equations for each control volume. Momentum conservation equations are not differential equations and can be considered as Bernoulli equations. The code models cover large and small break LOCAs and transients. Due to the relatively coarse nodalization, MAAP4 calculations require minimal computation time.

MELCOR code /IS 9/, /IRSN2007/is developed by the Sandia National Laboratories (SNL). The code has a modular structure with large number of physical models. It covers a broad range of severe accidents phenomena, such as core degradation, fission product (FP) release and transport, ex-vessel corium behaviour and fission product and aerosol behaviour in the containment building. The applied models are parametric-mechanistic, based on empirical correlations. The nodalization schemes could be more detailed. MELCOR runs at a moderately fast speed.

SCDAP/RELAP5 code /IS 10/, /IRSN 2007/ is developed by Idaho National Engineering Laboratory (INEEL). The code is based on detailed, mechanistic models of both thermal-hydraulic and severe accident phenomena. Nodally structured, the code uses a large number of components to describe the primary system. The simulations are time-consuming. Generally it is applied for LOCAs and transients within the primary system, reactor core phenomena and fission product release from the fuel.

The ICARE/CATHARE system is developed by IRSN /IS 11/, /IRSN 2007/. It is applied for accident analysis of light water reactor (PWR, VVER, EPR, etc.) and probabilistic safety analysis (PSA) level 2. This system is a combination of the ICARE2 mechanistic code for core degradation developed by IRSN and the CATHARE2 thermal-hydraulic code developed in

collaboration by CEA, IRSN, EDF and FRAMATOME-ANP. ICARE/CATHARE is modular code as each module deals with a specific phenomenon: thermal-hydraulics, mechanics, chemistry, fission products, movement of materials, debris beds, core meltdown.

Currently developed and in process of validation European integral severe accidents analysis code is ASTEC (Accident Source Term Evaluation Code). General description of the code structure and capabilities are given below.

3.3 ASTEC code

The integral code ASTEC is commonly developed by IRSN and GRS with the aim to get a fast running code for the simulation of severe accidents sequences in LWR from the initiating event up to the possible fission products (FPs) release out of the containment. The applications are:

- Source term determination studies
- PSA level 2 studies
- Accident management studies
- Physical analyses of experiments to improve the understanding of the phenomenology.

The code shall cover all important phenomena, which can occur in PWR, including VVER, BWR and new reactor designs like EPR. The purpose is code application to accident sequence studies, probabilistic safety assessments, investigations on accident management procedures and to the support to experiments. ASTEC plays a central role in SARNET (Severe Accident Research Network) project under the 6^{th} and 7^{th} European Framework Programme, in order to progressively become the reference European integral code.

The code has modular structure. The basic modules are /PIG 2002/, /ALL 2005/, /AST 2006/, /DOR 2006/, /GIL 2007a/, /GIL 2007b/:

CESAR

CESAR module simulates the early front-end phase of the accident. Accounted is two-phase thermal-hydraulic behaviour. The vessel and the loops are defined by a simplified modelling. After the beginning of the core degradation phase two-phase thermal-hydraulics is calculated in the loops and in the vessel upper plenum only. The physical models are based on the reference French thermal-hydraulic code CATHARE /GIO 2001/.

Two phases are considered: water and gas (steam and one non-condensable gas), as in present only one non-condensable gas is considered - hydrogen. The numerical approach is a five-equation one: two mass balance equations, two energy balance equations and one momentum equation for gas velocity with a drift flux correlation for water velocity. The state variables are total pressure, void fraction, gas enthalpy, water enthalpy, partial pressure of hydrogen and gas velocity.

The reactor coolant system is discretized into volumes, either homogeneous or with a swollen level model. A volume can be also nodalized in axial direction. The specified volumes are connected with junctions. The wall heat transfer models close the energy balance equations.

Special components represent pumps, valves and breaks.

DIVA

This module describes in-vessel core degradation. The module is directly derived from the IRSN mechanistic code ICARE2 for core degradation: same general structure and same modelling approach. The module simulates the early-phase degradation with fuel rod ballooning and failure, cladding oxidation, fuel rod heat-up, molten mixture candling, etc. and then the late-phase degradation with corium accumulation within the core channels and formation of blockages, corium slump into the lower head and corium behaviour in the lower head until vessel failure.

Some specific models were developed to avoid too high computation times:

- For core thermal-hydraulics: multi-1D channel liquid and 2D gas
- For corium behaviour in lower plenum: 2D meshing of vessel lower head, three 0-D corium layers (oxide layer, metal layer, debris).

The main models are:

- Heat conduction and heat transfer: between two walls, between rod and cladding (including the gap), convective heat transfer between fluid and wall, radiation in a reactor core or in a bundle. Radiation from the lower core structures to the residual water in lower plenum is also modelled, which favours vaporisation of water
- Power: simulated can be the nuclear power generated by fission products or electric power generated as in the case of experiments
- Chemistry: oxidation of Zr by steam, oxidation of stainless steel by steam, dissolution of UO_2 by solid and liquid Zr, dissolution of Zr by liquid steel, oxidation and degradation of B_4C control rods
- Rod mechanics: creep of zircaloy cladding, loss of integrity of fuel rods (using user-defined criteria)
- Material relocation: in early-phase of core degradation, radial/axial movement of a mixture of molten and solid masses within or along the rods and then slump into the lower plenum
- Vessel lower head mechanical failure: melt-through, or mechanical failure (either instantaneous plastic rupture or creep rupture) or user-defined criteria (such as temperature, degradation rate, stress)
- Reflooding of quasi-intact or slightly degraded cores (i.e. still in rod-like geometry).

The description of geometry of vessel lower head allows the modelling of any type of shape such as semi-elliptical one for VVER reactor types.

CPA

The CPA module simulates thermal-hydraulics and aerosol behaviour in the containment. It consists of two main sub-modules THY (thermal-hydraulics behaviour) and AFP (aerosol and fission product behaviour). The containment discretization through a "lumped-parameter" approach (volumes represented by nodes connected by junctions) simulates simple or multi-compartment containments (tunnels, pit, dome) with possible leakages to the environment or to normal buildings, with more or less large openings to the environment.

- Thermal-hydraulics in containment CPA-THY: describe phenomena such as pressure and temperature build-up and history, local temperature and pressure distributions, local gas, local heat transfer to walls (free and forced convection, radiation, condensation), 1D heat conduction in structures (plates or cylinders, consisting of several material layers), and hydrogen combustion
- Aerosol and fission product behaviour in containment CPA-AFP: describe phenomena such as volume condensation and growth of insoluble and soluble aerosol particles, behaviour of chemically different aerosol components, and agglomeration and deposition processes.

ELSA

This module simulates release of fission products and structure materials from the core. It is strongly coupled with the DIVA module. For intact fuel rods, the semi-empirical approach deals with three classes of fission products: volatile, semi-volatile and non-volatile.

SOPHAEROS

This module simulates transport of fission products vapours and aerosols in the reactor coolant system. Using families of species (elements, compounds, gas, volatile, non-volatile) and five states (suspended vapours, suspended aerosols, vapour condensed on walls, deposited aerosols, sorbed vapours), the mechanistic and semi-empirical approaches model the main vapour-phase and aerosol phenomena.

RUPUICUV

This module simulates the direct containment heating (DCH), i.e. ex-vessel corium discharge into the cavity (vessel blow-down, cavity pressurization) and potential corium oxidation and entrainment from the cavity to the containment.

Two kinds of cavity geometries are considered:

- "Closed" cavities such as in USA-type PWR, i.e. without direct connection with containment, but through a series of intermediate compartments
- "Open" cavities such as in Western European PWR, i.e. with an annular space towards the containment.

CORIUM

This module simulates the behaviour of corium droplets transported by high pressure melt ejection (HPME) into the containment atmosphere and sump. Hot gases entrain these droplets. Heat transfer between corium and gas is modelled in each containment zone (DCH).

MEDICIS

This module uses the lumped-parameter 0D approach with averaged melt/crust layers. It assumes either well-mixed or stratified (heavy oxide, metal, light oxide) corium, and it calculates concrete ablation and corium oxidation.

IODE

This module simulates iodine behaviour in the containment, i.e. the main chemical reactions in sump and gas phase. Transport of iodine species through compartments of the containment is computed by CPA module.

ISODOP

This module simulates decay of fission products and actinide isotopes in different zones of the reactor. It starts the calculation using an initial isotope inventory.

SYSYNT

This module simulates the management of engineered safety features (for instance spray system, safety injection system, management of steam generators).

MDB

This material data bank (MDB) library groups together all material properties under a unique simple readable format.

There are also some specific couplings between the modules, as during the front-end phase, CESAR alone calculates the thermal-hydraulics in the whole reactor coolant system, using a simplified core modelling of 1 radial mesh. An automatic switch to DIVA for simulation of in-vessel core degradation phenomena has been elaborated. This switch will be effective around time of start of core uncovery, and in any case before the start of rod zircaloy oxidation by steam. After the switch, CESAR calculates only the loops and the vessel upper plenum, and DIVA calculates the remaining part of the vessel (core, lower plenum, and downcomer).

For the accident analyses performed in the following Chapters, different release versions of the ASTEC code have been used. This is because of the fact that the code is still in validation process.

4 Validation of the ASTEC in-vessel modules against ISP46 PHEBUS FPT1 experiment

This Chapter focuses on the validation of the ASTEC code against the PHEBUS ISP-46 FPT1 experiment, investigating the release of fission products, their transport and deposition in a PWR during a hypothetical severe accident. Main issue of the presented investigation concerns representation of the severe accident phenomena, thus the ASTEC code application in simulation of severe accidents.

4.1 Description of PHEBUS FPT1 experiment

The PHEBUS Fission Product (FP) programme /PHE 2001/, /PHE 2004/ had been initiated in 1988 after major severe accidents in nuclear reactors at Three Mile Island (TMI), USA, in 1979 and at Chernobyl, Ukraine, in 1986. The main objective of the programme had been investigation of the release, transport and retention of fission products in an in-pile facility under conditions representative of severe accidents in a Light Water Reactor (LWR). Cooperation formed between the "Institut de Protection et de Sûreté Nucléaire" (IPSN) of the "Commissariat à l'Energie Atomique" (CEA) and the Commission of the European Communities (CEC) agreed in performing six tests in collaboration with other international partners, namely:

- The United States Nuclear Regulatory Commission (NRC)
- The Japanese Nuclear Power Engineering Corporation (NUPEC)
- The Japan Atomic Energy Research Institute (JAERI)
- The Canadian Candu Owners Group (COG)
- The Korean Atomic Energy Research Institute (KAERI)
- The Swiss Paul Scherrer Institute (PSI)
- The Swiss Federal Nuclear Safety Inspectorate (HSK).

The programme had been directed by the "Département de Recherche en Sécurité" (DRS) at CEA-Cadarache and the Joint Research Centre (JRC) of the CEC /PHE 2001/.

The FPT1 test is the second experiment of the international PHEBUS FP programme conducted by the French IPSN of the CEA. The programme is launched to study the severe accident phenomena in a light water reactor (LWR). Severe accident situations assume total or partial malfunction of the reactor protection and safety systems, leading to core meltdown. They also assume total or partial failure of emergency operating procedures intended to prevent these accidents or to mitigate their consequences. Thus, the PHEBUS FP experimental programme has been aimed at estimation of the amounts of radioactive fission products and aerosols, released by fuel elements, to investigate their behaviour both in the primary circuit and in the containment, and to provide an experimental basis for computer code validation.

The FPT1 test was conducted in July 1996, in order to study the release of fission products and their subsequent transport and deposition in primary circuit and the containment of a pressurized water reactor. ISP-46 provides the opportunity to assess the capability of severe accident modelling codes in an integral manner, covering core degradation through to the late phase with melt pool formation, hydrogen production, fission products release and transport, circuit and containment phenomena, and iodine chemistry. The general objective is to assess the capability of computer codes to model in an integrated way the physical processes taking place during a severe accident in a pressurized water reactor, from the initial stages of core degradation to the behaviour of released fission products in the containment. The codes are supposed to be used in a similar manner as they would be used for plant studies, employing standard models and options as far as possible, with representations of the facility in similar details as used for plant studies.

Figure 4-1shows the general scheme of the FPT1 experiment /PHE 2001/.

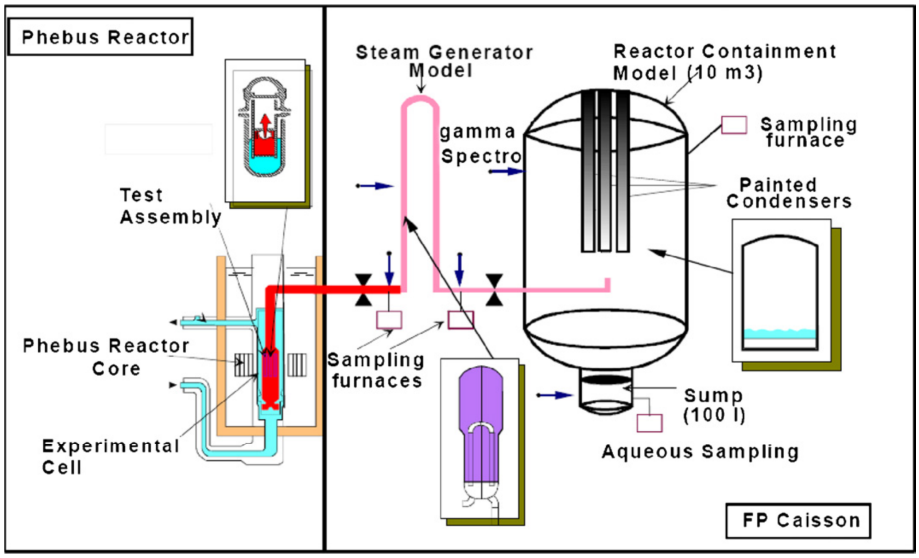

Figure 4-1: PHEBUS FPT 1 (ISP-46) general experimental scheme

The specific objectives of the FPT1 test could be described separately for the fuel rod bundle, the experimental circuit and the containment. The experimental circuit simulates some of the PWR components, including the primary side of a steam generator.

In the fuel rod bundle

The objective was to generate significant degradation of the bundle by reaching the liquefaction temperature of the fuel in order to produce large releases of fission products into the experimental circuit. This required that the liquefaction of at least ~2 kg of fuel (i.e. ~20% of the total mass of fuel) from the bundle had to take place under low pressure in a steam-rich carrier gas.

In the experimental circuit

The main objectives were to investigate fission product retention within the primary circuit of the reactor at low pressure (around 0.2 MPa) without steam condensation and to provide data on fission product chemistry including interactions of these fission products with pipe walls at high temperature.

A secondary objective was to explore phenomena in the section just above the bundle exit where sharp changes in the carrier gas temperature were expected. In the FPT1 test, a section of the liner, in the temperature controlled part of the vertical line above the bundle, was made of stainless steel, allowing differences in deposition on this material and the Inconel, which was used elsewhere in the circuit to be studied.

In the containment

The main objectives were to study fission product chemistry and especially iodine radiochemistry in the sump water and the atmosphere, and the effect of paints in the realistic chemical conditions of a severe accident. An additional objective was to take advantage of the actual aerosol source to assess aerosol physics codes, especially the models for deposition with steam condensation (diffusiophoresis) onto internal condensing surfaces (condensers). The reduced volumetric scale factor compared to a PWR with 900 MW power is approximately 1/5000. A further important objective is the study of core degradation phenomena, especially during the late phase of the process.

The FPT1 test bundle consists of 21 fuel rods, which are in a 5x5 lattice configuration with a pitch of 12.6 mm. The rods are hold by two zircaloy spacer grids. Among these 21 rods, 18 rods are PWR fuel rods (~3.75% enrichment in U235) previously irradiated to a mean burn-up of 23.4 GWd/tU and two instrumented fresh fuel rods (~3.5% enrichment in U235). These rods have a fissile length of 1 m, housed in a zircaloy (Zry) cladding of 1.12 m. The last rod is an absorber silver-indium-cadmium (AIC) control rod with stainless steel cladding housed in a zircaloy guide tube. The FPT1 test bundle was ~1 m in length and contained a total fuel mass of ~11 kg. The bundle was housed in an insulating shroud, limiting the radial heat losses, which was introduced into an in-pile tube cooled by a pressurized water circuit. The shroud is composed of four layers: a 2.5 mm thick thorium inner layer, 8 mm thick insulated region of porous zirconium and a 6 mm thick Inconel-625 pressure tube, flame-spray coated with a 2 mm thick high density zirconium

layer on its inner surface. There are two gaps in the shroud (0.5 mm at room temperature) surrounding the porous zirconium sleeve. The test train was set in a cell in the centre of the PHEBUS reactor. The bundle was pre-irradiated for ~7 days with a mean bundle power of ~205 kW in the PHEBUS reactor before the experimental phase of the test itself in order to generate short-lived fission products in the fuel. The main instrumentation in the PHEBUS core and the test train has been used to control the experiment on-line. After the pre-conditioning phase, a period of 36 hours was necessary to bring down reactor xenon poisoning and to establish the boundary conditions of the experimental circuits.

The fuel degradation phase had lasted five hours, during which the inlet steam flow rate injected at the bottom of the test train had been varied from 0.5 to 2.2 g/s providing oxidizing conditions, while the bundle power had been progressively increased from 0.65 kW up to 36.5 kW. The bundle degradation phase consisted of two main periods. The first one, devoted to the thermal calibration of the bundle lasted ~7900 s. During this period, the bundle power and the steam flow rate were changed step by step in order to check the thermal response of the bundle. The second period was the real temperature transient and degradation phase of the test, lasting from ~7900 s to ~17000 s. The degradation phase was especially devoted to the release of fission products, bundle, structure and control rod materials in order to study their transport and retention in the experimental circuit. After the degradation phase the experiment continued with aerosol phase, washing phase and chemistry phase.

4.2 ASTEC model

The investigation presented in Chapter 4 aims at modelling of the main phenomena arising during the late phase of a severe accident, such as molten pool formation, hydrogen production, fission products and aerosol releases. An ASTEC model, using ASTEC v1.1 code version, has been applied to simulate the PHEBUS FPT1 experiment. To model the main phenomena occurring in the late phase of a severe accident, the CESAR, DIVA, ELSA, SOPHAEROS, IODE and CPA modules have been activated (Chapter 3, Part 3.3). Special attention has been given to a proper modelling of the fuel rod bundle and different nodalizations schemes have been applied to study the sensitivity of the calculated results on the axial meshing.

The model consists of several main structures including simulation of the FPT1 reactor bundle, the circuit and the containment vessel, as follows (Figure 4-1):

- The fuel rod bundle consists of 20 fuel rods: 18 irradiated fuel rods, 2 fresh fuel rods and one silver-indium-cadmium (AIC) control rod. The reactor bundle is surrounded by insulated shroud composed by high density zirconium. The core is also surrounded by measurement instruments
- The circuit consists of: upper part section, which is represented as a vertical line ~3 m high; an isothermal horizontal line ~9 m long; vertical steam generator U-tube ~4 m high; and another isothermal horizontal line ~4 m long

- The vertical and the first horizontal line together simulate the hot leg of PWR primary circuit, while the second horizontal line simulates the cold leg
- The containment vessel reproduces the reactor containment. It is used for estimation of the released iodine isotopes.

Alternative nodalizations are concerned in order to investigate the code response according to the different meshing methods.

The primary circuit is represented by 23 volumes as follows (Figure 4-2):

- Upper part - consists of 6 volumes
- Hot leg - consists of 4 volumes
- Steam generator - divided into 11 volumes
- Cold leg - consists of 2 volumes.

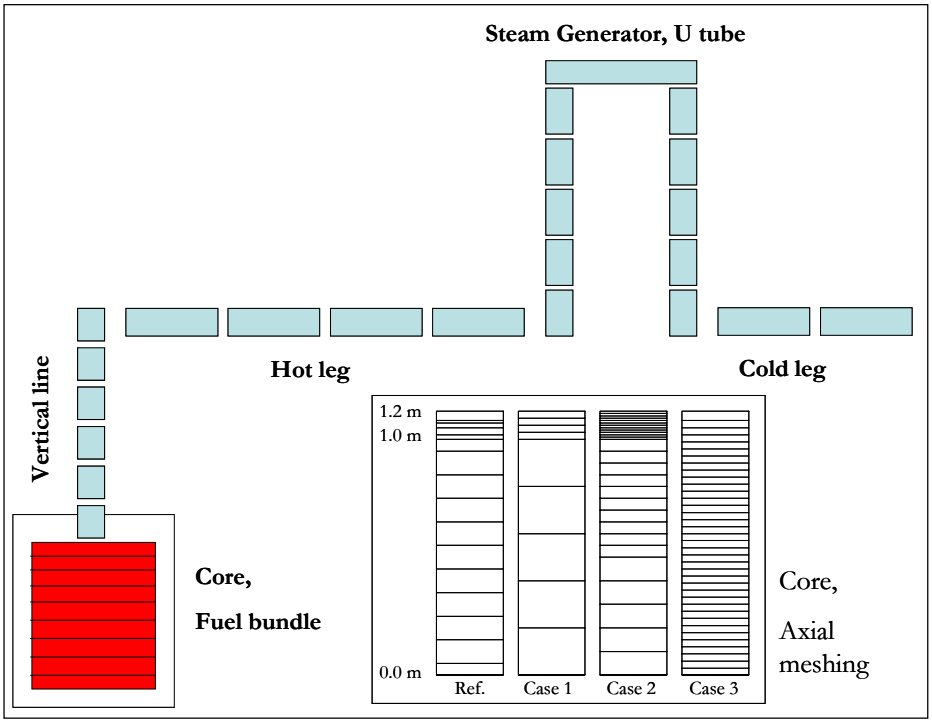

Figure 4-2: FPT 1 ASTEC nodalization for the primary circuit and the core axial meshing

By the axial meshing of the fuel bundle several cases have been investigated (Figure 4-2). As a reference, a case with 17 mesh points has been used. Three additional cases for comparison with the reference case have been applied to study the effect of the different nodalizations on the calculated results:

- Simplified case with 10 axial points, separated at 2 parts (0-1.0 m), and (1.0-1.12 m) with various steps/spaces between the mesh points in each part

- Three sectioned case with a sequence of 28 mesh points, separated at 3 parts (0-0.5 m), (0.5-1.0 m) and (1.0-1.12 m) with various space between mesh points in the each part
- Uniform case with a sequence of 38 mesh points with coextensive steps - space 0.03 between the all mesh points in the entire sequence (0-1.12 m) long.

All the cases are presented in Table 4-1. The finer nodalization in the upper part of the core model aims at calculation of the onset of the severe accident from the start of core uncovery. In radial position the meshing is kept as the basic input deck (as in the reference case). The radial meshing is composed of two adjacent channels inside the bundle. The 21 rods modelled (1 AIC and 20 fuel rods) are divided into 4 rings of rods. The containment is modelled as a single volume.

Table 4-1: Meshes of the FPT1 bundle axial meshing. Length coordinates in m

Mesh No/Cases	Ref. (Mesh 17)	Case 1 (Mesh 10)	Case 2 (Mesh 28)	Case 3 (Mesh 38)
1	0.00	0.00	0.00	0.00
2	0.05	0.20	0.10	0.03
3	0.15	0.40	0.20	0.06
4	0.25	0.60	0.30	0.09
5	0.35	0.80	0.40	0.12
6	0.45	1.00	0.50	0.15
7	0.55	1.03	0.55	0.18
8	0.65	1.06	0.60	0.21
9	0.75	1.09	0.65	0.24
10	0.85	1.12	0.70	0.27
11	0.95		0.75	0.30
12	1.00		0.80	0.33
13	1.02		0.85	0.36
14	1.05		0.90	0.39
15	1.07		0.95	0.42
16	1.08		1.00	0.45
17	1.12		1.01	0.48
18			1.02	0.51
19			1.03	0.54
20			1.04	0.57
21			1.05	0.60
22			1.06	0.63
23			1.07	0.66
24			1.08	0.69
25			1.09	0.72
26			1.10	0.75
27			1.11	0.78
28			1.12	0.81
29				0.84
30				0.87
31				0.90
32				0.93
33				0.96
34				0.99
35				1.02
36				1.05
37				1.08
38				1.12

4.3 Code-to-experiment comparison

4.3.1 Boundary conditions

The gaseous flow in the bundle is modelled according to the definition of two adjacent channels. An internal, which has 23.99 mm internal radius and external, which has the radius of the thorium layer of the shroud. The outlet pressure at elevation 1.12 m is set to 2.2 bars.

The inlet steam temperature is kept at a constant value of 438 K during the whole transient. The axial power profile is given in Figure 4-3:

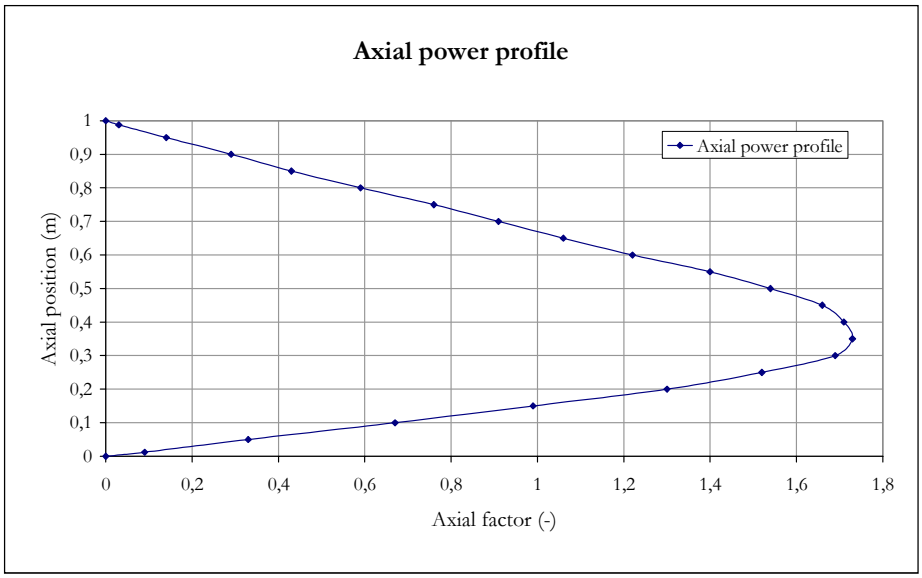

Figure 4-3: FPT1 experiment, axial power profile

The total duration of the test is 17039 s. The bundle degradation phase is divided into five representative periods:

- Calibration period (from 0 to 7900 seconds)
- Pre-oxidation period (from 7900 to 11060 seconds)
- Oxidation period (from 11060 to 13200 seconds)
- Power plateau (from 13200 to 14580 seconds)
- Heat-up period (from 14580 to 17039 seconds).

The calculation is ended by the isolation of the containment from the primary system.

4.3.2 Results of the simulations

The evaluation of the calculation focuses on the following phenomena:

- First fuel cladding rupture
- Thermal behaviour and fuel temperatures for the different mesh cases
- Hydrogen production during the calculations
- Relocation of materials at the end of the calculations.

In Table 4-2 are presented the main events calculated by ASTEC for the different cases and the results are compared to the experiment. Figure 4-4 to Figure 4-35 depict the calculated results by the ASTEC code. With the help of the selected parameters a comparison to the experimental results has been done and is described in the text below.

The first total core uncovery is at the beginning of the calculation for all the cases. According to the post-experimental analyses of the FPT1 test, the clad ballooning and bursting due to the internal overpressure had occurred during the third temperature plateau of the calibration period (~5700 s). The first fuel cladding rupture for the different cases is arising around 4960 s (Case 3, Mesh 38) – 5670 s (Case 1, Mesh 10), corresponding to the calibration period of the experiment. The closest results to the experimental ones are calculated in Case 1 with a coarse bundle nodalization: 5700 s experiment/5670 s calculated (Table 4-2).

The burst of the cladding results in a release of fission gas and aerosols from the fuel pellets. According to /PHE 2001/ it is supposed that probably the cladding failed at different times in the axially hottest region at 0.5 m elevation. At the time of the cladding failure, the maximum measured experimental temperature of ~845 °C (1118 K) is in a good agreement with the ASTEC code calculated results in all cases. The release of fission products from the fuel pellets is at 5690 s calculated by ASTEC in Case 1 versus 5800 s in the experiment. The calculated times in Case 2 (5110 s) and Case 3 (4980 s) are underestimated. The reference case with 17 meshes gave a time for the start of FP release around 5140 s, which is also underestimated.

The start of the structural material release for the different cases is varying between ~8740 s (Case 3, Mesh 38) and ~8970 s (Case 1, Mesh 10) corresponding to the pre-oxidation period of the experiment. In all cases the start of structural material release is underestimated in comparison to the experimental results of 9690 s.

Differences in the results are also observed for the time of beginning of oxidation. The experimental results have shown beginning of oxidation at about 8580 s from the first total core uncovery. Case 3 with 38 meshes gave the closest time to the experimental data (8800 s). The coarse meshing of the bundle (Case 1) as well as the reference case with 17 meshes largely overestimates the experimental results (10443 s and 10733 s respectively).

Figure 4-4 to Figure 4-15 show the evaluation of the thermal behaviour - temperature evolutions at levels 0.2 m, 0.5 m and 0.8 m. This is respectively the lower part, the mid-part and the upper part of the bundle. FUEL2, FUEL4 stay for the modelled fuel elements (inner and outer) and SHR11, SHR27 stays for the shroud elements (inner and outer).

According to the test data provided, during the first thermal calibration period of the test, the failure of zircaloy cladding due to internal over-pressure occurred at ~845 °C (referring to the maximum temperature measured at the bundle mid-plane). At the end of the calibration period (~7900 s) the maximum temperature measured in the bundle was stable at ~920 °C (1193 K). Referring to the FPT 1 Final Report /PHE 2001/ at ~7900 s of the transient, the nuclear power generated in the bundle was increased and the steam flow rate was increased from 0.5 g/s to 2.2 g/s in ~37 min (until ~10160 s). Respectively, the ASTEC code calculated results for that period of time are in a good agreement to the measured experimental data. The temperature escalations detected in the FPT1 experiment in the upper part of the fuel bundle with a peak around ~11300 s, which are due to the oxidation runaway, have been predicted by the code (Figure 4-12 to Figure 4-15) in all the simulated cases, but less pronounced in the Case 1 with 10 meshes bundle nodalization scheme (Figure 4-13). Correct agreement is predicted on the evolution of bundle temperatures in all the studied nodalization cases, but underestimation of the oxidation peak in comparison to the experimental data 2200 °C (2473 K).

The analyses of the thermal behaviour of the bundle and the shroud clearly indicate a large fuel relocation and accumulation during the last ~20 min of the test (until ~16000 - ~17039 s). The materials (fuel and cladding) relocated away from both the upper and the lower half of the bundle. At the end of the heat-up phase, as could be seen from Figure 4-32 to Figure 4-35, the molten material is progressively accumulated inside the molten pool at 0.19 - 0.26 m elevation. Figure 4-32 to Figure 4-35 show the distribution of the different materials depending on the height of the core and the core radius. Referring to /PHE 2001/, the temperature inside the molten pool at the lower elevation has probably reached ~2500 °C (2773 K) at the end of the degradation phase. The extension of the mass of the molten pool associated with the complete failure (melting and/or dissolution) of the lower grid has produced a second axial movement of materials. The hydrogen mass flow rate (Figure 4-28 to Figure 4-31) has increased during this phase too, and probably has been due to the second downward progression of the molten pool below the lower grid leading to temperature escalation and oxidation of the partially oxidized cladding.

Generally, the thermal behaviour does not vary much for the different cases viewing all the temperature evolution curves before the runaway oxidation period. Differences in the calculations appear locally later during the oxidation period and the heat-up period and these differences, observed mainly at the bottom of the bundle (Figure 4-4 to Figure 4-15 and Figure 4-32 to Figure 4-35) are due to relocation processes i.e. when hot masses become in contact with colder ones.

With the beginning of the zircaloy oxidation, hydrogen production in the experimental circuit (sensor in the containment) has been detected around 8580 s.

Table 4-2: Main events, FPT1 experiment vs ASTEC code simulations

Event/Cases	FPT1 Experiment	Reference (Mesh 17)	Case 1 (Mesh 10)	Case 2 (Mesh 28)	Case 3 (Mesh 38)
First total core uncovery, [s]	-	1.00000E+00	1.00000E+00	1.00000E+00	1.00000E+00
First fuel cladding rupture, [s]	5.700E+03	5.12078E+03	5.67078E+03	5.09078E+03	4.96078E+03
Start of FPs release from fuel pellets, [s]	5.800E+03	5.14078E+03	5.69078E+03	5.11078E+03	4.98078E+03
Start of structural material release, [s]	9.690E+03	8.83713E+03	8.97078E+03	8.90078E+03	8.74078E+03
Beginning of oxidation, [s]	8.580E+03	1.07333E+04	1.04436E+04	8.85078E+03	8.80078E+03
Containment isolation, [s]	1.86608E+04	1.86608E+04	1.86608E+04	1.86608E+04	1.86608E+04
Hydrogen production, [g]	~112	~115	~114	~118	~112

Figure 4-28 to Figure 4-31 show the total hydrogen production. The chemical reaction has started in the upper part of the bundle as fuel temperature has exceeded 1100 °C (1373 K). The experimental results, as well as the calculated ones, show that due to the exothermically chemical reaction, produced during the oxidation of the zircaloy cladding in the steam atmosphere, results in temperature increase of the fuel rods. Until ~8580 s there is only a minor hydrogen production. The hydrogen production increased slowly and progressively after that time, between ~8580 s and ~9140 s, as the maximum temperature in the fuel bundle exceeded ~1100 °C at 0.5 m elevation.

In accordance to the calculated results by the ASTEC code a good agreement to the experimental results for the total hydrogen production is received for Case 2 with 28 meshes and for Case 3 with 38 meshes. The oxidation rate of zircaloy is accelerated considerably at temperatures around 1675 °C (1948 K) at ~11300 s. A second smaller hydrogen generation peak is detected clearly as well in the reference case with 17 meshes as in the detailed case with 28 meshes (Case 2). According to the post-experimental results, this second hydrogen peak is observed in the last ~20 min of the test. That is explained with the download relocation of the molten pool to a zone where probably the cladding was not completely oxidized. The calculated hydrogen production results in Case 3 gave the exact value of 112 g as of the experiment. In the other nodalization cases the production of hydrogen is overestimated by the code (Table 4-2).

Figure 4-32 to Figure 4-35 show the final degraded state of the test bundle. In the figures with AIC is indicated the position of the Silver-Indium-Cadmium control rod, STEEL - indicates the position of the steel elements in the bundle, ZR – the zirconium elements, ZRO – the zirconium oxide elements, ZRO2 – the zirconium dioxide elements and MIXTU corresponds to the mixture (the molten) elements. A resolidified molten pool could be observed, which generally

consists of uranium and zirconium oxides, homogeneous pool. The most degradation of the fuel bundle and material slumping has been observed during the heat-up period of the experiment. The relocation of materials has started from the upper part of the fuel bundle and proceeded downwards to the lower parts. Melt is accumulated at elevation 0.2 m from the bottom of the test bundle, which leads to formation of a melt pool, trapped by the lower grid. The relocation processes calculated by the ASTEC code and according to the experimental results started at temperatures below ~2100 °C - 2200 °C (2373 K – 2473 K), as that process could be explained with the formation of eutectic mixtures between the material and the control rod from one side, and from another the oxidized cladding and the fuel rods, leading to fuel dissolution and loss of integrity of the fuel pellets.

According to the experiment the molten pool moved down probably because of the partial failure of the lower crust at the level of the grid. There is also a second movement of materials, which is probably due to the total failure of the lower bundle grid.

In Figure 4-16 to Figure 4-27 are depicted the release of fission products, separately for volatile, semi-volatile and low-volatile trends, calculated by the ASTEC code.

According to the FPT1 experimental results the first detection of most isotopes of volatile fission products (noble gases, isotopes of Cs, Te, I, Sb) at different locations in the circuit occurred between 10960 s and 11340 s. Good agreement in the ASTEC code calculated results to the experimental ones is observed. The high temperatures lead to almost complete release of the high volatile fission products. During that time period the escalation of the oxidation reaction resulted in strong material release in the circuit and significant increase of isotopes of volatile nuclides - Cs, Te, I, Sb (Figure 4-16 to Figure 4-19). The maximum fraction of volatile fission products release, according to the experimental results, is reached around 13500 s to 13800 s. The noble gases, such as Kr and Xe, which are highly volatile and non-reactive towards circuit surfaces, have reached a maximum release fraction of 84 % - 94 % calculated by the code. In comparison to that the experimental data indicate that 77.4 % of the initial bundle inventory of Xe135 reached the containment, and for Kr - respectively 84 % (fact that intact fuel remained at the bottom of the test bundle after the bundle degradation phase).

The semi-volatile fission products release (Figure 4-20 to Figure 4-23), such as Ba and Ru during the FPT1 test transient was very limited, with release fractions representing of the order of 1 % of their bundle inventory or less. The code calculated results show that the Ba release is largely overestimated.

The code calculated results for the low-volatile fission products are shown in Figure 4-24 to Figure 4-27. Zr arises mainly from bundle structure material. The low-volatiles have not been determined with sufficient accuracy in the FPT experiment.

The main phenomena that could occur during severe accidents in PWRs were reproduced in the FPT1 test and were simulated by the ASTEC code i.e.: (1) cladding burst, (2) zircaloy oxidation and hydrogen generation, (3) control rod failure and relocation of the absorber materials, (4) fuel rod liquefaction, material accumulation and molten pool formation and (5) fission product and aerosol releases, transport and retention in the primary circuit and the containment. During the

heat-up and transient phase the temperatures as well as the hydrogen generation are calculated in good agreement to the experiment. The onset of temperature escalation in all the calculated cases is very well predicted. The nodalization studies on the fuel bundle have shown that even with a coarse meshing Case 1, a good agreement of the experimental results is achieved. Case 3 with a detailed nodalization has represented the exact hydrogen production. The timing of key events is well predicted. The agreement of thermal-hydraulic variables is good. The simulation of the fission products release show reasonable agreement with the experiment, considering the uncertainties from the modelling and (partly indirect) comparison with the measurements. The total fractional releases from the bundle and circuit are satisfactory for most radionuclides. Good agreement has been obtained for the high volatile fission products, but for some, like ruthenium and uranium, the difference between simulation results and experimental measurements is by an order of magnitude.

According the different meshing the models with finer nodalization at the top of the bundle and a coarser nodalization in the lower part show that most of the main events can be predicted with good accuracy. The finer nodalization at the top is important to predict the onset of the severe accident phenomena following the first core uncovery as exact as possible.

The relatively low relocation temperature of the fuel rods as estimated in the FPT1 test (2100 °C - 2200 °C) is an important point. The melting temperature of the accumulated corium in the lower part of the FPT1 bundle as measured in the post-irradiation examinations (PIE) was found to be ~2500 °C. These parameters must be considered in the calculations simulating severe accidents in PWRs.

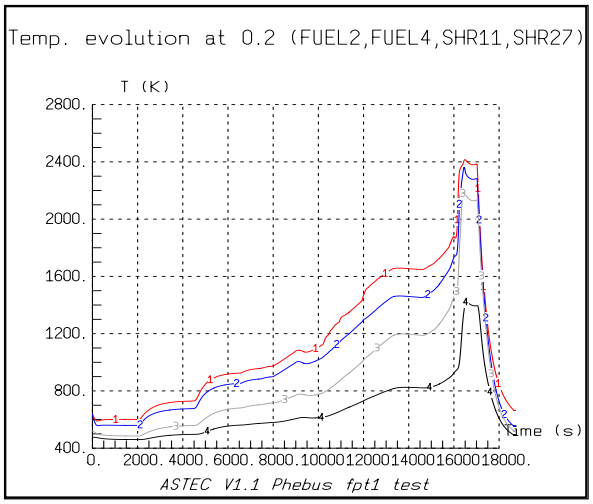

Figure 4-4: ASTEC v1.1, FPT1, Ref. Mesh 17, Temperature evolution at 0.2 m

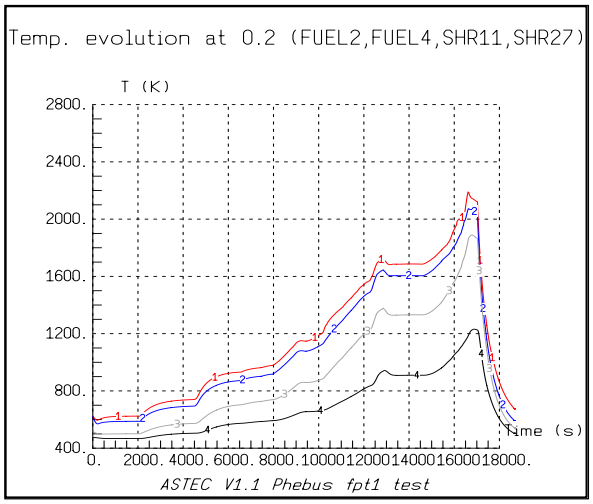

Figure 4-5: ASTEC v1.1, FPT1, Mesh 10, Temperature evolution at 0.2 m

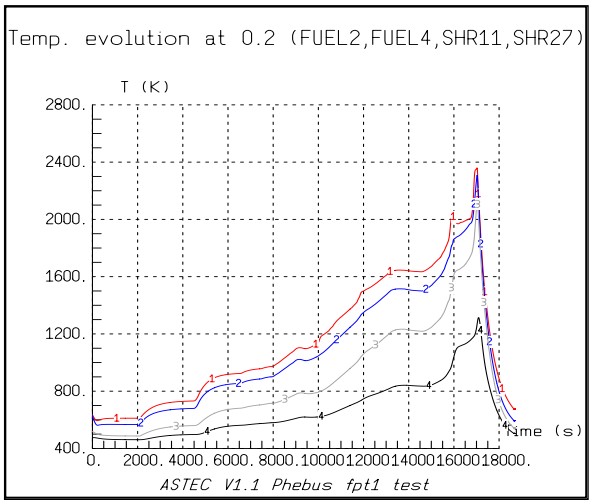

Figure 4-6: ASTEC v1.1, FTP1, Ref. Mesh 28, Temperature evolution at 0.2 m

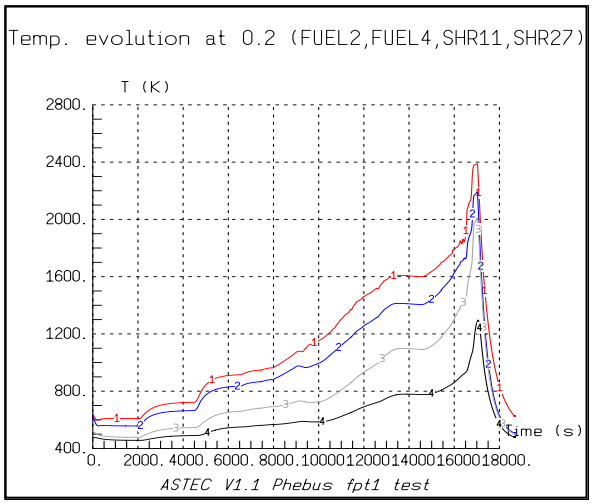

Figure 4-7: ASTEC v1.1, FTP1, Mesh 38, Temperature evolution at 0.2 m

Fuel elements: 1 FUEL2
2 FUEL4

Shroud elements: 3 SHR11
4 SHR27

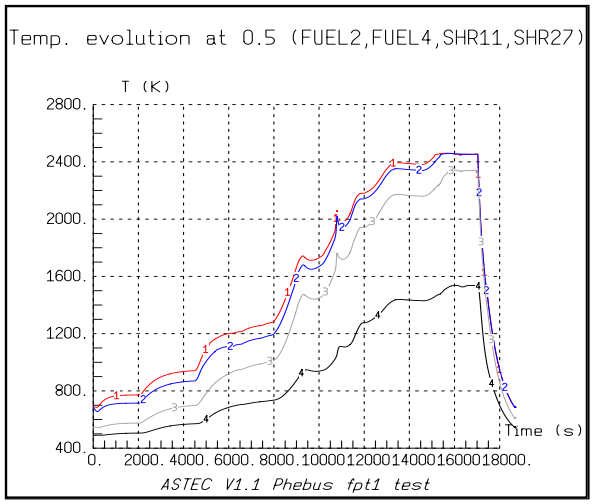

Figure 4-8: ASTEC v1.1, FPT1, Ref. Mesh 17, Temperature evolution at 0.5 m

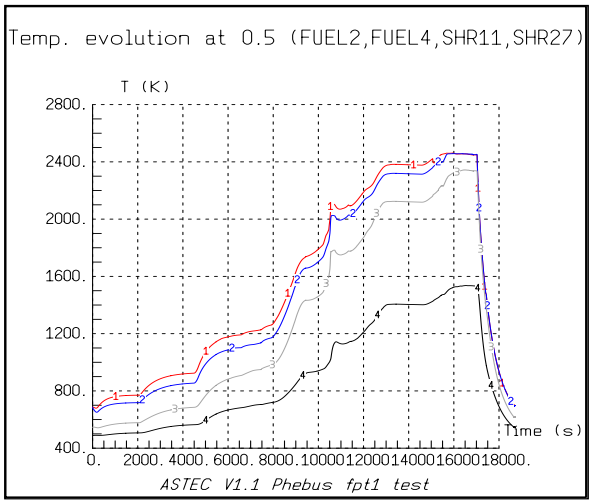

Figure 4-9: ASTEC v1.1, FPT1, Mesh 10, Temperature evolution at 0.5 m

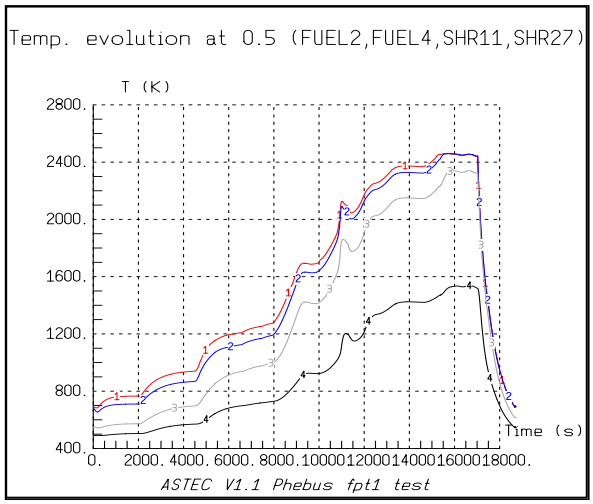

Figure 4-10: ASTEC v1.1, FPT1, Mesh 28, Temperature evolution at 0.5 m

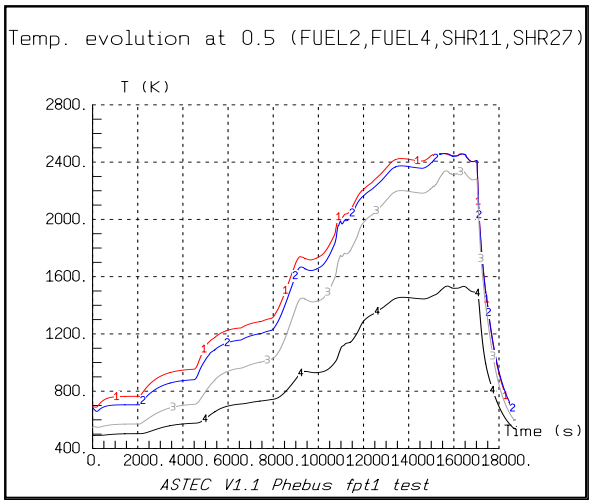

Figure 4-11: ASTEC v1.1, FPT1, Mesh 38, Temperature evolution at 0.5 m

Fuel elements: 1 FUEL2
2 FUEL4

Shroud elements: 3 SHR11
4 SHR27

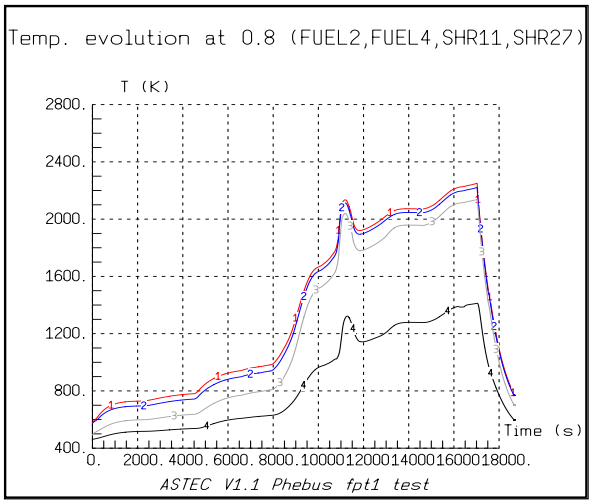

Figure 4-12: ASTEC v1.1, FPT1, Ref. Mesh 17, Temperature evolution at 0.8 m

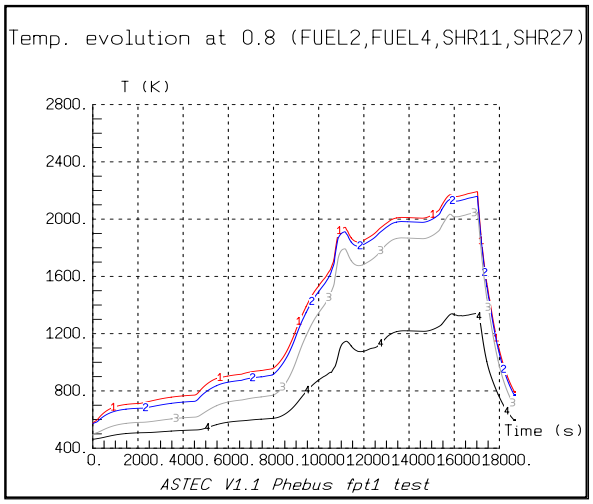

Figure 4-13: ASTEC v1.1, FPT1, Mesh 10, Temperature evolution at 0.8 m

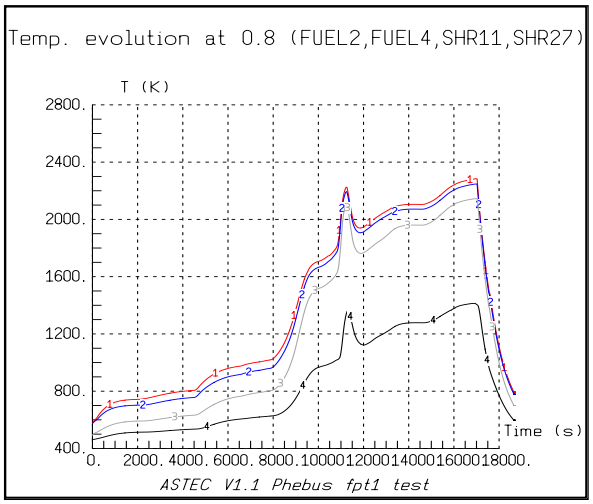

Figure 4-14: ASTEC v1.1, FPT1, Mesh 28, Temperature evolution at 0.8 m

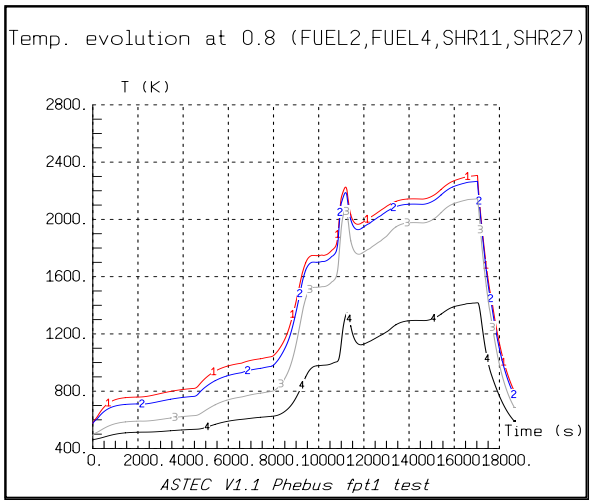

Figure 4-15: ASTEC v1.1, FPT1, Mesh 38, Temperature evolution at 0.8 m

Fuel elements: 1 FUEL2
2 FUEL4

Shroud elements: 3 SHR11
4 SHR27

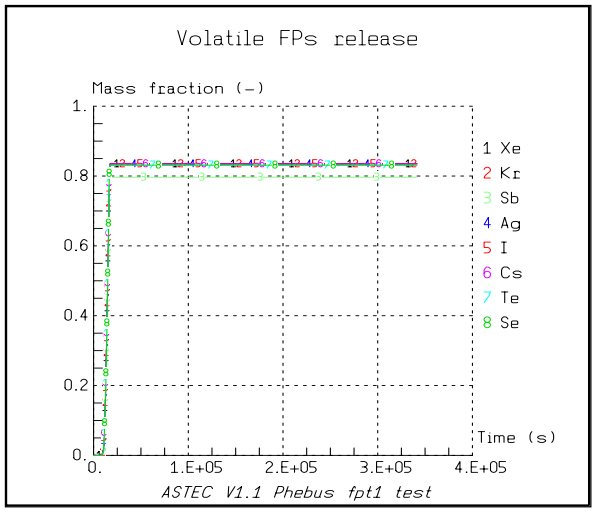

Figure 4-16: ASTEC v1.1, FPT1, Ref. Mesh 17, Volatile FPs release

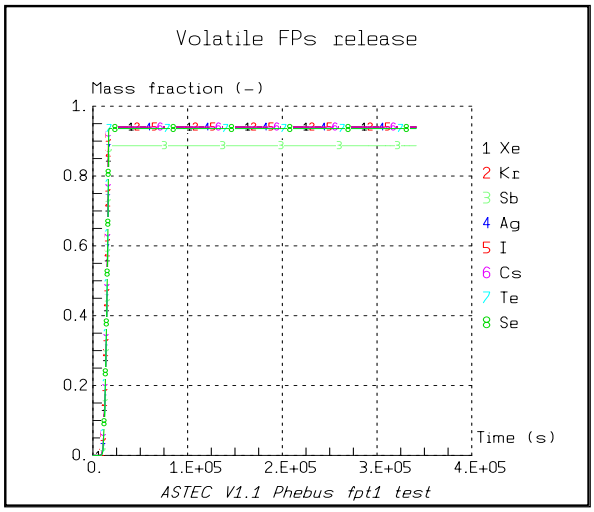

Figure 4-17: ASTEC v1.1, FPT1, Mesh 10, Volatile FPs release

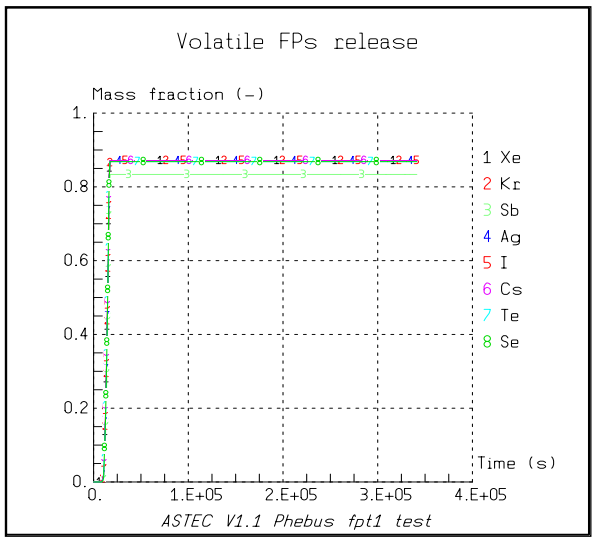

Figure 4-18: ASTEC v1.1, FPT1, Mesh 28, Volatile FPs release

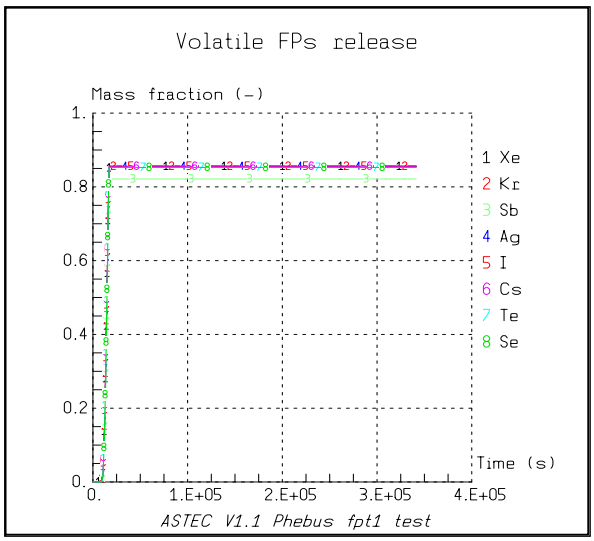

Figure 4-19: ASTEC v1.1, FPT1, Mesh 38, Volatile FPs release

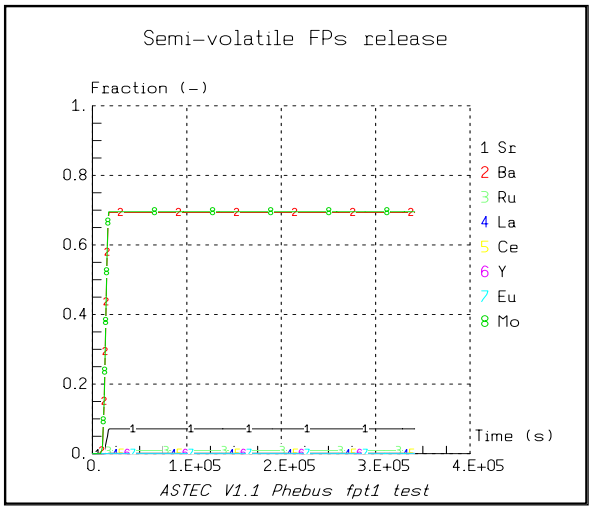

Figure 4-20: ASTEC v1.1, FPT1, Ref. Mesh 17, Semi-volatile FPs release

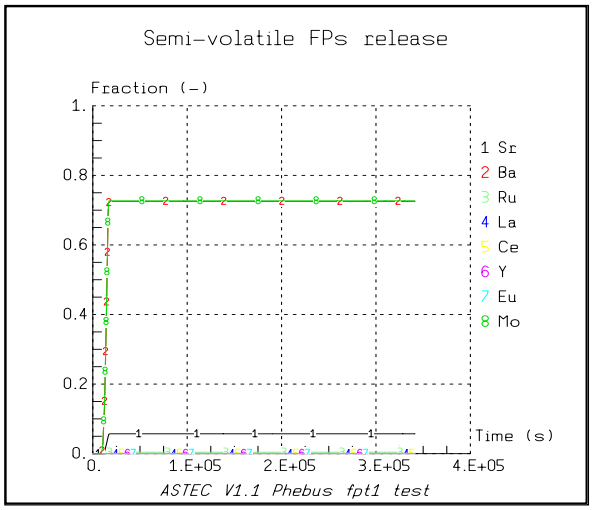

Figure 4-21: ASTEC v1.1, FPT1, Mesh 10, Semi-volatile FPs release

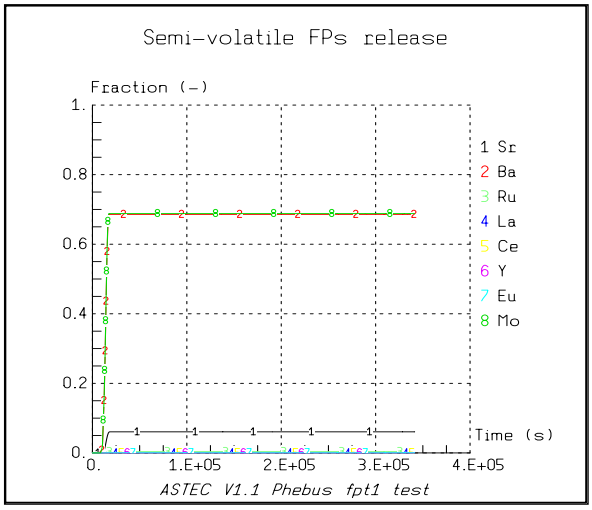

Figure 4-22: ASTEC v1.1, FPT1, Mesh 28, Semi-volatile FPs release

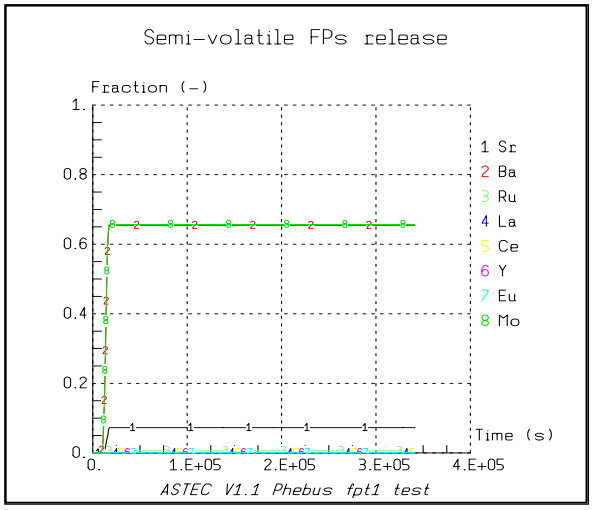

Figure 4-23: ASTEC v1.1, FPT1, Mesh 38, Semi-volatile FPs release

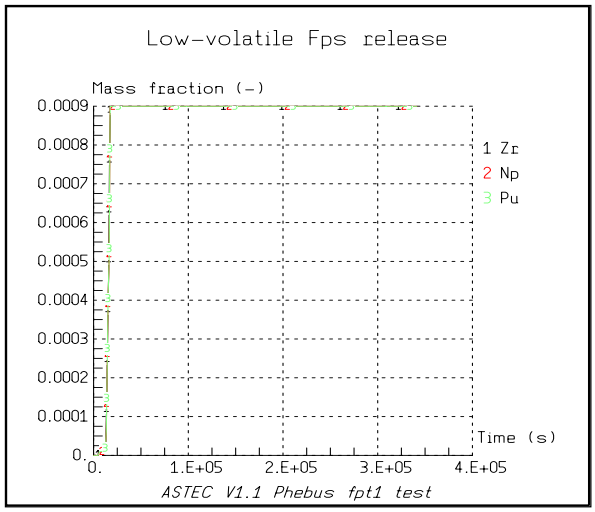

Figure 4-24: ASTEC v1.1, FPT1, Ref. Mesh 17, Low-volatile FPs release

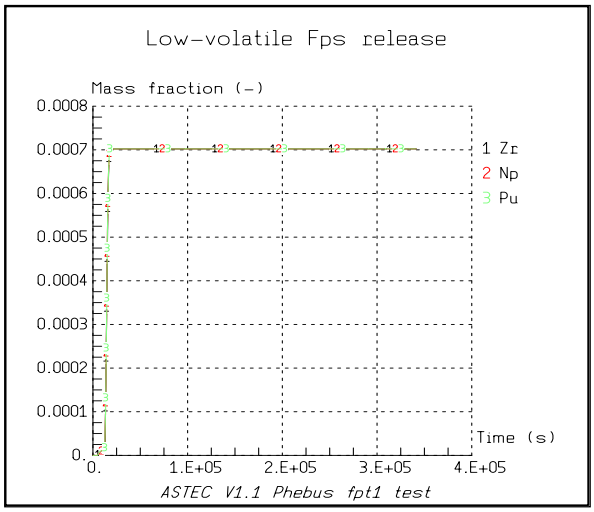

Figure 4-25: ASTEC v1.1, FPT1, Mesh 10, Low-volatile FPs release

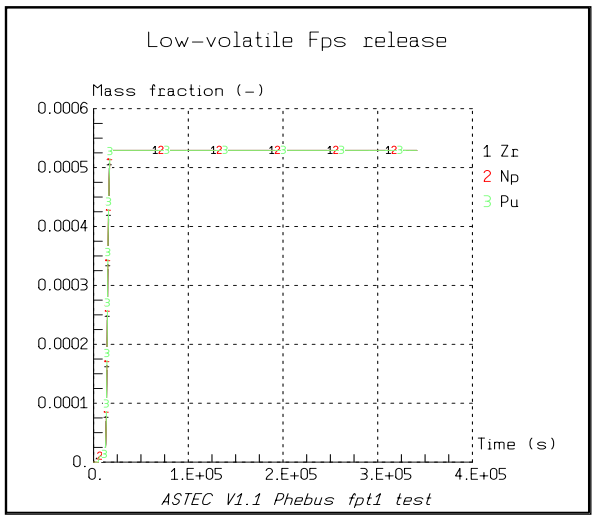

Figure 4-26: ASTEC v1.1, FPT1, Mesh 28, Low-volatile FPs release

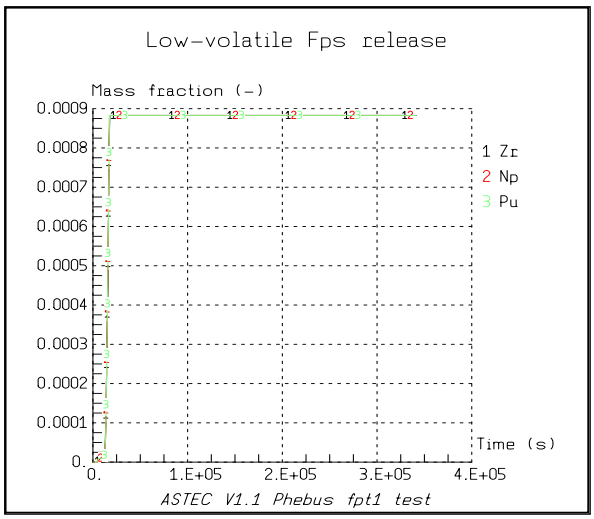

Figure 4-27: ASTEC v1.1, FPT1, Mesh 38, Low-volatile FPs release

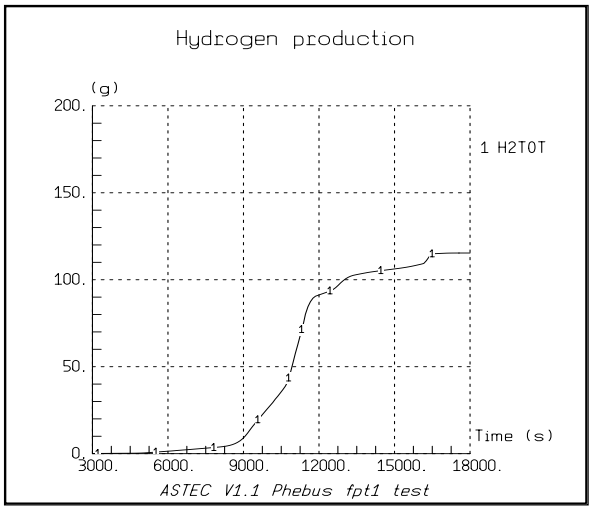

Figure 4-28: ASTEC v1.1, FPT1, Ref. Mesh 17, Hydrogen production

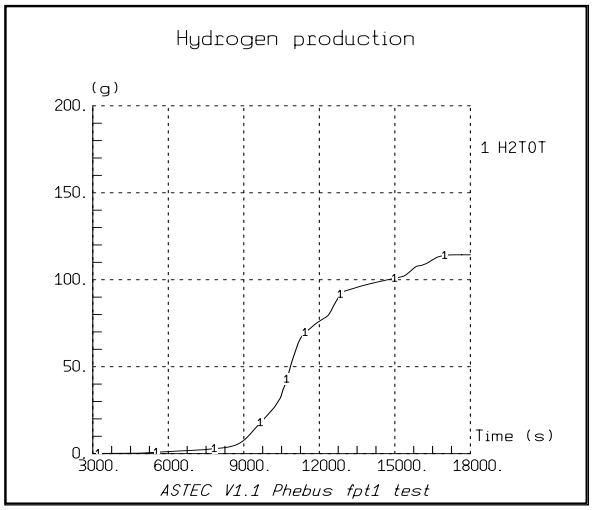

Figure 4-29: ASTEC v1.1, FPT1, Mesh 10, Hydrogen production

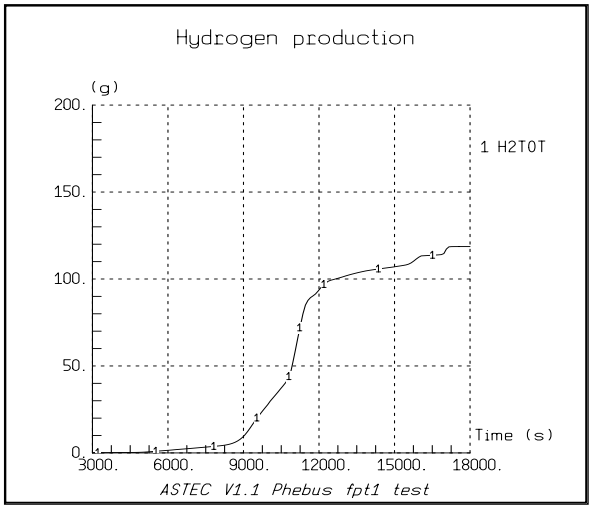

Figure 4-30: ASTEC v1.1, FPT1, Mesh 28, Hydrogen production

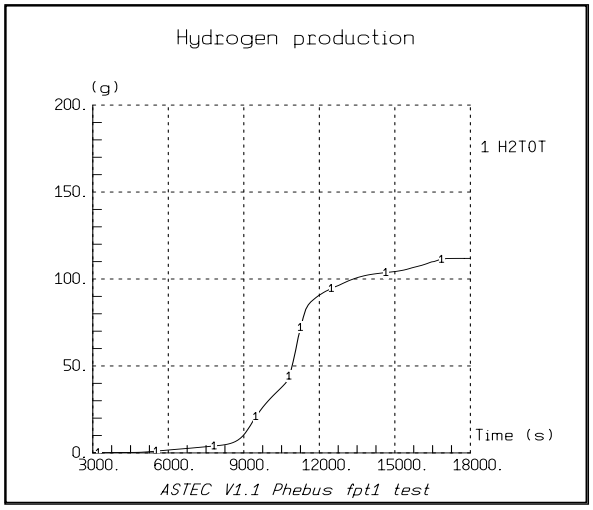

Figure 4-31: ASTEC v1.1, FPT1, Mesh 38, Hydrogen production

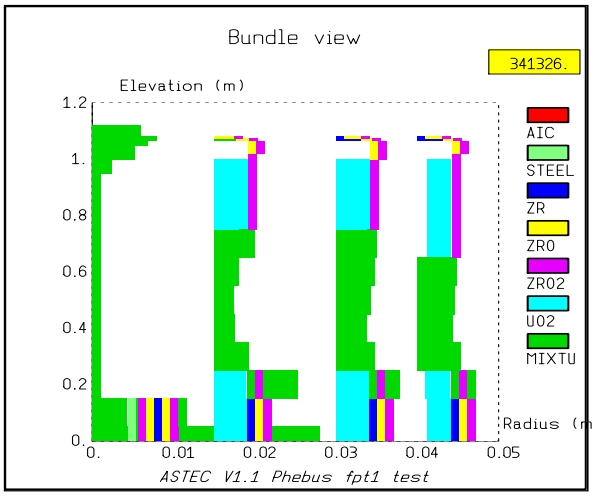

Figure 4-32: ASTEC v1.1, FPT1, Ref. Mesh 17, Bundle view

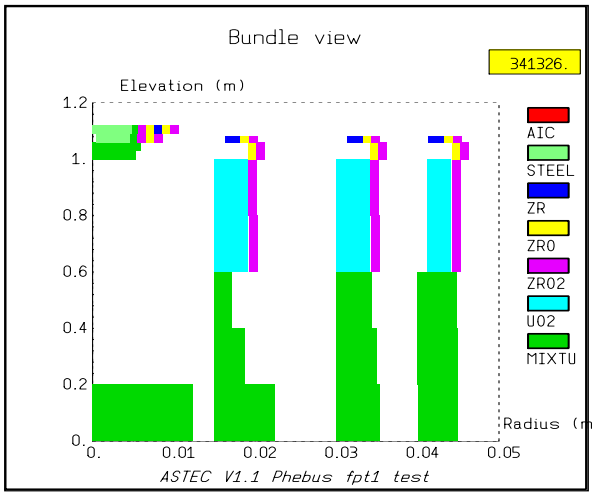

Figure 4-33: ASTEC v1.1, FPT1, Mesh 10, Bundle view

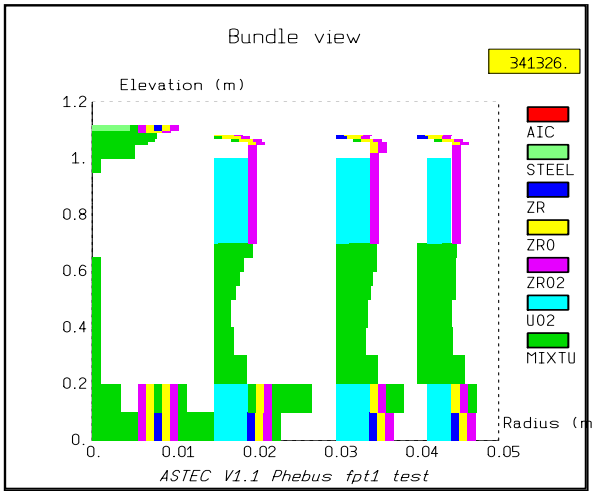

Figure 4-34: ASTEC v1.1, FPT1, Mesh 28, Bundle view

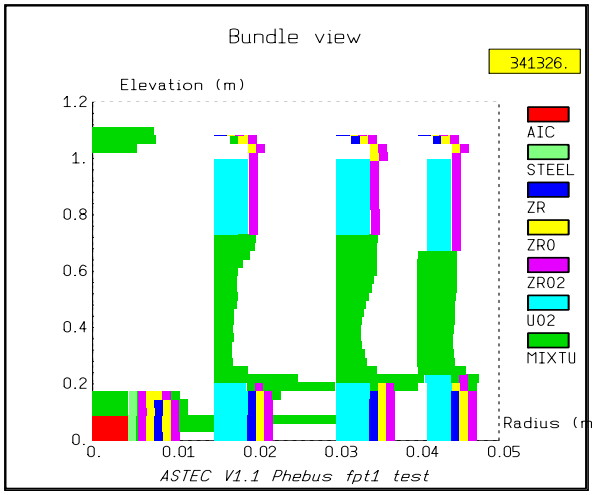

Figure 4-35: ASTEC v1.1, FPT1, Mesh 38, Bundle view

5 Modelling of VVER-1000 for early in-vessel phase simulation

Chapter five describes the modelling applied for the simulation of the early in-vessel phase. The applied codes are ASTEC and ATHLET. General description and main characteristics of a VVER-1000 nuclear power plant (NPP) are included /OVC 1992/, /NEA 1998/, /FOB 2005/, /GEN 2005/, /PAV 2007/, /CAC 2010/.

5.1 General description and main characteristics of a VVER-1000 NPP

The VVER-1000 reactors belong to the second generation nuclear reactor types (Gen. II), as in particular the model VVER-1000/V-320 has been developed during 1975-1985 period, as a new Soviet nuclear standard design covering the international operational and safety design experience.

Other plants of the V-320 type exist in Russia (Balakovo 1-4, Khmelniski-1, South Ukraine 3, Zaporozye 1-6), Czech Republic (Temelin) and Bulgaria (Kozloduy 5-6). The Temelin plant has been upgraded with Western instrumentation, control equipment and fuel but the reactor and containment design and safety systems of relevance to severe accident performance are of V-320 type. In general, the VVER-1000 reactor system resembles the Western pressurized water reactors (PWR).

The VVER-1000/V-320 is a PWR with a thermal electric power of 3000 MW and gross electric output of 1000 MW. The unit is with four circulation loops, each including a main circulation pump and a horizontal steam generator (Appendix F). All elements of the primary side are situated in a steel-lined, cylindrical, concrete containment building.

The main equipment of the primary side includes:

- Reactor with internals. Within the reactor the reactor core with its fuel assemblies is located

- Four main coolant pumps (MCPs), type GCN-195M, providing circulation of the coolant through the primary circuit
- Four steam generators (SGs), type PGV-1000, horizontally aligned, U-tube type. The heat, generated in the reactor core, is transferred through the steam generators to the secondary side
- Pressurizer (including the relief and safety valves, a heater and a spray system), connected to one of the main circulation loops
- Main circulation pipelines.

The secondary side includes:

- Secondary side of the steam generators, the steam lines, the collector, relief and safety valves
- Steam turbine type K-1000-60/ 1500
- Generator
- Condenser
- Deaerator
- Feed water pumps.

In the VVER-1000 primary system the coolant enters into the reactor vessel through four inlet pipelines with nominal diameter DN 850 mm associated with the four primary loops. The flow then passes into the downcomer between the reactor vessel and the inner vessel. The flow enters the lower plenum of the reactor vessel and passes through orifices in the inner vessel and then enters slots in the fuel support structures that lead directly to the fuel assemblies. The flow passes through the open bundles of the core. The pressure drop in the core is approximately 0.18 MPa at rated flow conditions. The fuel assemblies are in the configuration of a hexagon with each containing 312 fuel rods. There are 163 fuel assemblies of which 61 have control rods. The fuel pins are arranged on a triangular pitch. After exiting the reactor core, the coolant flows into the upper plenum, which contains the shielding block, and then out to the hot legs of each of the four primary loops in the system (Appendix F).

The hot leg nozzle for each loop of the reactor is located on the reactor pressure vessel directly above the cold leg nozzle for each corresponding primary loop. The distance between the centers of the hot and cold leg is 1800 mm. The hot leg pipeline runs directly to the nearest steam generator header and has only one elbow of 90 degrees. This configuration provides the shortest path to the steam generator and reduction of the hydraulic losses at the same time.

The coolant inventory in primary side is regulated by make-up and let down systems. The make-up system delivers water to cold legs of primary loops No 1, 2, 3 and 4. The letdown system (Drain system) is connected to cold legs of primary loops No 2 and 3.

The pressurizer is a vertical cylindrical vessel with electric heaters and sprays. The bottom of the pressurizer is connected to one of the hot legs of the loop by a piping system called surge line

while the top of the pressurizer has sprays with piping connected to a cold leg and the make-up system. This configuration for the spray injection inherently allows the high pressure in the cold leg to inject water into the pressurizer, but other systems are available to inject water to condense steam and to reduce the pressure in the system.

The pressurizer is the only location within the primary side of a pressurized water reactor that has a steam/liquid interface during normal operation. The interface reduces the risk from water hammer and provides a compressible steam (gas) space, which is used to set and regulate the pressure of the primary system. The function of the pressurizer is crucial for the regulation of the primary pressure.

The pressurizer system consists of the following components:

- Pressurizer
- Barbotage tank with a breaking membrane to the containment volume
- Spray system with spray valves
- Safety relief valves (SEMPELL type):
    - Control valve: opening pressure 18.11 MPa/closing pressure 16.67 MPa
    - First group of safety valves: opening pressure 18.60 MPa/closing pressure 17.07 MPa
    - Second group of safety valves: opening pressure 18.60 MPa/closing pressure 17.07 MPa
- Electromagnetic relief valve, which actuates and closes the regulating relief valve
- Electromagnetic relief valve, which actuates all SEMPELL type valves at specified setpoints.

The pressurizer logic is the following: the pressurizer controls the pressure in the primary system by several means. If the pressure decreases, the heaters are switched on. This increases the steam content, which increases the pressure in the system. If the pressure is too high, the spray system is initiated into the steam volume, which causes a decrease in the pressure.

For the normal operation of the main coolant pumps the following supporting systems are required:

- Oil lubrication system
- Intermediate circuit water system
- Sealing water system
- Service water system
- Independent cooling circuit.

In case of loss of service water or intermediate circuit water the operation of the main coolant pumps is available up to 180 s. In case of loss of sealing water – the operation of the main

coolant pumps is available up to 7200 s. In case of primary saturation (loosing of subcooling margin) or containment overpressure protection signals, 15 s after the closure of the isolation valves the main coolant pumps are stopped by self-protection on low oil pressure. The pump coast down time in case of loss of power supply is 55 s for 1 out of 4 main coolant pumps and 210 s for 4 out of 4 main coolant pumps.

Though VVER-1000 reactor types are in principal quite similar to the Western European reactor types, the behaviour of horizontal steam generators is very different in comparison to Western types, which have vertical steam generators. The steam generators play a very important role for safety and reliability of VVER nuclear power plants. The transient response of horizontal steam generators can be very different than that of Western type vertical steam generators due to the higher water mass and the larger water surface (water/steam interface) in horizontal steam generators. This higher water mass can affect the reactor transient response particularly during secondary side occurrences and in a station blackout scenario (SBO). The steam generators include horizontal U-shaped heat exchanger tubes and provide natural separation on the secondary side without the use of coarse separators. The lower part of the steam generator contains cylindrical primary collectors with 11000 horizontal U-tubes. There are moisture separators in the upper part. In the horizontal steam generator there is a relatively large secondary water volume of about 66 m^3.

The steam generators are fed by two different feedwater systems. Each feedwater system consists of turbine-driven pumps and piping connecting the feedwater line at four different locations to each steam generator.

The feedwater system supplies water from the condensate storage tank back into the steam generators through the high pressure heaters (or bypassing them), which controls the steam generator water level during plant operation. The system consists of:

- Two turbine driven feedwater pumps
- Two auxiliary electrically driven feedwater pumps
- Ten control valves.

The steam produced in the steam generators is transported to the turbine by the main steam lines. It is also used for in- house supply of steam to the turbo-pumps. The main steam lines system includes the following components:

- 8 steam generator safety valves
- 4 steam dump to condenser valves BRU-K
- 4 steam dump to atmosphere valves BRU-A
- 4 fast actuation isolation valves BZOK
- 4 check valves CV
- 4 main steam isolation valves.

Depending on the state of the plant, the safe operation is ensured by the reactor control and protection systems and by the activation or interaction of the operational and safety systems. These systems respond to the changes in the state of the nuclear power plant and activate certain operations that assure that the plant remains in a stable and safe condition.

Besides the retention of radioactivity and the control of reactivity the cooling of the reactor core is an important protection goal in all transients and accidents. In LOCA the emergency core cooling system (ECCS), as a part of the safety systems will be activated to inject water into the reactor and the primary loops and to ensure that the reactor core is covered with water. Two types of safety systems are used: passive and active ECCS.

Active system: The active systems are those that need a power supply to operate, e.g. motor driven pumps. These systems are automatically activated when the set-points are reached and without any operator intervention. Three active systems (each of them consists of three trains) are used to inject water in the primary circuit depending on the pressure of the primary system:

- High pressure injection system (HPIS): capable to inject concentrated boric acid solution if the primary pressure is in the interval 0.1 to 17.8 MPa
- Medium pressure injection system (MPIS): starts to inject water at primary pressure below 11 MPa
- Low pressure injection system (LPIS): starts to inject water at primary pressure below 2.16 MPa.

Passive system: Beside the active safety systems in the plant, there are also several systems that respond in a passive manner. These systems respond without operator action. The passive systems utilize the basic laws of the physics to function without electric power supply, e.g. hydro-accumulators as a part of the ECCS.

The nuclear power plant has four hydro-accumulators, which are located in different parts. They are located at diagonally opposite positions near the inner surface of the containment wall. Within each part, they are at different levels. The accumulators located at higher elevation discharge into the lower elevation nozzles; they are injecting water into the downcomer of the reactor vessel. The lower elevation accumulators discharge water into the higher level nozzles, connected to the upper plenum of the reactor pressure vessel (RPV), (Appendix F). The hydro-accumulators start automatically to inject into the primary circuit if the primary pressure drops below 5.8 MPa.

The VVER-1000 reactor core is characterized by hexagonal geometry: the fuel assemblies have hexagonal form and the control rods/assemblies are arranged also on a basis of hexagonal symmetry. The fuel rods are arranged in a triangular lattice. The fresh UO_2 pellets have central holes, which can affect the fission gas release mechanism. The hole disappears at higher burn-ups.

The cladding material is a Zr+1%Nb alloy. It has good operational experience in the low temperature range and it is more resistant to oxidation in comparison to the Zircaloy (ZrSn) applied in the Western PWRs. The cladding thermo-mechanical phenomena (as plastic

deformation) take place at 800 °C - 1000 °C. The cladding is capable to take slightly more hydrogen at high temperatures in comparison to the Western PWRs claddings, and the material becomes brittle at lower oxidation rates.

Operation of the equipment during severe accidents (SA)

The availability and operation of essential safety systems and components like pumps or valves depend on the availability of electric power supply. The different systems and components are assigned to different categories of electrical supply, mainly category I and II. The VVER-1000 has 3 diesel generator (DG) stations with a nominal active capacity of 6.2 MW plus 1 additional DG station. At loss of offsite power accidents the DGs provide the power supply to all systems of category II. Operability of the available equipment during severe accident sequences is of primary importance for prevention or mitigation of the accident. Depending on the applied accident management strategy, availability of different equipment is issued (Appendix F). The following severe accident management strategies have been implemented in the VVER-1000 reactor type:

- Primary side depressurization

Using of the pressurizer safety valves is the most appropriate and effective way to depressurize the primary circuit. The pressurizer safety valves are available due to first category supply. In all the initiating events: design basis accidents (DBAs), beyond design basis accidents (BDBAs) and severe accidents, including SBO, the pressurizer relief and safety valves are available. The efficiency of the gas removal system is as that of the pressurizer safety valve. The valves of the gas removal system are second category electric power supply. In severe accidents with SBO it will be impossible to use these valves for primary circuit depressurization.

- Depressurization on the secondary circuit

The secondary side has a large amount of water and using steam dump to atmosphere valves (the BRU-A valves) the operators have extra time for avoiding heating-up of the primary circuit. Depressurization of the secondary side can be realized either by the steam dump to condenser, steam dump to the atmosphere, house load steam system, or by the steam generator safety valves. Application of the strategy is possible when coolant is available in the steam generators. When electrical supply is available and when the normal operation systems are available, the strategy is realized with the steam dump to condenser and the steam dump to the atmosphere valves. Application of the strategy is possible when the steam generators are not isolated from the main steam header through the fast acting isolation valve.

At loss-of-offsite power only electrical supplies of categories I and II are available. When entering severe accident management guidelines (SAMG) this strategy is possible to be implemented by the steam dump to atmosphere and the steam generator safety valves only. At total loss of electrical supply for the secondary side depressurization procedure the operator must use the steam dump to the atmosphere or the steam generator safety valves. In SBO scenario, after loss of battery supply (after two or more hours), the operator should use manual manner to open the steam dump to the atmosphere valves or the steam generator safety valves at place.

As condition of use of the procedure the operator must ensure feeding of the steam generators together with steam generators' depressurization procedure to avoid the risk of tube creep rupture or mechanical damage of the U-tubes and the steam generator header due to thermal shock, if cold water is injected into a dry steam generator. Steam generator tube rupture or crack of the steam generator header would lead to a leakage from primary to secondary side with subsequent release of radioactivity to the environment. In case of SBO, applying secondary side depressurization at the earliest possible time will start passive feeding as early as possible with the relatively hot water stored in the feedwater system and the steam generators' depletion can be delayed. In that way the risk for damages to the steam generator U-tubes or the steam generator header due to high temperature differences can be reduced. Under the conditions of a severe accident the steam dump to the atmosphere valves and the steam generator safety valves can be opened in place by the operator, in all beyond the design basis modes of operation, even at SBO. Disadvantage is when there is no power supply, it is impossible to execute remote control of the valves.

- Injection into primary circuit

The strategy is realized by the usage of the design specific features: high pressure injection system, medium pressure injection system, low pressure injection system and the passive safety system - the hydro-accumulators. Preceding the application of this strategy is the depressurization of the primary side. Availability of the diesel generator station is necessary for the active ECCS.

- Injection into secondary circuit

The entering criterion in this case is the level in the steam generator. In case of SBO the turbine driven feedwater pump, the auxiliary feedwater pumps, the emergency feedwater pumps (EFWP) and the steam generator blowdown system are not available. Before passive feeding can be organized, secondary side depressurization has to be performed (see above). Passive feed of the steam generator from the deaerators on the feed part can not be provided in case of feed water collector rupture.

If the initial event has not brought to a loss of the turbine driven feedwater pump and there is enough steam receipt in the on-site service steam head, the make up of the steam generator can be realized by one turbine driven feedwater pump, while the second one will be put to recirculation mode of operation by the operator. In case of an off-site electrical power supply loss it is possible to supply auxiliary feedwater pump by an all-unit diesel-generator station. When the turbine driven pump and the auxiliary feedwater pump are unavailable for make up of the steam generator the operators can use the emergency feedwater system to the steam generator. The pumps are with category II electric power supply and they are available at a "Loss of house power supply" mode of operation. In case that it is impossible to pass water up to the damaged steam generator, this steam generator is left to be dried.

The application of the strategies "Secondary bleed and feed" and "Primary bleed and feed" in a SBO accident is discussed in Chapter 6, Parts 6.2.4 – 6.2.8.

- Containment depressurization

When entering SAMG there are two possibilities: the spray system starts under interlock or the operator starts the spray system if there is a failure in the automatic actions. In loss of offsite power only electrical supplies of categories I and II are available. The spray system can operate by category II power supply (diesel generator). In case of SBO accident, the spray system is not available. In this case the only filtered venting system will operate and protect the containment against overpressurization. The catalytic recombiners are passive system too, and will operate in SBO conditions.

5.2 ASTEC and ATHLET models for the reference VVER-1000 NPP

Two thermal-hydraulic codes have been used for the early in-vessel phase simulations presented in Chapter 6. The main goal for applying two codes is validation of the ASTEC code with help of ATHLET for the early in-vessel phase. In this Chapter (Part 5.2) a common description of both ASTEC and ATHLET models is given. Specific aspects related to the physical models of the codes, as well as difficulties met by the modelling are discussed in Chapter 5, Parts 5.3 – 5.5.

The reactor coolant system models for both ASTEC and ATHLET include all the major components of the primary and the secondary side, as well as the necessary safety injection systems. The models describe the main components of a VVER-1000 - the reactor pressure vessel, the reactor core, upper plenum, lower plenum and downcomer, the main coolant pipes, main coolant pumps, the pressurizer, steam generators, feed water systems and steam lines, turbine, pressure regulation and safety valves for the primary and secondary side, respectively. Besides the coolant circuits all necessary reactor protection systems, as reactor power control, reactor SCRAM and turbine trip, as well as activation of safety systems, are also taken into consideration.

For both codes a multi channel approach (parallel 1-D fluid channels) has been used to model the reactor core. In ASTEC the core is discretized in axial and in radial direction - ten positions in axial direction and five rings in radial direction, including additionally the baffle and the barrel. An additional ring has been added to take into account the downcomer and the reactor vessel. For ATHLET the core is subdivided into two thermal-hydraulic channels, each including two fuel rod models with different axial profile and linear rod power. In axial direction the core channels are discretized in ten nodes.

The ASTEC v1.3.0 input file developed for the SBO sequence (Chapter 6, Part 6.2) includes the modules CESAR, DIVA and CPA, and it has been modified for a proper modelling of steam generator safety valves - the BRU-A valves, which function is a controlled discharge of steam from the steam generators to the atmosphere. The valve starts operating at abnormal increase in steam pressure and after a sudden drop of turbine load. They must maintain the preset steam pressure in the main steam header. The safety valves of the steam generators have been also modelled.

The ATHLET input deck was elaborated in co-operation with GRS, the Kurchatov-Institute and OKB Gidropress. Requirements for a realistic simulation of the sophisticated performance of safety and regulation valves (BRU-A and pressurizer safety valves) in VVER-1000 plants, which were not considered in ATHLET, led to some source code modifications. This specially developed version has consequently been used for this analysis, too.

In the ATHLET model for the horizontal type steam generators no main flow direction exists as it is the case for vertically oriented steam generators. The steam generators play an important role for the safety and reliability of the nuclear power plants. The heat, generated in the reactor core, is transferred through the steam generators to the secondary side. In a SBO scenario the decreasing water level on the steam generators' secondary side leads to reduction of the steam generator power (primary to secondary heat transfer) and as a consequence to increase of the primary pressure. After reaching the set-point of the pressurizer relief valve the mass loss on the primary side could lead to a core heat-up. For preparing countermeasures the time for steam generators' depletion is an important factor. Because of that, special attention has been paid to the modelling of the horizontal steam generators of the VVER-1000 with respect to the mass inventory and the spatial orientation with the specificities in the heat transfer characteristic (Chapter 5, Part 5.4).

For ATHLET a thorough investigation was performed to account the specific conditions in VVER-1000 steam generators. Finally, a so called 2-path nodalization for the steam generator's secondary side has been realised for the calculation at hand (Figure 5-1). This approach allows for circulation of the water inventory. Within the channel (S1-OP) where the tube bundle is located the water is heated, thereby establishing an upward flow direction. Consequently a downward flow direction is induced for the other channel (S1-PO) with the relatively colder water inventory. The main feed water injection is connected to the non-heated part and the heat transfer from the primary to the secondary side is modelled within the heated part of the drum. On the primary side the horizontal oriented U-tubes have been subdivided into three parallel bundles with five nodes in horizontal direction (Figure 5-4) and the flooding based drift model with a special option for horizontal tubes has been applied. Like the tube bundles, the heated section of the secondary side has been subdivided into three vertical parts, so that a more realistic behaviour can be simulated for scenarios, where the water inventory in the steam generators is decreasing.

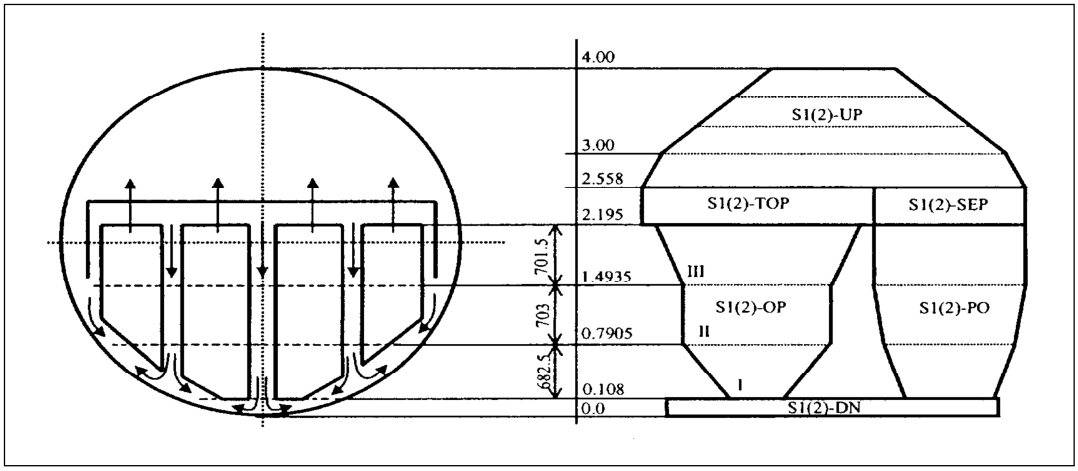

Figure 5-1: ATHLET model of 2-channel approach for secondary side of SG with horizontal design /BEL 1995/

In ASTEC the steam generator is modelled as a VOLUME for the primary and secondary side, containing cold and hot collectors and the U-tubes. In axial direction the tubes are grouped into three parts (described as VOLUMEs), and horizontally the tubes are divided into four CELLs.

The ASTEC and ATHLET nodalization schemes are depicted in Figures 5-3 and 5-4, respectively. The ASTEC scheme represents the reactor pressure vessel, two of the four main circulation loops, the pressurizer and the hydro-accumulators, which are connected to the upper plenum and the downcomer, respectively. For ATHLET a similar schematic representation of the reactor pressure vessel, pressurizer, main circulation loops No 1 and No 4 and the hydro-accumulators is given. A more detailed nodalization scheme including all four loops is given in Appendix A.

The decay power modelled in the input of ASTEC and ATHLET is graphically presented in Figure 5-2.

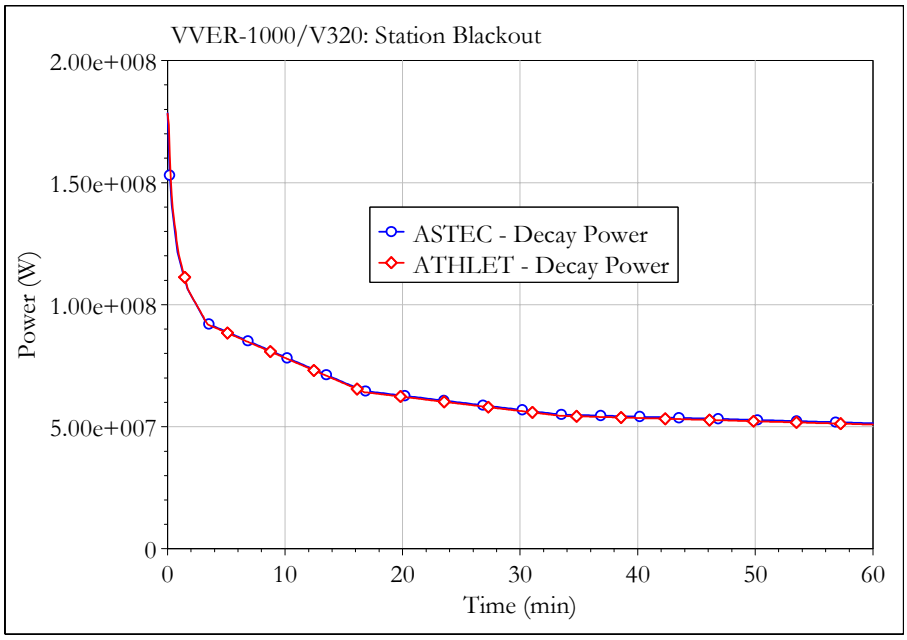

Figure 5-2: Decay power as a function of time

The applied nodalization schemes are shown in the following figures.

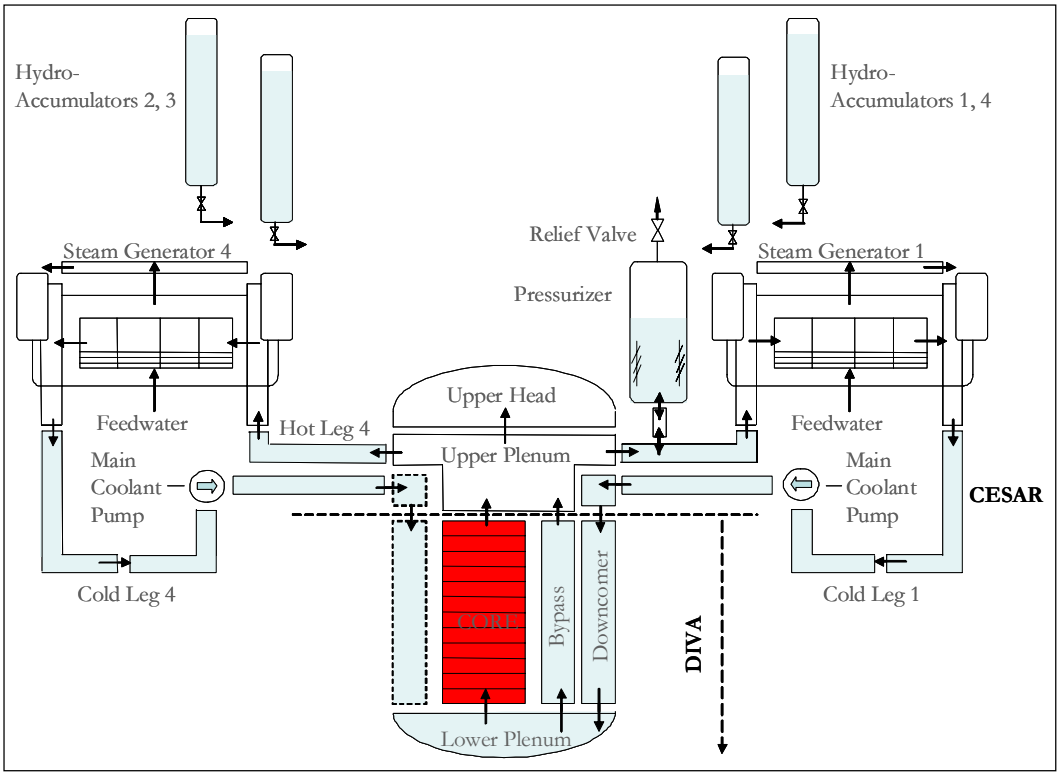

Figure 5-3: VVER-1000, ASTEC simplified nodalization scheme

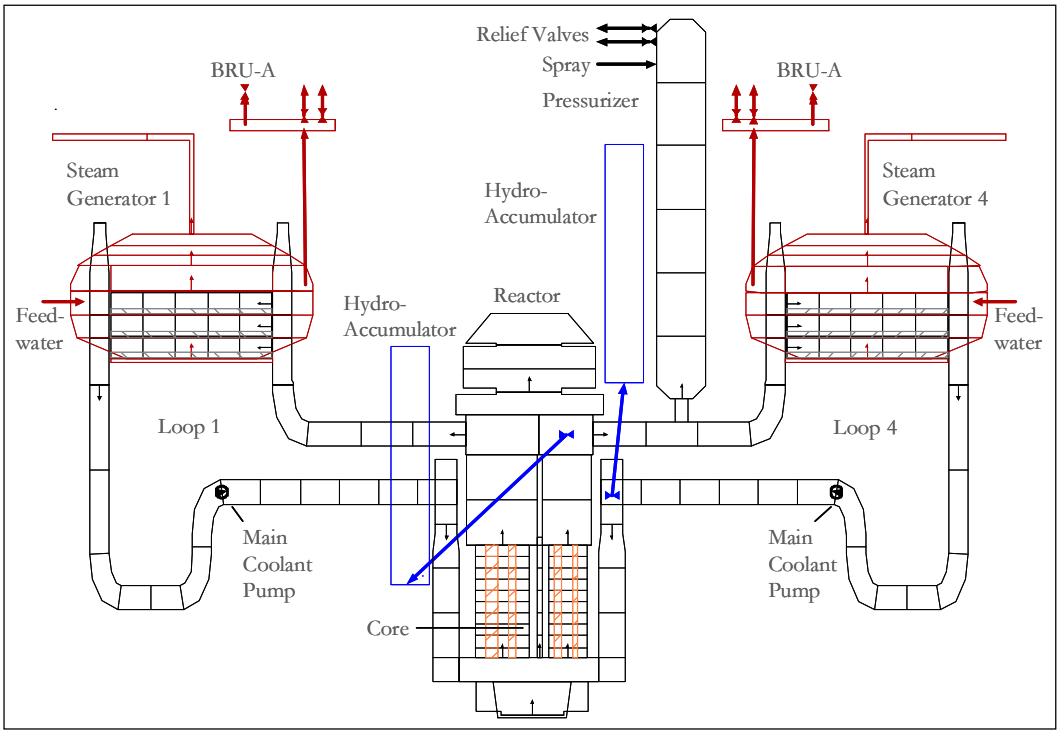

Figure 5-4: VVER-1000, ATHLET simplified nodalization scheme

5.3 ASTEC model specifics

The ASTEC modules used for the modelling, in a coupled mode, of the in-vessel phase, are CESAR, DIVA and CPA.

The input model includes the description of the following nuclear plant sub-components:

- Reactor core
- Reactor pressure vessel
- Primary loops
- Pressurizer
- Hydro-accumulators
- Steam generator secondary side
- Containment geometry.

5.3.1 Core model

The reactor core in ASTEC is specified by the DIVA module, described with the VESSEL_D structure (Appendix B). The reactor core has been divided into five radial rings. One more ring has been added to model the downcomer. The axial discretization consists of ten identical meshes. The fuel, the fuel cladding, the control rods, the control rod cladding, the guide tubes, the barrel, the baffle and the vessel are defined in structures (STRU MACR) with a type TYPG CYLINDER (Appendix B). The height of the respective elements, as well as the internal and external radii and the initial element temperature are specified.

The following elements of the reactor core and in-vessel structures are modelled:

- Fuel rods consisting of the fuel column and cladding. The total number of fuel rods is 50856
- Absorber rods of boron carbide. Modelled are the absorber rods themselves, their claddings and guide tubes. The total number of such rods is 1098
- Baffle
- Barrel
- Part of reactor vessel
- Part of downcomer
- Lower plenum
- Bottom head.

All the fuel rods located in five internal radial zones are modelled with one representative rod. The representative fuel rod is described in the input deck by two macro-components: fuel

column and cladding. Respectively, every representative absorber rod is modelled by three macro-components: guide tube, cladding and absorber of boron carbide.

Additional structure (STRU LOWE) is modelling the reactor pressure vessel lower plenum. The bottom of the reactor vessel is modelled by a hemisphere connected with the cylindrical part of the reactor vessel. The bottom is represented by one macro-component and is split into 15 cells in the spherical part, 2 cells in the cylindrical part and 5 cells in radial direction. Coolant in the lower plenum is modelled by two macro-components – fluid and gas. Separately in the special thermal-hydraulic data the pressure losses in the reactor core are specified.

The components of the modelled system consist of the following materials:

- UO_2 – fuel
- Zr+1%Nb – fuel rod cladding and guide tube material
- B_4C – absorber material
- Stainless steel – material of the claddings of the absorber rods, the baffle, the barrel, the reactor vessel, the lower plenum.

The physical interaction between the fuel, cladding, control rods and guide tubes are described in STRU COND (Appendix B). The creep of the cladding is described under STRU CREE. The stainless steel oxidation by vapour (FEOX), the dissolution of UO_2 by molten Zr (UZRL), oxidation model used for cladding, shroud or debris oxidation by steam (ZROX), the liquefaction of B_4C by solid stainless steel (BCSS), the oxidation of B_4C (BCOX) are implemented.

The usual applied temperature criterion in the severe accidents codes for liquefaction and relocation of core materials is 2800 K, corresponding to liquefaction of the ceramic phase mixture at the eutectic point in the UO_2-ZrO_2 phase diagram. "*Nevertheless, poor representations of the observed relocation of core debris in the FPT0 test are produced by the codes when this default criterion is used. Much better representations of relocation are obtained in codes predictions by artificially reducing the "melting point" of fuel to 2500-2600 K to simulate the effects of non-equilibrium material interactions in the Zr-U-O system."* /PHE 2007/. Such artificial temperature reduction is needed to obtain an adequate simulation of the thermal evolution in the core.

The core input parameters have been defined as follows:

- Fuel rod cladding melts at 2400 K
- Fuel relocation occurs at 2550 K
- Relocation of control rod cladding occurs at 1730 K.

The CAND structure is implemented to account the axial relocation of molten U-O-Zr mixture, the radial relocation is taken into account due to the decanting model. The radiation in the core is implemented. The material properties are specified in STRU MATE.

Figure 5-5 gives the fission and decay power, the fission power is approximately one order of magnitude larger at the beginning of the transient, but negligible after a few hundreds of seconds.

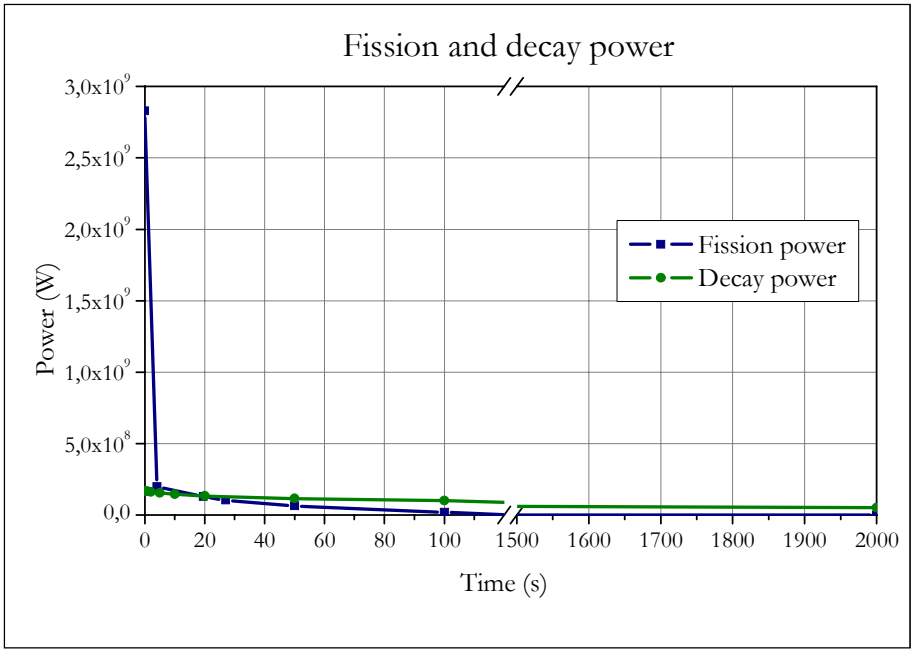

Figure 5-5: Fission power and decay power as function of time

5.3.2 Primary side

The description of the primary circuit (STRU PRIMARY) is treated by the CESAR module. The reactor downcomer, the upper plenum (subdivided into two volumes), the hot legs, the steam generator primary side (the tubes), the cold legs, the hydro-accumulators and the pressurizer are specified as volumes (STRU VOLUME).

Every circulation loop is split into the following volumes (Figure 5-3): hot leg, hot header of the steam generator, steam generator tubing is modelled by 3 volumes in vertical direction, cold header of the steam generator, downward oriented part of the cold leg, raising section of the cold leg including main coolant pump, horizontal section of the pipeline from the main coolant pump to the reactor inlet nozzle. Every volume is defined with its geometry data, the elevation at which the volume is situated, the hydraulic diameter and the heat exchange surface area. The thermal data describing the volume are pressure, temperature, enthalpy and void fraction.

The volumes are interconnected by junctions (STRU JUNCTION). The primary to secondary interface is defined in STRU WALL (Appendix B). The walls are specified in every steam generator cell. They represent the total surface of the sections of the tubing located in this cell. The heat exchange between the primary and secondary circuits is modelled by STRU CONNECTI between the tubing walls facing the primary circuit and the tubing walls facing the secondary circuit.

As mentioned above, the steam generator's U-tubes are modelled by three vertically separated parts (tube bundles). In ASTEC a tube bundle is defined as a VOLUME. For each bundle the total volume, hydraulic diameter and the elevation of the center line have to be specified. The total heat transfer area of all 11000 tubes is 6115 m^2. The secondary side is modelled as a single

volume. The following characteristic data have been used for the tube bundles (Chapter 5, Part 5.4, Figure 5-6):

	Elevation of bundle center line	No. of tubes	Heat transfer area
Bundle 1:	9.6185 m (above zero level)	2418	1344.2 m^2
Bundle 2:	10.293 m (above zero level)	4060	2257.0 m^2
Bundle 3:	10.996 m (above zero level)	4522	2513.8 m^2

The NPP components as pumps and systems are defined in a separate structure (STRU SYSTEMS). The characteristics of the main coolant pumps are specified in the STRU SYSTEMS. The pump connection to the section of the primary pipeline is done with the help of STRU CONNECTI.

The pressurizer and the pipeline connecting it with the primary circuit are modelled by PRZ and SRG_LINE volumes. The regulations are defined in STRU REGU.

5.3.3 Secondary side

The secondary side is defined similar to the primary side by volumes, walls and junctions. The secondary circuit is modelled with the following volumes: four steam generators from the side of the secondary circuit; four corresponding steam headers; main steam header. The characteristics of the feedwater pump are specified in the STRU SYSTEMS, and feedwater supply to steam generators from the side of the secondary circuit is introduced with the help of STRU CONNECTI. The heat exchange between the primary and secondary circuits (as was mentioned above) is modelled with the help of STRU CONNECTI between the tubing walls facing the primary circuit and the tubing walls facing the secondary circuit.

5.3.4 Containment

The containment is modelled with five volumes (three zones, where large components are located, a main containment dome and a cavity). The environment is modelled as a very large volume.

5.4 ATHLET model specifics

The thermo-fluiddynamic (TFD) module is the basic module of ATHLET /ATH 2001/, /ATH 2003/. In a first step the simulated system is discretized in space. It is partitioned into a net of adjacent spatial entities, called control volumes (CV), interconnected by junctions. The control domain of the junctions is defined between the centers of the left and right CVs. In a second step the partial differential equations are spatially integrated using the CV as integration domain for those model equations based on the mass and energy conservation law and the junction as

integration domain for those model equations based on the momentum conservation law. In the ATHLET case this system of ordinary differential equations is of first order and non-linear.

The thermo-hydraulic model describes the main components of the VVER-1000 (Figure 5-4) - the RPV, the reactor core (multi-channel modelling), upper plenum and lower plenum, the main coolant pipes, main coolant pumps, the pressurizer, steam generators, feed water and steam lines, pressure regulation and safety valves for the primary and secondary side respectively. All the four primary circulation loops are modelled, as the pressurizer is connected to the loop number four (Appendix A).

The nuclear heat generation is simulated in ATHLET within the module NEUKIN. The power generation in the reactor core consists of two parts: the prompt power from fission (kinetic energy of fission fragments) and the decay heat from the short- and long-lived fission products. The time dependent behaviour of the prompt power generation is calculated either from a point-kinetics model or from a one-dimensional neutron kinetics model. For the simulations presented in Chapter 6, the point-kinetics model has been applied.

The simulation of the heat conduction in structures, fuel rods, and electrical heaters is performed within the basic module HECU. It permits assigning of heat conduction objects (HCOs) to all thermal-fluiddynamic objects of a given network. The one-dimensional heat conductor module HECU provides the calculation of the temperature profile and the energy transport in solid materials, as well as the heat transfer between structures and fluid.

The regulation and control of the operational and safety systems is realized within the GCSM block-oriented simulation language for the description of balance-of-plant systems in ATHLET. In the GCSM module the signals for the reactor control, reactor protection and activation of the safety systems have been modelled. For the SBO simulations, presented in Chapter 6, the following types of signals have been taken into account:

- Nominal values and lower/upper limits for primary/secondary pressures and temperatures as well as for the RPV, the pressurizer and steam generator levels
- Signals for core outlet temperature and unavailability of power supply to activate the PSD and SSD procedures, as well as modified regulation and control of pressurizer and steam generator relief and safety valves for the procedures
- Set points for activation of SCRAM, turbine trip, main coolant pumps' coastdown and ECCS.

As already mentioned in Chapter 5, Part 5.2, the geometric and thermal-hydraulic characteristics of the horizontal oriented steam generators play an important role during a SBO accident. The continuous mass release through the steam generators' relief valves (BRU-A) after the loss of the main heat sink leads to a decrease of the steam generator level. To predict the time for steam generators' depletion and the following primary side pressure increase and core heat-up as accurate as possible, special attention has been paid to the modelling of the steam generators and their heat transfer characteristic, e.g. the effective heat transfer area of the steam generator U-tubes depending on the water level on the steam generators' secondary side (part of the U-tubes

covered by water). With decreasing steam generator level the effective heat transfer area is more and more reduced and as a result the primary to secondary heat transfer (steam generator power) decreases too. After depletion of the steam generators the primary to secondary heat transfer breaks down, leading to the pressure increase on the primary side.

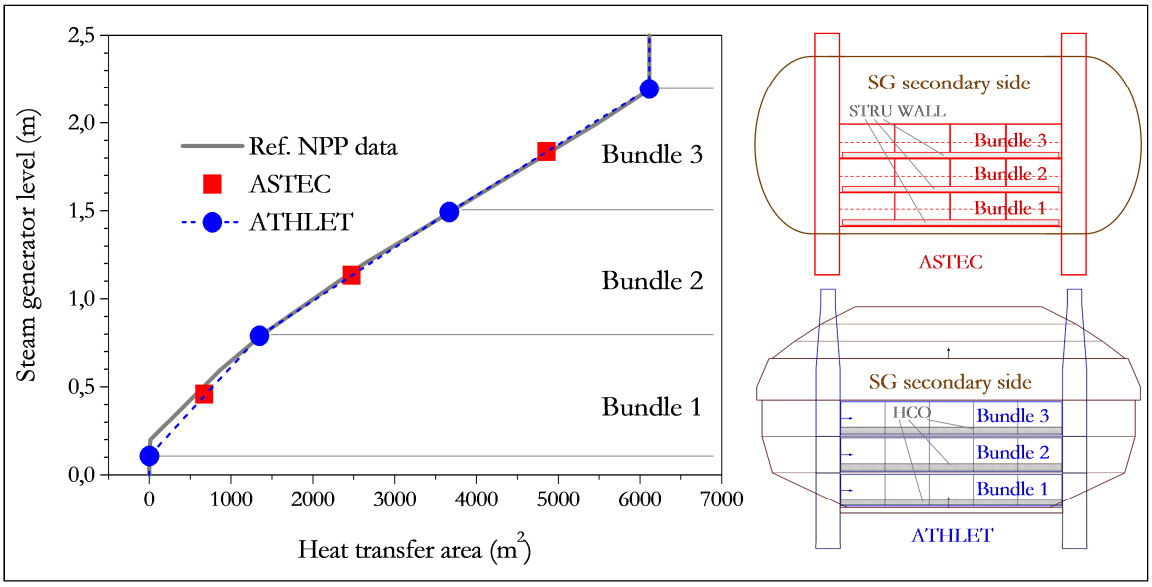

Figure 5-6: Heat transfer characteristic of the VVER1000-type steam generator (NPP data vs. ASTEC- and ATHLET-model) and simplified nodalization schemes

In Figure 5-6 the heat transfer characteristic for a reference VVER-1000 steam generator is compared to the steam generator model in the ATHLET and ASTEC input decks (Chapter 5, Part 5.3.2).

In the ATHLET model the total number of 11000 U-tubes for one steam generator has been sub-divided into three tube bundles, each bundle models a U-tube with an average length multiplied by a factor for parallel thermo-fluiddynamic objects (TFO). With the help of the corresponding heat conduction objects (HCO) the heat transfer from primary to secondary side is modelled, thereby connecting the primary side of each tube bundle to one of the three vertical oriented parts of the steam generators' secondary side (Figure 5-6). The following data have been used for the three tube bundles:

	Elevation on sec. side	**No. of tubes**	**Heat transfer area**
Bundle 1:	0.108 – 0.790 m	2424	1347.6 m^2
Bundle 2:	0.790 – 1.493 m	4172	2319.4 m^2
Bundle 3:	1.493 – 2.195 m	4404	2448.3 m^2

The steam generator U-tubes have an outer diameter of 16 mm and an average length of 11.06 m. Total heat transfer area for all 11000 U-tubes is 6115.3 m^2.

Additional modelling for simulation of the primary side depressurization (PSD) and secondary side depressurization (SSD) procedures for the SBO sequence is included (Chapter 6, Part 6.2.4). Both procedures utilize the bleed and feed strategy, feed of the primary and secondary side, respectively, is provided by use of passive systems. The PSD procedure is performed by fully opening of the PRZ relief and safety valves. After sufficient primary pressure reduction the passive ECCS (hydro-accumulators) start to inject water into the RPV. In the ATHLET input deck the hydro-accumulators and their connections to the RPV have been modelled (Chapter 5, Part 5.2, Figure 5-4), considering the pressure losses in the connecting pipelines. The input deck has been modified to activate the PSD-procedure by using a temperature criterion (core exit temperature, Chapter 6, Part 6.2.4, 6.2.5 and 6.2.7).

To simulate the passive feeding of the steam generators for the SSD-procedure, the complete feedwater system has been modelled. The system consists of two feedwater tanks, the feedwater lines including the preheaters, the feedwater distribution header and the connections to each of the four steam generators. A check valve in the feedwater connection line prevents a possible backflow from the steam generator towards the feedwater system. The check valve is opening/closing depending on the pressure difference, measured between the downstream and upstream sides of the valve position. For the pipelines the pressure losses, important for an accurate modelling of the passive feeding of the steam generators, have been considered. In Figure 5-7 the nodalization scheme for the feedwater system and the connection to SG1 is depicted. The ATHLET input deck has been modified to activate the SSD procedure by full opening of two BRU-A valves 30 minutes after the initiating event (Chapter 6, Part 6.2.4). The passive feeding of the steam generators' secondary side starts if the secondary pressure has been reduced below the pressure in the feedwater system. First the relatively hot water, stored in the feedwater pipelines behind the preheaters, starts to feed the steam generators. After sufficient pressure reduction the colder water from these tanks provides an additional quantity of coolant to feed the steam generators' secondary side. In this way the continuous decrease of the steam generator levels during a SBO accident can be temporarily stopped and the depletion can be significantly delayed, thus partially re-establishing the primary to secondary heat transfer via the steam generators.

To avoid a possible damage of the steam generators, the possibilities for secondary depressurization and cool-down procedures are restricted if the steam generator levels drop below a certain limit /PAV 2007/. For that the operators have to follow the plant specific instructions. As already mentioned in Chapter 5, Part 5.1, starting SSD as early as possible would reduce the risk for tube rupture or crack of the steam generator header. For the generic investigations in Chapter 6, Part 6.2.6, additional feeding with cold water (e.g. with help of mobile pumps), what could cause damage due to thermal shock, as well as plant specific measures or restrictions for secondary side oriented procedures after a significant decrease of the steam generator levels have not been taken into account.

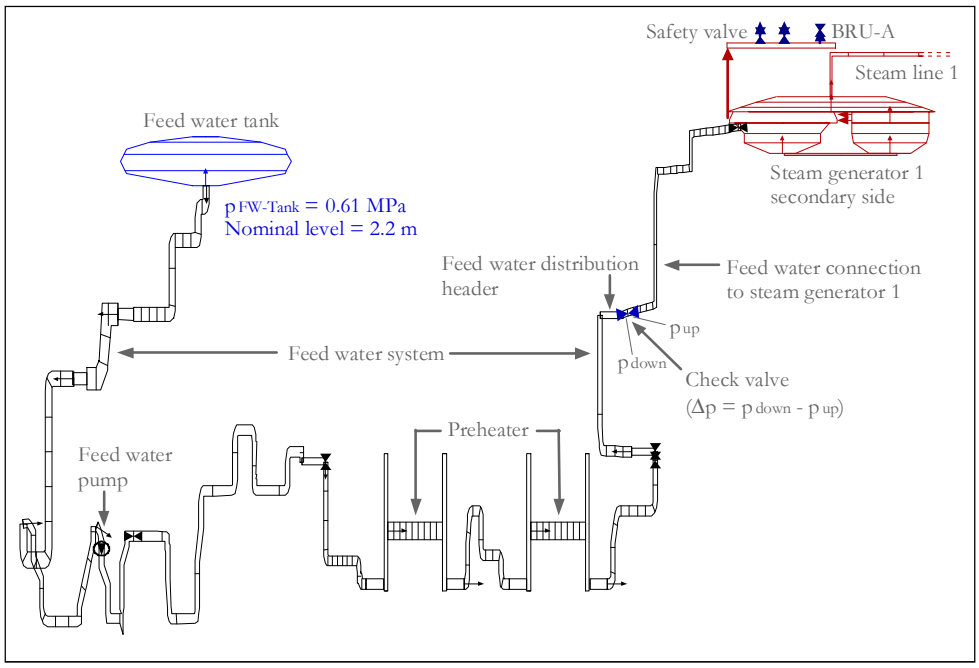

Figure 5-7: VVER-1000, ATHLET nodalization for feedwater system, connection to SG 1

The characteristic data presented in Table 5-1 have been applied to the ATHLET feedwater model:

Table 5-1: Main characteristics for the secondary side feedwater system

Feedwater tank	
Pressure, [MPa]	0.61
Total volume (one FW tank, water/steam), [m^3]	210
Water mass (one FW tank), [t]	131
Temperature, [°C]	159
Nominal level, [m]	2.2
Feedwater pipelines	
Total water mass stored between FW tanks and FW distribution header, [t]	218
Water mass stored in the connection line between FW distribution header and steam generator (one SG), [t]	23.5
Temperature (in FW distribution header), normal operation / after SBO, [°C]	225
Steam generator, secondary side	
Water mass during normal operation (one SG), [t]	46.5

5.5 Difficulties met by the modelling

Difficulties are met at the process of unification of the both applied input decks for simulation of a SBO accident.

The SBO sequence without any active safety systems has been applied, as to be easily studied the thermal-hydraulic response of the reactor coolant system, main phenomena arising during the in-vessel phase, i.e. up to beginning of core heat-up process. Such scenario is suitable for checking of the correct modelling of the reactor coolant system heat sinks, heat transfer from primary to secondary side, heat losses from the reactor coolant system surfaces and proper function of the pressurizer and steam generators relief and safety valves.

Despite the very different structure used for the input files of the codes, an in-depth analysis of the input data for specification of the boundary conditions has been performed. The most important data like, e.g. decay heat, water inventory, and heat transfer area have been compared and, if necessary, adjusted. Besides, the codes do not always use identical approaches for modelling of specific phenomena, so an exact match could not be ensured. As an example, the form-loss coefficient for a valve can be defined for valves within ATHLET calculations, whereas it is in general not possible for a valve in ASTEC.

A reference input file, reviewed and approved by the ASTEC maintenance team in IRSN, September 2005, for VVER-1000 plants, has been used as a basis for the ASTEC calculations here performed. General description of the input deck is provided in /FOB 2005/.

The first ASTEC calculations were performed with the standard valve type for the steam generator safety valves (TYPE SGVALVE), i.e. the BRU-A valves, and the respective valve type for the pressurizer safety valve (TYPE PRESSUVA). A comparison of the calculation results obtained with this input data with those results calculated with ATHLET revealed major discrepancies. As for the primary and secondary pressure ASTEC predicted some kind of cycling behaviour for the BRU-A valves, which influenced the whole sequence. A thorough investigation of the real behaviour of the valve suggested, that the ATHLET results seemed to be more realistic, as explained below.

The steam dump to the atmosphere valves (BRU-A): there is one relief valve per steam generator (opening pressure 7.26 MPa, closing pressure 6.28 MPa, flow rate 4x900 t/h). They are emergency power supplied and resistant to external impacts. After failure of the bypass station BRU-K and the auxiliary power reducing station BRU-SN relieve excess steam to the atmosphere and so reducing the pressure. They can be controlled automatically or manually. In the automatic position, the cool down process is controlled by cool down rate. The maximum section of the BRU-A steam dump valves is 0.0225 m^2. At steam generator pressure above 7.26 MPa the BRU-A valve is forced to open until the pressure decreases below 7.26 MPa, afterwards a controller is switched on with a set value of 6.67 MPa. After the full closing of the BRU-A valve with delay 100 s the controller switches over in awaiting mode. When the pressure decreases below 6.27 MPa the BRU-A valve closes fully.

Pressurizer safety valves (SEMPELL): the first group of the pressurizer valves opens at a pressure of 18.11 MPa and closes at a pressure of 16.67 MPa, whilst the second and third group of valves open at a pressure of 18.60 MPa and close at a pressure of 17.07 MPa. The maximum section of the pressurizer valves is 0.007854 m^2. There are three independent parallel valve units, installed on a pipe connected to the pressurizer.

A series of ASTEC calculations have been performed in order to choose the most proper type of valve, available in the ASTEC code, in order to simulate the real plant behaviour during the operation of the designated valve.

Several options for valve simulation in ASTEC could be chosen in STRU SYSTEM/VALVE:

- TYPE SAFETYVA
- TYPE PRESSUVA
- TYPE SGVALVE
- TYPE STANDARD
- TYPE KEVALVE
- TYPE CHECKVAL
- TYPE CPA_OLD.

The only valve type available in ASTEC that could simulate the behaviour of the BRU-A valve more realistically was found to be a valve of type PRESSUVA. According to the CESAR manual /GIO 2001/ this type of valve aims at simulating the pressurizer operated relief valves- as this type of valve will open if the upstream volume pressure exceeds p_{open} and be closed if the pressure becomes below p_{close}. In between, a hysteresis is taken into account. After modification of the ASTEC input data the results showed a similar trend as the ATHLET results.

For the pressurizer safety valves a similar phenomenon could be detected, as the assumed cycling of the pressurizer safety valves could not be realized by defining the valve as of type PRESSUVA. As the behaviour of the pressurizer safety valve is opening when the primary pressure reached a set value for opening, and closing when the pressure limit for valve closing is reached, in accordance to this cycling with opening/closing pressure values, a valve of TYPE SGVALVE will simulate the behaviour of the pressurizer safety valve in more realistic way. A very similar behaviour comparable to the ATHLET results could be achieved. The differences in the behaviour of both types of valves are graphically represented in Figure 5-8.

Besides, it is interesting to note, that independently of the valve type chosen for the calculation, the general trend and the integral mass released through the PRZ valves is almost identical (Figure 5-9). On the other hand, the mass flow rates are quite different and for the SGVALVE they are too high with view to the nominal value.

For the calculations discussed in the next Chapter a type PRESSUVA valve was taken for the BRU-A and a type SGVALVE was taken for the pressurizer valves.

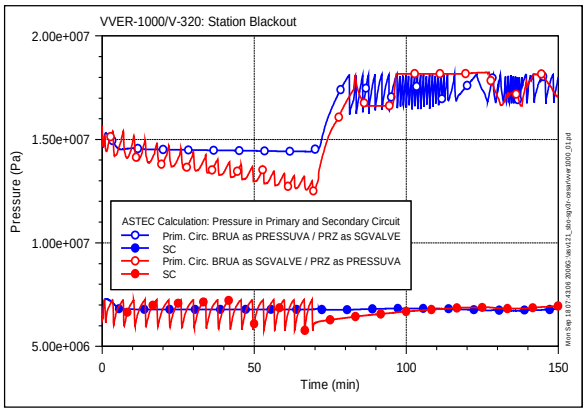

Figure 5-8: Comparison of two ASTEC calculations varying valve types chosen for the steam generator BRU-A valves and the pressurizer safety valves

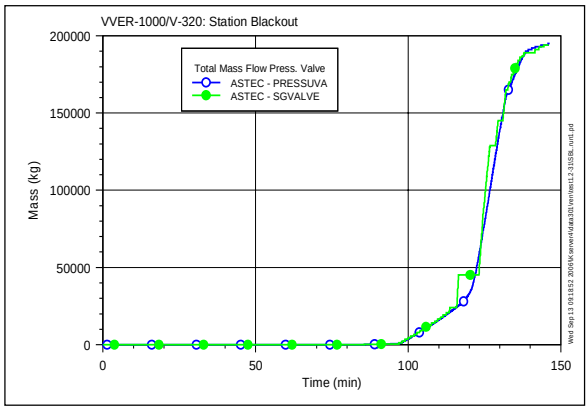

Figure 5-9: Comparison of integral mass flow through two different types of valves- PRESSUVA and SGVALVE in ASTEC for simulation of pressurizer valve

6 Investigations on the early in-vessel phase of severe accident for VVER-1000

The dominant accident sequences starting from normal operation and leading to a core melt in VVER-1000 /NEA 1998/ could result from the following initiating events:

- Loss of in-site and/or off-site power
- Loss of heat removal in the secondary side
- Feedwater and steamline rupture
- Loss of coolant accidents (LOCA).

In this Chapter a cold leg break to represent LOCA accident response and a total loss of electric power supply (station blackout - SBO) with core degradation until failure of the reactor pressure vessel (RPV) are scrutinized.

6.1 Small break loss of coolant accident

The LOCA events are postulated accidents characterized with loss of coolant from the reactor during which the make-up system of the reactor can not compensate the leakage. LOCAs are subdivided mainly into three categories: small (SBLOCA), medium-sized (MBLOCA) and large (LBLOCA) breaks. The SBLOCAs are characterized by an extended period after the occurrence of the break, during which the primary system remains at a relatively high pressure and the core remains covered /AKS 2007/. The rates of coolant discharge, the pressure variations with time and the decay heat removal via the steam generators and/or the leak are major characteristic differences between the three LOCA categories.

This investigation has been performed within the framework of the SARNET Project WP4 RAB under the EURATOM 6th framework programme. It emphasizes the modelling approach of a SBLOCA sequence for VVER-1000 reactors and describes the input assumptions for the integral ASTEC v1.2 computer code. Purpose of this study is to estimate the behaviour of the ASTEC

code, its capability for simulation of severe accidents and to determine the primary/secondary and the containment response to such accident. It is a contribution to the validation of the ASTEC code.

6.1.1 Initial and boundary conditions, assumptions for the simulation

Activated modules are CESAR for the thermal-hydraulic behaviour in the circuits, DIVA for the core degradation and CPA for the containment. In order to achieve proper initial conditions for the transient calculation the steady-state iteration procedure has been applied. After 500 s a stable stationary state has been obtained. The imposed reactor nominal parameters are controlled during steady-state by regulation procedures for pressurizer water mass, primary and secondary mass flow, as well as system pressure and temperatures.

The following assumptions were made:

- 60 mm leak in the cold leg of the pressurizer loop next to the RPV
- The isolation valves are closed in the steam pipeline, thus preventing steam supply to the turbine
- Stop of feedwater supply to the steam generators
- All the active emergency core cooling systems and hydro-accumulators fail
- Failure of secondary side heat removal (BRU-K, BRU-A, secondary cooldown procedures)
- No feeding with the auxiliary borating system
- No fission products/aerosol calculation.

This calculation has been performed for a total "problem time" of 8.3 hours (about 30000 s) therefore it is focused only on the "in-vessel phase" of the accident (up to lower head vessel failure). The ASTEC model is described in Chapter 5, Part 5.2.

The initial state of the plant is a full power of 3000 MW_{th} and normal operation of all relevant systems. The structure CONNECTI of the type "BREAK" is defined in the input deck to model the break. This structure is connected to the volume, which models the cold leg between the main coolant pump and the RPV in the thermal-hydraulic system PRIMARY. The EVENT structure defined in the input deck for transient calculation changes the status of this connection from "OFF" to "ON" at time zero, thereby opening the leak in the cold leg of loop 1.

Switch CESAR-DIVA (TH-core degradation)
Two factors were taken into account on choosing the time of the DIVA module switching on (key-word: tstar_di). On one hand, the steam content in the primary circuit must be quite high that provides for the DIVA module normal functioning. On the other hand, the time of the DIVA module switching on should be early enough to detect the first degradation. This time was chosen as 2400 s.

6.1.2 Results of the simulation, course of the transient

In Table 6-1 the main events of the accident sequence are listed.

At 0 s simulation time a 60 mm SBLOCA occurs in the cold leg of the pressurizer loop next to the RPV. The SCRAM, TURBINE TRIP and MCP OFF signals are actuated by the reactor protection system. The turbine isolation valve closes 10 seconds after the reactor SCRAM signal. As a consequence, the feedwater supply to the steam generators stops, being provided by the turbine driven pumps.

In the beginning of the accident sequence (during the first 250 s), the primary pressure decreases very rapidly due to the loss of coolant through the break. In Figure 6-1 is depicted the reactor coolant system primary and secondary pressure. With P-prima is noted the primary pressure, with P-secon – the secondary side pressure and UP-plenu stays for the pressure in the upper plenum of the reactor. The leak mass flow leads to a decrease of the pressirizer level. The water level in the reactor drops. At the beginning of the accident the secondary pressure is immediately increasing and at around 60 s when the set points for opening of the secondary side safety valves are reached, the steam generator safety valves open and start cycling. From approximately 250 s till 2500 s the primary pressure follows the secondary pressure. The decreasing primary inventory and the increasing void fraction lead to deteriorated primary to secondary heat transfer. After 2500 s the primary to secondary heat transfer breaks down and the primary pressure decreases below the secondary pressure. From this time the decay heat is only removed via the leak. The steam generators are in hot standby. The continuous loss of coolant leads to the beginning of core heat-up. With the propagation of the dry out, and without injection from the ECCS, the core starts to heat-up, the fluid and the rod temperatures start rapidly to increase.

The thermal-hydraulic phenomena related to the break behaviour can be described as follows. At the beginning of the transient only single phase fluid (water) is released through the break, thus the RPV level starts to decrease. Voiding is observed in the reactor upper plenum and in the primary loops and starts to increase. Due to the increasing void fraction the decrease of the primary pressure is slowing down. At approximately 550 s – 600 s the void fraction at the break position (in the cold leg) starts to increase (Figure 6-3) and after that there is a release of two-phase fluid through the break. After 2500 s only single-phase fluid (steam) is released through the break.

The continuous loss of coolant leads to heating-up of the core (Figure 6-2). At about 6000 s up to 10000 s the simulation shows an increase of the primary pressure due to corium slumping (Figure 6-1 and Figure 6-5). After this the pressure continues to decrease till the vessel failure.

After core uncovery the fuel temperature increases due to the low heat transfer to steam. The predicted fuel temperatures are shown in Figure 6-4, where Tfu105, Tfu110 and Tfu114 indicate the temperature of the fuel at different elevations in the core: bottom, middle and top, respectively. The fuel temperatures are calculated by the DIVA module, as the core degradation has started at 4042 s. Because of that from 0 till 4042 s the temperatures in Figure 6-4 are not calculated from the core degradation module, but from the thermal-hydraulic module CESAR. The high temperatures lead in the low pressure sequences to the mechanical deformation of the

cladding: ballooning and rupture. The ASTEC calculated maximum fuel temperature is about 3200 K. Melting of the core components and break-up of the fuel rods lead to the loss of rod-like geometry and to subsequent debris formation (Figure 6-5). The UO_2 fuel pellets are liquefied by the dissolution of the molten Zr1%Nb or by the interaction of the UO_2 and the ZrO_2 below their melting points /NEA 1998/.

Extended dry-out in the reactor core is observed. The high temperature interaction of steam and cladding results in oxidation and hydrogen generation. Beginning of the noticeable hydrogen generation (time moment by which > 1 % of hydrogen is generated) corresponds to 4900 s. Figure 6-6 shows the in-vessel hydrogen mass released during the degradation of the core. Fe stays for the hydrogen produced by the iron, B_4C stays for the hydrogen produced by the contact with the boron carbide, UO_2-Zr stays for the hydrogen generated by the contact uranium dioxide-zirconium and Total stays for the total hydrogen production. The total mass of hydrogen generated by the end of the reviewed time interval is 252 kg.

The beginning of the release of fission products takes place at 5398 s (Table 6-1).

If the accident is unmitigated, the molten material of the degraded core relocates to the lower regions of the core. Figure 6-5 shows the mass of the relocated corium in the lower plenum of the RPV.

From the thermal-hydraulic point of view the typical phases of a SBLOCA accident (e.g. the depressurization phase, the coupling of primary and secondary pressures and the break down of primary to secondary heat transfer followed by a decrease of the primary pressure below the secondary pressure) are predicted very well. The major parts of expected severe accident phenomena in VVER-1000 were modelled in ASTEC v1.2 calculation, namely: the core heat-up; the cladding oxidation, the degradation of the core components, the melt relocation and the vessel failure. Lower head vessel failure time predicted by ASTEC is at around 17995 s (~ 5 h).

Table 6-1: ASTEC, SBLOCA 60 simulation without active and passive ECCS, Main events

No	Event	ASTEC v1.2 Time, [s]
1	Opening of the break with D=60 mm equivalent diameter in (Loop1) cold leg next to the nozzle, SCRAM, the main coolant pumps are switched off	0
2	Turbine stop valves are closed	10
3	Start of DIVA module	4042
4	First total core uncovery	4587
5	Start of FP release from fuel pellets	5398
6	First corium slump	5622
7	Pool formation into the lower plenum	9500-10000
8	Lower head vessel failure	17995

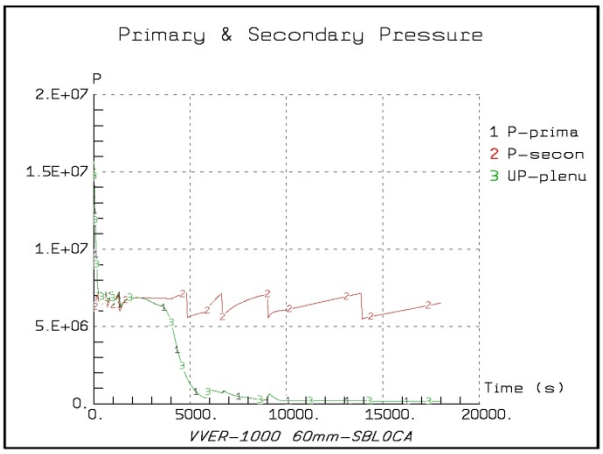

Figure 6-1: ASTEC v1.2, SBLOCA 60mm, Primary and secondary pressure

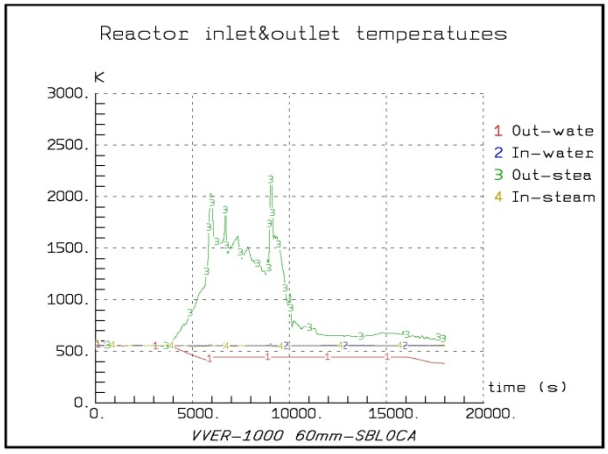

Figure 6-2: ASTEC v1.2, SBLOCA 60mm, Reactor inlet and outlet temperature

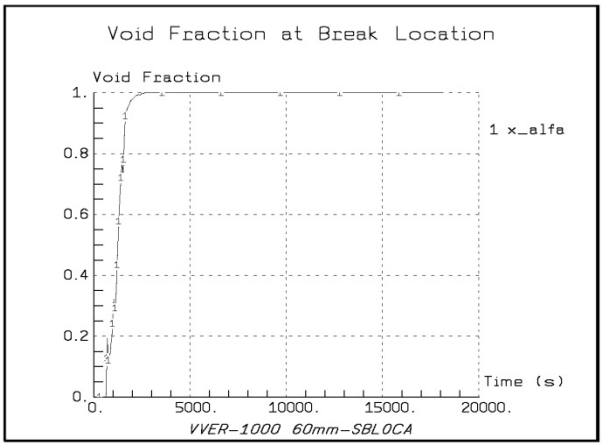

Figure 6-3: ASTEC v1.2, SBLOCA 60mm, Void fraction at break location

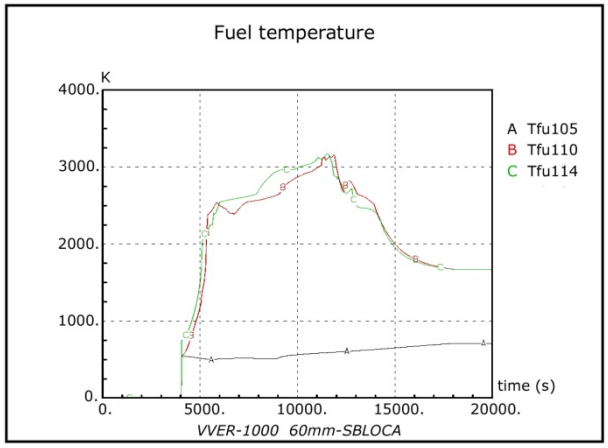

Figure 6-4: ASTEC v1.2, SBLOCA 60mm, Fuel temperatures calculated by DIVA module

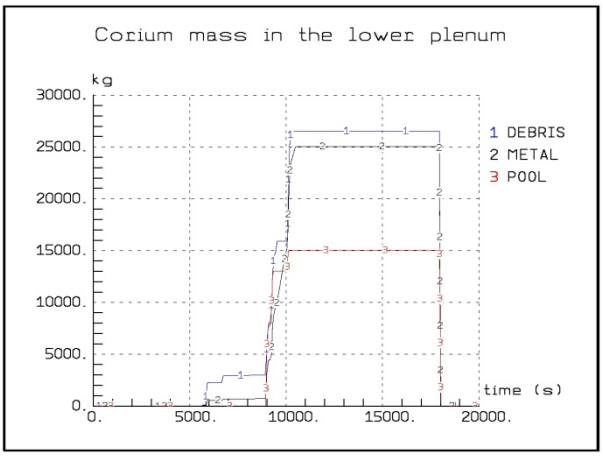

Figure 6-5: ASTEC v1.2, SBLOCA 60mm, Corium mass in the lower plenum

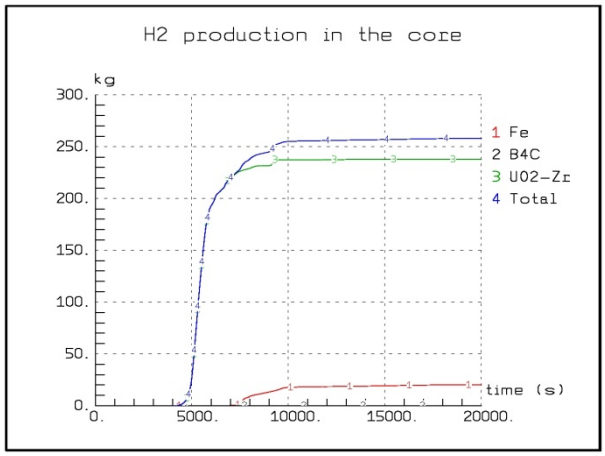

Figure 6-6: ASTEC v1.2, SBLOCA 60mm, Hydrogen production

6.2 Station blackout

A comparative investigation on a SBO accident scenario with ASTEC v1.3.0 and ATHLET 1.2d codes has been performed. The purpose of this study is to assess ASTEC code behaviour in the modelling of main thermal-hydraulic phenomena in the primary and secondary circuit arising during a hypothetical severe accident, in this case a station blackout sequence. The performed analyses cover a SBO sequence without and with passive safety injection systems (hydro-accumulators) and without diesel generators (DGs) operation, in order to investigate the thermal-hydraulic response of the ASTEC code.

The main targets of this study are:

- Estimate of the behaviour of the ASTEC code, its capability for simulation of the main thermal-hydraulic phenomena arising during the early in-vessel phase of severe accidents, including safety systems and accident management (AM) procedures; i.e. estimation of the maximum period of time for taking appropriate measures and particular decisions by the plant personnel
- Understanding of the discrepancies between ASTEC v1.3.0 and ATHLET 1.2d
- Formulation of proposals for improvement of ASTEC capability in the simulation of the early phase (in-vessel phase) of severe accident scenarios.

The investigation on the ASTEC code has been elaborated within the framework of WP19 Spreading of Excellence of the SARNET Project of the EURATOM 6th framework programme. It presents the modelling approach of a SBO sequence for VVER-1000 reactors with ASTEC v1.3.0.

The ATHLET calculations have been performed with a reference input file for a VVER-1000 and it has been modified to simulate a SBO sequence without and with consideration of passive and active emergency core cooling systems. Moreover, the two basic accident management measures – secondary and primary side depressurization – have been implemented, to investigate the effectiveness of the secondary bleed and feed and the primary bleed and feed procedures in a SBO accident. A more detailed description of the applied ASTEC and ATHLET models is given in Chapter 5.

The ATHLET code has been used as a reference computer code for the comparison study with the ASTEC code. The main topics considered for this comparison study are: primary system pressurization/depressurization during the in-vessel phase, operation of steam generator BRU-A, operation of pressurizer relief and safety valves (SEMPELL), and their influence on the thermal-hydraulic behaviour during the early phase of the SBO sequence.

The calculation results demonstrate the capability of the ASTEC code to model the early phase of the accident with satisfactory agreement in a reasonable period of time. Major events characterizing this phase, e.g. the relief and safety valves' operation and their effect on the thermal-hydraulics, the time for steam generators dry-out, the break down of the natural circulation and the start of the core heat-up have been successfully modelled.

The discrepancies attributed to the behaviour of both the steam generator relief valves and the pressurizer safety valves have been reduced by modifying the valve type within the ASTEC calculation (Chapter 5, Part 5.5). Furthermore, it is an outcome of this investigation that a proper nodalization to account for the specific requirements of the horizontal steam generators typical for VVERs is necessary for evaluation of the accident management measures (Chapter 5, Parts 5.2 – 5.4).

It has to be stressed that the objective of these analyses was by no means to deduce statements in order to assess the safety standards of any specific nuclear power plant.

In the following Chapters after a general description of the SBO scenario a detailed discussion of the main phenomena related to the early phase of the accident is given. With the help of the comparative study, using both ATHLET and ASTEC codes, an evaluation of the capabilities of ASTEC to model the main thermal-hydraulic phenomena is provided. By applying secondary and primary bleed and feed, the effectiveness and a possible optimization of the AM strategies are investigated.

6.2.1 General description of the SBO scenario

The analyses have been performed assuming a station blackout (loss of the offsite electric power system concurrent with a turbine trip and unavailability of the emergency AC power system), leading to unavailability of all major active safety systems, such as the high pressure injection system (HPIS), the low pressure injection system (LPIS) and the emergency feedwater system (EFWS) /TUS 2007/. The initiating event results in reactor trip, trip of all main coolant pumps and feedwater pumps. With the main coolant pumps coast down the coolant flow rate through the reactor decreases and the decay heat is removed from the core in natural circulation mode. After the reactor SCRAM and main coolant pumps' trip, the steam content in the water on the steam generators' secondary side decreases and the mixture level in the steam generators decreases, too. With closing of the turbine stop valves, the heat generated on the primary side can not be transferred through steam dump to the condenser and consequently the pressure in the secondary circuit is increasing. After reaching the set-point of the steam generator BRU-A valves (steam dump to atmosphere) the secondary pressure is stabilized from the operation of the valves, and is maintained constant at a value of 6.67 MPa. The steam mass flow is determined by the BRU-A valves operation.

Because the feedwater is stopped and the secondary water inventory is continuously evaporating, the steam generators' level is decreasing. When the secondary side heat sink is depleted the core decay heat causes a gradual increase of primary coolant temperature and pressure followed by the opening of pressurizer relief valves and drainage of primary coolant first to the relief tank in the containment and later on to the containment itself.

The effect of the sprays on the containment atmosphere has not been studied, as the sequence here investigated refers to the accident phase prior to vessel failure and assumes no intervention of systems power supplied by diesel generators.

Without additional measures the described scenario would lead to further depletion of the primary side, resulting in core uncovery and core heat-up at high pressure (Appendix E).

6.2.2 Initial and boundary conditions

Before performing a transient simulation, for both input decks a steady-state calculation for adjusting the boundary conditions necessary for the analyses of the discussed accident sequences has been performed. In that way the initial plant conditions as reactor power, steam generators power, pressure and temperatures on primary and secondary side and mass flow rates are achieved. In Table 6-2, the main steady state parameters before initiation of the transient simulation are listed.

Table 6-2: Steady state parameters of the reference VVER-1000 plant

Parameters	Plant Data	ASTEC	ATHLET
Reactor power, [MW_{th}]	3000	3000	3000
Primary pressure – upper plenum, [MPa]	15.70	15.66	15.67
Average coolant temperature at reactor outlet, [°C]	320.1	319.2	319.5
Maximum coolant temperature at reactor inlet, [°C]	290.0	288.7	288.8
Mass flow rate through one loop, [kg/s]	4400	4400	4440
Pressure in steam generator (steam dome), [MPa]	6.27	6.26	6.25
Mass flow rate through one steam generator, [kg/s]	408.0	408.0	410.5

The following assumptions have been applied to both ASTEC and ATHLET simulations:

- Start at nominal operating conditions (100 % reactor power)
- Conservative approach for decay heat curve (high limit), Figure 5-2
- Steam generator pressure regulation is available (BRU-A)
- BRU-A stops at 7200 s (after batteries depletion)
- Pressurizer relief and safety valves are available
- Active safety injection systems are not available
- Passive safety injection systems are available.

Additionally to the unavailability of all active safety injection systems a conservative approach for the decay heat curve has been applied. With this assumption the general course of the transient is accelerated, leading to an earlier core heat-up with the minimum time margin available for the operators to prepare counter-measures. For the generic investigations the applied assumptions lead to conservative results.

For the SBO accident with primary side depressurization (PSD) applied as an accident management measure an additional simulation, assuming start of one diesel generator and one

LPIS-train has been performed (Chapter 6, Part 6.2.7.2), to evaluate the latest possible time for restoration of the power supply and thus avoiding heating-up of the core.

In order to make an assessment of the phenomenology and the thermal-hydraulic behaviour (only of the in-vessel phase), several characteristic parameters in ASTEC and ATHLET have been chosen. These parameters, listed here below, have been also used for a graphical representation and discussion of the results, presented in Chapter 6, Parts 6.2.3-6.2.7:

- Primary and secondary pressure
- Reactor inlet and outlet temperatures
- Cladding temperatures
- Primary to secondary heat transfer (steam generators power)
- Hydro-accumulators mass inventory
- Coolant amount in the steam generators (water mass/liquid level)
- Mass flow in the primary loops
- Coolant amount in pressurizer
- Mass loss through BRU-A valves
- Mass loss through the PRZ valves (SEMPELL).

6.2.3 Results of the ASTEC simulation – accident progression without application of accident management measures

The SBO calculations (Chapter 6, Part 6.2) have been performed with the ASTEC v1.3.0 code. The analysis presented in this Part 6.2.3 has been restricted to a total "problem time" of 8.3 h (about 30000 s) and focuses only on the "in-vessel phase" of the accident. The analysis has been performed assuming no accident management measures like primary or secondary depressurization and no external cooling of the RPV (Appendix E, Appendix F).

In the table below (Table 6-3) are pointed out the main events of the transient sequence:

Table 6-3: ASTEC, SBO sequence, Main events

No	Event	ASTEC V1.3.0 Time, [s]
1	Initiating event – SBO, SCRAM, main coolant pumps are switched off	0
2	Turbine stop valves are closed	10
3	Feedwater terminated	11
4	Opening of BRU- A valves	65
5	Steam generators dry- out	4310
6	Actuation of the pressurizer valves	5100
7	Heating-up of the core	8750
8	Start of fission products release from fuel pellets	9658
9	First material slump in lower plenum	9705
10	Pressurizer (SEMPELL) valves fully opened	No AMM
11	Start of hydro-accumulators injection	No AMM
12	Stop of hydro-accumulators injection (empty)	No AMM
13	Lower head vessel failure	15452
14	Corium mass in the lower head, [kg]	67942

After the reactor SCRAM and main coolant pumps coast down, the gravitational forces are dominating the flow and the distribution of coolant inside the primary system. The primary side pressure is decreasing for a short time as a result of the reactor SCRAM and the decreasing reactor power (Figure 5-2).

Due to the isolation of the secondary side, the secondary pressure increases and the decay heat is removed from the primary circuit via the steam generators by opening the BRU-A valves, leading to a continuous decrease of water inventory on the secondary side of the steam generators. During this phase the primary pressure remains nearly constant at around 15 MPa. After the depletion of the steam generators (4310 s), the primary to secondary heat removal breaks down and an instantaneous pressure increase on the primary side occurs (Figure 6-7). Later on the core undergoes a high-pressure boil-off. In Figure 6-7 P-prim stays for the primary pressure and P-sec stays for the secondary pressure.

After reaching the set point of the pressurizer relief valve continuous depletion of the primary coolant inventory through the valves uncovers the core and leads to temperature increase in the core (Figure 6-8). In Figure 6-8: T_out_li/T_out_st corresponds to the outlet liquid/steam temperatures and T_in_liq/T_in_ste are the inlet liquid/steam temperatures. The fuel cladding temperature is also increasing and at temperatures above 1100 °C the Zirconium in the fuel cladding is oxidized by steam.

The amount of energy that is released during the steam-oxidation reaction is comparable to the residual power. A layer of ZrO_2 is forming on the external cladding surface. Strong hydrogen production is observed. Because of the significant decay heat and the high pressure in the primary side of the reactor coolant system, and due to the unavailability of emergency coolant

injection, the necessary core cooling is not provided and the maximum allowed cladding temperature criteria of 1200 °C is exceeded. Without any additional measures the BDBA is turning into a severe accident.

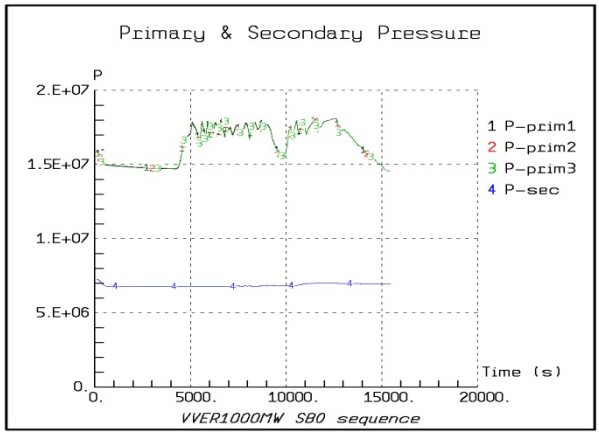

Figure 6-7: ASTEC SBO, no AMM, Primary and secondary pressure

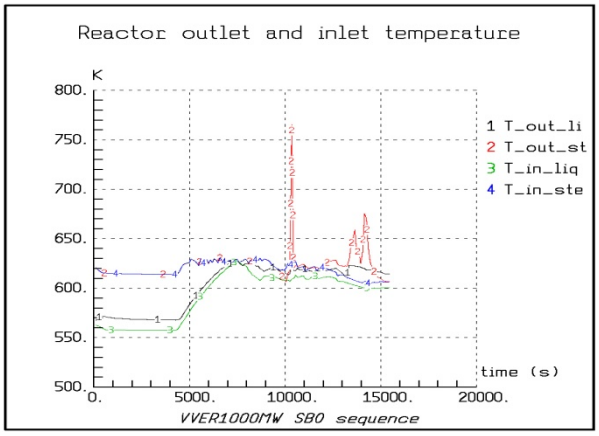

Figure 6-8: ASTEC SBO, no AMM, Reactor inlet and outlet temperature

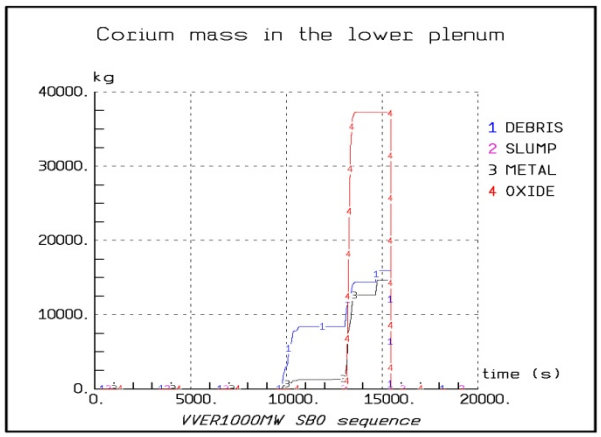

Figure 6-9: ASTEC SBO, no AMM, Corium mass in the lower plenum

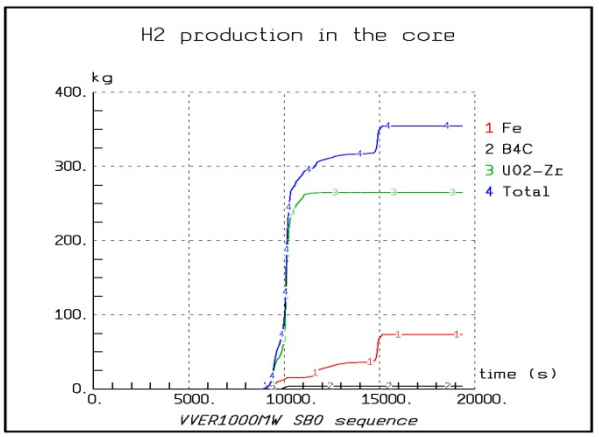

Figure 6-10: ASTEC SBO, no AMM, Hydrogen production

The boron carbide B_4C control rods undergo degradation at lower temperatures than the fuel rods. The control rod materials start relocating downwards in the reactor core. The continuously increasing temperature in the fuel pellets and the fission products generation inside the fuel elements increases the internal pressure of the fuel rods. The overpressure causes swelling and creeping of the cladding material, ballooning and crack. With the crack of the fuel claddings starts the release of fission products from the fuel pellets at 9658 s from the beginning of the transient. The further corium progression depends on the physical properties of the corium, particularly the solidus/liquidus temperatures, the viscosity of the molten mixtures formed in the core as a function of the degree of oxidation. The temperature in the core continues rising, the fuel melts and molten pool forms in the core, relocates, and followed later on by slumping of materials into the lower plenum of the reactor (9705 s) and failure of the RPV wall (15452 s).

The total slumped corium mass in the reactor lower plenum at the time of the reactor vessel failure is approx. ~ 68 t (Figure 6-9). In Figure 6-9 the total corium mass is summed from the debris mass, the slumped mass, the mass of the metal and the mass of the oxide. Figure 6-10 shows the in-vessel hydrogen production according to the different core materials. Fe: stays for the hydrogen produced by the iron; B_4C: stays for the hydrogen produced by the contact with the boron carbide; UO_2-Zr: stays for the hydrogen generated by the contact uranium dioxide-zirconium and Total: stay for the total hydrogen production. The calculated quantity of the cumulative in-vessel hydrogen production is approximately ~355 kg.

A similar simulation without application of accident management measures has been performed with the mechanistic code ATHLET /TUS 2010b/. The results show that after the depletion of the steam generators and increasingly mass loss from the primary side the reactor core starts to heat up and the cladding temperatures exceed the safety margin of 1200 °C (Chapter 6, Part 6.2.8, Figure 6-35).

6.2.4 Application of accident management measures

During severe accident sequences it is of prime importance to depressurize the primary circuit in order to allow injection from the passive and/or active safety injection systems and to avoid RPV failure at high pressure that could cause direct containment heating and subsequent challenge to the containment structure. Two basic procedures can be applied for managing of accidents to prevent growing into a severe one: primary side depressurization (PSD) and secondary side depressurization (SSD). The both procedures play an important role in the preventive and the mitigative domain of an accident sequence (Appendix E, Appendix F). Main goals are:

- To preserve the integrity of the primary circuit
- To preserve the integrity of the pressurized premises
- To create conditions for cooling down of the core or of the debris after core damage.

It is the aim of both procedures to delay an extended core heat-up and to prevent failure of the RPV under high pressure. Even more, by gaining additional time for recovery of electricity (in case of station blackout accident) and for additional water supply the failure of the vessel might be prevented at all.

By reduction of the primary pressure from one side the load on the RPV is reduced and from the other side conditions for efficient operation of the passive and active safety systems are created. Depressurizing the secondary side is a very efficient way to reduce the primary circuit pressure without early release of primary coolant to the pressurizer relief tank or to the containment. In emergency conditions when the reactor control and protection system is actuated the secondary side depressurization is realized by the steam dump to condenser or steam dump to the atmosphere valves (the BRU-A valves). In emergency condition with loss of vacuum in the condenser, when the reactor control and protection system is actuated, the steam dump to condenser valves are unavailable and cool-down process by secondary circuit is provided by steam dump to atmosphere with cooldown speed of 20 K per hour or 60 K per hour. It is

necessary to feed up the steam generators with available equipment from the emergency feedwater system or passively with water from the feedwater tanks (Figure 6-11) – secondary Bleed and Feed procedure. If heat removal by secondary circuit is unavailable or not effective, the primary circuit heat removing procedure requires starting the depressurization and the cooling of the primary circuit by opening of the pressurizer relief and safety valves – primary Bleed and Feed procedure. In case that power supply is available, feeding from the HPIS will start. In case of station blackout water delivery to the reactor core can be provided only from the passive safety systems (hydro-accumulators). Therefore the primary pressure must be reduced below the hydro-accumulators' set point of 5.8 MPa.

After SBO in VVER-1000, SSD can be performed by full opening of a certain number of the BRU-A valves. Different criteria can be used to start the procedure, e.g. if the core exit temperature exceeds or if the SG levels drop below a special limit. In the presented simulations, SSD is started 30 minutes after the SBO. It is assumed that 30 minutes after initiation of the accident is the earliest possible time for operators' intervention. Like in the Western PWRs, PSD is performed by fully opening of the pressurizer relief and safety valves (Appendix E, Appendix F). To activate the PSD procedure, different criteria (like RPV level or core exit temperature) can be used. In the simulations PSD is started, when the core exit temperature exceeds 350 °C or 650 °C respectively (earliest/latest time criterion for PSD).

Figure 6-11 shows the generic scheme of the SSD and PSD procedures for the SBO accident. These procedures have been applied for the simulations presented in Chapter 6, Parts 6.2.5 - 6.2.7. By applying PSD Chapter 6, Part 6.2.5 presents a comparative study using both ASTEC and ATHLET codes. A detailed discussion of the thermal-hydraulic phenomena related to the early in-vessel phase of the accident is given. Chapter 6, Parts 6.2.6 and 6.2.7 present results from ATHLET simulations for the SBO accident with application of the SSD procedure, and for a possible optimization of the PSD procedure.

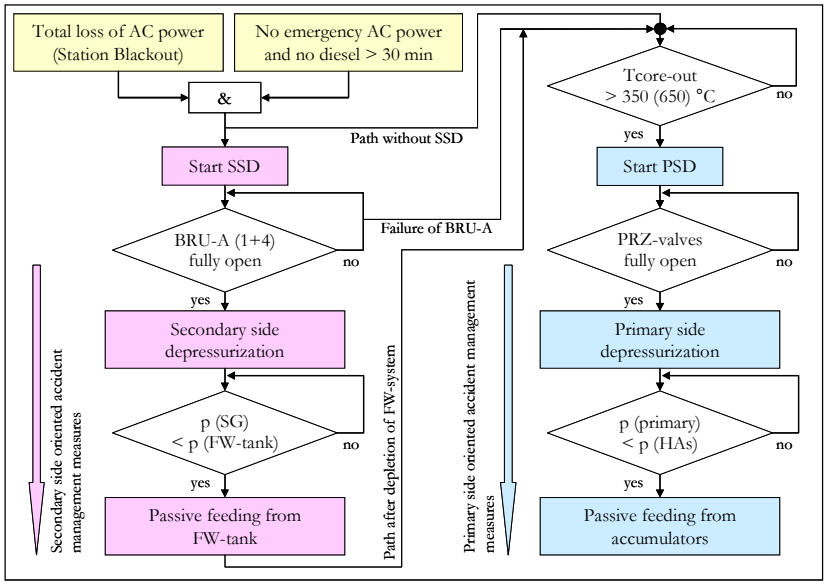

Figure 6-11: Generic scheme of the SSD and PSD procedures applied in the SBO simulations

6.2.5 Course of the station blackout transient with primary side depressurization (PSD)

With the help of the ASTEC and ATHLET simulations this Chapter gives a more detailed description of the main phenomena arising during a SBO accident. The results of the comparative analyses will be used to assess the capabilities of ASTEC to model the thermal-hydraulic phenomena during the early phase of the transient. For both simulations the initial conditions and assumptions as described in Chapter 6, Part 6.2, have been applied. The primary side depressurization as an accident management measure has been taken into account for the both simulations. It is activated at core outlet temperature $T_{core\text{-}out}$>650 °C (Figure 6-11).

The ASTEC v1.3.0 calculation for a SBO sequence has been performed for a total "problem time" of 8.3 hours (about 30000 s) therefore it focuses only on the "in-vessel phase" of the accident. The ATHLET simulation has been performed for 4.4 hours (16000 s) after SCRAM.

In the following pages the ASTEC results, for the chosen parameters, are compared to the respective ATHLET trends (Figure 6-12 to Figure 6-17).

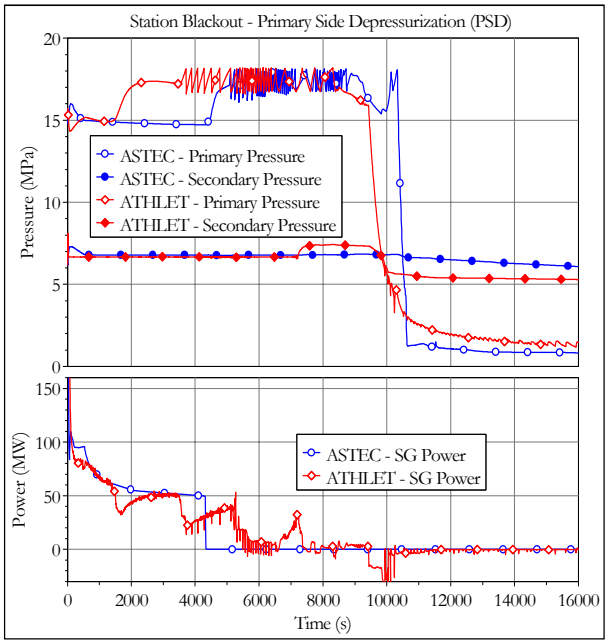

Figure 6-12: Primary/secondary pressure and total steam generator (SG1-4) power (ASTEC and ATHLET simulation)

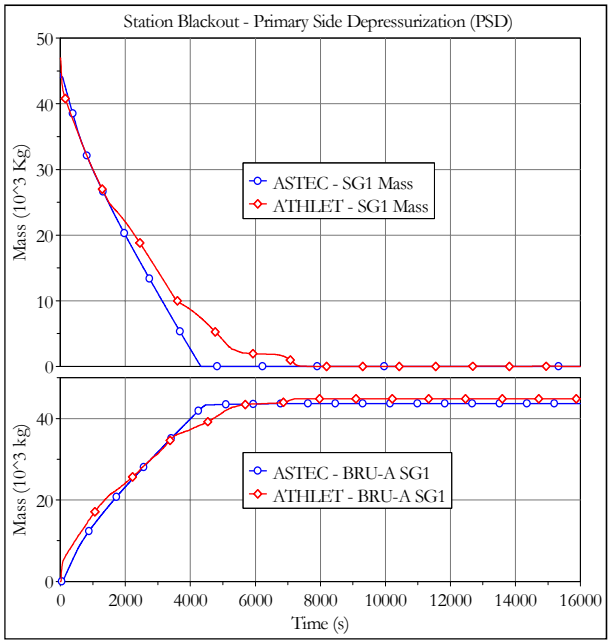

Figure 6-13: Steam generator (SG1) water mass and integral BRU-A mass flow (ASTEC and ATHLET simulation)

The initial event (SBO) leads to reactor SCRAM, stop of all main coolant pumps, closure of the turbine stop valves and loss of feedwater supply. The primary and secondary pressures are given in Figure 6-12 for the discussed scenario. Shortly after plant blackout the secondary pressure increases to the set point pressure thresholds of the steam dump to atmosphere and after opening the BRU-A valves the secondary pressure is maintained at 6.67 MPa. The integral mass flow of the BRU-valves is shown in Figure 6-13. At the beginning of the accident, the primary

pressure is dropping due to the decrease of the reactor power after SCRAM and start of the main coolant pumps coast down. After that the different behaviour of the primary pressure up to 500 s is caused by differences in the applied pump models (particularly the coast down curves), the nodalizations used for the steam generators and the different BRU-A valves behaviour (valve modelling). In that phase in the ATHLET simulation the BRU-A valves open much faster and as a consequence of the higher steam and energy release the secondary and primary pressures stay below the respective values calculated by ASTEC (Figure 6-12 and Figure 6-13).

In this phase, for a first time the steam generator power drops below the reactor power and consequently the primary pressure increases. In general the both codes predict the same behaviour, but the pressure increase starts at different times. Due to the pump coast down the coolant flow rate through the reactor and the main circulation loops decreases (Figure 6-14). In the early phase, the decay heat is still removed by natural circulation. The heat transferred from the primary to secondary side evaporates the secondary water inventory and the mass of water on the secondary side is decreasing, as depicted in Figure 6-13.

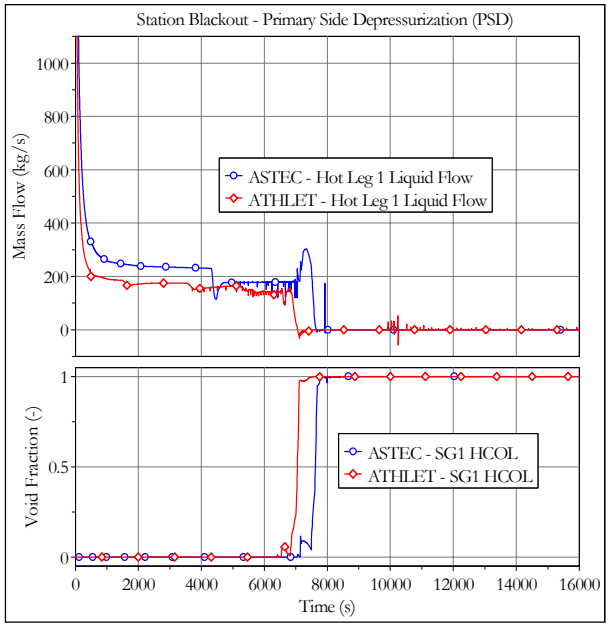

Figure 6-14: Hot leg mass flow and void fraction in steam generator hot collector (HCOL), (ASTEC and ATHLET simulation)

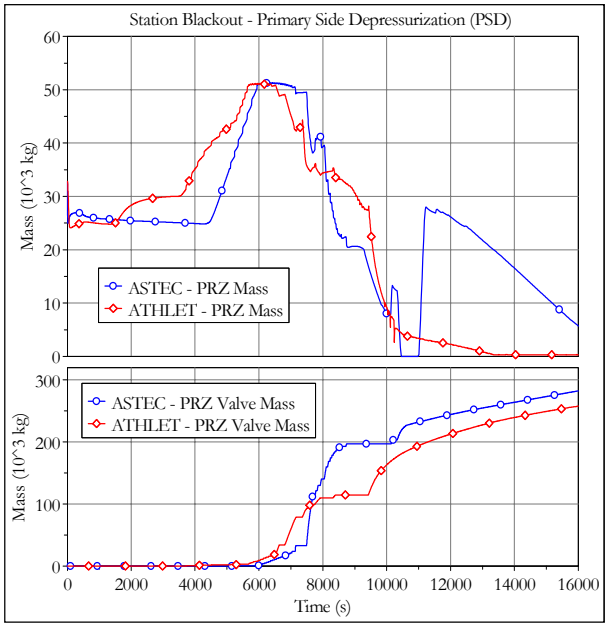

Figure 6-15: Pressurizer (PRZ) mass and integral valve mass flow (ASTEC and ATHLET simulation)

The decreasing water level in the steam generators also decreases the effective heat transfer area (Chapter 5, Part 5.4, Figure 5-6). As already mentioned, when the steam generator power drops below the reactor power, the primary pressure increases.

The stepwise reduction of the steam generator power (Figure 6-12) and the earlier increase of the primary pressure in the ATHLET simulation are caused by a more detailed steam generator model (e.g. vertical subdivision of the heated part of the secondary side into three parts, Figure 5-1, Figure 5-4 and Figure 5-6). After the uncovery of a part of the tube bundles, a drop in the

steam generator power and a significant increase of the primary pressure can be observed (t=1400 s and t=3500 s). The ASTEC simulation with a simplified nodalization for the steam generators (Figure 5-3) provides a smoother decrease of the steam generator power. The primary pressure starts to increase only when the steam generators are completely emptied (t=4310 s). Later on, the primary pressure reaches the threshold for opening the pressurizer relief valve (t=3710 s in ATHLET and t=5100 s in ASTEC).

The minimum steam generator level is reached at approximately 4310 s in the ASTEC simulation. In the ATHLET simulation the steam generator level drops below the lowest part of the horizontal oriented U-tubes at 5200 s. After that the heat transfer from the primary to the secondary side (steam generator power) breaks down and in the ATHLET simulation the pressurizer relief valve opens and closes much faster, Figure 6-12.

Because of the delayed pressure increase in the ASTEC simulation the threshold of the pressurizer relief valve is reached much later in the transient. With the actuation of the pressurizer relief valve the pressurizer level (water mass) is increasing (Figure 6-15). When the level reaches the position of the relief valve, a transition from two-phase to single-phase water flow with a higher mass release through the valve is observed.

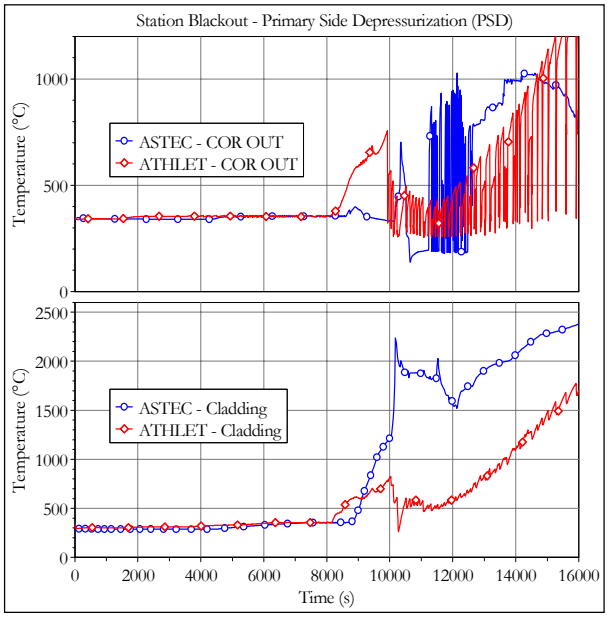

Figure 6-16: Steam temperature at core outlet (COR OUT) and cladding temperatures in the upper part of the core (ASTEC and ATHLET simulation)

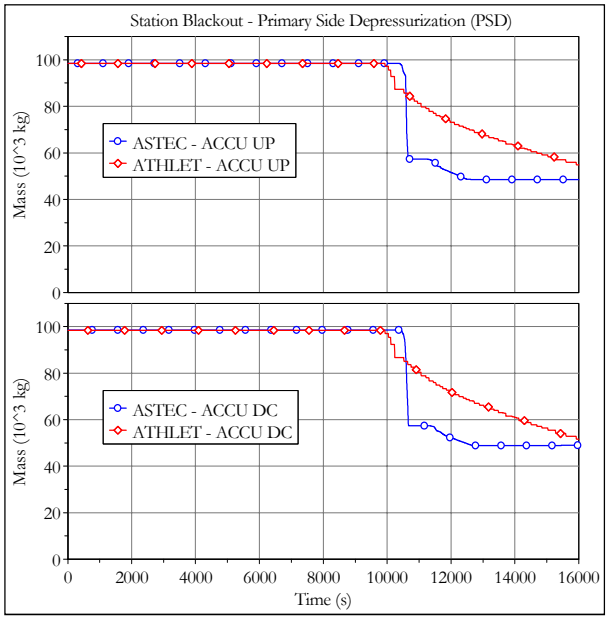

Figure 6-17: Mass inventory of hydro- accumulators – injection to upper plenum (UP) and downcomer (DC), (ASTEC and ATHLET simulation)

The integral mass flow through the pressurizer relief and safety valves is presented in Figure 6-15. Due to the increasing loss of primary coolant through the pressurizer relief valves, the primary mass inventory is decreasing and the RPV cover bubble appears. When the water level in reactor vessel drops below the hot nozzles, steam appears also in the main circulation loops, resulting in the break down of natural circulation in the primary system (see mass flow and void fraction in

Figure 6-14). As there is no water supply to the primary circuit, the core starts to heat-up in the further course of the transient (Figure 6-16). The reduced primary water mass leads to core uncovery and its consequent dry-out.

At a core outlet temperature of $T_{core\text{-}out}$>650 °C (Figure 6-16) depressurization of the primary side is initiated manually by the operator. For this accident management measure the pressurizer relief and safety valves are fully opened, which allows a fast reduction of the primary pressure below the set point of the hydro-accumulators (p_{prim}<5.8 MPa) and in this way an injection of water from the passive safety injection systems (Figure 6-12 and Figure 6-17).

The accumulators injection leads to an increasing water level in the RPV and the rise of the cladding temperatures is temporarily stopped (Figure 6-16). Due to the evaporation in the reactor core and caused by a reversed heat transfer in the steam generators the decrease of the primary pressure is slowing down. As a consequence the injected mass from the hydro-accumulators is decreasing. This effect can be clearly seen in the ATHLET simulation (Figure 6-12 and Figure 6-17). The reversed heat transfer (negative steam generator power) is not predicted by ASTEC. Therefore the decrease of the primary pressure calculated by ASTEC is much faster, leading to more effective hydro-accumulators injection. After the primary side depressurization and the start of the hydro-accumulators injection the secondary pressure slightly decreases. This effect is predicted by both ASTEC and ATHLET codes (Figure 6-12).

Feeding from the hydro-accumulators in the both simulations lowers the core temperatures for a limited period of time (Figure 6-16). After the first injection phase the hydro-accumulators' injection is decreasing (in the ASTEC simulation it is stopped at p_{prim}<1 MPa) and later on the cladding temperatures start to increase again. Without additional measures, recovery of electricity supply and start of active safety injection systems, a further increase of the cladding temperatures can not be prevented. Even though the ASTEC code predicts a more effective accumulator injection during the first injection phase (Figure 6-17), the accumulated water mass in the reactor core is underestimated, whereas the pressurizer level (water mass, Figure 6-15) increases much faster. As a consequence ASTEC predicts much higher cladding temperatures, reaching more than 1200 °C. In the ATHLET simulation the cladding temperatures also exceeds the critical limit of 1200 °C, but much later in time (Figure 6-16). In the later phase of the accident exothermic oxidation of the fuel rod cladding contributes significantly to the heat-up of the core, thus initiating the core degradation phase. ASTEC uses the special module DIVA for the simulation of core degradation. Hence, the differences in the physical models between ASTEC and ATHLET could also be responsible for the differences in the cladding temperatures.

The both codes predict the general course of the transient and most of the discussed thermal-hydraulic phenomena with a good qualitative agreement. From a safety point of view both simulations clearly show the positive effect of the applied accident management measure. The codes predict a time margin for the operators of at least 2.6 h between the initiating event until the activation of the accident management procedure from the criterion $T_{core\text{-}out}$>650 °C. To assess the time margin for additional measures after primary side depressurization, the behaviour of the accumulator injection and the differences in the predicted cladding temperatures have to be detailed investigated.

Compared to the simulation in Chapter 6, Part 6.2.3 the ASTEC simulation with applying PSD as an accident management measure shows a time delay for the lower head vessel failure of approximately 1.5 hours (without PSD the lower head vessel failure occurs at t=15452 s and with PSD at t=20886 s respectively), also /TUS 2008/ and /TUS 2009/.

Table 6-4 summarizes the timings of the main events derived from the both codes.

Table 6-4: ASTEC/ATHLET SBO simulations, Main events

Event	ASTEC With PSD Time, [s]	ATHLET With PSD Time, [s]
Initiating event – SBO, SCRAM and main coolant pumps switched off	0	0
Turbine stop valves are closed	10	0
Feed water terminated	11	0
Opening of the steam dump to atmosphere (BRU-A)	65	15
Steam generators dry-out (break down of steam generator power)	4310	5200
Actuation of the pressurizer valves	5100	3710
Pressurizer valve mass flow transition from two-phase to single-phase water	5940	5680
Upper plenum temperature reaches saturation conditions (voiding start-up)	7140	6520
Closing of BRU-A valves (batteries depletion)	7200	7200
Break down of natural circulation on primary side	7640	7160
Heating-up of the core	8750	8150
PSD, pressurizer valves fully opened	10340	9420
Start of hydro-accumulators' injection	10514	9930
Stop of hydro-accumulators' injection	12650	-
Lower head vessel failure	20886	Not calculated
Corium mass in the lower plenum, [kg]	73248	Not calculated

6.2.6 Course of the station blackout transient with secondary side depressurization (SSD)

As already described without additional measures and without recovery of electricity supply the SBO accident would lead to an extended core heat-up under high pressure conditions. By means of the SSD procedure the secondary pressure can be reduced to allow the passive feeding of the steam generators' secondary side from the feed water system. In this way, the heat removal from the primary to the secondary side can be enhanced and the primary pressure can be reduced. The PSD procedure can be additionally applied to reduce the primary pressure by fully opening of the pressurizer relief and safety valves and so to trigger the injection from the passive emergency core

cooling system (hydro-accumulators). The aim of the both procedures is to delay an extended core heat-up and to prevent failure of the RPV under high pressure (Appendix E, Appendix F).

For a successful realization of the secondary bleed and feed strategy the fulfillment of another strategy is necessary i.e. "secondary circuit feed-up", with water from the emergency feedwater system or passively from the feedwater lines and the feedwater tank (Figure 5-7). Applying the SSD procedure will delay the pressure rise in the primary circuit for several hours and during this time the primary pressure remains below the limits of the pressurizer relief and safety valves operation.

In this Chapter the effect of SSD on the course of the SBO transient is discussed. The investigations are realized with the ATHLET code. For the description of the specific model applied to the steam generators' secondary side and the feedwater system see Chapter 5, Part 5.4.

The earliest criterion was applied to activate the corresponding accident management measures (Figure 6-11). It is assumed that two BRU-A valves could be fully opened by the operators 30 min after the initiating event. In case of failure of BRU-A valves to stay in open position (after the depletion of the batteries) or after depletion of the feedwater system a second increase of the primary pressure could be expected. In that case additionally to the SSD, PSD can be applied to reduce the primary pressure by full opening of the pressurizer relief and safety valves and so to trigger the injection from the passive emergency core cooling system (hydro-accumulators), Chapter 6, Part 6.2.4, Figure 6-11. To investigate the effectiveness of SSD, two simulations with the following assumptions have been performed:

1st simulation (SSD-Case1), Figure 6-18 to Figure 6-22:

- 30 min after Station Blackout, BRU-A 1+4 fully opened (earliest criterion)
- If SSD cannot be activated at all or if the procedure is not successful (e.g. conservative assumption for failure of BRU-As after the depletion of the batteries), later on PSD is applied to reduce the primary pressure and to start passive feeding of the primary side from the accumulators. The 1st temperature criterion ($T_{core\text{-}out}$>350 °C) has been applied to activate PSD (Chapter 6.2.4, Figure 6-11).

2nd simulation (SSD-Case2), Figure 6-23 to Figure 6-26:

- Manual opening of the BRU-A valves 1+4 from 30 min after Station Blackout, till end of the simulation both valves stay in open position.

For the both simulations the course of the accident sequence before starting SSD (0-1800 s) corresponds to the ATHLET simulation described in Chapter 6, Part 6.2.5.

Results of the 1st simulation (SSD-Case1)

During the first 1800 s the BRU-A valve's normal operation (Figure 6-20) maintains the secondary pressure at 6.67 MPa. Because the normal feedwater supply has stopped and the auxiliary feedwater pumps are not available, the mass loss through BRU-A valves leads to continuous depletion of the steam generators' secondary side and steam generator levels are decreasing (Figure 6-19, also Chapter 6, Part 6.2.5). 30 minutes after SBO the BRU-A valves 1

and 4 are opened from the shift operator by a button from the main control room for starting of the SSD procedure. After initiation of SSD (Figure 6-20) the pressure in steam generators SG 1 and SG 4 is decreasing whereas the pressure in SG 2 and SG 3 remains approximately constant and below the set-point of the BRU-As operation (Figure 6-18).

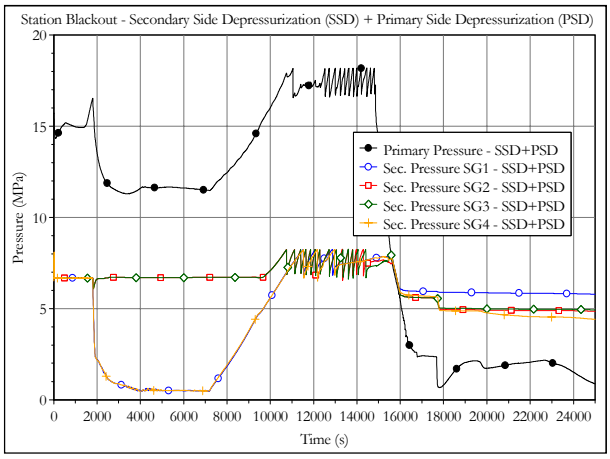

Figure 6-18: ATHLET, SBO; SSD-Case1, Primary and secondary pressure

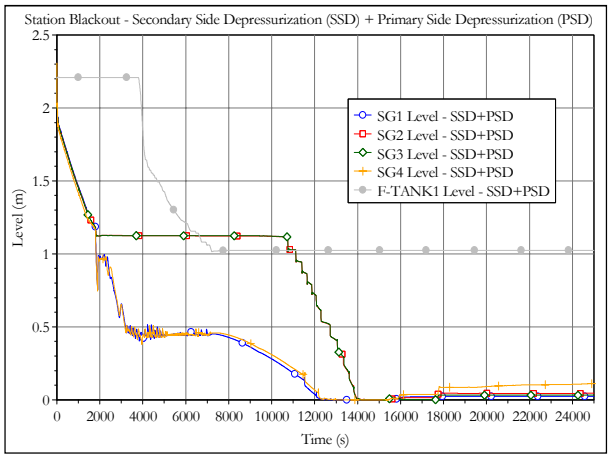

Figure 6-19: ATHLET, SBO, SSD-Case1, Steam generator level and level in FW-tank

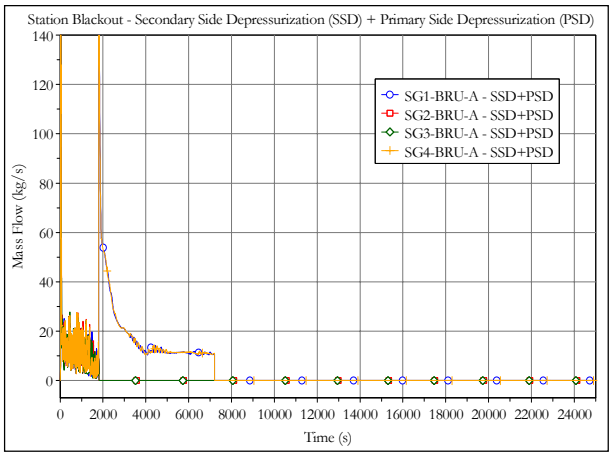

Figure 6-20: ATHLET, SBO, SSD-Case1, BRU-A mass flow

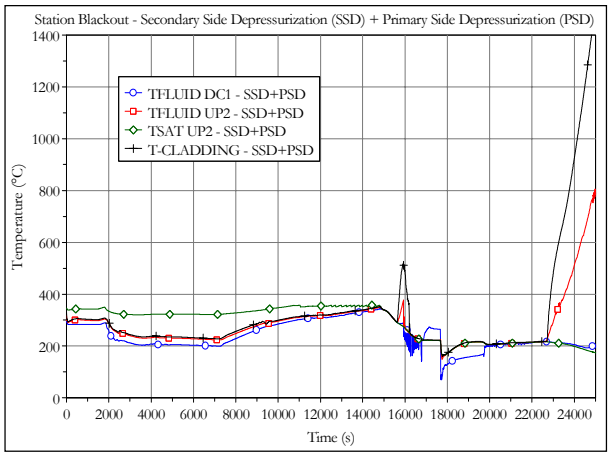

Figure 6-21: ATHLET, SBO, SSD-Case1, Fluid and cladding temperatures

The fast pressure reduction allows the passive feeding of the SG 1 and SG 4 first from the feed water pipes and later on from the feed water tanks (Chapter 5, Part 5.4, Figure 5-7). Figure 6-19 shows the level in the four steam generators and in the feedwater tank (FW-tank). After depressurization the feedwater can be partly evaporated (if the feedwater temperature exceeds the saturation temperature), thus reducing the effectiveness of the feeding procedure. A more

detailed discussion of this effect is presented in the following part in the results of the second SSD simulation (SSD-Case2).

By applying SSD and passive feeding the depletion of the steam generators can be significantly delayed and due to the enhanced heat transfer from the primary to the secondary side, the primary pressure is also decreasing (Figure 6-18).

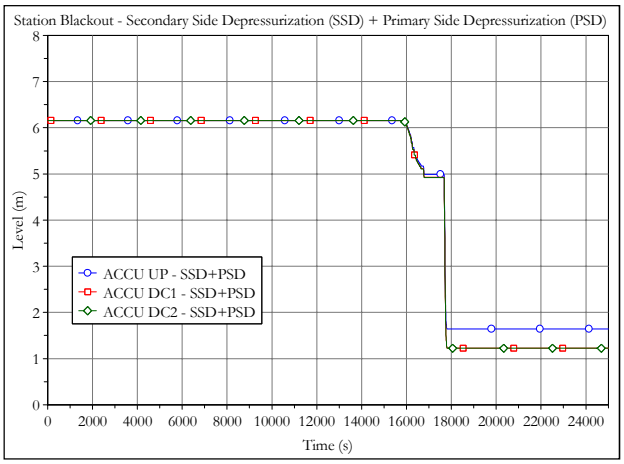

Figure 6-22: ATHLET, SBO, SSD-Case1, Accumulator level

From approximately 3200 s till 7200 s the mass loss through the fully opened BRU-A valves in SGs 1 and 4 is compensated by the passive feedwater injection and the depletion of the steam generators' secondary side is stopped. Because of the closed BRU-As in SGs 2 and 3 the corresponding water levels remain at higher values (Figure 6-19, Figure 6-20). It is assumed that after 2 hours all BRU-As fail in closed position (conservative assumption for depletion of batteries). The manual opening of BRU-A valves is not considered after batteries depletion. After closing the BRU-A valves the remaining water in SGs 1 and 4 is continuously evaporated and the liquid level is decreasing (Figure 6-19). As a consequence the pressure in SGs 1 and 4 starts to increase (Figure 6-18) and the passive feeding from the feedwater system is stopped. For SGs 2 and 3 already after initiation of SSD the steam generator power has broken down and these steam generators remain in hot stand by. Because of the decreasing heat transfer from primary to secondary side also the primary pressure starts to increase.

At t=10750 s the secondary pressure in SGs 2 and 3, and at t=11500 s in SGs 1 and 4 reaches the set-point of the safety valves. Due to the mass loss through the valves the steam generators' levels further decrease (Figure 6-19). The reduced heat removal from the steam generators' secondary side leads to further increase of the primary pressure and temperature. At t=12500 s the primary pressure reaches the set-point of the pressurizer relief valve (Figure 6-18).

The core outlet temperature reaches the set-point for activation of PSD ($T_{core\text{-}out}$>350 °C, Figure 6-11) at t=14860 s (~ 4 hours after SBO). The full opening of the pressurizer relief and safety valves (Figure 6-18) leads to decreasing primary pressure. Due to the mass loss through the valves and evaporation on primary side a first increase of cladding temperatures can be observed at approx. t=15640 s (Figure 6-21). At t=15920 s the primary pressure drops below the set-point of accumulator injection (5.8 MPa) and the passive feeding from accumulators stops the core heat-up. After depletion of the accumulators (t=17800 s, Figure 6-22), the fluid and cladding temperatures rise again and due to the mass loss through the pressurizer valves the primary water mass is continuously decreasing. A second core heat-up with a fast increase of cladding temperatures takes place at t=22720 s (Figure 6-21). At t=24500 s the cladding temperature exceeds the critical limit of 1200 °C.

Results of the 2nd simulation (SSD-Case2)

For the first simulation with SSD it was assumed that the BRU-As fail in closed position (SSD+PSD simulation) after 2 hours. To investigate the effect of BRU-As operation on the transient, full opening of the valves was simulated in a second code run from 30 minutes after SBO up to the end of the transient (BRU-A valves remain in open position, Figure 6-24). It has to be pointed out that the operators have to open the BRU-A valves manually for this procedure.

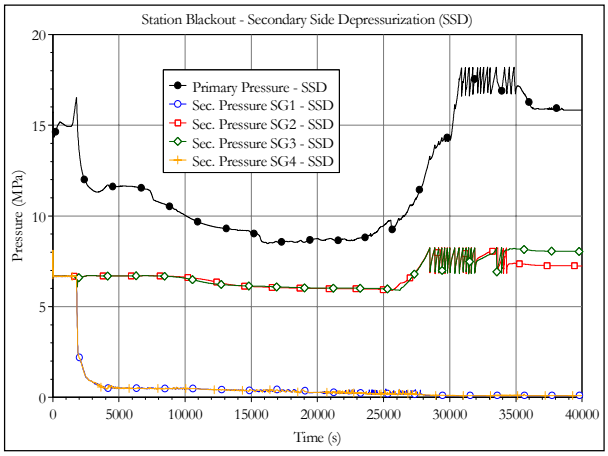

Figure 6-23: ATHLET, SBO, SSD-Case2, BRU-A 1+4 fully opened, Primary and secondary pressure

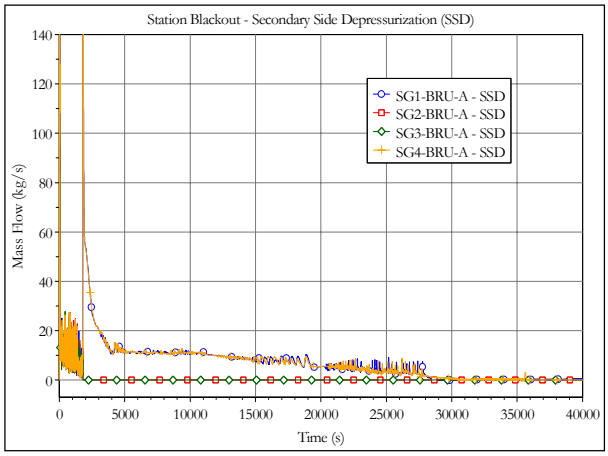

Figure 6-24: ATHLET, SBO, SSD-Case2, BRU-A 1+4 fully opened, BRU-A mass flow

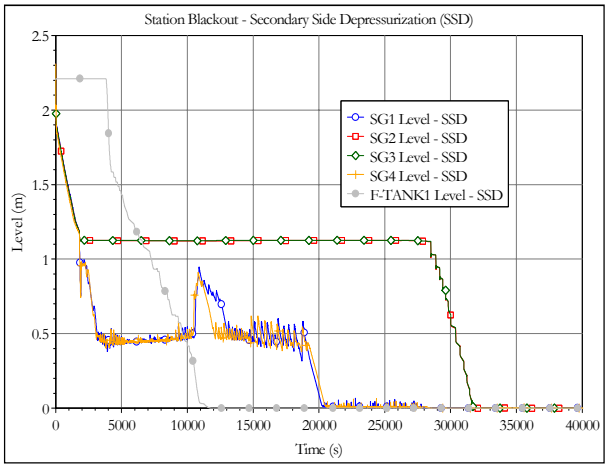

Figure 6-25: ATHLET, SBO, SSD-Case2, BRU-A 1+4 fully opened, Steam generator level and level in FW-tank

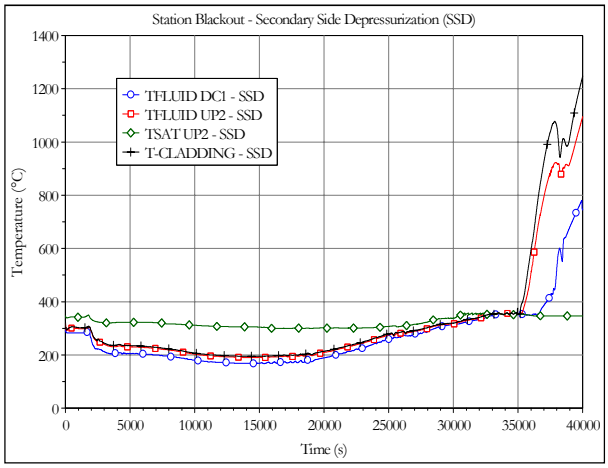

Figure 6-26: ATHLET, SBO, SSD-Case2, BRU-A 1+4 fully opened, Fluid and cladding temperatures

Till 7200 s the course of events corresponds to the 1st simulation, SSD of SGs 1 and 4 leads to passive feeding from the feedwater system and a depletion of the steam generators' secondary side can be avoided (Figure 6-23 and Figure 6-25). The secondary depressurization is much more effective with full opening of two BRU-A valves (SG 1 and SG 4) during the whole transient. As can be seen from Figure 6-23, compared to the 1st simulation the primary pressure stays below the set point of the pressurizer relief valve for a much longer period. During this time the fluid

temperatures on the primary side are kept below the saturation temperature and the primary circuit remains sub-cooled (Figure 6-26).

As in the previous simulation, SSD-Case1, because of the closed BRU-As the water levels in SGs 2 and 3 remain at higher values (Figure 6-25).

Before final depletion of SGs 1 and 4 the oscillations in the steam generators' levels, in the secondary mass flow rates and in the pressures are partly caused by evaporation of the injected water and operation of a check valve of the feedwater system, which opens and closes depending on the pressure difference (Chapter 5, Part 5.4 and Figure 5-7). The hysteresis of this valve is stepwise and it operates on the following way: if the pressure difference is greater than 1 bar the valve opens and at a pressure difference lower than 0.5 bar it starts to close. In the following part for SG1 a brief description of the main phenomena occurring during passive feeding is given (Appendix G, Appendix H).

For a short time, after starting the depressurization, the secondary side of the steam generator is fed with sub-cooled water from the feedwater system and the depletion is temporarily stopped. Due to the fast depressurization, later on the fluid temperature at the upper most part of the feedwater connection line (Figure 5-7) exceeds the saturation temperature and the feedwater starts to evaporate before it enters in the steam generator. As a consequence the passive feeding is less effective and the steam generator level continues to drop. The changing density in the feedwater connection line has an effect on the pressure difference between upstream and downstream sides of the check valve and as a result the valve is periodically opening and closing. This behaviour can be seen in Appendix G, e.g. distribution of the void fraction in the feedwater connection line, valve operation, liquid mass flow, pressure and the steam generator level. In the time between 2000 s and 4000 s evaporation takes place also in the lower part of the feedwater connection line. After that plugs of sub-cooled water from the feedwater system enter the connection line to the steam generator and the corresponding void fraction is decreasing. During the whole feeding process strong oscillations with different period and amplitude can be observed (Figure 6-25, Appendix G). These oscillations are partly caused by flashing. If the fluid temperature reaches the saturation temperature, the void fraction increases and the mass flow is accelerated. Then colder water from the feedwater system is entering the connection line and stops the flashing, as a consequence the void fraction decreases. With the changing fluid mass in the connection line during the flashing process the check valve opens and closes periodically. With the continuous pressure reduction in the feedwater system voiding can be also observed in the vertical part of the feedwater line below the feedwater tank (Appendix H). Probably the changing period of the oscillations is caused by different effects, like flashing or evaporation at different points of the feedwater system and an oscillating behaviour of the remaining water mass in the lower parts of the system. The peak in the steam generator level at ~ 10500 s, which can be seen in Figure 6-25, is induced by flashing of the total volume of the feedwater connection line. The significant reduction of the water mass above the check valve forces the valve to stay in open position for a longer period and after that a plug with colder water is entering the feedwater connection line and the steam generator is fed with more water. Later on in the lower part of the connection line evaporation starts again, the feeding process is stopped and the steam generator

level starts to decrease. Despite of this level peak and the oscillations, from 3000 s till 19000 s the steam generator level remains approximately at 0.45 m to 0.5 m (Figure 6-25). The stagnating level is caused by equilibrium between the injected mass and the mass, which is released through the BRU-A valve. The observed phenomena like evaporation and flashing are responsible for the limited water injection from the feedwater system to the steam generators. At the steam generators' entrance the water is periodically evaporated, which makes the injection in the steam generators less effective.

With the depletion of SGs 1 and 4 the primary to the secondary heat transfer is more and more reduced and from 25800 s till 28500 s the pressure in SGs 2 and 3 and the primary pressure as well increase rapidly. With reaching the set-point of the steam generators' safety valves the levels in SGs 2 and 3 start to decrease and the continuous mass release through the valves leads to steam generators' depletion (Figure 6-25). Due to an enhanced, but limited heat removal in SGs 2 and 3 the increase of the primary pressure is temporarily delayed. At t=30890 s the primary pressure reaches the set-point of the pressurizer relief valve (Figure 6-23). After that the mass loss from primary side leads to core heat-up (Figure 6-26). At t=35150 s a fast increase of the cladding temperature can be observed, exceeding the critical limit of 1200 °C at t=39750 s.

For the 2nd simulation depressurization of the primary side (PSD) was not taken into account. The earliest/latest temperature criteria for initiation of the PSD procedure ($T_{core\text{-}out}$>350 °C/$T_{core\text{-}out}$>650 °C) are reached at t=32700 s and t=36400 s respectively. With the assumptions for this simulation, SSD with two BRU-A valves manually opened would give the operators a time margin of at least 9 hours before starting the PSD procedure (compared to 4 hours for the 1st simulation with BRU-As closed after batteries depletion).

6.2.7 Investigations on the effectiveness and possible optimization of the primary side depressurization procedures

6.2.7.1 Initiation of PSD by different temperature criteria

The PSD is a basic strategy by application of which the high pressure accident scenarios could be avoided. It would provide the necessary conditions for ECCS actuation.

Investigation on the effectiveness of the PSD by variation of the initiation criteria was performed by the ATHLET code (Chapter 6, Part 6.2.4, Figure 6-11). Two cases were studied:

- 1st simulation (PSD350): depressurization of the primary side at a temperature criterion $T_{core\text{-}out}$>350 °C (earliest criterion)
- 2nd simulation (PSD650): depressurization of the primary side at a temperature criterion $T_{core\text{-}out}$>650 °C (latest criterion).

With a core outlet temperature of 350 °C the fluid temperature reaches the saturation temperature and steam appears in the RPV. This criterion corresponds to the earliest possible time to detect a core heat-up before the cladding temperatures start to rise. The second criterion corresponds to the latest possible time to start PSD and to delay an excessive increase of the

cladding temperatures by passive feeding from the hydro-accumulators. With activating PSD at a core outlet temperature 650 °C the cladding temperatures already start to rise.

It is the main purpose of this study to assess the maximum response time for the operator in a way to be seen the effectiveness of the measure on the accident progression. Figure 6-27 to Figure 6-30 show the main results of the simulations. For the both simulations the course of events before activation of the PSD procedure corresponds to the ATHLET simulation described in Chapter 6, Part 6.2.5.

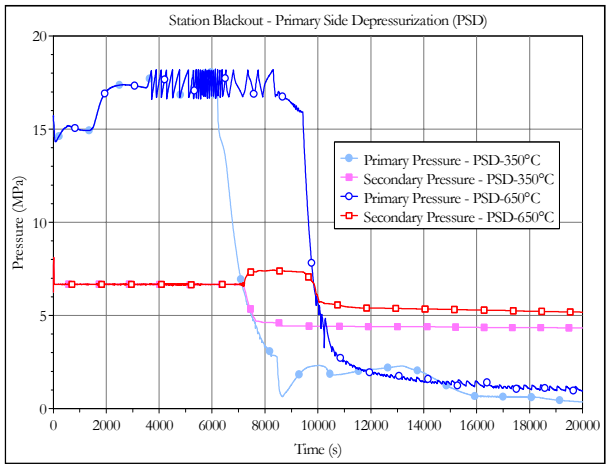

Figure 6-27: Primary and secondary pressure (PSD350 vs. PSD650 simulation)

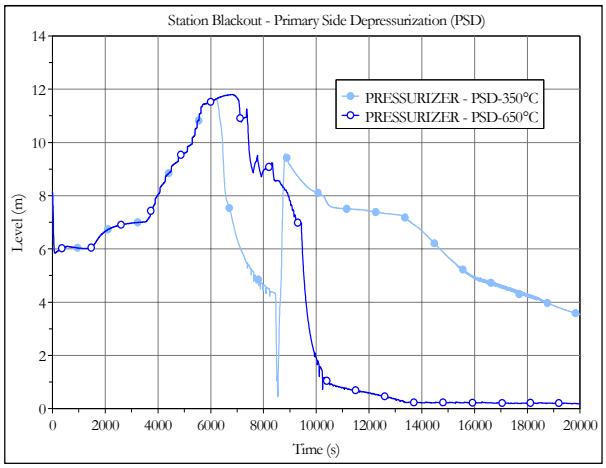

Figure 6-28: Pressurizer level (PSD350 vs. PSD650 simulation)

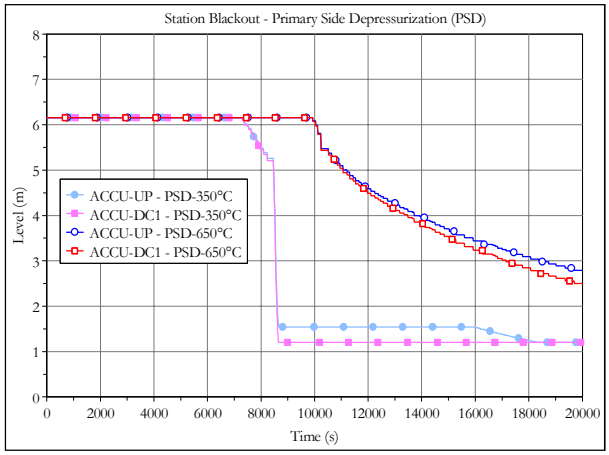

Figure 6-29: Accumulator level (PSD350 vs PSD650 simulation)

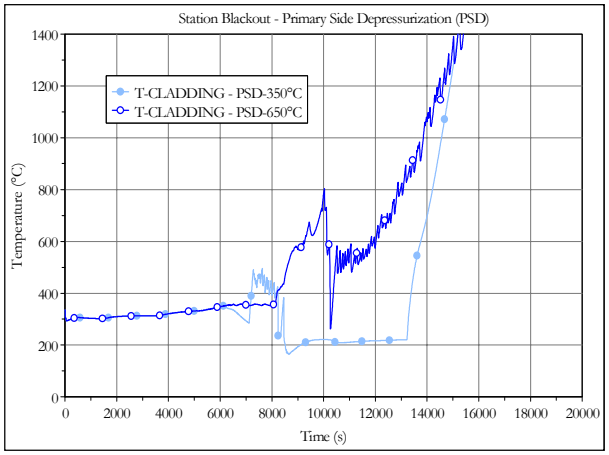

Figure 6-30: Cladding temperature (PSD350 vs. PSD650 simulation)

With the depletion of the steam generators and the decreasing primary to secondary heat transfer the primary pressure and the fluid temperatures start to rise. Later on the pressure increase is limited by the operation of the pressurizer relief valve. For the first simulation the criterion to activate PSD is reached at t=6205 s, in the second simulation PSD is started at t=9420 s. The

reduction of the primary pressure earlier in time (Figure 6-27) also allows earlier water delivery to the core from the passive safety system. The immediate effect can be seen from the peak cladding temperature (Figure 6-30). For the simulation with PSD triggered at $T_{core\text{-}out}$>350 °C the first peak in the cladding temperature is observed around 7200 s. This peak is much smaller than with later initiated PSD.

The first peaks (heat-ups) in the cladding temperature, which occur due to the first core uncovery are mitigated by the reflooding from the hydro-accumulators' water independently from the PSD temperature actuation criterion. For the PSD350 simulation the hydro-accumulators injection starts at t=7200 s and the hydro-accumulators depletion of is observed at t=8600 s (Figure 6-29).

For the simulation with PSD650 the primary pressure reaches the limit for the accumulators' injection at t=9930 s. The feeding from the accumulators lowers the core temperatures for a limited period of time. Due to the evaporation in the reactor core and caused by a reversed heat transfer in the steam generators the decrease of the primary pressure is slowing down and the secondary pressure slightly decreases (Figure 6-27). As a consequence the injected mass from the accumulators' is decreasing (Figure 6-29). After the first injection phase of the hydro-accumulators the cladding temperatures start to rise again (Figure 6-30).

For the case with the higher core outlet temperature criterion for PSD actuation, the second increase in the cladding temperature is observed at around 11500 s from the beginning of the transient. This compares to 13200 s for the case with earlier actuation of the PSD.

The simulation with PSD at a core outlet temperature of 350 °C has shown that the cladding temperature is kept constant at a low level for a period of time of 1.3 hours. This is due to the full water injection from the passive safety system into the downcomer and the upper plenum of the pressure vessel. The more effective accumulator injection in the PSD350 simulation leads to an increasing water level in the RPV and also in the pressurizer (Figure 6-28). In the PSD650 simulation the accumulator injection starts later in time and due to the presence of overheated steam in the primary circuit (steam temperature is much higher than saturation temperature) the primary pressure decrease caused by condensation of steam is lower than in the PSD350 simulation. Consequently the accumulator injection is not that effective as in the PSD350 simulation.

Earlier initiation of the primary side depressurization would keep the fluid and the cladding temperatures lower for a longer period of time, while later initiation of the PSD shows continuous increase in the cladding temperatures. Despite the differences in both simulations the results show that the critical limit of 1200 °C for the cladding temperatures is reached at approx. the same time (Figure 6-30).

From the results of the simulations there is no clear indication that one of the temperature criteria, applied to activate PSD, is more effective. With the limited amount of water in the hydro-accumulators and without restoration of power supply in both cases an extensive core heat-up can be delayed, but not avoided. From an operational point of view, PSD activated at the latest possible time ($T_{core\text{-}out}$>650 °C) would give the operators an additional time margin to restore an active emergency core cooling pump (Chapter 6, Part 6.2.7.2) and to avoid a significant

release of primary coolant to the relief tank and the containment due to full opening of the pressurizer relief and safety valves. Based on the performed simulations the time difference between earliest and latest PSD criterion is approximately 54 minutes.

6.2.7.2 SBO scenario with start of one active emergency core cooling pump

Figure 6-31 to Figure 6-34 show the reactor coolant system response during the PSD650 procedure with later restoration of one diesel and one low pressure injection train. The additional water delivery provides sufficient cooling of the reactor core. The excessive increase in the cladding temperature and consequent later core damage can be avoided.

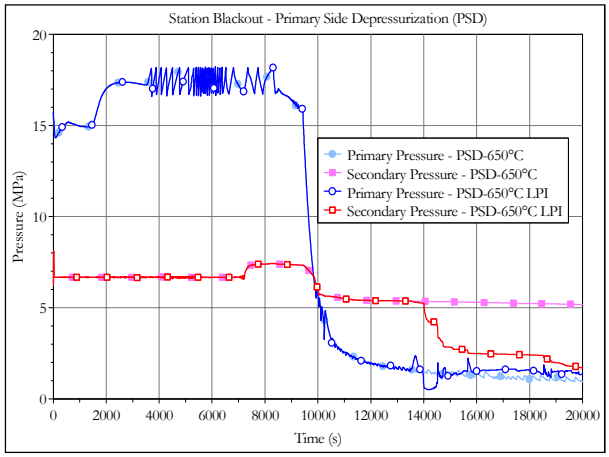

Figure 6-31: Primary and secondary pressure (PSD650 without and with 1LPIP simulation)

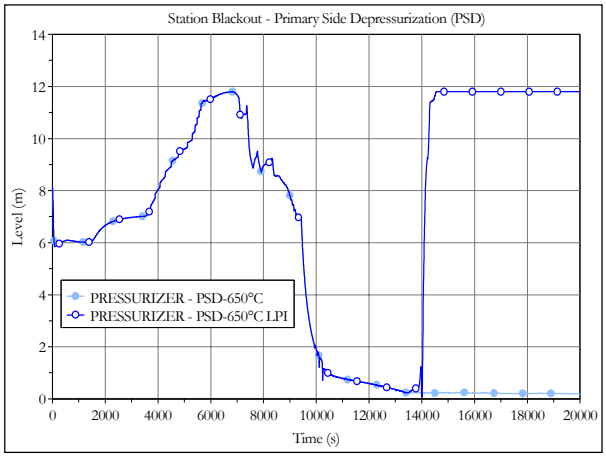

Figure 6-32: Pressurizer level (PSD650 without and with 1LPIP simulation)

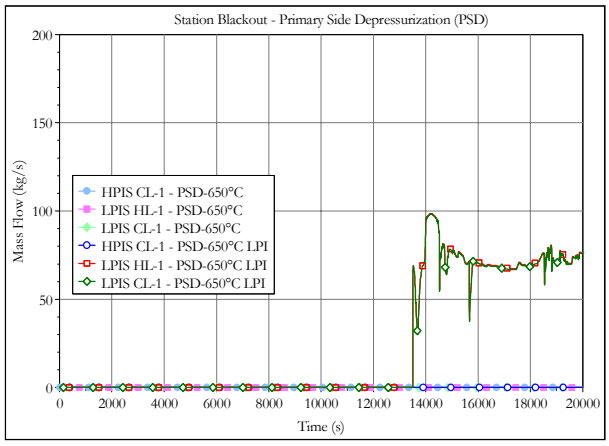

Figure 6-33: Mass flow LPIS (PSD650 without and with 1LPIP simulation

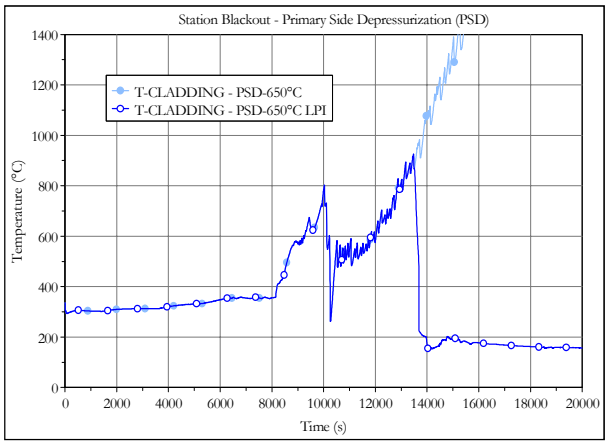

Figure 6-34: Cladding temperatures (PSD650 without and with 1LPIP simulation)

The course of the events before start of one low pressure injection pump (LPIP) is described in Chapter 6, Part 6.2.5 and Part 6.2.7.1. The first peak in the cladding temperature (Figure 6-34) at

t=10000 s from the beginning of the transient simulation is mitigated by the injection from the hydro-accumulators. As there is no additional water supply later on, the core starts to heat-up again and the fuel and cladding temperatures continue to increase.

By means of the PSD the start of the extended core dry-out can be delayed, but if there is no water delivery from active ECCSs to the reactor, the core will start to melt. It has to be pointed out, that for preventing severe core damage a recovery of the electricity supply as early as possible and the start of active ECCSs is an essential requirement.

It is postulated that after three hours and forty-five minutes (t=13500 s) from the beginning of the transient (as latest possible time for preventing a severe accident) one train of the low pressure injection system will be recovered and will start injecting borated water with maximum mass flow rate of approximately ~ 100 kg/s into the hot and the cold leg of loop 1 (Figure 6-33).

At approximately t=14500 s the feeding with the available LPIS has filled up the pressurizer (Figure 6-32). Due to the LPIS injection the steam on primary side is partially condensed and caused by a reversed heat transfer in the steam generators the secondary pressure starts to decrease (cool-down of secondary side, Figure 6-31).

From Figure 6-34 can be seen that with restoration of one LPIS train the excessive heating-up of the core will be avoided and the safety criteria for the peak cladding temperature are kept.

6.2.8 Summary of the main results of the SBO simulations

The analyses of in-vessel phase of hypothetical SBO severe accident sequence in a nuclear power plant with a VVER-1000 reactor with the integral computer code ASTEC have shown that in case that no accident management measures are performed, like depressurization of the primary circuit, the vessel will fail under high pressure. The depressurization of the primary side would delay the failure of the RPV, as slowing the core damage would allow more time for systems to be recovered to mitigate or terminate the accident. This would give more time and different possibilities for operator interventions e.g. joining a train of the ECCS in case that electrical power supply is available or providing additional power supply by mobile diesel generators and mobile pumps for feeding the reactor coolant system, or initiation of measures for flooding the reactor cavity /TUS 2008/, /TUS 2009/.

The ASTEC simulations without and with PSD have shown, that with primary side depressurization and feeding from the hydro-accumulators the time for lower head vessel failure can be delayed by 1.5 hours. The comparative simulations with ASTEC and ATHLET for the SBO scenario with PSD applied as an accident management measure predict a time margin for the operators of at least 2.6 hours between the initiating event and the activation of the PSD procedure. The time margin to final core heat-up is calculated by ASTEC as 2 hours and 26 minutes against 3 hours and 12 minutes in the ATHLET simulation. For the case that no accident management measures have been applied, from ATHLET core heat-up is predicted already at 2 hours and 17 minutes /TUS 2010b/, whereas the ASTEC simulations without and with PSD show no difference for the time margin till core heat-up. The course of the primary pressure and the time margins for ASTEC and ATHLET simulations are summarized in the

upper and respectively lower part of Figure 6-35. The ASTEC results are valid up to failure of the RPV and the ATHLET results up to the time when cladding temperatures exceed 1200 °C. The comparative simulations with PSD applied at $T_{core\text{-}out}$>650 °C show, that feeding from the hydro-accumulators lowers the core and cladding temperatures for a limited period of time, but without additional measures (e.g. recovery of electricity supply and start of active safety injection) a further core heat-up can not be avoided.

The ATHLET code simulations for PSD applied at different core outlet temperatures have shown, that with starting PSD later in time (temperature criterion of 650 °C) the effectiveness of the accumulator injection is lower. With both temperature criteria (350 °C and 650 °C) the critical limit of 1200 °C for the cladding temperatures is reached at approximately the same time, 14500 s – 15000 s (3.9 – 4 hours). PSD with start of one LPIS train after 3 hours and 45 minutes at the latest would avoid the excessive heating-up of the core.

The ATHLET code simulations for SSD have shown that with the reduction of the secondary pressure and the passive feeding from the feedwater system, the time for steam generators depletion is significantly delayed. Also because of the enhanced primary to secondary heat transfer, after starting SSD, there is an effective reduction of the primary pressure. The assumption, that after two hours the BRU-A valves fail in closed position, leads to an activation of the PSD, because after closing BRU-As the primary pressure starts to increase again. SSD combined with PSD after failure of BRU-A (SSD-Case1) will delay the extended heating-up of the core until approximately 22720 s (6.3 hours) after initiation of the transient and the critical limit of 1200 °C for the cladding temperatures is reached at approximately 24500 s (6.8 hours). With full opening of two BRU-A valves up to the end of the transient (SSD-Case2), SSD is more effective and the primary pressure remains below the set-point of the pressurizer relief valve for a much longer time. After the depletion of the feedwater tanks and pipelines, the decreasing steam generator levels and the reduced primary to secondary heat transfer lead to an increasing primary pressure.

By manual opening of the BRU-A valves and a more effective (passive) feedwater injection, the initiation of PSD can be delayed by additional 5 hours (compared to the simulation with BRU-A valves closed after batteries' depletion).

The effectiveness of passive feeding after depressurization strongly depends on the ability to inject as much water as possible into the reactor coolant system. Due to reversed heat transfer in the steam generators or caused by the depressurization itself a part of the injected water can be evaporated, thus reducing the effectiveness of the feed procedures. Caused by flashing in the feedwater system, after the SSD, the feeding procedure can be periodically interrupted.

The performed investigations demonstrate the applicability of SSD and PSD as accident management measures in the preventive domain. Based on the ATHLET simulations described in Chapter 6, Parts 6.2.5 - 6.2.7, the lower part of Figure 6-35 summarizes the time margins for the operators before the corresponding accident management procedures have to be initiated, as well as the remaining time before the final core heat-up takes place. The results are relevant up to heating up of the reactor core with cladding temperatures of approx. 1200 °C. By applying PSD

as the first accident management procedure, an extended core heat-up can be delayed by 3 hours 40 minutes for the first criterion ($T_{core-out}$>350 °C) and 3 hours 12 minutes for the second criterion ($T_{core-out}$>650 °C) respectively. With SSD initiated 30 minutes after SBO as the first accident management procedure, an early mass loss from the primary side can be avoided. Due to the effective reduction of the primary pressure after SSD (Figure 6-35) the criteria for initiating PSD are reached much later in time. With the assumption that after 2 hours BRU-A valves fail in closed position (SSD-Case1), the final core heat-up occurs at 6 hours 19 minutes after SBO. By manual opening of two BRU-A valves (SSD-Case2), the final core heat-up can be delayed until 9 hours 46 minutes after SBO (for the 2nd simulation activation of PSD is not considered).

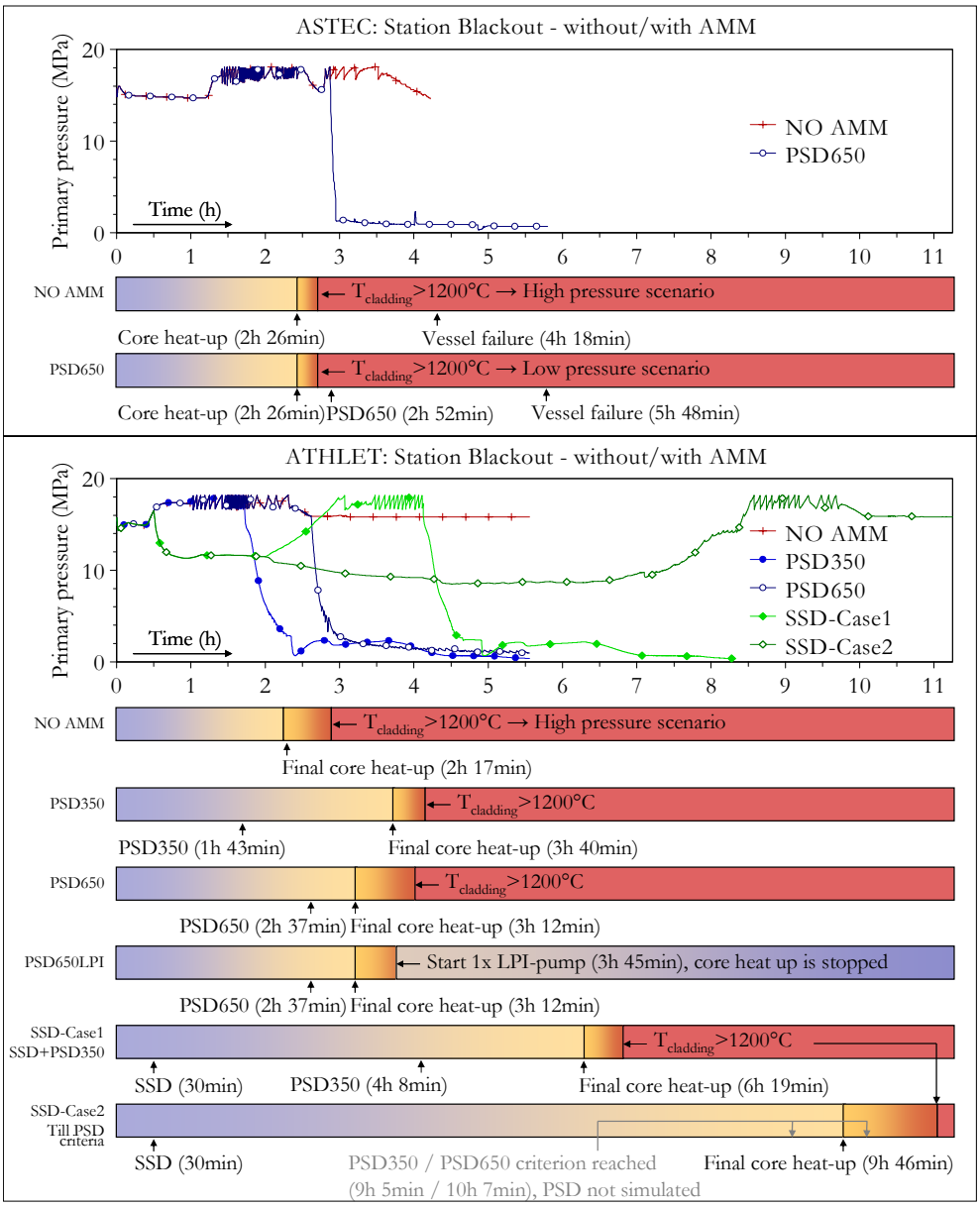

Figure 6-35: Course of the primary pressure and time margins for the operators – NO AMM and PSD650 simulations with ASTEC (upper part); NO AMM, PSD350, PSD650, SSD-Case1 and SSD-Case2 calculated with ATHLET (lower part)

The initiation of the PSD at the latest possible time after the SSD would give the operators an additional time margin to restore electric power supply and to start an active ECC pump. With start of one active ECC pump at the latest possible time after PSD, the safety functions important to prevent core damage are preserved.

If SSD and PSD are not successful as accident management measures or if after applying the accident management measures in the preventive domain the core starts to heat-up again and electrical power supply is not available, severe core damage can not be avoided. To keep the integrity of the RPV after start of core meltdown, an additional severe accident management strategy can be applied e.g. in-vessel melt retention (IVR) by ex-vessel cooling (EVC). In Chapter 7 for a hypothetical station blackout scenario the applicability and the effectiveness of ex-vessel cooling is investigated.

The uncertainties, regarding the simulations with ASTEC and ATHLET, and having influence on the calculated results concern the estimation of the pressure losses in the circuit, the estimation of the form loss coefficients with respect to the nuclear power plant, the pressure losses in the lines between the hydro-accumulators and the RPV and especially the difficulties in the modelling of the hydro-accumulators' injection. The predicted time margins after SSD mainly depends on the effectiveness of the passive feeding procedure, which can be influenced by evaporation, flashing and mass oscillations in the feedwater system. To assess the behaviour during secondary bleed and feed procedures and the corresponding time margins for a specific plant, the geometry of the feedwater system including the mass and temperature distribution within the system have to be modelled as correct as possible.

The main thermal-hydraulic phenomena as well as the main physical events of a severe accident sequence are simulated by the ASTEC code. The capability of the code has been demonstrated in the code-to-code comparison with the mechanistic code ATHLET. Part of the differences between the codes comes from the difficulties in the unification and consistency of the input decks, due to the very heavy task on such complex reactor input decks.

Improvement of the primary to secondary heat exchanges (steam generator modelling) in the ASTEC code, as well as of the numerical robustness of the code is needed to cover the various thermal-hydraulic phenomena.

A specific management of time step was necessary for accounting the intense hydro-accumulator injection after primary circuit depressurisation. The ASTEC computing time is globally around real accident time.

7 Investigations on the late in-vessel phase of severe accident for VVER-1000

This Chapter focuses on investigations on the late in-vessel phase of a severe SBO accident and the possibilities for severe accident management during the late in-vessel core melt processes. As a late phase severe accident management strategy, the in-vessel melt retention (IVR) by external cooling (EVC) of the reactor pressure vessel (RPV) is analysed. The investigations are based on two different melt pool configurations: homogeneous melt pool and segregated melt pool. Thermal and structural analyses have been conducted with the Finite Element code ANSYS /ANS 2001/, /ANS 2002/, /ANS 2003/. The investigations have been done on the basis and as a continuation and extension of previous work performed at HZDR /ALT 2005/, /WIL 2005/, /ALT 2008/.

7.1 Severe accident management procedures related to the late in-vessel phase

In a hypothetical severe accident the materials in the reactor core might melt and slump downwards from the reactor core region to the distributor grids in the reactor pressure vessel and in the later in-vessel stage of a severe accident - to the lower head of the reactor vessel. There a molten pool (corium) consisting of relocated materials might form. The major energy source to be removed is the decay heat in the pool. The decay heat generated in the melt pool is transported to the reactor pressure vessel wall and to the upper part of the vessel. The heat transport to the lateral wall is by natural convection and to the inner part of the vessel by radiation through the melt surface. The reactor pressure vessel is the last barrier to the melt release to the containment.

The late in-vessel phase of a severe accident can be characterized by two "accident exit paths":

- Failure of the reactor pressure vessel caused by the thermal, mechanical or chemical load of the corium pool on the reactor pressure vessel wall. Afterwards the molten mass relocates to the lower cavity and the load is concentrated on the containment structures.

For assessment of the load to the containment important parameters are the time till vessel failure, the load caused failure of the vessel, reactor system pressure at the moment of the reactor pressure vessel failure (high pressure or low pressure scenario, Chapter 6), the breach location and size

- To keep as long as possible the last barrier of the melt release to the containment intact, focus is given on the retention of the molten materials within the vessel (IVR). A possible way is to flood the reactor cavity (Appendix F). Investigated is if by cooling of the reactor pressure vessel from outside, the significant energy caused by the decay heat of the molten pool could be successfully removed through the vessel wall. In this case important parameters are if sufficient water cooling of the outside reactor pressure vessel wall can be realized, the heat transfer from the melt pool-to the vessel wall-to the water from outside.

Development and implementation of severe accident management guidelines (SAMG) is applied practice in many NPPs. Objective of the SAMG is prevention or mitigation of severe accidents by keeping the reactor pressure vessel integrity and reducing the load to the containment. The in-vessel melt retention by ex-vessel cooling concept has already been approved by the Finnish Regulatory Agency (STUK) to be a part of the severe accident management procedures for the Loviisa NPP, Finland, with a VVER-440 reactor /KYM 1997/. Besides its feasibility for such smaller power reactors, the concept is also investigated for some GEN III and advanced light water reactors with higher core power, such as the Westinghouse AP-1000. By applying the strategy of in-vessel retention of corium, the possible fuel-coolant interaction in the reactor cavity and thus the pressure loads in the cavity could be avoided.

When the adopted strategy for managing the severe accident is external cooling of the vessel, water must be supplied to the reactor cavity. The means like availability of power supply, equipment availability like pumps, path for water delivery, for realization of the external flooding strategy should be also defined. The heat flux from the melt pool to the vessel wall should be kept below the critical heat flux (CHF) on the outer surface (Appendix E). The outer surface wall temperature should be kept near the saturation temperature of water, so that sufficient cooling of the vessel could be provided.

Up to the moment the in-vessel melt retention by external cooling of the reactor pressure vessel is not considered as a SAM strategy for VVER-1000 reactors.

7.2 Thermal-hydraulic parameters related to the late in-vessel phase

From accident analyses point of view main events, which could lead to vessel failure are: station blackout (SBO), anticipated transients without SCRAM (ATWS) and loss of coolant accident (LOCA). Important thermal-hydraulic parameters are:

- Pressure

The reactor coolant system pressure prior to the failure of the reactor pressure vessel determines the internal load over the vessel and respectively to the containment. If the vessel fails under high pressure, the load on the containment will be also high due to the high-pressure melt ejection effects. The system pressure depends on one side on the reactor design and from other side on the accident scenario and the phenomena occurring during the accident (e.g. mass loss through breaks and valves, heat transfer from primary to secondary side)

During a SBO without accident management measures applied, and in case of unavailability of the diesel generators, the vessel is predicted to fail under high pressure. The reactor system pressure at the time of the vessel failure strongly depends on the capacity of the pressurizer relief and safety valves.

- Power level

For the analysed severe accident sequence SBO, Chapter 6, full reactor power level is chosen. These initial conditions provide high temperatures, higher hydrogen production rates, the release of fission products occurs at high power rates

- Water level (inventory)

The presence of water influences the way energy is exchanged in the late in-vessel phase of a severe accident i.e. the core damage progression

- Lower head thermal history

During core degradation molten materials slump into the lower vessel head with much higher temperature than the temperature of the vessel wall, which is initially cool. This will cause additional thermal and mechanical stresses on the reactor pressure vessel wall

- State of the molten pool

The quantity of the heat transferred from the molten pool to the reactor vessel wall is dependent on the decay heat of the pool related to the fission products retained in the corium, the composition of the pool and the configuration of the pool.

For the performed analyses below about the investigated SBO event it was assumed that the primary circuit of the reactor system is depressurized by opening the primary side safety valves (the pressurizer valves), Chapter 6. Assumed is also that the investigations start from fully developed molten corium pool in the lower head of the reactor pressure vessel.

7.3 Molten pool behaviour

A crucial question regarding the feasibility of the IVR is whether all the decay heat can be transferred through the vessel wall into the water in the reactor cavity. The heat flux distribution from the molten corium to the RPV wall is therefore of great importance.

After slumping of molten core material into the reactor pressure vessel lower plenum, the molten pool could be considered either as a homogeneous mixture or as stratified pool containing oxidic

and metallic components, with oxide layer situated at the bottom and metallic layer settling on the top.

A homogeneous corium pool might form in air-steam atmosphere conditions /BEC 2008/, for example when water is injected into the vessel by means of active or passive safety systems during the process of core degradation. The heat transfer in the pool is governed by turbulent natural convection, which is characterized by the internal Rayleigh number (Ra'). The internal Rayleigh number is a function of the decay heat generation, the properties of the corium melt and the height of the corium melt relocated into the lower plenum. The values are around 10^{16} /KOL 1996/, /THF 1996/, /THF 1997b/.

Stratified molten pool might form due to density differences of the relocated materials (Figure 7-1). The stratified pool formation depends on the progression of the accident scenario, the physical phenomena arising during the core degradation, the physical and chemical interactions into the core and the pool. Two characteristic layers will form: oxide layer and metal layer. The metallic layer consists of light molten metal components. With the time progression each layer will be cooled and a solid crust might form along the vessel wall and at the contact surface molten oxide/metal /ASF 1996/. The heat generation is mainly concentrated at the oxidic part of the pool. In the metallic layer, the heat generation basically depends on redistribution of the fission products. Regarding that, the main heat source for the metal layer is due to the heat coming from the underlaying oxide layer. The heat removal from the upper surface of the metal layer is through radiative heat transfer and through conduction to the vessel wall.

A matter of debate is the question whether the metal layer on top of the oxidic pool causes a so called focussing effect, i.e. the concentration of the heat flow through the reactor pressure vessel wall in the vertical position of the metal layer. Moreover, the influence of the thickness of this metal layer on the peak heat flux has to be investigated.

The thermal-fluid dynamics in molten pools is either done by numerical simulations applying CFD codes on the basis of FEM, or by simplified models based on experimental correlations e.g. effective conduction-convection model /WIL 2005/. Predictions on the basis of computer codes are limited from the uncertainty of the implemented models and at the same time from the limited data, with which these models could be verified and validated. The problems related to the corium behaviour are focused on the liquid/solid phase transition modelling, whether stratification of the corium will occur, heat transfer, properties of the materials and temperature dependent physical properties of the materials.

ASTEC thermal-hydraulic analyses have been performed to obtain boundary conditions such as event timing of full molten pool formation, initial pool and reactor pressure vessel wall temperatures (Chapter 6, Appendix D, Appendix E). Important issues considered in performing thermal and mechanical analysis of the molten pool behaviour and the behaviour of the reactor pressure vessel are the geometry of the lower plenum, the thickness of the lower head (reactor type specific), the decay heat generation rate, the state of the molten pool, the material composition of the melt, the characteristics of the melt, the temperature range, the heat fluxes and the pressure load on the vessel needed to induce failure. When temperature and stress level

in a significant portion of the vessel lower head wall exceed a certain limit, the lower head may fail immediately by ultimate strength failure or over time by global rupture /ALT 2005/, /WIL 2005/.

In this work, the late in-vessel phase of a VVER-1000 reactor SBO accident, applying external cooling of the RPV wall as mitigative severe accident management measure (SAMM), is investigated /TUS 2010a/. The study is based on the FEM computer code ANSYS, accounting the temperature distribution in the vessel lower head as well as the mechanical behaviour of the reactor pressure vessel wall.

For the heat transfer analyses an axisymmetric model of the relocated corium and the vessel has been built. The thermal model considers a corium bed composed primarily of UO_2, ZrO_2 and stainless steel. Two configurations have been analysed: a homogeneous pool and a stratified pool.

The natural convection phenomena are described by the Grashof (Gr), Prandtl (Pr) and in case of internal heating, by the Damköhler (Da) numbers, as /VDI 2002/:

$$Gr = \frac{g \cdot \beta \cdot \Delta T \cdot H^3}{\nu^2} \quad \text{(Eq. 7.1)}$$

$$\mathrm{Pr} = \frac{\nu}{\alpha} \quad \text{(Eq. 7.2)}$$

$$Da = \frac{\dot{q}_v \cdot H^2}{\lambda \cdot \Delta T} \quad \text{(Eq. 7.3)}$$

The ratio between the buoyant forces and the viscous forces within a fluid (described by the Gr number) multiplied with the ratio of convective and conduction heat transfer (described by the Pr number) is the so called Rayleigh number. In case that the liquid volume is heated externally, this number is called "external" Rayleigh number and usually is denoted by Ra. If the heating is caused by internal heat sources (decay heat), this number is called "internal" or "modified" Rayleigh number.

These two dimensionless numbers are defined as:

$$Ra = \frac{g \cdot \beta \cdot \Delta T \cdot H^3}{\alpha \cdot \nu} \quad \text{(Eq. 7.4)}$$

$$Ra' = \frac{g \cdot \beta \cdot \dot{q}_v \cdot H^5}{\alpha \cdot \nu \cdot \lambda} \quad \text{(Eq. 7.5)}$$

where:

g - acceleration due to gravity, [m/s^2]

β - coefficient of thermal expansion, [1/K]

ΔT - temperature difference between bulk liquid and boundary, [K]

H - characteristic length, [m]

$\dot{q}_v$ - volumetric heat generation, [W/m^3]

α - thermal diffusivity, [m^2/s]

ν - kinematic viscosity, [m^2/s]

λ - thermal conductivity, [W/m·K]

The heat transfer is characterized by the Nusselt number:

$$Nu = f(Gr \cdot \mathrm{Pr}) \qquad \text{(Eq. 7.6)}$$

7.3.1 Heat transfer from the molten oxidic pool

For the oxide layer with internal heat sources the energy balance equation could be written as:

$$\frac{\lambda}{H_{ol,t}} \cdot \Delta T_{ol,\max} \cdot \left(Nu_{up,ol} \cdot S_{up,ol} \cdot \frac{H_{ol}}{H_{ol,TML}} + Nu_{dn,ol} \cdot S_{dn,ol} \right) = q_v \cdot V \qquad \text{(Eq. 7.7)}$$

Here q_v is the volumetric heat, $Nu_{ol,up}$ and $Nu_{ol,dn}$ are the average values of the Nusselt-numbers for the melt pool surface ($S_{up,ol}$) and the side surface ($S_{dn,ol}$), λ is the thermal conductivity coefficient for the oxide pool, H_{ol} - is the total height of the oxide layer and $H_{ol,TML}$ - is the height of the turbulent mixing zone of the oxide layer.

The melt pool is described by the following characteristic numbers:

- The Prandtl-number is calculated as:

$$\mathrm{Pr}_n = \frac{\eta_0 \cdot c_{p,0}}{\lambda} \qquad \text{(Eq. 7.8)}$$

- The main parameter that governs the free convection in the molten oxidic layer is the internal Rayleigh number. It is calculated as:

$$Ra_{i,ol} = \frac{g_0 \cdot \beta \cdot \dot{q}_{gen,0} \cdot H^5 \cdot \rho_0^2 \cdot c_{p,0}}{\eta_0 \cdot \lambda^2} \qquad \text{(Eq. 7.9)}$$

- The average Nusselt number in the upward direction can be expressed with equation according to the Bernaz correlation /BER 1998/, /WIL 2005/ as:

$$Nu_{up,ol} = 0.382 \cdot Ra_{i,ol}^{0.233} \qquad \text{(Eq. 7.10)}$$

- The down Nusselt-number is calculated according to the Bernaz correlation /BER 1998/, /WIL 2005/ as:

$$Nu_{dn,ol} = 2.202 \cdot Ra_{i,ol}^{0.174} \qquad \text{(Eq. 7.11)}$$

- The modified conductivity in vertical direction is described as:

$$\lambda_{eff,ol} = Nu_{up,ol} \cdot \lambda \qquad \text{(Eq. 7.12)}$$

7.3.2 Heat transfer from the molten metallic pool

For part of the ANSYS simulations it has been assumed that stratification takes place and the molten metal will be situated in the upper part of the corium pool. Contrary to the oxide layer, which contains almost all of the decay heat generated into the corium pool, the metallic layer contains only a very small part of it /REM 1997/, /SEH 2005/. For the segregated pool simulations this small part is neglected and it is assumed that the molten metal has no internal heat generation, but it is heated by the oxide corium pool from below. Considering this assumption only the external Rayleigh-number (Ra_e) will play a role in description of the natural convection heat transfer processes. The metal layer is cooled from the top and also from the side. For this investigation appropriate empirical correlations derived on the basis of infinite layers available in the literature are applied.

The ANSYS model for determination of the heat fluxes through the metallic layer is the following:

- The height of the metal layer in ANSYS is described as:

$$H_{met} = YMELT - YMXOX \qquad \text{(Eq. 7.13)},$$

where H_{met} stays for the height of the metal layer, YMELT is the total height of the molten pool and YMXOX is the height of the oxide pool.

The following correlations have been applied:

- The nominal heat conductivity is applied according to /BEC 2008/ equal to:

$$\lambda_{met,0} = 40 \frac{W}{m \cdot K} \qquad \text{(Eq. 7.14)}$$

- The dynamic viscosity is applied according to /BEC 2008/ equal to:

$$\eta_{met} = 3.3 \cdot 10^{-3}\, Pa \cdot s \qquad \text{(Eq. 7.15)}$$

- The Prandtl-number is calculated as:

$$\mathrm{Pr}_{met} = \frac{\eta_{met} \cdot c_{p,met}}{\lambda_{met,0}} \qquad \text{(Eq. 7.16)}$$

- The external Rayleigh-number is calculated as:

$$Ra_{e,met} = \frac{g_0 \cdot \beta \cdot \Delta T_{met} \cdot H_{met}^3 \cdot \rho_{met}^2 \cdot c_{p,met}}{\lambda_{met,0} \cdot \eta_{met}} \qquad \text{(Eq. 7.17)}$$

- The assumed outer surface – bulk temperature difference is /BEC 2008/:

$$\Delta T_{met} = 152 K \qquad \text{(Eq. 7.18)}$$

- The heat flux from the top surface is determined by the Raleigh-Benard convection and is defined by the upper Nusselt-number according to the BALI and COPO II /BON 1998/, /KRE 2008/ experiments:

$$Nu_{up,met} = 0.069 \cdot Ra_{e,met}^{0.333} \cdot \mathrm{Pr}_{met}^{0.074} \qquad \text{(Eq. 7.19)}$$

The range of validity of this correlation is: $3x10^5<Ra<7x10^9$; $0.02<Pr<8750$

- The heat transfer to the vertical RPV wall is defined with the side Nusselt-number according to the Churchill-Chu /CHU 1975/ and the BALI experiment correlation for an isothermal vertical plate and for any Pr and Ra-number less than 10^{12}:

$$Nu_{sd,met} = \frac{0.15 \cdot Ra_{e,met}^{1/3}}{\left[1+\left(\frac{0.492}{\mathrm{Pr}_{met}}\right)^{9/16}\right]^{16/27}} \qquad \text{(Eq. 7.20)}$$

- The modified conductivity in vertical direction is calculated as :

$$\lambda_{eff,met,y} = Nu_{up,met} \cdot \lambda_{met,0} \qquad \text{(Eq. 7.21)}$$

- The modified conductivity in radial direction is calculated as:

$$\lambda_{eff,met,x} = Nu_{sd,met} \cdot \lambda_{met,0} \qquad \text{(Eq. 7.22)}$$

7.4 Thermal ANSYS model

7.4.1 Geometry and elements

In the present work a specific approach has been developed to simulate the late phase of an accident scenario for a VVER-1000 reactor. The studies are focused on the governing physical phenomena in the lower plenum geometry of the reactor pressure vessel.

Due to the heat generation in the corium pool, the reactor pressure vessel lower plenum is a subject of high thermal loads, which could lead to failure of the reactor pressure vessel. The failure of the vessel is a combination of thermal, mechanical and eventually chemical (erosion or corrosion of the reactor pressure vessel wall due to the molten pool) loads. For the simulation and the analyses of the processes in the reactor pressure vessel lower plenum, as a first step, a geometrical model within ANSYS has been built. As programming language for the simulations, the APDL macro-language (ANSYS parametric design language) has been utilized. The whole VVER-1000 vessel has been modelled with its real dimensions. For the thermal analyses the FE-model includes the reactor pressure vessel and the relocated molten corium pool in the lower plenum. Figure 7-1 shows the main VVER-1000 geometry data of the reactor pressure vessel lower plenum. The internal radius of the vessel is 2.068 m, the vessel wall thickness in the cylindrical part of the vessel is 0.2 m. With B_i is defined the inner elliptical radius, with B_e – the external elliptical radius and s – shows the meridian path along the outer vessel wall, starting from the south pole of the reactor pressure vessel bottom.

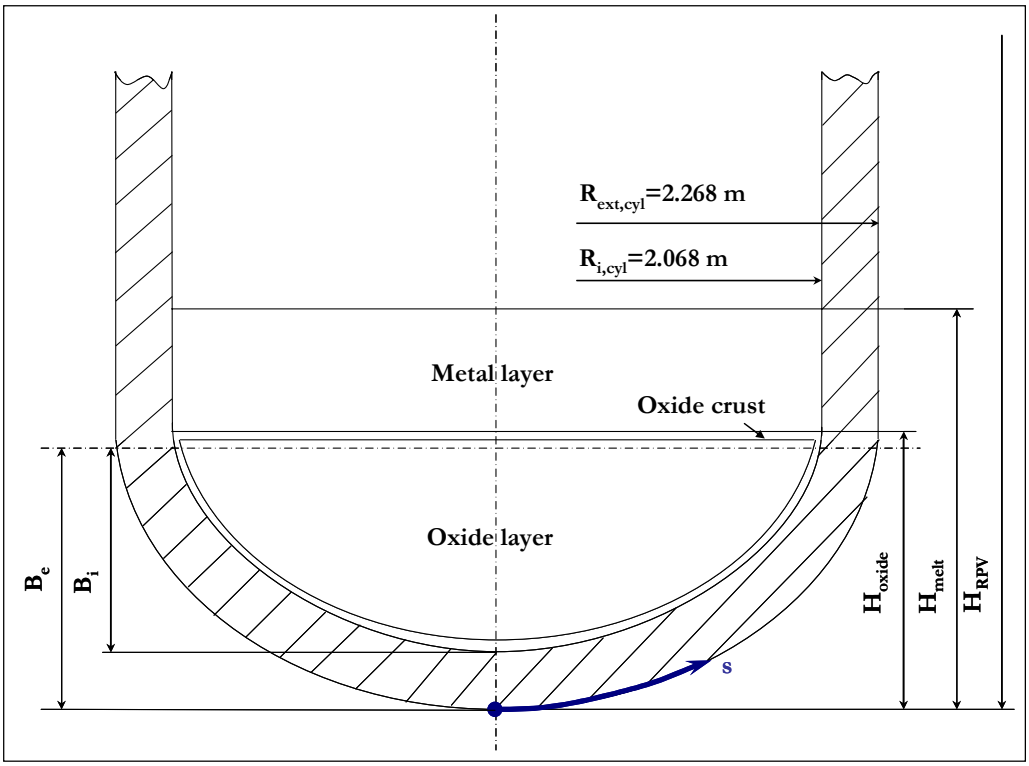

Figure 7-1: General scheme of VVER-1000 lower vessel head

The heat conduction in the area of the reactor pressure vessel wall is calculated with 2D-temperature elements type PLANE55. The area of the molten pool with the internal heat generation is also meshed with 2D thermal elements type PLANE55. The internal heat sources are defined as so called "body force". At the interface between the molten pool and the vessel wall are used contact (CONTA171) and target (TARGE169) elements, which describe the heat transfer between the pool and the vessel wall. The thermal radiation inside the reactor pressure vessel is modelled as a Superelement MATRIX50, which allows the correct representation of the radiation view factors. At the outer vessel surface heat radiation and convection are considered. Since the thermal elements PLANE55 allow only one boundary condition at their free surface, the nodes at the outer surface are additionally meshed with "surface effect elements" SURF151. These elements consider the heat exchange with an environment of constant temperature. In case of a dry environment a convection boundary condition with a fixed heat transfer coefficient and constant ambient temperature is applied. In case of external flooding, a heat flux density depending on the excess temperature is applied. The thermal model is axisymmetric.

Figure 7-2 depicts the geometrical model areas.

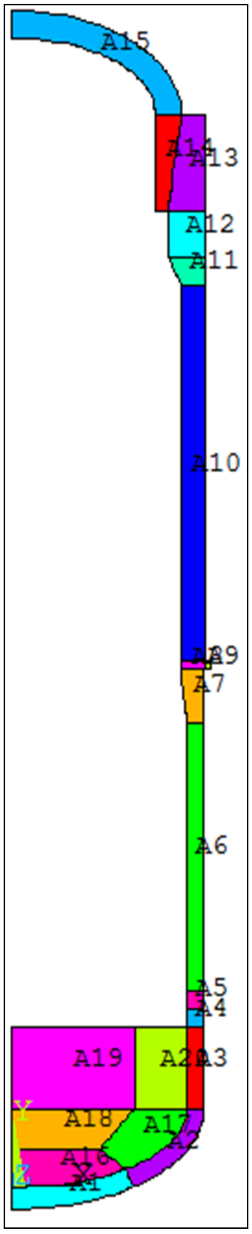

Figure 7-2: ANSYS Solid model areas

7.4.2 Corium composition

The developed model has been applied for simulation of the both homogeneous and stratified melt pools. The boundary conditions as initial corium temperatures, reactor pressure vessel wall temperatures, corium quantity and material properties, necessary for determination of the lower plenum melt pool configuration, are deduced from a thermal-hydraulic simulation of a SBO scenario with depressurization of the primary side, using the integral severe accident code ASTEC (Chapter 6, Part 6.2.5/Appendix C). The simulation has shown that the mass of the relocated corium in the reactor pressure vessel lower plenum is about ~73 t. This pool quantity is additionally increased with ~ 45 t, which describes the mass of the support structures in the lower plenum (the core support thimbles), as this mass has not been taken into account by the summing of the total melted mass in the ASTEC code. The corium thermal properties such as specific heat, density, thermal conductivity, latent heat and viscosity of the corium are calculated on the basis of the corium composition. The structural material thermal properties are considered on the basis of temperature-dependent functions.

Table 7-1 shows the masses of components in a reference VVER-1000 NPP, which are fully or partially involved into the molten pool formation in the lower head of the reactor pressure vessel.

Table 7-1: Reference VVER-1000 NPP Masses of core components and in-vessel structures

Component	Mass, [kg]
Core Parameters	
• Fuel mass	74249.76
• Zr mass (Zr cladding and guide tube)	21650.5
• Steel mass (guide tube, control rod cladding, spacers, core baffle and 6 tubes of the core baffle)	46099.7
Steel mass of lower tail	2963.9
Steel mass of upper tail	4075
Steel in lower plenum	
• Curved part of core basket	11559.07
• Cylindrical part of core basket	5659.489
Core support plate (without the heads of the fuel assemblies)	2360.1
Mass of the curved part of the RPV	37954.8
Core baffle mass	29607
6 tubes mass	868
Total weight of control assemblies	
• Steel mass of Control rod cladding	10990.98
• B_4C mass of Control assemblies	365.39
Mass of the guide tubes	
• Steel mass of guide tubes	3374.589

According to the ASTEC simulation, a fully developed molten pool has formed approximately 17000 s after the beginning of the SBO transient (time after SCRAM). This time is taken as initial time (equal to 0 s) in the ANSYS simulation.

In the ASTEC calculations a segregated molten pool is simulated, which properties are mainly described according to uranium dioxide, zirconium oxide and zirconium dioxide, zirconium and steel. For getting the data for the simulation of a homogeneous pool in ANSYS, the melted pool quantity from ASTEC is additionally oxidized.

7.4.2.1 Homogeneous pool

The total initial melt mass of the homogeneous pool equals approximately to 148 t with total height of the melt pool of 1.76 m. The volume of the melt fills fully the elliptical part of the reactor lower plenum and a melt height of 0.9 m situates in the cylindrical part of the vessel.

Table 7-2 gives a detailed description of the component masses derived from the ASTEC simulation for the homogeneous melt pool configuration.

Table 7-2: Homogeneous melt pool composition

Component	Mass, [kg]
From oxide layer	
UO_2	49772.633
ZrO_2	2579.964
FeO	35.829
NiO	0.553
ZrO	5073.381
Cr_2FeO_4	1.586
Fe_3O_4	3.897
B_4CO	2.408
From debris	
Zr	8.711
UO_2	4857.828
B_4C	876.776
FeO	223.578
NiO	50.582
ZrO	2833.806
ZrO_2	2234.901
Steel	3294.770
BSteel	361.343
Cr_2FeO_4	155.677
Fe_3O_4	14.997
B_4CO	8.286
From metal layer	
Zr	6967.610
B_4C	248.252
Steel	252.958
BSteel	1197.220
Steel (from LSTRUCT)	70781.175
Total	**147953.268**
Volume, [m^3]	**~ 19.872**
H_{melt}=1.76 m	

7.4.2.2 Segregated pool

Table 7-3 gives a detailed description of the component masses derived from the ASTEC simulation for the segregated melt pool configuration.

Table 7-3: Segregated melt pool composition

Component	Mass, [kg]
From oxide layer	
UO_2	49772.633
ZrO_2	2579.964
FeO	35.823
NiO	0.553
ZrO	5073.381
Cr_2FeO_4	1.586
Fe_3O_4	3.897
B_4CO	2.408
From debris	
Zr	6.449
UO_2	972.374
B_4C	679.899
FeO	223.578
NiO	50.582
ZrO	2833.806
ZrO_2	2234.901
Steel	2094.558
BSteel	229.714
Cr_2FeO_4	155.677
Fe_3O_4	14.997
B_4CO	8.286
From metal Layer	
Zr	5158.135
B_4C	192.508
Steel	160.811
BSteel	761.099
Steel (from LSTRUCT)	44997.151
Total	**118244.776**
Volume, [m^3]	**~ 15.409**
H_{melt}=1.43 m	

7.4.3 Initial and boundary conditions

7.4.3.1 Initial temperature

The initial conditions in case of a homogeneous pool are the following:

- Uniform initial temperature distribution for the vessel wall: $T_{wall,init} = 563\ K$
- Uniform initial homogeneous melt pool temperature: $T_{melt,init} = 2050\ K$.

The total relocated corium mass of the segregated pool is approximately ~ 118 t and occupies a volume of 15.4 m^3. For the purpose of this analysis a two-layered stratified molten pool is assumed to develop in the reactor vessel lower head: an oxide layer and a metal layer atop. The configuration assumes that the oxide pool contains all the oxidic core components, and the metal layer contains all unoxidized metallic components. The volume of the oxide pool is 7.73 m^3, which totally fits in the semi-elliptical head of the reactor pressure vessel with a total height of 0.86 m. The volume of the metal layer is approx. 7.68 m^3 with a total height of 0.57 m. A small part of the oxide layer occupies the lower part of the cylindrical bottom, while the metal is totally situated in the cylindrical part of the vessel lower head.

It is assumed that the residual heat is entirely generated in the oxide layer. The molten metal has no internal heat generation, but it is heated by the oxide corium pool from below. According to this configuration, the volumetric heat in the oxide pool is 2.01 MW/m^3. The initial conditions in case of a segregated pool are the following:

- Uniform initial temperature distribution for the vessel wall: $T_{wall,init} = 563\ K$
- Uniform initial segregated melt pool temperature: $T_{melt,init} = 2730\ K$.

7.4.3.2 Radiation and convection at free surfaces

The release of the heat generated in the melt pool is by radiative heat transfer and convection at free surfaces. They are applied as boundary conditions for the ECCM analysis (Chapter 7, Part 7.4.4). Due to the high temperatures the heat transfer processes are governed by radiative transfer, specified inside and outside of the vessel.

The heat transfer due to radiation is determined by the Stefan-Boltzmann law for black body radiation /VDI 2002/:

$$q_{rad} = \sigma_{SB} \cdot \varepsilon \cdot \left(T_s^4 - T_{amb}^4\right) \qquad \text{(Eq. 7.23)}$$

Here σ_{SB}=5.67032·10^{-8} W/m^2K^4 is the black body radiation constant (Stefan-Boltzmann constant), ε is the surface emission coefficient, $0<\varepsilon<1$, T_s is the surface temperature and T_{amb} is the ambient temperature.

The heat transfer by convection at free surfaces is described by:

$$q_{conv} = \alpha \cdot \left(T_s - T_{amb}\right) \qquad \text{(Eq. 7.24)}$$

Here α is the heat transfer coefficient for gases.

It should be noted here that there are existing uncertainties in the calculations concerning the applied emissivity coefficients. The main results, i.e. the top surface temperature of the metallic layer and the maximum sideward heat flux from the metallic layer are closely related to the choice of the emissivity coefficient on the surface of the molten metallic layer and in that way influence the efficiency of the radiation heat transfer. This influence is discussed separately in Chapter 7, Part 7.6. For the basic simulations Chapter 7, Part 7.5, the emissivity coefficient of the internal surfaces is chosen to be equal to a value of 0.3 and for the external surfaces - 0.7.

7.4.3.3 Nukiyama curve

Primary objective of the external vessel cooling concept in case of molten pool formation in the lower plenum of the reactor pressure vessel is to determine whether the calculated heat flux exceeds the heat removal capability (i.e. the critical heat flux, CHF) on the external vessel surface considering the partial melting of the vessel wall. On the contact surface water/vessel wall the heat flux should be kept below the CHF to ensure a sufficiently low temperature of outer wall region and to avoid film boiling at the outer wall surface. Figure 7-3 shows the Nukiyama curve for water at a pressure of 0.1 MPa /VDI 2002/, /WIL 2005/. The Nukiyama curve characterizes the heat transfer from a heated horizontal surface to an upper water volume depending on the temperature difference between wall surface and fluid for different boiling regimes. Up to the point A the heat transfer occurs by forced convection. The A-B region is the nucleate boiling region. The point B with q_{max}=850 kW/m^2 describes the critical heat flux. After reaching the critical heat flux (transition from A to B), the heat transfer from the heated surface to the surrounding fluid can be considerably reduced. The region between point B and point D is an unstable transition region. In this region first the heat flux will be reduced while the wall temperature increases, afterwards the heat transfer increases and stabilizes in the film boiling region at point D with much higher surface temperature. If the CHF is reached and the heat flux is fixed, the heat transfer regime jumps from point B to point D (stable film boiling) and the temperature difference between wall and fluid as well as the surface temperature itself rapidly increases.

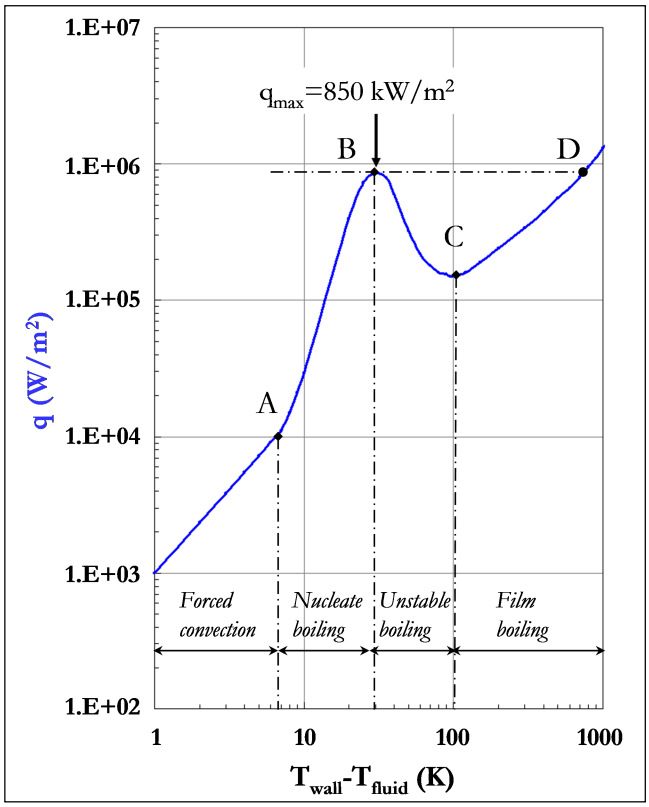

Figure 7-3: The Nukiyama boiling curve for water at 1 bar

If external cooling is applied to an already very hot surface, a transition from point D to point C can be observed. On the

outer surface stable or unstable film boiling with reduced heat transfer capacity from wall to fluid takes place. After cooling down of the heated surface and reaching point C, a transition to the boiling curve between points A and B can occur (rewetting).

For a vertical wall with water in a surrounding cavity, the fluid is heated-up and moving in upward direction, whereas colder fluid is moving down, thereby establishing a circulation and causing an enhanced heat transfer from the wall to the fluid. For that reason the application of the Nukiyama curve for a horizontal surface is a conservative approach to describe the heat flux from the reactor pressure vessel wall into the external water.

7.4.4 Effective material properties

Computational Fluid Dynamic (CFD) simulations require very high computational power, which makes it difficult to perform many variation calculations. A question is the suitability of the available turbulence models in the CFD-codes in case of prototypic scenarios with Rayleigh numbers of up to 10^{14} to 10^{16} /DIN 1997/. For investigation of the melt pool temperature distributions as well as the corresponding heat fluxes from the melt pool to the reactor pressure vessel wall and to the inner area of the vessel, an effective conduction convection model (ECCM), originally developed at KTH Royal Institute of Technology, Sweden, and implemented in ANSYS from FZD /WIL 2005/, /ALT 2008/, has been applied.

The goal of the ECCM is to give a detailed description of the heat transfer processes in the reactor lower plenum and in that way to provide an estimation of the temperature field in a melt pool with internal heat sources. The appliance of effective diffusivity to model heat transfer in a fluid layer is to be found in /CHE 1992/. In /SEH 1999/ is to be found an extension of this concept for generic pool geometries, named ECCM and implemented in MVITA code. Simplified heat transfer models based on ECCM are to be found also in the /DOM 1998/ and /WIL 2005/.

Special attention is given to heat fluxes at the melt region boundaries by applying suitable empirical correlations. The convection is described as a pure heat conduction calculation with an inhomogeneous and anisotropic heat conduction tensor. The volumetric heat generation in the pool is so strong that it is in a state of a turbulent natural convection. In the lower part of the pool there is an almost stagnant region with a downward temperature gradient. A substantial amount of the heat goes upwards and the maximum side heat flow is close to the top and almost no heat at the bottom.

By the ECCM the processes and the phenomena within a hemispherical melt pool are analysed. The corium pool is subdivided into several liquid regions (Figure 7-4):

- Stratified temperature layer (STL)
- Turbulent mixing layer (TML)
- Side-wall boundary layer (SBL).

The stratified temperature region is located in the lower part of the molten pool. It is characterized by an approximately parabolic temperature distribution in the vertical direction

/WIL 2005/. Within this region the melt is slowly rising upwards and heating itself due to the internal heat sources. The relations in the lower part of the pool are influenced by the strong convective movement along the vessel wall. The stream lines of this convection regime continue downwards, parallel to the vessel wall. Due to the flow momentum of the downwards streaming fluid it can penetrate into an environment of lower temperatures and therefore higher density despite its own higher temperatures and lower density. Within the temperature stratified region the melt is slowly rising upwards. While rising the melt is heated-up due to the internal heat sources. This interrelationship is accounted for in the model by anisotropic heat conductivity. This process is correlated indirectly with the down flow at the vessel wall.

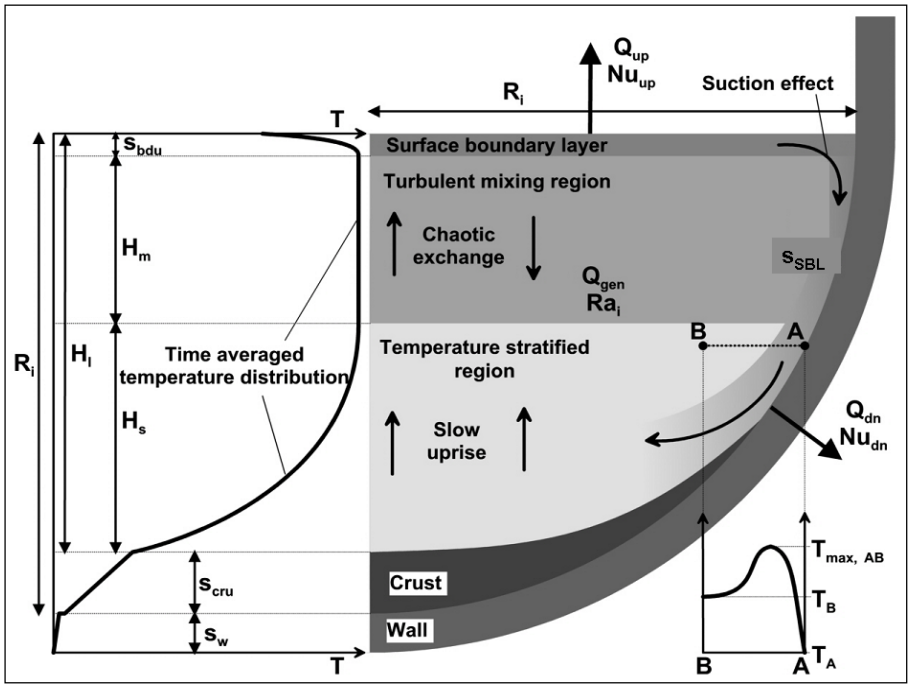

Figure 7-4: ECCM principal scheme of a melt pool with internal heat sources /WIL 2005/, /WIL 2006/

The vertical conductivity in the stratified region refers to the nominal conductivity of the fluid:

$$\lambda_{eff,y}^{STL} = \lambda_0(T) \qquad \text{(Eq. 7.25)}$$

The horizontal conductivity is calculated as:

$$\lambda_{eff,x}^{STL} = \lambda_0(T) \cdot Nu_{dn} \qquad \text{(Eq. 7.26)}$$

The turbulent mixing region is located above the stratified temperature region. According to experimental observations the turbulent mixing region is characterized by homogeneous temperature, if the temperature fluctuations resulting from the falling down cold plumes are averaged over the time. This region is modelled with the approach of Bui /BUI 1998/ with a very high effective conductivity to account for the high turbulent mixing regime. The heat flux

from the upper melt surface is characterized by the Nu_{up} number and the heat flux through the side wall - by the Nu_{dn} number. The Nusselt numbers are expressed by experimentally derived correlations with the Rayleigh number.

The conductivities in horizontal and vertical directions are expressed as:

$$\lambda_{eff,x}^{TML} = \lambda_{eff,y}^{TML} = \lambda_0(T) \cdot Nu_{up} \qquad \text{(Eq. 7.27)}$$

The relations in the lower part of the pool are influenced by the strong convective movement along the vessel wall. The side-wall boundary layer thickness is calculated as a relation between the dimensions of the pool and the Nu_{dn} number:

$$s_{SBL} = \frac{R_i}{Nu_{dn}} \qquad \text{(Eq. 7.28)}$$

The conductivity within the boundary layer corresponds to the nominal temperature dependent conductivity.

This model was further developed for the calculation of the heat transport within the metallic melt. The model includes solidification of the corium (crust formation around the oxidic layer) and vessel melting.

Table 7-4 summarizes the nominal melt properties for the different pool configurations, on which the calculation of the effective properties is based:

Table 7-4: Melt properties for different pool configurations

No	Parameter	Segregated pool		Homogeneous pool
		Oxide layer	Metal layer	
1	Solidus temperature, [K]	2500	1766	1560
2	Liquidus temperature, [K]	2720	1780	2030
3	Density, [kg/m^3]	9692	6619	7593
4	Heat conductivity, [W/(m·K)]	4.0	40	3.5
5	Thermal expansion, [1/K]	$6.5 \cdot 10^{-5}$	$3.2 \cdot 10^{-5}$	$3.2 \cdot 10^{-5}$
6	Dynamic viscosity, [Pa·s]	$4.5 \cdot 10^{-3}$	$3.3 \cdot 10^{-3}$	$4.5 \cdot 10^{-3}$
7	Kinematic viscosity, [m^2/s]	$6.8 \cdot 10^{-7}$	$4.5 \cdot 10^{-7}$	$3.5 \cdot 10^{-6}$
8	Specific heat capacity, [J/(kg·K)]	600	660	720

7.4.5 Internal heat sources. Decay power of the pool

After the reactor SCRAM the decay heat generated from the fission products decreases with the time. The decay power of the molten pool is applied to be lower than the decay heat in an intact core due to volatile fission products, which will be released to the primary circuit and to the containment. This has been taken into account in the estimates. It has been roughly assumed that 80 % of Xe, Kr, I, Br, Cs and Rb are released.

Graphical representation of the decay power and the molten pool power, calculated from approximately ~2.8 h after SCRAM can be seen in Figure 7-5. The decay heat curve (the blue one) is derived from a simulation with the BGCore computer code and is verified against the ANSI-ANS-5.1-2005 Standard /FRI 2008/. The red curve describes the pool power.

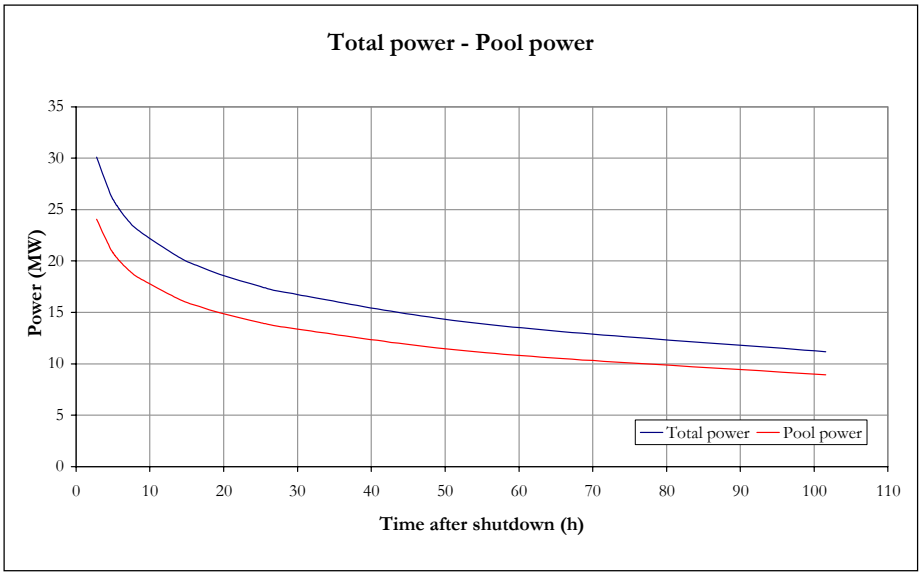

Figure 7-5: Decay heat: reactor - molten pool power as a function of time

7.4.6 Redistribution of the heat from stratified temperature layer (STL) – turbulent mixing layer (TML)

The ECCM is not completely capable of reproducing the temperature distributions in the pool for high Ra_i. Especially for non-spherical pool geometry the maximum temperatures occur at too low positions (in the STL). Therefore it is necessary to introduce additionally an effective heat generation.

According to the made assumption that all the decay power is contained in the oxide layer, the following correlations describe the distribution of the heat:

$$Q_{gen,ox} = Q_{gen,total} \qquad \text{(Eq. 7.29)},$$

where:

$Q_{gen,ox}$ - stands for the generated heat in the oxide layer, MW

$Q_{gen,total}$ - stands for the total heat, MW.

The volumetric heat in the oxide layer q_{ox}^{v} is derived as:

$$q_{ox}^{v} = \frac{Q_{gen,ox}}{V_{ox}} \qquad \text{(Eq. 7.30)},$$

where V_{ox} - stands for the volume of the oxide layer, m^3.

As described in Part 7.4.4, there is an exchange of fluid between TML and STL through the SBL. To evaluate the heat transport, the between TML and STL one has to analyse the temperature profile and the velocity profile near the side. Since the temperature in the SBL is higher than the pool temperature (T_B) in the range directed to the pool centre and lower than T_B close to the side wall, the heat transfer depends on the concrete shape of $v_y(s)$ and T(s). The heat power, which is transported from the STL to the TML (or which is removed from the STL) can be expressed as:

$$Q_{SBL} = \overline{c_p \cdot \dot{m} \cdot \Delta T} = c_p \cdot \rho \cdot 2\pi \cdot (R_i - s_{SBL}) \cdot \int_{s=0}^{s_{SBL}} v_y(s) \cdot (T(s) - T_B) \cdot ds \qquad \text{(Eq. 7.31)},$$

where v_y is positive in upwards direction.

To simplify the evaluation of the integrals, the dimensionless quantities are defined as follows:

$$\xi(s) = \frac{s}{s_{SBL}} \qquad (0 \le \xi \le 1) \qquad \text{(Eq. 7.32)}$$

$$\vartheta(\xi) = \frac{T(s) - T_B}{T_B - T_{liq}} = \frac{T(s) - T_B}{\Delta T} \qquad (-1 \le \vartheta \le 1) \qquad \text{(Eq. 7.33)}$$

$$T(s) = \Delta T \cdot \vartheta(\xi) + T_B \qquad (T_{liq} \le T \le T_{\max}) \qquad \text{(Eq. 7.34)}$$

$$v_y(s) = \hat{v}_y \cdot \psi(\xi) \qquad (0 \le \psi \le 1) \qquad \text{(Eq. 7.35)}$$

with ξ - dimensionless thickness coordinate

ϑ -dimensionless temperature

ψ -dimensionless velocity profile.

In /WIL 2005/ a CFD analysis for the FOREVER test was performed. From this analysis the dimensionless velocity and temperature profiles in the SBL have been extracted at $y=s_{cr}+H_S$ (y=0 at inner south pole). The profiles are shown in Figure 7-6:

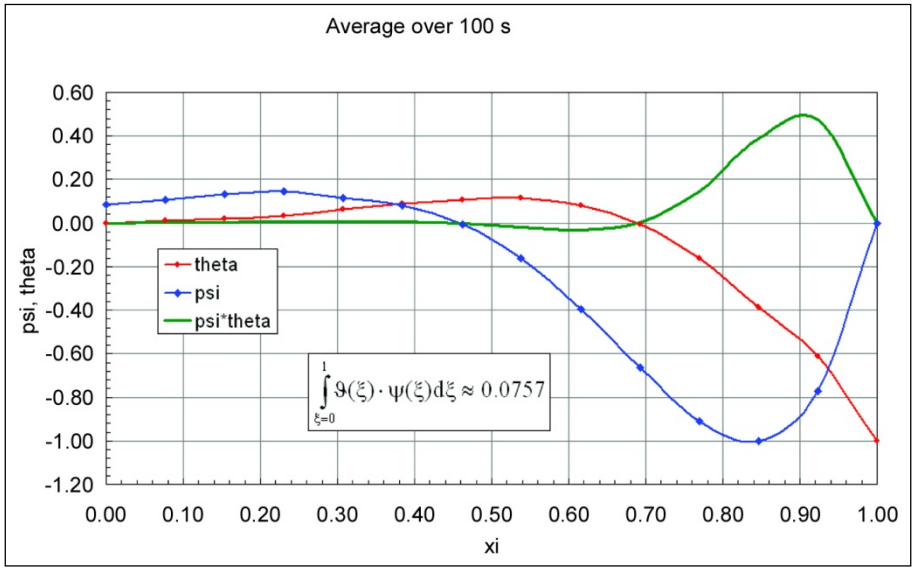

Figure 7-6: Temperature and velocity profile in the side boundary layer obtained from a CFD analysis

The temperature gradient and the average temperature then can be expressed as:

$$\frac{\partial T}{\partial s} = \frac{\Delta T}{s_{SBL}} \cdot \vartheta' \qquad \text{(Eq. 7.36)}$$

$$\bar{T} = \Delta T \cdot \int_0^1 \vartheta(\xi)\, d\xi + T_B \qquad \text{(Eq. 7.37)}$$

The expression for the transported heat Q_{SBL} becomes:

$$Q_{SBL} = c_p \cdot \rho \cdot 2\pi \cdot (R_i - s_{SBL}) \cdot s_{SBL} \cdot \hat{v}_y \cdot \Delta T \cdot \int_{\xi=0}^{1} \psi(\xi) \cdot \vartheta(\xi) d\xi \qquad \text{(Eq. 7.38)}$$

With respect to Figure 7-6 one can obtain:

$$\begin{aligned} Q_{SBL} &= c_p \cdot \rho \cdot 2\pi \cdot (R_i - s_{SBL}) \cdot s_{SBL} \cdot \hat{v}_y \cdot \Delta T \cdot 0.0757 \approx \\ &\approx c_p \cdot \rho \cdot 2\pi \cdot R_i \cdot s_{SBL} \cdot \hat{v}_y \cdot \Delta T \cdot 0.0757 \end{aligned} \qquad \text{(Eq. 7.39)}$$

To keep $Q_{SBL} / V_{STL} > 0$, correction of Q_{SBL} is done:

$$Q_{SBL} = Q_{SBL} \cdot \frac{(1 - V_{ox,cr})}{V_{ox}} \qquad \text{(Eq. 7.40)}$$

$$\text{If } Q_{SBL} \geq Q_{gen,ox} \cdot \frac{V_{ox,STL}}{V_{ox}} \quad \text{then} \quad Q_{SBL} = Q_{gen,ox} \cdot \frac{V_{ox,STL}}{V_{ox}} \qquad \text{(Eq. 7.41)}$$

The effective heat generation rates in the STL and in the TML are calculated as follows:

$$q^{v}_{ox,STL} = q^{v}_{ox} - \frac{Q_{SBL}}{V_{ox,STL}} \quad \text{(Eq. 7.42)}$$

$$q^{v}_{ox,TML} = q^{v}_{ox} + \frac{Q_{SBL}}{V_{ox,TML}} \quad \text{(Eq. 7.43)}$$

The total balance of the heat generation is maintained:

$$Q_{gen} = q^{v}_{ox} \cdot V_{ox,cr} + q^{v}_{ox,STL} \cdot V_{ox,STL} + q^{v}_{ox,TML} \cdot V_{ox,TML} \quad \text{(Eq. 7.44)}$$

The parameters used in the ANSYS model are the following:

- Temperature difference T_{bulk}-T_{liq} for the stratified temperature layer of the oxidic melt:

$$\Delta T = 1000\,K \quad \text{(Eq. 7.45)}$$

- Maximum downward velocity in the side boundary layer according to /HEU 2005/:

$$\hat{v}_y = 0.01 m/s \quad \text{(Eq. 7.46)}$$

- Side boundary layer thickness, referring to Eq.7.28:

$$s_{SBL} = 0.002\,m \quad \text{(Eq. 7.47)}$$

7.4.7 Estimation of the critical outside temperature

For assessment of the reactor pressure vessel failure for the cases without external flooding, an estimation of the critical outside temperature is done.

Assessment of the outer surface heat flux due to radiation:

$$q_{out} \approx \varepsilon \cdot \sigma_{SB} \cdot T^{4}_{out} \quad \text{(Eq. 7.48)}$$

The temperature gradient in the RPV wall according the Fourier's law is:

$$q = -\lambda_{steel} \cdot \nabla T \quad \text{(Eq. 7.49)}$$

As the reactor pressure vessel wall thickness s is small in comparison to the internal radius of the RPV, then the Fourier's law in one dimensional form in direction x can be written as:

$$q_x = -\lambda_{steel} \cdot \frac{dT}{dx} \quad \text{(Eq. 7.50)}$$

Referring to Eq. 7.46 and Eq. 7.48 one can derive:

$$\frac{dT}{dx} = -\frac{q_{out}}{\lambda_{steel}} = -\frac{\varepsilon \cdot \sigma_{SB} \cdot T_{out}^4}{\lambda_{steel}} \qquad \text{(Eq. 7.51)}$$

Estimation of the remaining wall thickness:

The temperature of the outer side of the reactor pressure vessel wall is T_{out}. At the inner side of the vessel wall is always the liquidus temperature of the steel T_{liq}. The thickness of the vessel wall is given by s, respectively the remaining wall thickness is defined as s_{rem}. Then one can derive:

$$\frac{T_{liq} - T_{out}}{s_{rem}} = -\frac{dT}{dx} \qquad \text{(Eq. 7.52)}$$

$$\frac{T_{liq} - T_{out}}{s_{rem}} = \frac{\varepsilon \cdot \sigma_{SB} \cdot T_{out}^4}{\lambda_{steel}} \qquad \text{(Eq. 7.53)}$$

From Eq. 7.53 for s_{rem} is derived:

$$s_{rem} = \frac{T_{liq} - T_{out}}{\varepsilon \cdot \sigma_{SB} \cdot T_{out}^4} \cdot \lambda_{steel} \qquad \text{(Eq. 7.54)}$$

From another side estimation of the wall thickness is required. The forces acting on the body are described with the equivalent stress (Figure 7-7, left side):

$$\sigma_{eqv} = \sqrt{\sigma_{ax}^2 + \sigma_{tg}^2 - \sigma_{ax} \cdot \sigma_{tg}} \qquad \text{(Eq. 7.55)}$$

Here σ_{ax} is the axial stress and σ_{tg} is the tangential stress. They can be expressed as:

$$\sigma_{ax} = \frac{m \cdot g}{2 \cdot \pi \cdot R_i \cdot s_{rem}} + \frac{p_i \cdot R_i}{2 \cdot s_{rem}} \qquad \text{(Eq. 7.56)}$$

$$\sigma_{tg} = \frac{p_i \cdot R_i}{s_{rem}} \qquad \text{(Eq. 7.57)}$$

The $m \cdot g$ component in Eq. 7.56 describes the dead-weight of the vessel and the melt, where m is the mass of the reactor pressure vessel lower plenum and the melt (m=155 t).

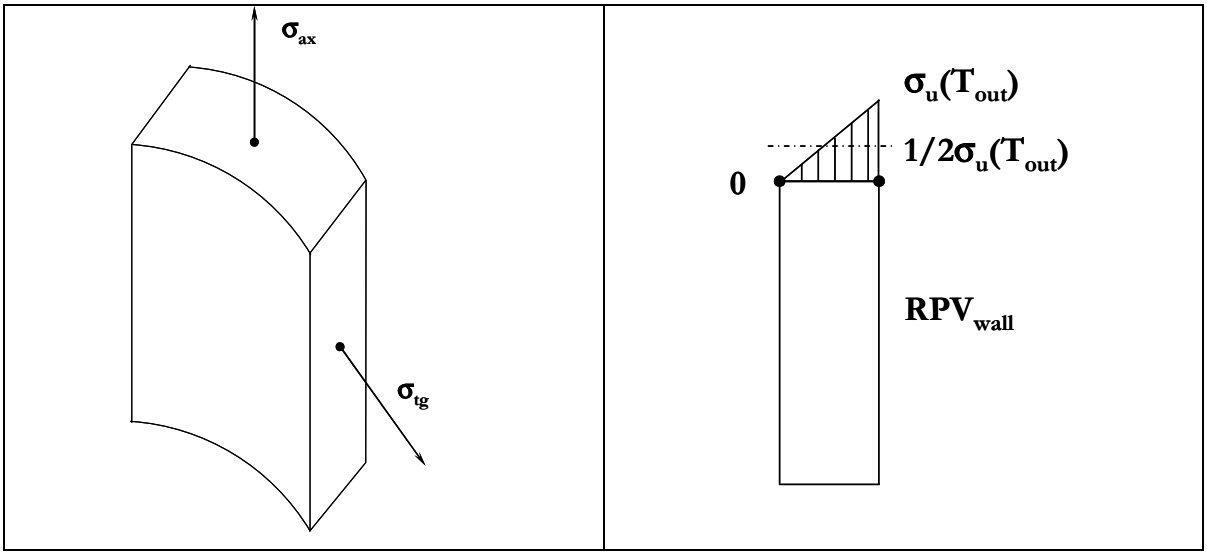

Figure 7-7: Schematic representation of the stresses

At the inner side of the reactor pressure vessel wall the stress is equal to 0 and at the outer side of the wall the stress is the ultimate stress σ_u (Figure 7-7, right side). Then:

$$\frac{1}{2}\cdot\sigma_u\left(T_{out}\right)=\sigma_{eqv} \qquad \text{(Eq. 7.58)}$$

A comparison between the load from the dead-weight and the load from the internal pressure is done. The first component in Eq. 7.56, describing the load from the dead-weight $\frac{m\cdot g}{2\cdot\pi\cdot R_i.s_{rem}} equals\ to\ 5.84\cdot10^5\ Pa$, whereas $\frac{p_i\cdot R_i}{s_{rem}} equals\ to\ 2.59\cdot10^7\ Pa$, which difference is two orders of magnitude. Taking into account this for σ_{eqv} one can write:

$$\sigma_{eqv}\approx\frac{p_i\cdot R_i}{s_{rem}}\cdot\frac{\sqrt{3}}{2} \qquad \text{(Eq. 7.59)}$$

Then from Eq. 7.54 and Eq. 7.59 for $\sigma_u\left(T_{out}\right)$ one can write:

$$\sigma_u\left(T_{out}\right)=\frac{\sqrt{3}\cdot p_i\cdot\pi\cdot R_i^2}{\pi\cdot R_i}\cdot\frac{\varepsilon\cdot\sigma_{SB}\cdot T_{out}^4}{\lambda_{steel}\cdot\left(T_{liq}-T_{out}\right)} \qquad \text{(Eq. 7.60)}$$

The parameters used in Eq. 7.60 are:

- Emissivity $\varepsilon=0.7$
- Stefan-Boltzmann constant $\sigma_{SB}=5.67\cdot10^{-8}\,W/m^2\cdot K^4$
- Internal pressure $p_i=2.5\,MPa$
- RPV internal radius $R_i=2.068\,m$ (Figure 7-1)

- Thermal conductivity of the vessel steel: $\lambda_{steel} = 28 \div 40 W/m \cdot K$, temperature dependent
- Liquidus temperature of the steel $T_{liq} = 1780\,K$.

Figure 7-8 shows the analytical solution of Eq. 7.60 for $\sigma_u\left(T_{out}\right)$, noted as Stress($T_{out}$) in the plot. It represents the outer wall temperature in the outer reactor pressure vessel node. The temperature T_{liq}=1780 K corresponds to the steel melting temperature. From one side on the graph is plotted the stress dependence on the outer wall temperature and from another side the true ultimate stress of the steel depending on the temperature is mapped. The cross section point represents the critical reactor pressure vessel wall temperature, which is applied later for detection of the vessel failure in ANSYS for the cases without external flooding.

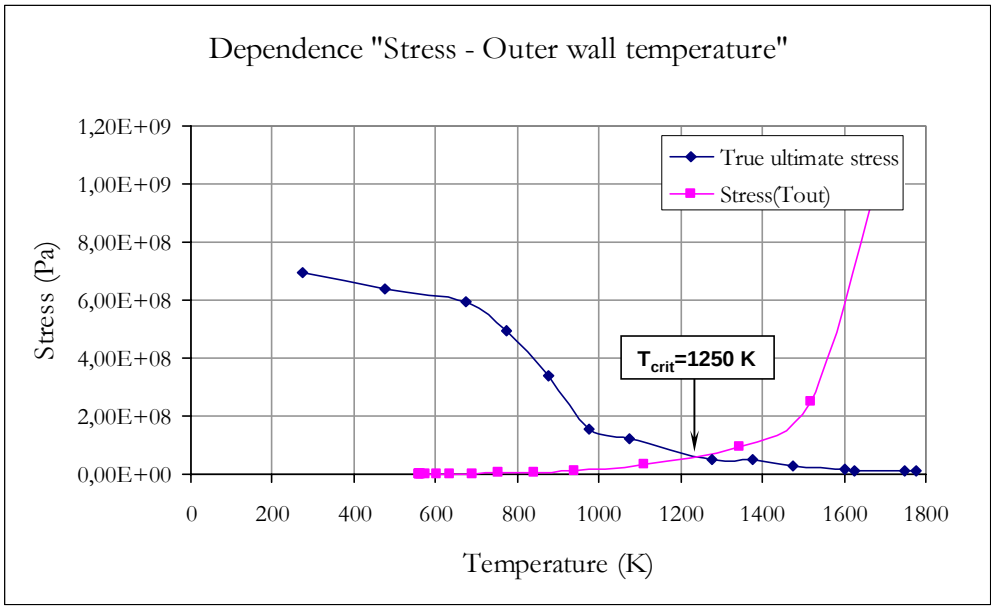

Figure 7-8: Dependence "Stress - Outer wall temperature"

7.5 Results of the ANSYS thermal analysis

7.5.1 Accident scenario 1: Homogeneous melt pool without external flooding

If the melt pool is in contact with the vessel wall the thermal loads from the molten pool on the vessel wall are sufficient to cause failure of the vessel /SARNET 2006/. Without applying any accident management strategies to keep the molten pool in the reactor pressure vessel, thermal failure of the vessel is expected. On the basis of the ANSYS simulation the time margin to vessel failure is assessed.

To consider the convection of the oxidic melt and the heat transfer to the lower head, the vessel wall and the solidified or the liquid melt are simulated with thermal elements. Figure 7-9 shows the geometrical model of the homogeneous melt pool material distribution at the beginning of the simulation.

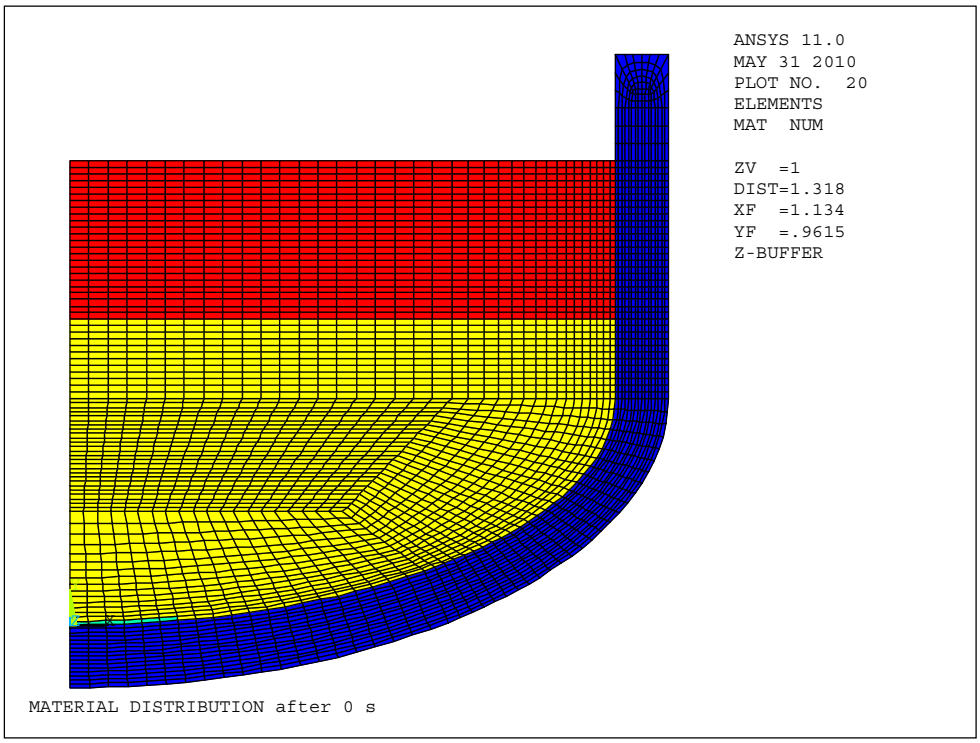

Figure 7-9: ANSYS, Homogeneous pool, Material distribution at 0s, red: TML, yellow: STL, green: crust, blue: RPV wall

The different materials are represented by different colours. The vessel wall (steel) is blue, the yellow region describes the stratified zone, the red area describes the turbulent mixing zone of the model, and the green colour represents the crust.

Since the vessel is at low temperature and a good heat conductor, an insulating crust forms at the lower boundary, which is in direct contact with the vessel wall. The crust thickness depends on the temperature of the corresponding elements in contact. If the temperature of an element lies below the solidus temperature, the material number is automatically changed and the element does not belong anymore to the liquid elements array, but to the solid array elements. In case that the temperature is above the liquidus temperature, the corresponding element is transformed to the liquid elements array.

The thermal calculation starts at 17000 s after the beginning of the SBO scenario. At this time the formation of the molten pool in the lower head is finished and the decay heat is about 21 MW. In Figure 7-10 are depicted the total power and the heat generation areas (Part 7.4.6).

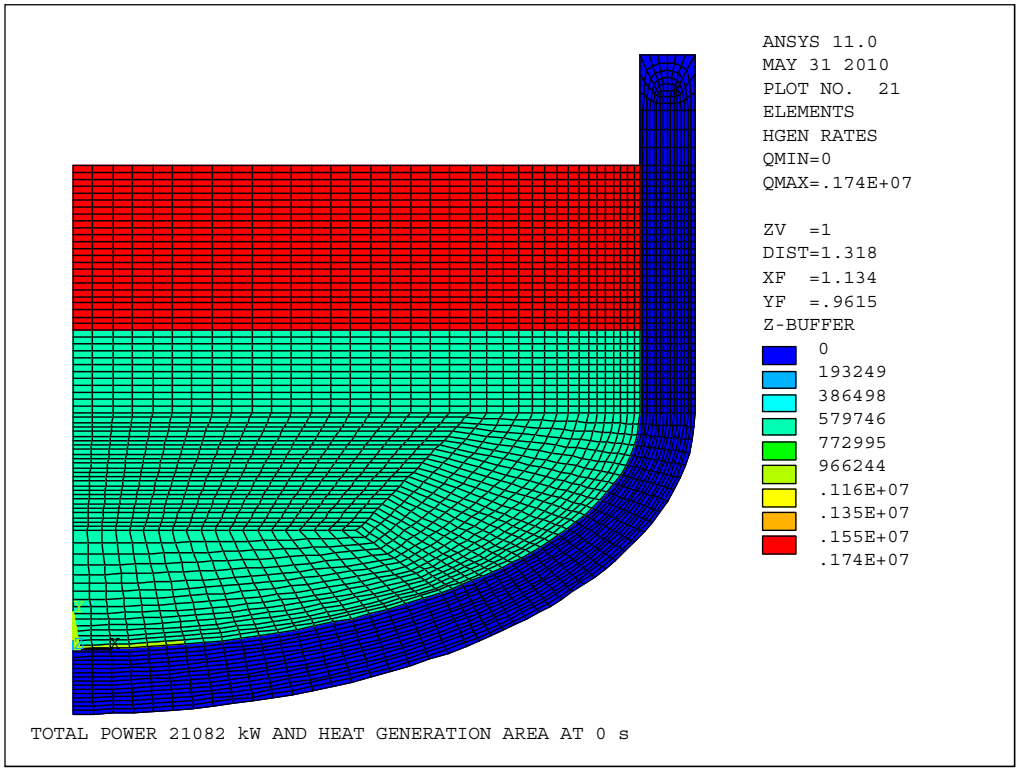

Figure 7-10: ANSYS, Homogeneous pool, Total power and heat generation at 0s, cyan: STL, red: TML, blue: RPV wall

The thermo-dynamical parameters are pointed out below in Table 7-5.

Table 7-5: Homogeneous melt pool thermo-dynamical parameters

No	Parameter	Value
1	Modified conductivity λ_{eff}, [W/(m·K)] (Eq. 7.12)	7566
2	Pr (Eq. 7.8)	0.926
3	Ra_i (Eq. 7.9)	$1.28 \cdot 10^{16}$
4	Nu_{up} (Eq. 7.10)	2162
5	Nu_{dn} (Eq. 7.11)	1397

Figure 7-11 shows the molten pool temperature field distribution for different timings. The total time for the simulation is 4000 s. The material properties are specified according Table 7-4. The vessel wall temperature at t=0 s is around 555 K. In the first steady-state solution step the temperature field is adjusted to the boundary conditions. The heat that is transferred from the molten pool to the vessel causes heating-up of the vessel wall and reduction of the mechanical strength of the vessel material. Consequently the reactor pressure vessel lower head exposes significant thermal and pressure loadings. Due to the high temperature difference between the outer vessel wall and the melt pool, a high temperature gradient from the pool to the wall is observed. The vessel wall temperatures initially increase slowly (Figure 7-11) and later on faster because of the increased effective conductivity. A crust is formed between the pool and the vessel wall, which serves as a temporary isolation from the higher corium temperatures for the vessel wall. If more heat it added than removed, the crust is shrinking consistent with the conservation of energy. The temperature of the outer vessel wall is increasing to critical limits of the material strength and leading to deterioration of the structural stability of the material itself.

The elements, which exceed the melting temperature of steel (1780 K) are removed (i.e. the material properties of those elements are switched: very high heat conductivity, very low density and specific heat capacity).

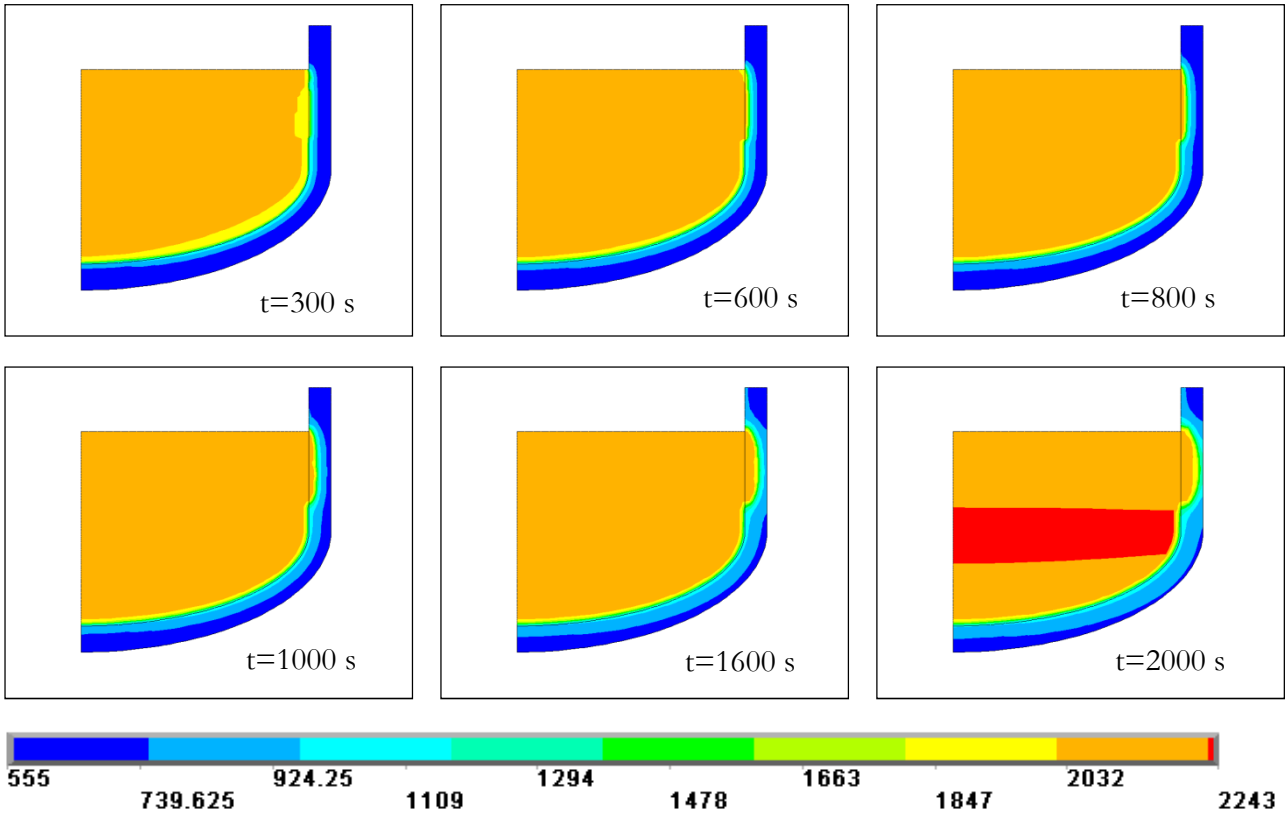

Figure 7-11: ANSYS, Homogeneous pool, no EVC, Temperature distribution

The released energy from the reactor pressure vessel is only due to heat radiation and natural convection with the surrounding air. With the accident progression the highest pool temperatures are observed in the upper part of the temperature stratified region. As the pool temperature increases, the heat flux from the pool to the vessel increases too. The top of the homogeneous pool is cooled by radiative exchange with the air above the pool.

The results of the analysis indicate vessel failure time of 2010 s from fully developed molten pool. In Figure 7-12 are depicted the outer surface temperatures at different meridian positions. Position y=1.76 m indicates the maximum height of the melt pool y=0.858 m indicates the transition zone between the elliptical and the cylindrical part of the vessel lower head and y=1.4 m corresponds to 0.36 m below the melt surface. T_crit indicates the vertical coordinate from the vessel wall, where the temperature of the material has reached 1250 K (critical temperature, Chapter 7, Part 7.4.7).

As no cooling of the outer reactor pressure vessel wall is provided, the vessel wall fails due to the extremely high thermal loads. The pressure and the initial boundary conditions have the greatest effect on the failure time.

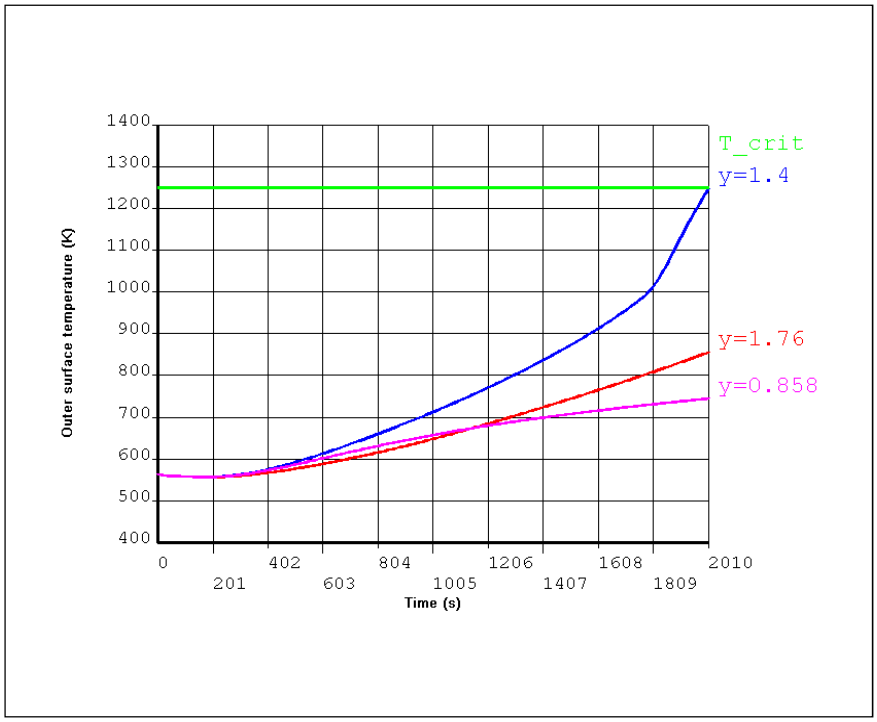

Figure 7-12: ANSYS, Homogeneous pool, Outer surface temperature at different vertical positions

7.5.2 Accident scenario 2: Homogeneous melt pool with external flooding

For this analysis it has been assumed that the reactor vessel wall is externally cooled by water. Necessary condition for keeping efficient heat transfer on the external surface of the reactor pressure vessel is that the boiling crisis will be avoided and the heat transfer mode remains in subcooled single-phase convection or nucleate boiling mode. The purpose of the external cooling is to keep the outside wall cool and thus to prevent its failure and retain the melt inside. Efficient heat removal from the vessel wall to the flooded reactor cavity and respectively to the containment should be established.

For the simulation of the external flooding the Nukiyama curve (Figure 7-3), which characterizes the heat transfer from a heated horizontal plane to an upper water layer depending on the temperature difference T_{wall}-T_{water}, has been applied.

In this variant with cavity flooding the simulation has been performed for 8.3 h from the formation of the molten pool in the reactor pressure vessel lower plenum, in order to demonstrate the localization and the stabilization of the corium inside the reactor vessel. Figure 7-13 shows the temperature distribution in the corium pool. 2000 s after the beginning of the simulation, the maximum pool temperature is around 2285 K and continuously increasing to 2867 K at 10000 s.

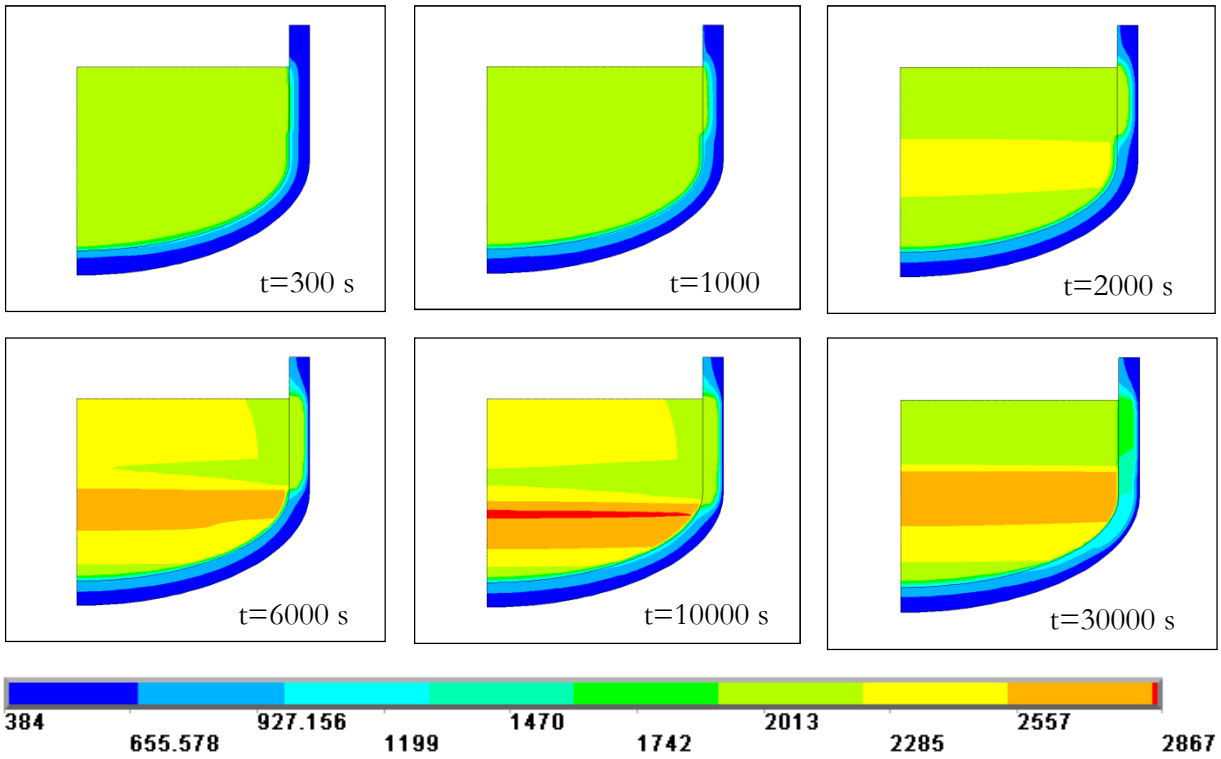

Figure 7-13: ANSYS, Homogeneous pool, with EVC, Temperature distribution

With increasing wall temperature, bubbly regime forms at the heated wall. The liquid close to the wall is set into motion. The result of this is that on one hand this regime promotes heat transfer from the wall to the liquid. On the other hand the vapour serves as insulation between the wall and the liquid. In that case the heat transfer is limited, determined by the vapour amount (big vapour amount – limited heat transfer). With continuous increasing of the wall temperature the insulating effect of the vapour dominates and so despite the rising temperatures the heat flux decreases /BAE 2006/. The thickness of the vessel wall is determined by the heat flux coming imposed from the molten pool. At the same time the thinning of the vessel wall is limited by the presence of water outside. The heat flow rate to the surrounding water is larger than the generated heat rate.

Figure 7-14 shows the outer vessel surface heat fluxes along the meridian line starting from the vessel south pole to the melt pool surface for different timings: 300 s, 1000 s, 2000 s, 6000 s, 10000 s and 30000 s (also Figure 7-1). The heat fluxes to the vessel wall from a volumetrically heated oxidized pool vary with angle change. Near the base of the hemisphere, the heat fluxes are considerably smaller than in the upper part of the melt. This is in agreement with the measured data of the COPO experiment (Rayleigh numbers of 10^{14}-10^{15}) /HEL 1997/, which have shown that the heat flux is extremely low at the bottom part of the vessel and rises with increase of the azimuthal angle along the vessel head.

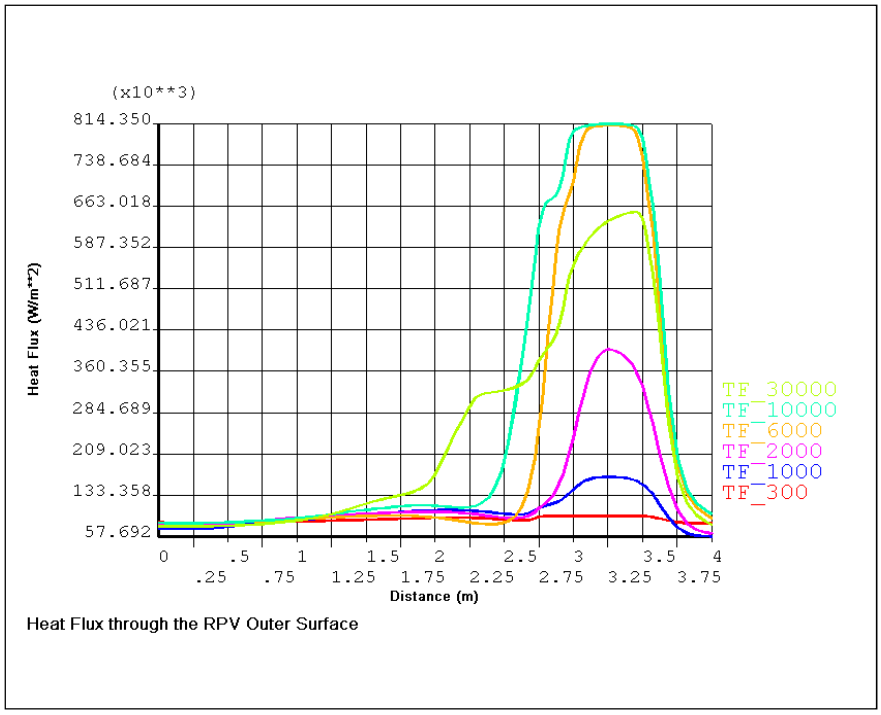

Figure 7-14: ANSYS, Homogeneous pool, with EVC, Heat flux through the RPV outer surface

TF-100: Heat flux at t=300 s *TF-600: Heat flux at t=1600 s* *TF-1000: Heat flux at t=3000 s*

TF-1600: Heat flux at t=6000 s *TF-2000: Heat flux at t=10000 s* *TF-3000: Heat flux at t=30000 s*

The maximum thermal load on the reactor wall was predicted at about 1.7 h from the beginning of the simulation with decreasing tendency later on consistent with the decreasing of the decay heat. At that time the maximum heat flux value is about 814 kW/m^2, which is below the CHF (Figure 7-3).

In Figure 7-15 are depicted the corresponding integral heat flows, which form the overall heat balance, where: HGEN is the generated heat in the pool (pool decay heat), PMSF is the released heat through the melt pool surface (top pool surface), POUTUP is the heat released from the upper part of the reactor pressure vessel (only this part of the vessel, which is situated above the molten pool in the vessel lower head) and POUTLP stands for the heat released from the pool (only the reactor pressure vessel lower plenum part), which is transferred to the water outside.

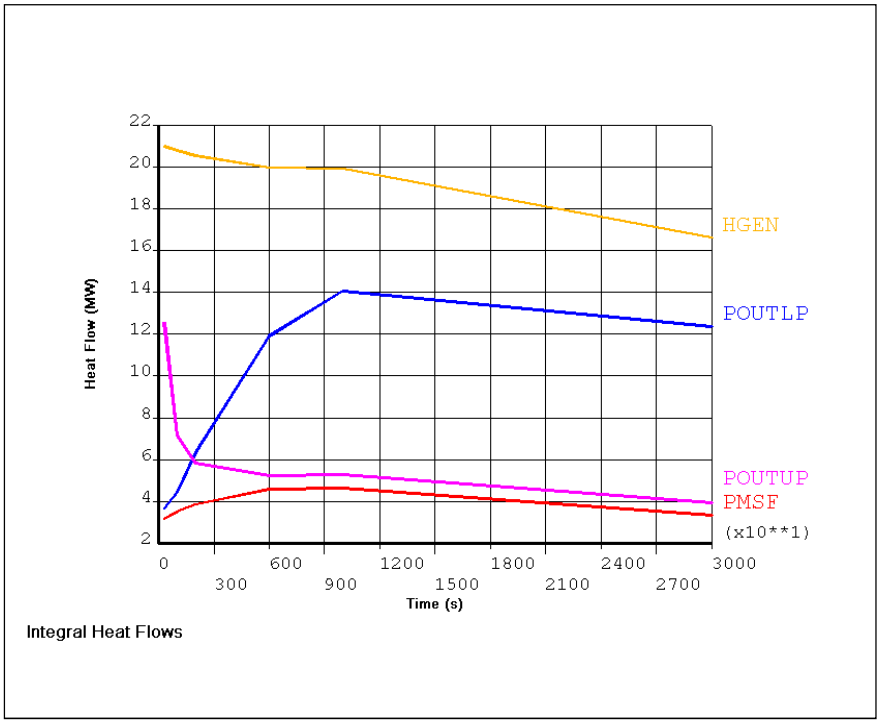

Figure 7-15: ANSYS, Homogeneous pool, with EVC, Integral heat flows

Figure 7-16 shows the outer vessel temperatures. As it can be seen the temperature at the outer surface is varying between 384 K – 402 K, remaining much below 1250 K (Chapter 7, Part 7.4.7) throughout the whole transient. The peak vessel temperatures are predicted to occur at the surface/vessel wall interface. The thermal analyses with the FE-model have shown that the reactor pressure vessel wall is not fully melted. It could be seen that in the area of the hot focus ¼ of the vessel wall has a temperature below the melting temperature of the steel. In spite of the remaining vessel wall thickness, if no cooling is provided, the vessel will fail due to the high thermal loads.

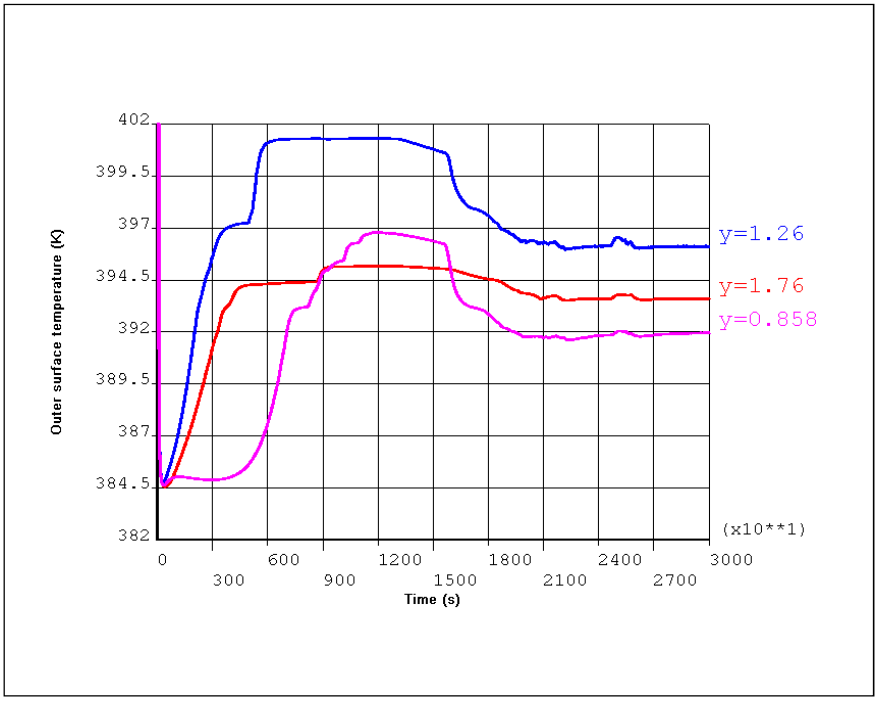

Figure 7-16: ANSYS, Homogeneous pool, with EVC, Outer surface temperature

7.5.3 Accident scenario 3: Segregated melt pool without external flooding

For this investigated scenario it is assumed that the relocated in the reactor pressure vessel lower head molten materials are separated due to their density differences and have formed a two-layered metal/oxide stratified pool. The oxidic layer is a mixture of uranium oxide and zirconium oxide and is heavier than metallic layer composed of steel and zirconium. In that way the oxide layer occupies the lower part of the molten pool and the metal layer is situated above the oxide layer. The oxidic pool is bounded thermally and fluid-dynamically by a crust. The decay heat generated from the molten pool is transferred to the vessel wall and upper structures in the reactor vessel by natural convection.

The thermal boundary condition of the pool at the beginning of the simulation is specified with constant initial melting temperature for the oxidic and the metal pool. The decay heat is transferred to the side wall (with crust formed around vessel inner surface) and upper interface between oxidic and metallic layer (crust formed between them) /REM 2005/. The heat is transferred from the bottom oxidic layer to the upper metallic layer, as the metal layer is heated from the located below oxide pool. This transferred heat in the metallic pool is removed through side and upper surface by natural convection developed in the pool and radiation with the vessel atmosphere.

Figure 7-17 shows the geometrical model of the segregated melt pool material distribution at the beginning of the simulation.

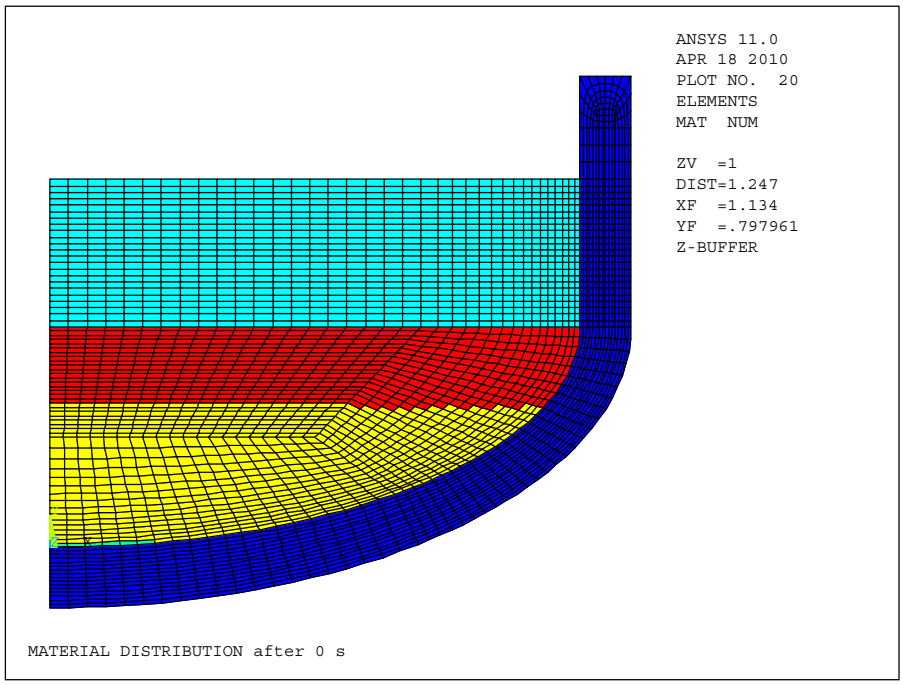

Figure 7-17: ANSYS, Segregated pool, Material distribution at 0s, yellow: STL, red: TML, cyan: metal layer, green: crust, blue: RPV wall

The yellow and red colours show the zones of the oxidic part of the pool (yellow: stratified zone and red: turbulent mixing zone) and the cyan colour depicts the borders of the metallic layer.

Figure 7-18 shows the total power and the distribution of the heat between the pool layers at the beginning of the simulation. The oxide layer contains all the decay power, whilst the metal layer is only heated from the underlying oxide pool.

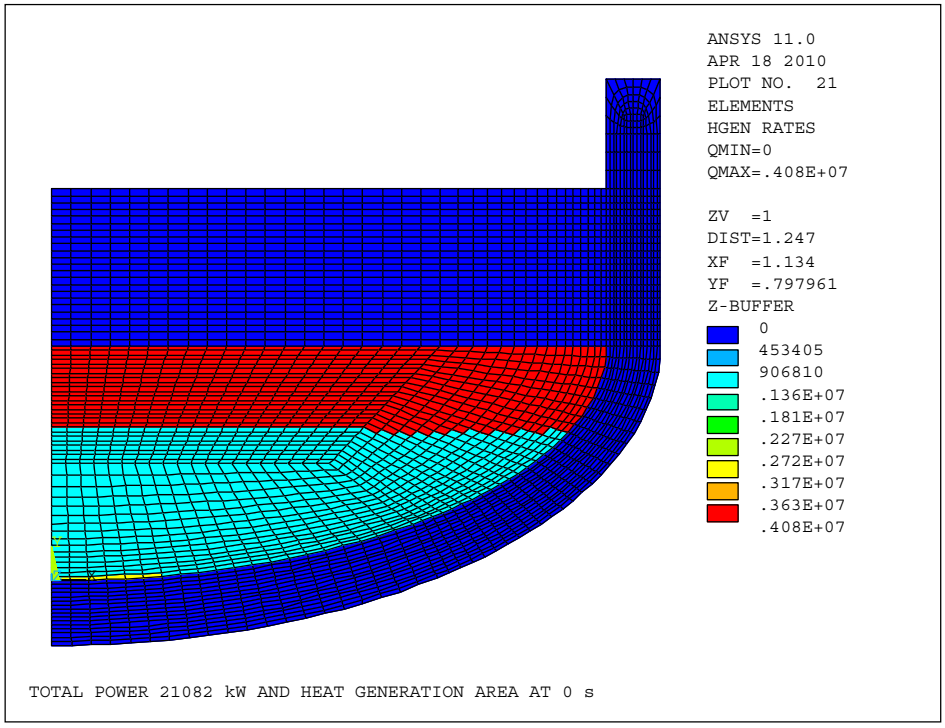

Figure 7-18: ANSYS, Segregated pool, Total power and heat generation at 0s, cyan: STL, red: TML, blue: metal layer and RPV wall

In Table 7-6 are pointed out the thermo-dynamical parameters of the segregated pool.

Table 7-6: Segregated melt pool thermo-dynamical parameters

No	Parameter	Segregated pool	
		Oxide layer	Metal layer
1	Effective conductivity λ_{eff} , [W/(m·K)] (Eq. 7.12/ Eq.7.21/Eq.7.22)	TML: $\lambda_{eff,x} = \lambda_{eff,y} = 4533$ STL: $\lambda_{eff,x} = 4533; \lambda_{eff,y} = 4$	$\lambda_{eff,x} = 4546$ $\lambda_{eff,y} = 4083$
2	Pr (Eq. 7.8/Eq. 7.16)	0.675	$5.445 \cdot 10^{-2}$
3	Nu_{up} (Eq. 7.10/Eq. 7.19)	1133	102
4	Nu_{dn}, $Nu_{sd,metal}$ (Eq. 7.11/Eq. 7.20)	863	114
5	Ra_e (Eq. 7.17)	-	$6.32 \cdot 10^{9}$
6	Ra_i (Eq. 7.9)	$7.99 \cdot 10^{14}$	-
7	Temperature difference, [K]	-	152

The natural convection heat transfer in the oxidic pool is realized with the volumetric heat generation from the decay heat. Some part of the heat is released through the downward surface and the remaining part of the heat is transferred to the upper surface by turbulent natural convection. The upward heat from the oxidic layer is transferred to the lower surface of the metallic layer /REM 2005/. A radiative heat transfer mechanism between melt pool surface and the inner parts of the reactor vessel is envisaged. For the current investigation, a radiative heat transfer boundary condition is imposed on the upper surface of the metallic pool.

The Rayleigh number of the oxidic layer ranges around $Ra_i=6\cdot10^{14}$ (Eq. 7.9) because of the high values of the volumetric heat generation in the pool, which is above 2 MW/m^3. It means that the natural convection in the oxidic layer by decay heat is in highly turbulent regime. The upward heat from the oxidic layer directly affects the natural heat transfer in the metal layer. The calculated Rayleigh number for the metallic layer is around $Ra_e=6\cdot10^9$ (Eq. 7.17). This means that the turbulent natural convection regimes are different in the two layers.

Figure 7-19 depicts the calculated temperature distribution in the segregated pool without cavity flooding for different times.

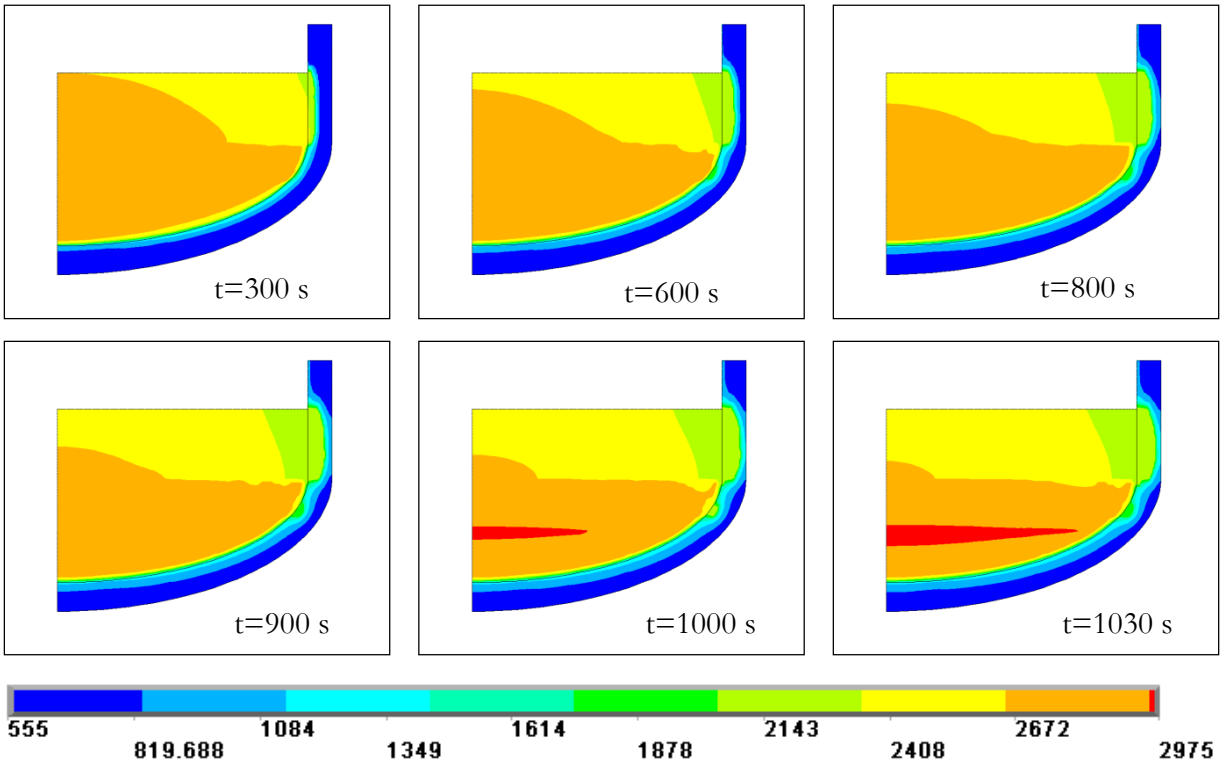

Figure 7-19: ANSYS, Segregated pool, no EVC, Temperature field distribution

At the beginning of the simulation a thermal boundary layer, crust, is developed around the oxidic pool. With the time progression the non-cooled reactor pressure vessel wall starts quickly to heat-up. The maximum pool temperature reaches 2975 K (middle of the oxide pool). The graphical results indicate that the minimum margins-to-failure occur at vessel locations that are in contact with the metallic layer. The vessel wall close to the metal layer undergoes the strongest thermal attack.

Figure 7-20 shows the vessel wall temperatures for different coordinates of the outer vessel wall. Indicated with y=1.43 m is the maximum melt height, y=0.858 m is the transition zone between the elliptical and the vertical part of the vessel and y=1.07 m stands for elevation 0.36 m below the melt pool surface. T_crit indicates the vertical coordinate from the reactor pressure vessel wall, where the temperature of the material has reached 1250 K (Chapter 7, Part 7.4.7). The calculation results indicate vessel failure time of 1040 s from fully developed molten pool. The vessel failure time depends from one side on the applied initial boundary conditions (initial temperatures) for the melt pool, the applied downward velocities in the stratified boundary layer of the oxidic pool, the temperature difference between the bulk and the liquidus temperatures, and from other side as shown in some additional calculations - on the applied time-step of the calculation.

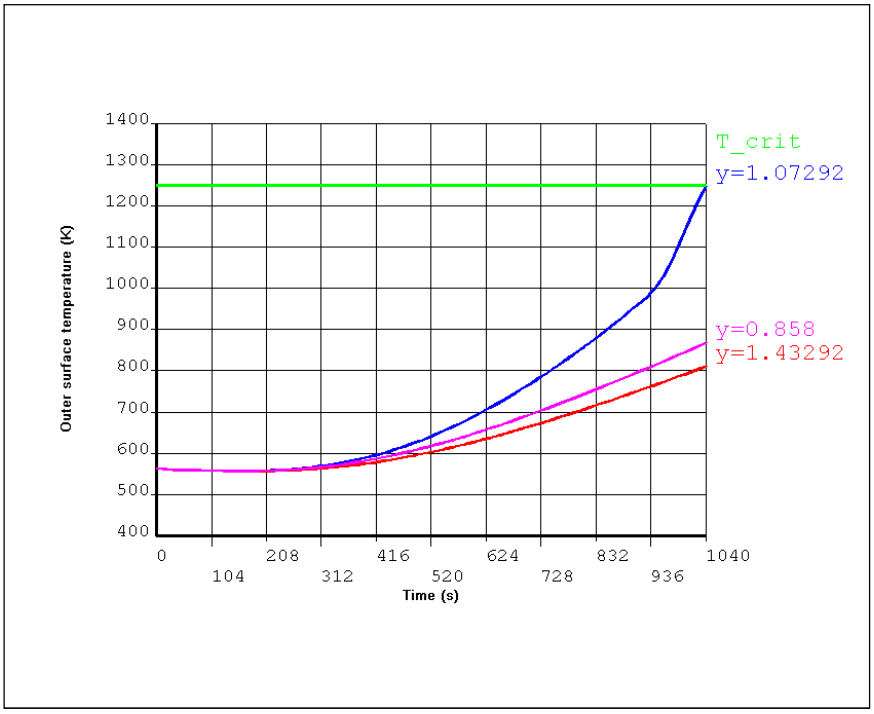

Figure 7-20: ANSYS, Segregated pool, no EVC, Outer surface temperature at different vertical positions

Comparing the results provided by the ASTEC code (failure of the reactor pressure vessel is calculated at 20866 s, Chapter 6), and the time from fully developed molten pool (17000 s ASTEC/0 s in ANSYS), 2826 s is the time difference between ASTEC and ANSYS in prediction of the time for failure of the reactor pressure vessel.

7.5.4 Accident scenario 4: Segregated melt pool with external flooding

For the current scenario an external cooling of the reactor pressure vessel has been applied. It is assumed that the whole reactor pressure vessel is flooded.

The analyses have been performed for a total problem time of 8.3 hours (30000 s) after fully developed molten pool. In Figure 7-21 is shown the temperature distribution in the corium pool for different times of the accident progression. At t=300 s, the vessel wall temperature is 383 K and the maximum pool temperature is 2810 K. Due to the large temperature differences of the melting points between the metal and the oxide, the oxide pool is bounded by a crust that avoids direct contact between the molten oxide and the vessel. The thermal attack of the vessel begins in the cylindrical part of the vessel, where the metal is situated. With the accident progression the temperature of the vessel increases and the vessel wall slowly ablates.

At the same time, the pool temperature is also increasing; the maximum pool temperature is reached in the centre of the oxidic layer. At t=2000 s (Figure 7-21), the maximum pool temperature is 3416 K. In the upper region of the oxide layer and along the inner bottom vessel wall, the pool temperature is approximately 3079 K. Roughly in one hour from the beginning of the transient the vessel reaches a stable thermal solution with minor changes up to the end of the simulation.

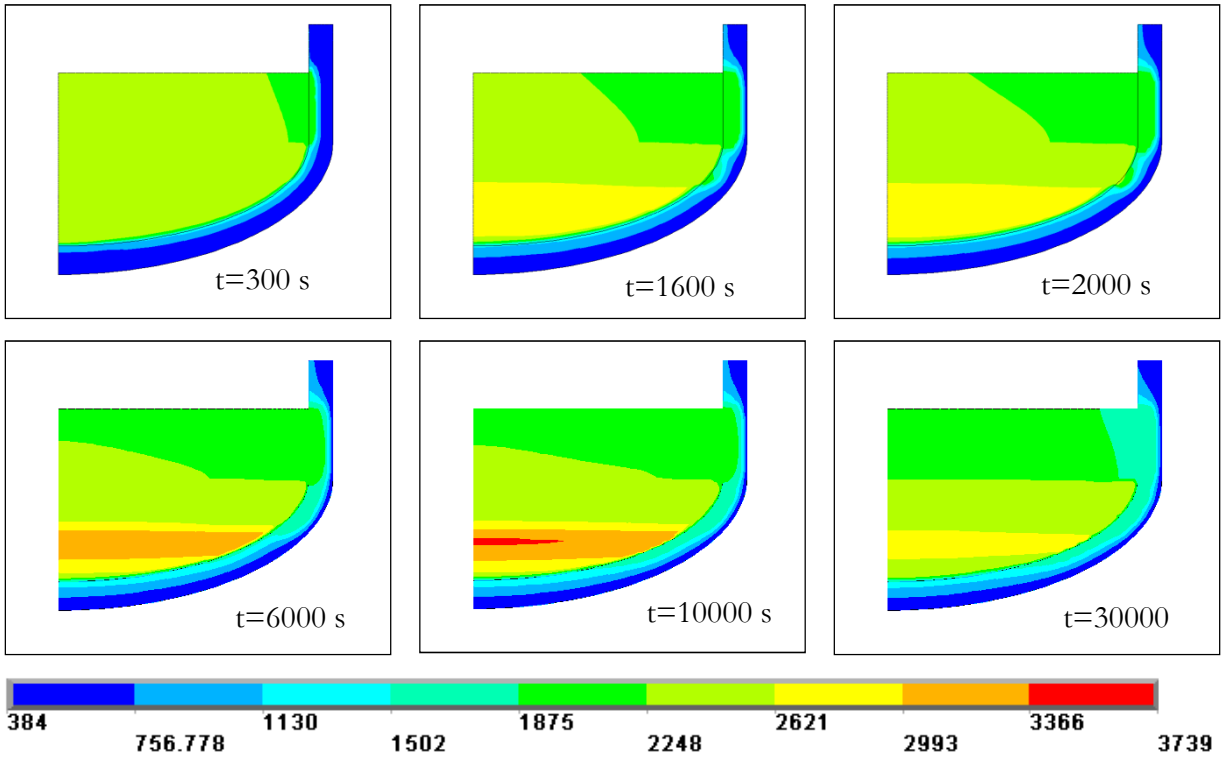

Figure 7-21: ANSYS, Segregated pool, with EVC, Temperature distribution

A maximum pool temperature of 3739 K has been reached at t=10000 s. The high conductivity of the metal and the effective heat transfer from the top reduces significantly the temperature of the metal layer. This reduction in the temperature results in crust formation on the top of the oxidic pool.

The water cooled external surface of the vessel is under nucleate boiling conditions and the outer vessel wall is kept at low temperature. The heat from the molten pool is transferred through the vessel wall and to the water outside. Decrease in the corium and wall temperatures is observed. The melting temperature of the metallic pool of the upper layer is about 1000 K lower than the oxide pool of the lower layer. The strongest thermal loading is in the cylindrical part of the vessel, in the region of the metal layer. The residual thickness of the vessel wall is ≈ 43 mm.

Figure 7-22 depicts the heat flux through the melt pool surface for different timings from the beginning of the simulation: 100 s, 600 s, 1000 s, 1600 s, 2000 s and 3000 s, starting from the vessel axis (distance = 0) to the vessel wall (distance = 2.1 m). Figure 7-23 shows the heat flux from the outer reactor pressure vessel surface into the water for the same above mentioned times. The path is along the vessel meridian starting at the south pole and ending at the top melt surface (also Figure 7-1).

The generated heat is partly transported to the upper region of the vessel by radiation. The radiative heat transfer is a strong function of the surface temperature (T^4). At the early stage (0 - 1000 s), the radiative heat transfer is more effective (Figure 7-22). Later on the most of the heat is released through the vessel wall to the surrounding water (Figure 7-23). The heat transfer from the pool through the vessel wall is compensated from the flooding water outside. Cooling from the top, and at the same time from the side, causes a temperature decrease versus time in the upper pool region (as can be seen from Figure 7-21). The temperature in the middle of the metal layer is around 2742 K.

Although the metal layer has no residual power, the highest thermal attack of the vessel wall is observed in this region. This is due to the low thermal conductivity of the formed crust, which limits the heat flux from the oxide layer towards the vessel. At 1000 s from the beginning of the simulation, the maximum outer heat flux is approximately 532 kW/m^2. For the molten pool configuration considered in this study, the maximum outer surface heat flux is reached at 1600 s and is approximately equal to 833 kW/m^2 (Figure 7-23), with a tendency of decreasing during the accident progression consistent with the decrease of the decay heat. At the time of the peak outer wall heat flux (reached at 1600 s), the ratio between the peak heat flux released through the vessel wall and the maximum heat released through the melt pool surface is around 1.38.

The changes in the heat flux are balanced by the crust thickness. The analyses have shown that the heat flux is very low at the bottom part of the vessel and increases upwards along the reactor pressure vessel wall (Figure 7-23).

Figure 7-24 depicts the overall heat balance, where: HGEN is the generated heat in the pool (pool decay heat), PMSF is the released heat through the melt pool surface (top pool surface), POUTUP is the heat released from the upper part of the reactor pressure vessel (only this part of the vessel, which is situated above the molten pool in the vessel lower head) and POUTLP stands

for the heat released from the pool (only the reactor pressure vessel lower plenum part), which is transferred to the water outside.

In Figure 7-25 are plotted the reactor pressure vessel outer surface temperature, which in direct contact with the water from outside. With position y=1.43 m is shown the full height of the molten pool (oxide layer and metal layer), position y=0.858 m is the transition metal/oxide (coincides with the elliptic bottom part transition to cylindrical part of the reactor pressure vessel lower plenum) and position y=0.93 m corresponds to 0.5 m below the top melt pool surface. One could notice that at the beginning of the simulation the outer vessel wall temperature rapidly increases from 385 K to 400 K. The peak is reached around 1980 s, as later on until the end of the transient (30000 s) the temperature tendency is decreasing. It is obvious that within this temperature range (385 K- 400 K), the outer part of the vessel wall is kept well below the melting temperature of the steel.

For the discussed SBO scenario, the thermal loads from the molten pool in the reactor vessel are below the enhanced CHF on the vessel outer wall. It means that for that severe accident the corium pool in the reactor vessels could be cooled by the external reactor vessel flooding. It is discussed that the SBO accidents are thought to be bounding cases /REM 2005/ for the external vessel cooling. Though the application of the external vessel cooling as accident management measure increases the magnitudes of the heat fluxes, the enhanced subcooling in the current simulation has shown that the thermal loads imposed on the RPV wall from a molten segregated pool could be effectively removed.

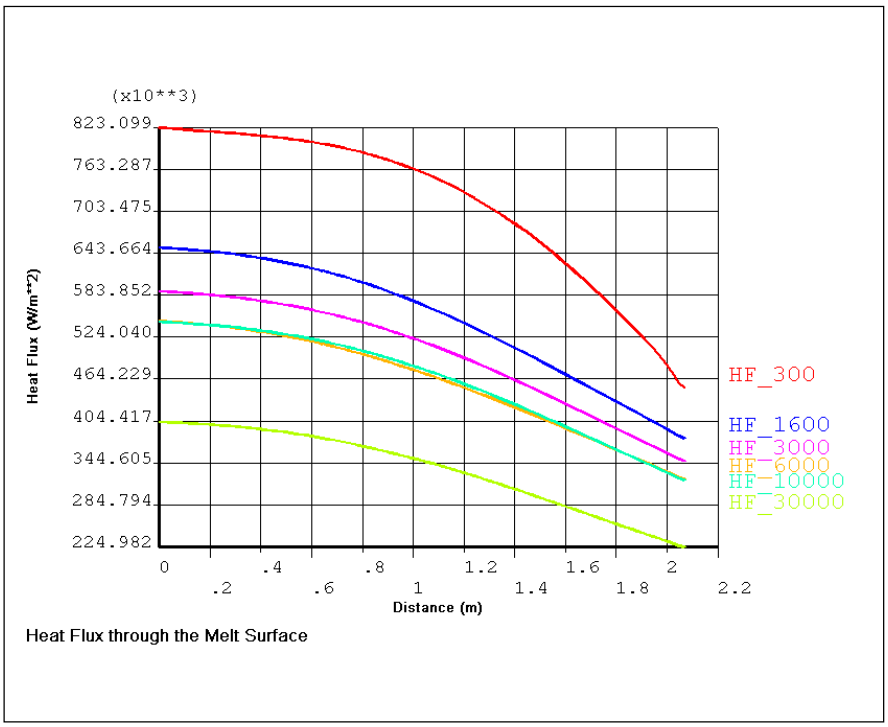

Figure 7-22: ANSYS, Segregated pool, with EVC, Heat flux through the melt surface

HF-100: Heat flux at t=300 s *HF-600: Heat flux at t=1600 s* *HF-1000: Heat flux at t=3000 s*

HF-1600: Heat flux at t=6000 s *HF-2000: Heat flux at t=10000 s* *HF-3000: Heat flux at t=30000 s*

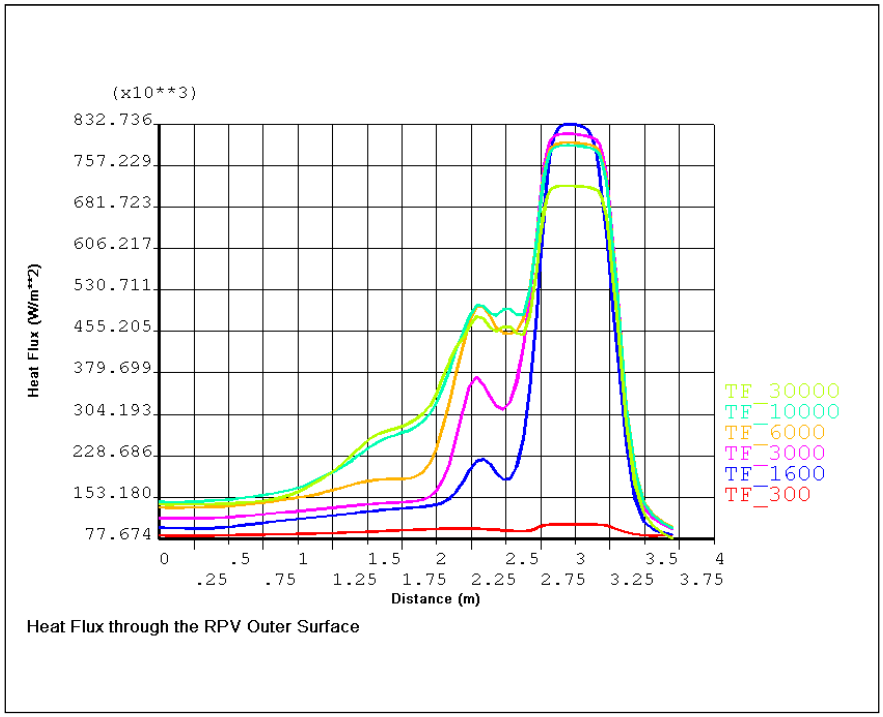

Figure 7-23: ANSYS, Segregated pool, with EVC, Heat flux through the RPV outer surface

TF-100: Heat flux at t=300 s *TF-600: Heat flux at t=1600 s* *TF-1000: Heat flux at t=3000 s*

TF-1600: Heat flux at t=6000 s *TF-2000: Heat flux at t=10000 s* *TF-3000: Heat flux at t=30000 s*

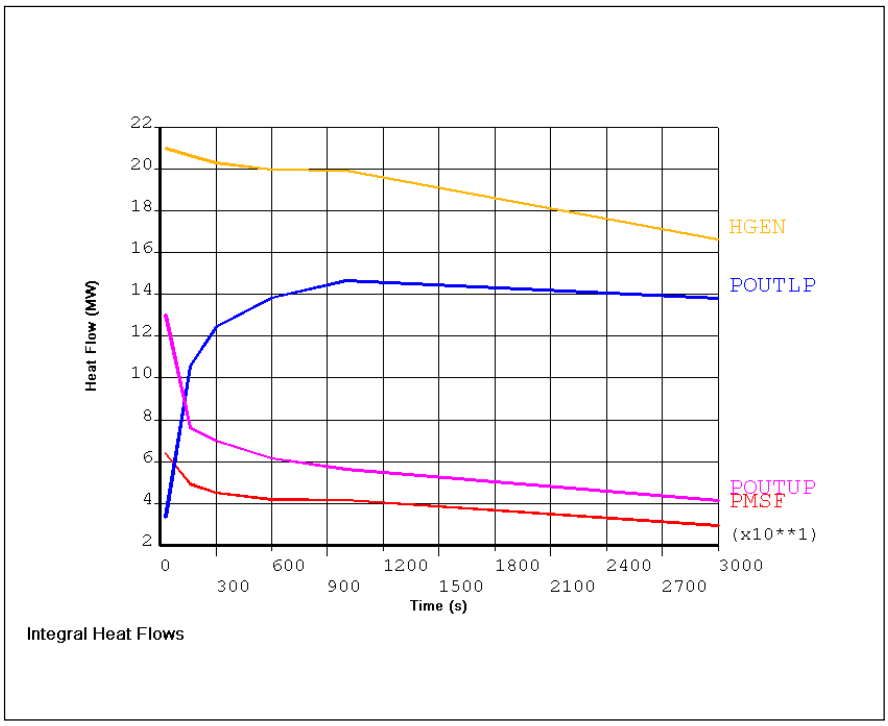

Figure 7-24: ANSYS, Segregated pool, with EVC, Integral heat flows

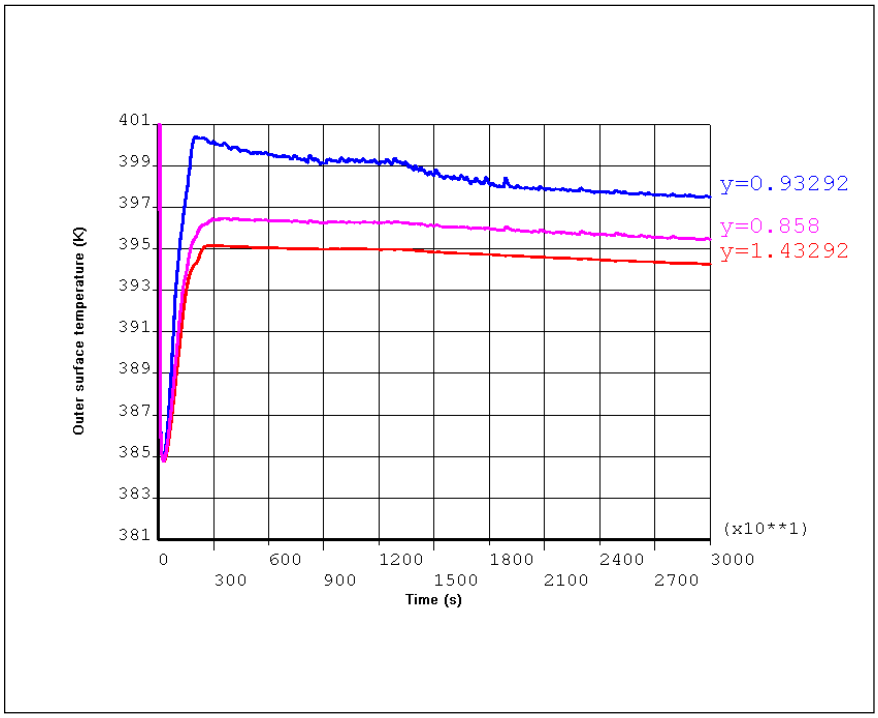

Figure 7-25: ANSYS, Segregated pool, with EVC, Outer vessel wall temperature

7.6 Parameter studies on the thickness of the molten metal layer

Uncertainties in the relocated metallic melt mass are basically due to different modelling assumptions made in the process of simulation of the severe accident, the models implemented in the codes themselves and how the melt progression would proceed before slumping of the molten materials into the reactor pressure vessel lower plenum. Key assumption is what would be the mass of the slumped vessel internal structures in the metallic layer. The heat flow from the molten metallic layer also depends on the decay power level, which defines the heat flow from the oxidic layer into the metallic one. As discussed earlier matter of debate is the question if the metal layer on top of the oxidic pool causes a so called focussing effect.

The influence of the thickness of the metal layer on the peak heat flux is investigated. The heat transfer behaviour is analyzed with decreased and increased molten steel mass to evaluate the sensitivity of heat transfer to the steel mass. The mass of the molten metallic layer may be reduced for example if the core barrel and baffle melt less than expected or if some of the metals re-solidify in the bottom of the reactor pressure vessel and the oxidic layer is formed on top of this metal. And in case that more metallic structures melt, then the height of the metal layer will increase.

A parameter study on the critical thickness of the metal layer has been performed. For the purpose of this analysis, ten simulations with varying thickness of the molten metal have been performed. The mass of the molten metal has been selected on the basis of rough engineering judgement. Complete accurate analyses on the amount of relocated material are not possible due to the lack of missing experimental data, the restrictions in the severe accidents code predictions etc.. As a basic case is applied the case of a segregated pool with cooling on the external surface (discussed in Chapter 7, Part 7.5.4) with total height of the metal layer of H_{met}=57 cm. Additionally ten separate cases with metal thickness of 10 cm, 20 cm, 28 cm, 40 cm, 70 cm, 80 cm, 90 cm, 120 cm, 140 cm and 160 cm were investigated.

Figure 7-26 represents the results for the peak heat flux dependency on the metal layer thickness. The blue dots represent the peak heat flux through the lower reactor pressure vessel outer wall to the water from outside. The red dots represent the peak heat flux through the melt surface, released heat by radiation. Because the metal layer has a higher thermal conductivity, the mass of metal assumed in the metallic layer significantly affects the estimated magnitude of the heat fluxes towards the adjacent vessel sidewall.

The simulation results have shown that with increasing thickness of the metal above the oxide, the heat flux is also increasing. For the cases with 10 cm, 20 cm, 28 cm and 40 cm metal layer, the heat that could be released through the side reactor pressure vessel wall is lower in comparison to the higher metal layer thickness. The lower the metal thickness, the higher the upper melt surface temperature is. More heat is released by radiation through the pool surface.

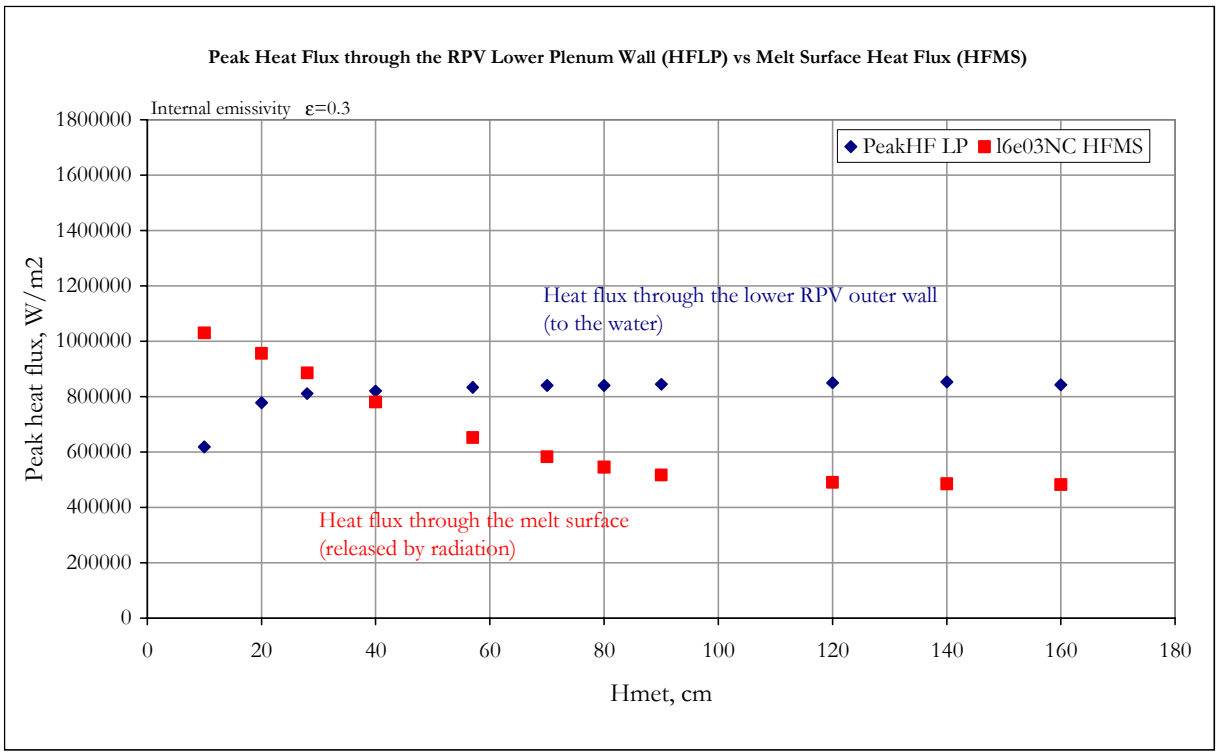

Figure 7-26: ANSYS, Segregated pool, with EVC, Heat flux dependency on the metal layer thickness

With decreasing of the thickness of the metal layer (metal layer height), the Rayleigh number is also decreasing, leading to decrease of the peak heat flux on the outer vessel wall. In spite of the fact of increasing of the available surface area for releasing of the heat through the vessel wall (at increasing metal layer height), the peak heat flux is increasing.

One could notice that at thin metal layer (e.g. H_{met}=10 cm), the melt surface temperature is kept high between 2700 K – 2800 K. The heat released by radiation is also high, because of the high melt surface temperature. At the same time, the heat that is released through the vessel outer wall is considerably low (~ factor of two) in comparison to the heat released through the pool surface. With increasing thickness of the metal layer, the surface temperature of the pool is decreasing. At H_{met}=57 cm, the pool surface temperature for the first 3000 s is about 2460 K (compared to 2800 K at H_{met}=10 cm). The heat released through the melt pool surface in this case is lower, decreased with the lower pool surface temperature.

The simulations were performed until the moment, at which decrease of the outer wall peak heat flux is observed (point H_{met}=160 cm).

It should be said that the above-discussed results have been compared to studies concerning the critical thickness of the metal layer found in the literature /THF 1996/, /REM 1997/, /SEH 1999/, /SEH 2000/, /SEH 2005/. The investigations performed there have pointed out, that reducing of the molten metal mass leads to increasing of the side wall heat fluxes. In /REM 1997/ the heat flux that exceeds the CHF was found to be for a height of the metallic layer of 0.25 m. In /THF 1996/ investigations had been done on the flux distributions for a 5 cm metal

layer on top of a 0.8 m deep oxidic pool. The results indicate that the outer heat flux values exceed the CHF. Part of these investigations, found in the literature, are obtained with 1D modelling.

In /SEH 1999/ a comparison of 1D and 2D representation of the heat of the vessel has been done. It was found that in case of 2D modelling the peak heat flux on the outer vessel wall is significantly lower than in case of 1D model representation. Based on the simulations in case of multi-dimensional representation, as in real reactor dimensions, the focusing effect is still existing, but is reduced as in case of 1D representation.

A careful comparison of the different results in /SEH 1999/, /SEH 2005/ and the analysis performed in Chapter 7, Part 7.5.4 shows, that the amount of heat, which is released from the melt surface by radiation is probably the key phenomenon. In /SEH 1999/ the initial melt pool temperature (2000 K) was considerably lower than in our case, which results in a lower fraction of heat released through radiation. In the current ANSYS model, Chapter 7, Part 7.5.4 there is a radiation heat transfer model to calculate the heat transferred from the free metal melt surface to all visible areas of the reactor pressure vessel above melt level. A difference is also that in the investigated case in Chapter 7, Part 7.5.4 in the current model the reactor pressure vessel above the melt is empty. There are uncertainties related to the material properties of the molten pools and in the emissivities of the pool surface.

Further detailed analyses were performed on the molten metal layer behaviour for understanding the different pool behaviour from the one cited in the literature /THF 1996/, /REM 1997/ and /SEH 1999/. For this purpose the above mentioned cases with different heights of the metal layer were recalculated, as all initial conditions as pool characteristics, properties and decay power were kept the same, except the internal emissivity, for which very low value ε=0.01 was specified.

Graphical representation of the results is shown in Figure 7-27. The blue and red dots represent respectively the heat released through the reactor pressure vessel later wall and the heat released by radiation. It can be seen that by reduction of the radiated heat (by setting very low emissivity of the internal vessel structures), the peak heat flux is increasing with decreasing of the metal layer thickness, as the highest (peak) outer vessel wall heat flux is at H_{met}=10 cm, and is approximately equal to 1.6 MW/m^2, which exceeds the CHF value according to the Nukiyama curve (Figure 7-3). Going in the right direction of the graph with increasing of the thickness of the metal layer, a rapid decrease in the peak heat flux value between H_{met}=40 cm and H_{met}=57 cm can be observed. The reason is the decreasing temperature difference T_{wall}-T_{fluid} according to the Nukiyama curve (Figure 7-3). For the basic case of H_{met}=57 cm, the peak heat flux is approximately equal to 1.15 MW/m^2, value also above the critical heat flux value of 850 kW/m^2 (Figure 7-3), meaning that the reactor pressure vessel integrity is destroyed.

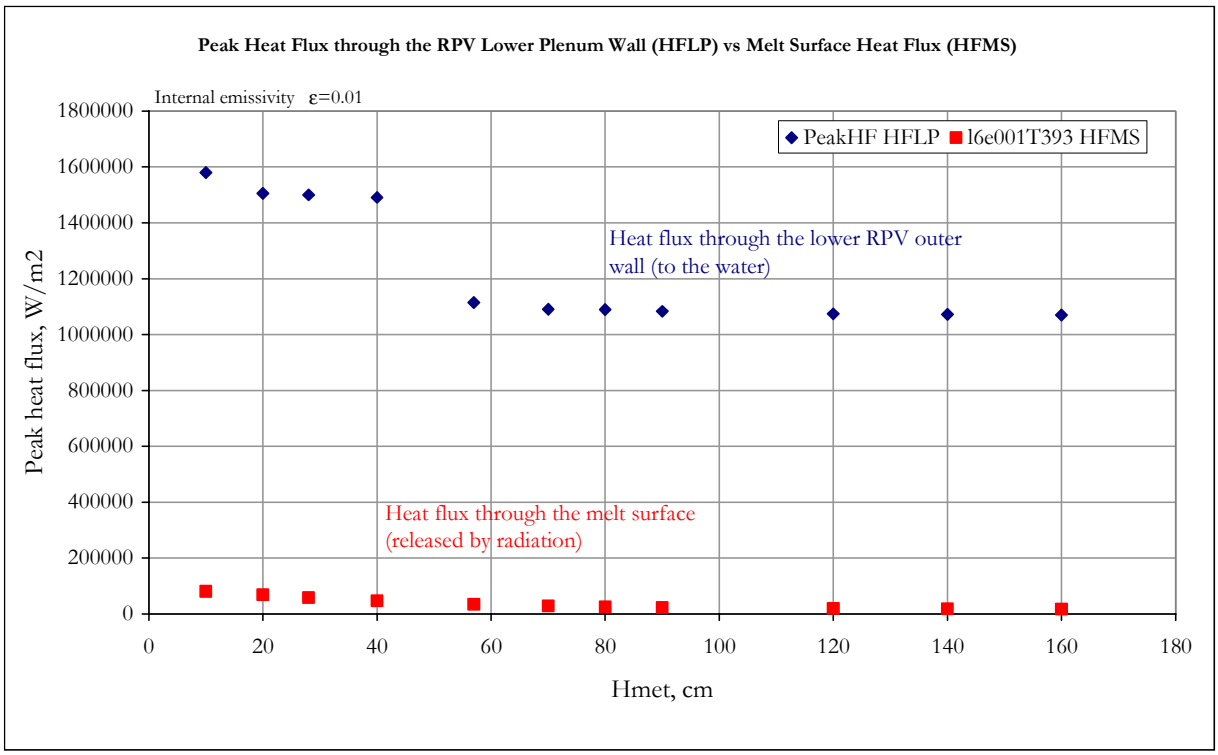

Figure 7-27: ANSYS, Segregated pool, with EVC, Heat flux dependency on the metal layer thickness with lowered internal emissivity ε=0.01

7.7 Structure mechanical modelling

The analyses performed with ANSYS are structural analysis evaluating elastic-plastic behaviour throughout the accident history after the relocation of the materials in the lower vessel head. In the following FE-mechanical analysis, the internal pressure, at which the RPV would fail is evaluated.

7.7.1 Axis symmetric mesh of the vessel

The lower vessel head is modelled with 2D-structural elements considering the temperature dependent material behaviour. For this purpose the FE code ANSYS is used. The model embraces only the remaining (not melted) part of the vessel wall. The meshing is kept likewise the one of the thermal model axisymmetric. The node positions and the element geometries of the vessel wall correspond exactly to those of the thermal model. Thus an easy transfer of the temperature loads from the thermal model is possible. The structural analysis uses the temperature history distribution form the ANSYS thermal model, with temperature dependent material properties, loads and boundary conditions. The ANSYS element type PLANE182 is used for the meshing.

7.7.2 Loads

The following loads are considered within the mechanical calculation:

- Internal pressure
- Gravity: dead-weight of melt and vessel
- Temperature field in the vessel wall.

The internal pressure and the gravity loads cause primary stresses. Their tendency is to increase with the reducing of the thickness of the reactor pressure vessel wall. The vessel failure could happen a) at high pressure or b) at low internal pressure, because the contribution of the weight is significant. The maximum temperature is above the melt temperature of steel. A part of the remaining thickness of the wall would be heated to relatively high temperatures. This influences strongly the structural capabilities of the steel and above a certain limit the reactor pressure vessel material would not sustain the high loads. Therefore it is important that the pressure of the primary circuit to be reduced close to the pressure of the containment. When the primary circuit has been depressurized, only a very small fraction of the original vessel wall thickness would be enough to support the weight of the vessel head and the corium. The thickness s, [m], needed could be roughly estimated by the following equations:

$$\sigma_{\text{tang}} = p \cdot \frac{r}{s} \qquad \text{(Eq. 7.61)}$$

$$s = \frac{p \cdot r}{\sigma_{\text{tang}}} \qquad \text{(Eq. 7.62),}$$

where p is the pressure [Pa], r is the average radius of the wall [m] and σ_{tang} is the strength of the steel [Pa].

If buoyancy is neglected and the same pressures in the cavity and inside the vessel are assumed, the pressure is caused only by the weight to be supported and may be obtained using the following equation:

$$p = \frac{m \cdot g}{\pi \cdot R_{in}^2} \qquad \text{(Eq. 7.63),}$$

where m - is the mass to be supported [kg], g – is the acceleration of gravity [m/s^2] and R_{in} – is the inner radius of the vessel wall [m].

In the FE model, the internal pressure is applied as a surface load. Two phenomena lead to an increasing primary stress with ongoing deformation: 1. the enlargement of the surface subjected to pressure load and 2. the reduction of the wall thickness. The weight of the vessel is considered by an accelerated coordinate system while the weight of the melt is modelled as an equivalent surface load. The temperature field is transferred from the thermal model at the time, at which the highest outer vessel surface temperature is reached.

7.7.3 Elastic and viscoplastic material properties

Three parts of the deformation of the material have to be taken into account /WIL 2005/: elastic deformation, creep and plasticity. The creep, also designated as viscoplasticity, is a time-dependent process. It plays a role at high temperatures as in the case of steel above 500 °C, and it occurs at arbitrary low stresses. Regarding this for the performed analyses creep effects were not included. The plastic deformation is prompt process, occurring only above a stress threshold (yield strength). It can occur already at room temperature, however, the yield strength increases with decreasing temperatures. Both deformation parts can occur simultaneously.

The elastic deformation is small compared to the creep and the plastic deformation, but it causes the stresses. The elastic material properties are assumed to be isotropic and can therefore completely be characterized by the temperature dependent Young's modulus and the constant Poisson number (ν=0.3).

The generation of the plastic and viscoplastic material data base is premised on the experimental results of the REVISA project of the 4th framework programme /MON 1999/, /IKO 1999/, /WIL 2003/. In this project tensile tests and also creep tests had been performed in the temperature range from 600 °C to 1300 °C for the French reactor pressure vessel steel 16MND5. In these tests the nominal stresses (tension force divided by initial cross section) and the nominal strain (increase of length divided by initial length) are measured. In the FE simulation the true stress and strain are needed. The convertion is done according to well known equations:

$$\varepsilon = \varepsilon^{tr} = \ln\left(1+\varepsilon^{nom}\right) \qquad \text{(Eq. 7.64)}$$

$$\sigma = \sigma^{tr} = \sigma^{nom}\cdot\left(1+\varepsilon^{nom}\right) \qquad \text{(Eq. 7.65),}$$

where the index "tr" refers to "true values".

The elaboration and the validation of the viscoplastic material database are briefly described in /ALT 2005/.

7.7.4 Results

The results from the mechanical analyses for the both pool configurations (homogeneous and segregated) are presented in Figure 7-28 to Figure 7-31.

Figure 7-28 shows the part of the lower head of the mechanical model for the homogeneous pool (left) and for the mechanical model for the segregated pool (right). The sharp cut shows the pool top position (maximum height of the melt). Molten elements are represented in grey colour. The ablation of the vessel wall is modelled in ANSYS in the following way: those elements are selected, which have at least one node with a temperature above the solidus temperature of the steel. These elements get the material properties of the adjacent melt region for the thermal solution. In the area of the hot focus the wall thickness reduction due to ablation is more than the half of the original vessel thickness. Solidification processes at later times are not considered.

One reason is that especially the mechanical material properties of resolidified areas are unknown.

According to the general experience there are no relevant creep processes in the considered reactor pressure vessel steel at temperatures below 700 K. Vessel failure occurs when the equivalent stress at the outside exceeds the ultimate strength of the vessel steel. Plasticity is considered for all temperatures.

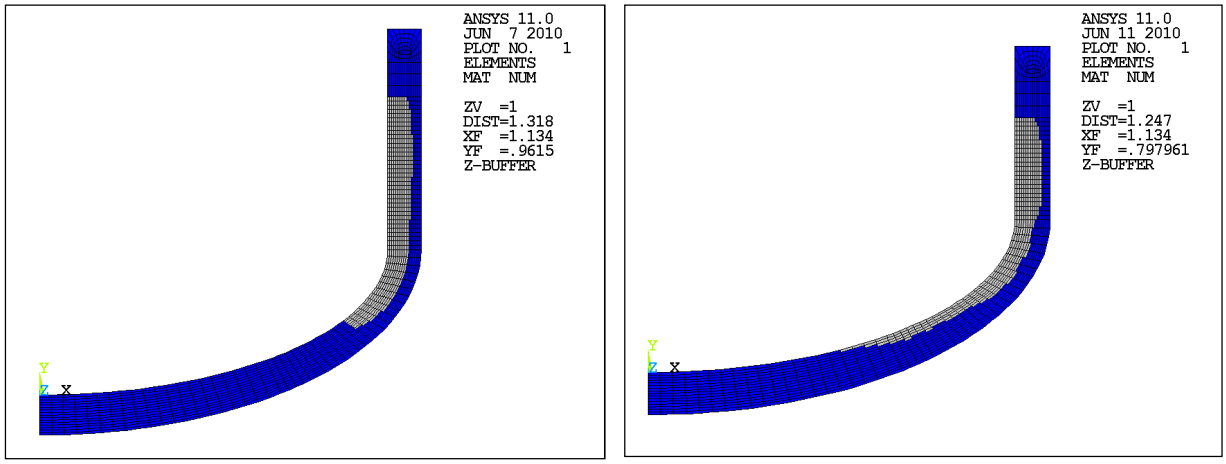

Figure 7-28: ANSYS, Ablated vessel wall, left: homogeneous pool, right: segregated pool

The ANSYS analysis has started with low pressure, and consequently the pressure has been increased to a limit, at which failure of the reactor pressure vessel wall will occur. The stresses have to be close to the ultimate stress to cause a failure of the RPV. The temperature dependent allowable stress is shown in Figure 7-29. It corresponds to the true ultimate strength. The ultimate strength is compared to the true stress of the vessel steel, which gives temperature-dependent stress-strain curves of the vessel steel /ALT 2005/. It is assumed that the vessel fails when a certain maximum (or allowable) stress is exceeded in the outer part of the vessel wall.

With T_{liq} is defined the liquidus temperature of the steel and $T_{allow,crit}$ stays for the temperature at which the strength of the steel starts significantly to decrease.

At low stress level the vessel wall temperatures have to be near the melting point of the vessel material for vessel failure to occur.

As can be seen from the temperature plots (Figure 7-21), the outer vessel wall is kept in the low temperature region and is much below the T_{liq} in Figure 7-29. The area of interest in our case lies in the left side field of $T_{allow,crit}$. It is assumed that the vessel will fail if in one element at the outer surface the allowable stress is exceeded.

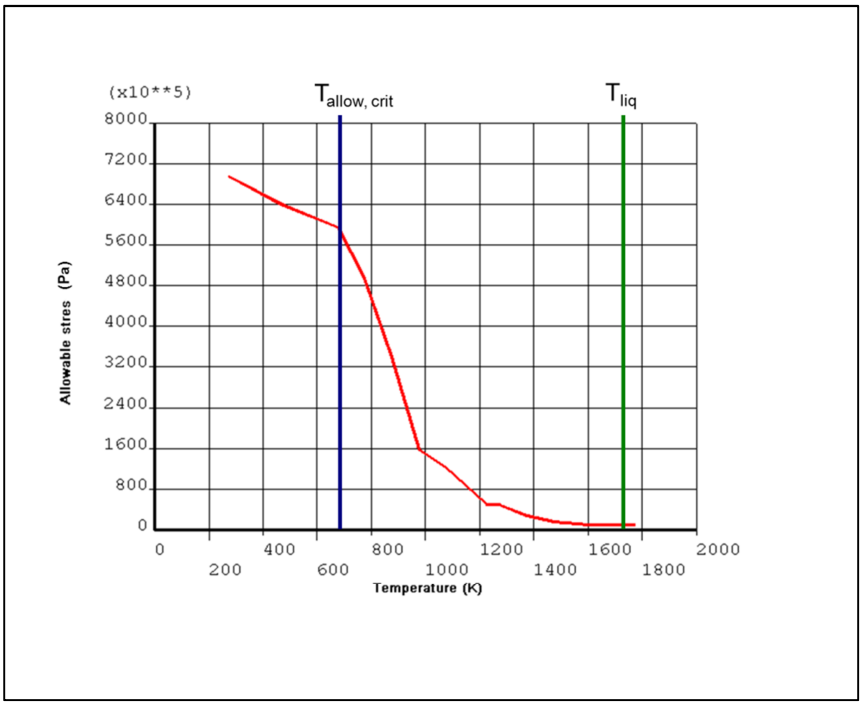

Figure 7-29: Allowable stress versus temperature for the RPV steel

The simulation of the failure pressure has been performed by elastic-plastic approach with stepwise increase of the internal vessel pressure. Figure 7-30 depicts the stress state and the relation between the equivalent stress and the allowable stress for the homogeneous melt pool. The results indicated that the rupture of the vessel occurs when the hot inner portion of the vessel wall degrades in strength and the vessel fails when the cooler outer wall cannot withstand the pressure stress. The most stressed location is the cylindrical part of the vessel. The failure pressure in this case equals approximately to 13.09 MPa.

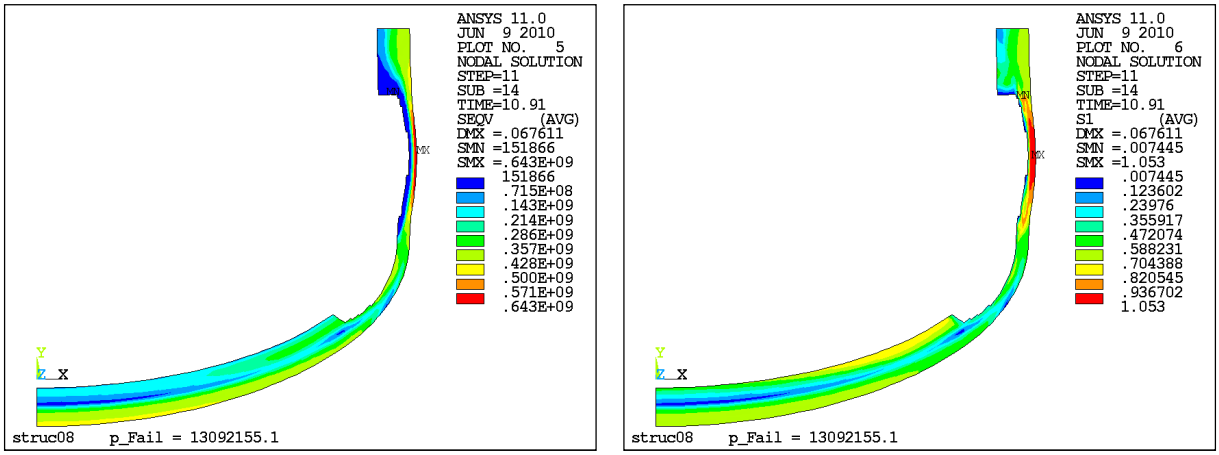

Figure 7-30: ANSYS, Homogeneous pool, left: equivalent stress [Pa], right: load (stress) factor

Figure 7-31 shows the results from the mechanical analyses for the segregated pool. Collapse occurred when the head could no longer support the internal pressure load with failure pressure of 13.56 MPa, only slightly higher than the failure pressure calculated for the homogeneous melt. This is due to the almost same remaining wall thickness at the hot spot region.

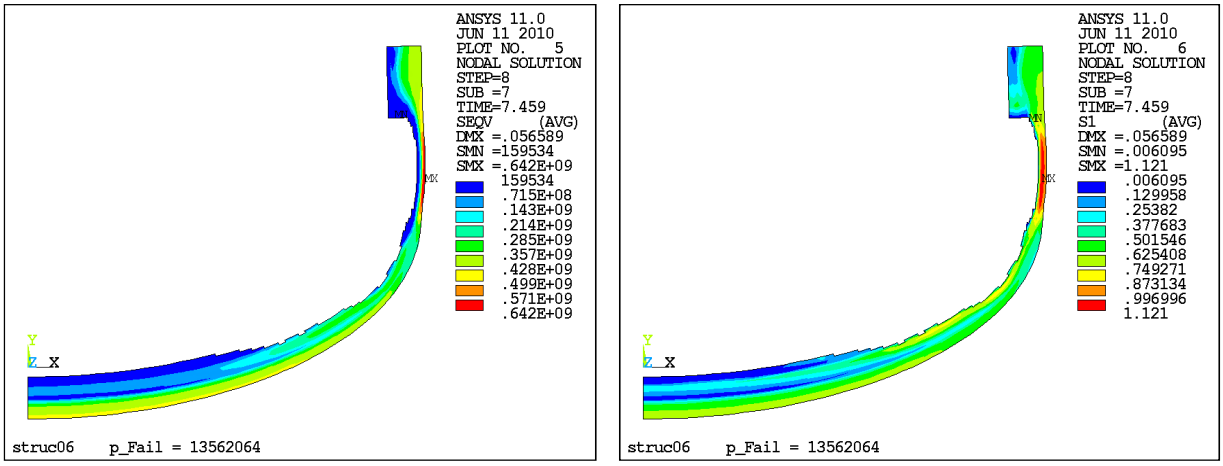

Figure 7-31: ANSYS, Segregated pool, left: equivalent stress [Pa], right: load (stress) factor

8 Summary

The performed investigations in this work aim at the analysis of the in-vessel phase of a hypothetical severe accident sequence in a nuclear power plant with a VVER-1000/V-320 reactor. The severe accident analyses were separated into two main parts: early in-vessel phase and late in-vessel phase.

Two accident scenarios were assessed which could lead to core damage, vessel failure and consequently challenge the containment – small break loss of coolant accident and station blackout scenario. The main goal of the investigation on both scenarios was the assessment of the ASTEC code capabilities in representation of severe accident scenarios and phenomena. It was the objective of the investigation on the station blackout transient to assess the severe accident management procedures for VVER-1000 reactors, i.e. estimation of the maximum period of time for taking appropriate decisions and measures. The performed analyses also contribute to the validation of the integral severe accidents code ASTEC.

Before performing the VVER-1000 severe accident analyses, the severe accident core degradation experiment ISP-46 FPT1 has been simulated with the ASTEC code. The investigations on the experiment have shown that the ASTEC code represents the measured experimental data with a good accuracy. The typical severe accident phenomena have been well reproduced (e.g. cladding rupture, zircaloy oxidation and hydrogen production, release of fission gas and aerosols, relocation of the different materials and molten pool formation). Differences were found in the release of the low-volatile fission products.

For the early in-vessel phase investigations, several simulations were performed by using the ASTEC and ATHLET codes, including a detailed evaluation of the calculated results and the observed phenomena. The simulation for the small break loss of coolant accident has shown, that ASTEC can predict the typical phases of the accident very well i.e. the depressurization phase, the thermal-hydraulic coupling between primary and secondary side as well as the break-down of primary to secondary heat transfer after extended voiding on the primary side. The severe accident phenomena following the expressed core heat-up, like cladding oxidation, core degradation, melt relocation and vessel failure were successfully modelled.

Detailed analyses have been done for the early thermal-hydraulic phase of the VVER-1000 station blackout accident with the ASTEC code and with the mechanistic code ATHLET. The ASTEC code simulations without and with primary side depressurization have shown, that applying primary side depressurization as a severe accident management measure allows prolongation of the time of vessel failure by approximately 1.5 hours, as the the vessel fails under low pressure. Slowing the core damage would allow more time for systems to be recovered to mitigate or terminate the accident. This would give more time and different possibilities for operator interventions. The code-to-code comparative analyses demonstrate the capability of the ASTEC code to model the accident sequence with a good accuracy. Despite the considerable differences in the codes themselves, the results are similar in terms of thermal-hydraulic response. There are discrepancies in timings of phenomena, which are within the limitations of the physical models and the applied nodalizations. Moreover it has to be considered that ASTEC is a fast running integral code, optimized for the calculation of entire sequences of severe accidents in light water reactors from the initiating event up to the release of fission products into the environment, while ATHLET focuses on the behaviour during the early phase of the discussed accident, using more detailed models for components, operational, safety and reactor protection systems. The simulations have shown that the effectiveness of the primary bleed and feed strategy in a station blackout scenario mainly depends on the behaviour of the hydro-accumulators and the capability to inject the full amount of water into the reactor pressure vessel. Due to evaporation of a part of the injected water in the core and also during the reversed heat transfer through the steam generators, the decrease of the primary pressure can be slowed down, so that the injection can be lowered or temporarily stopped.

A station blackout sequence without additional measures and without recovery of electricity supply would lead to an extended core heat-up under high pressure conditions. To prevent or at least to mitigate possible core damage, in-depth investigations were conducted on secondary and primary side depressurization as possible accident management measures for a station blackout scenario to estimate the remaining time margins for the operators.

The ATHLET code simulations for the secondary side depressurization have shown that:

- With the reduction of the secondary pressure and the passive feeding from the feed water system, the time for steam generators depletion is significantly prolonged
- The enhanced primary to secondary heat transfer after starting secondary side depressurization also leads to an effective reduction of the primary pressure
- The assumption, that after two hours the BRU-A valves fail in closed position, leads to a further activation of primary side depressurization, because after closing BRU-As the primary pressure starts to increase again. In that case secondary side depressurization combined with primary side depressurization will delay an extended heating-up of the core until approximately 6.3 hours and the critical limit of 1200 °C for the cladding temperatures is reached at approximately 6.8 hours after initiation of the transient
- With full (manual) opening of two BRU-A valves up to the end of the transient, the secondary side depressurization and the passive feeding from the feedwater system are

more effective. In that way an increase of the primary pressure after steam generators depletion and a mass loss through the pressurizer relieve valve can be significantly postponed. Compared to the simulation with BRU-A valves closed after batteries' depletion, the first criterion for primary side depressurization is reached 5 hours later in time. Without considering primary side depressurization as an additional accident management measure, the extended core heat-up can be delayed until approximately 9.8 hours after initiation of the transient and the critical limit of 1200 °C for the cladding temperatures is reached at approximately 11 hours

- The effectiveness of the secondary side bleed and feed strategy mainly depends on the availability of the BRU-A valves and the ability to inject as much water as possible from the feedwater system into the steam generators' secondary side. Caused by evaporation or by flashing in the feedwater system the passive feeding can be temporarily interrupted and the effectiveness of the feeding procedure can be reduced.

The simulations for the primary side depressurization have shown the following:

- By applying only primary side depressurization with both temperature criteria (350 °C and 650 °C) the critical limit of 1200 °C for the cladding temperatures is reached at approximately the same time, 3.9 – 4 hours
- The simulation with starting primary side depressurization later in time (temperature criterion of 650 °C) shows less effective accumulator injection
- The simulations with both temperature criteria show, that feeding from the hydro-accumulators lowers the cladding temperatures for a limited period of time, but without additional measures (e.g. recovery of electricity supply and start of active safety injection) a further core heat-up can not be avoided
- Primary side depressurization with start of one low pressure safety injection train after 3 hours and 45 minutes at the latest would avoid the excessive heating-up of the core.

The performed studies demonstrate the applicability of secondary side depressurization and primary side depressurization as accident management measures in the preventive domain. Passive systems and especially passive feeding of the reactor pressure vessel and the steam generators play an important role in a station blackout accident. An optimization of the accident management procedures (e.g. initiation criteria, control and operation of valves used for the depressurization) is crucial to maximize the effectiveness of the corresponding bleed and feed strategies, and to mitigate the consequences of the accident. The simulations proved that by first applying the secondary side depressurization the final core heat-up occurs much later in time compared to the case when primary side depressurization is applied as the first accident management measure (6.3 – 9.8 hours for secondary side depressurization compared to 3.2 – 3.7 hours for primary side depressurization). This would give the operators an additional time margin to restore the electric power supply. With start of one active emergency core cooling pump at the latest possible time after primary side depressurization, the safety functions important to prevent core damage are preserved.

Analyses for the late in-vessel phase of the accident and the possibilities for in-vessel melt retention have been studied with the finite element code ANSYS. An effective conduction convection model, originally developed at KTH and implemented in ANSYS by FZD, has served as a basis model. This basis model was further developed for the simulation of the heat transfer within a segregated molten pool.

The thermal ANSYS analyses reveal that:

- Without external flooding of the vessel, a pure thermal failure (melt-through) is highly probable due to the high thermal loads imposed by the decay heat in the molten corium
- The pressure and the boundary conditions i.e. the initial pool and vessel wall temperatures, and the decay heat, have the greatest effect on the failure times. The stratified pool composition substantially decreases the time to vessel failure compared to the homogeneous melt pool composition
- The failure will occur at the position of the highest temperatures. Close to the cylindrical part is disadvantageous in comparison to spherical/elliptical part, since the primary stresses in the cylinder are higher than those in a sphere, and the maximum temperatures occurring in the cylindrical part
- Applying external vessel cooling would help the stabilization of the vessel and the retention of the molten corium inside the reactor pressure vessel and can prevent the vessel failure. However, if the radiation from the melt surface is hindered, as for example in the case of remaining in-vessel structures, the critical heat flux is exceeded
- The homogeneous pool shows higher safety margin than the segregated pool. The molten pool is completely bounded by a corium crust that avoids direct contact with the vessel. The corium crust, thick at the lower boundary of the corium pool (south pole of the reactor pressure vessel) and is thinning in upward direction along the pool boundary. The vessel temperature is characterised by the external surface at low temperature (lower than 500 K) and an inner surface which reaches the melting point in a limited section of the reactor pressure vessel wall
- For both pool configurations the peak heat fluxes in the area of the hot focus are clearly visible. The maximum values are in the range of approximately 810 kW/m^2 to 830 kW/m^2. At the lower head south pole and at the high vessel locations in the cylindrical part, the resulting heat fluxes are below 50 kW/m^2
- In case of segregated pool the thermal attack of the vessel is observed primarily in the area of the metal layer. The vessel temperature is low at the external surface where the cooling efficiency is very good. Nevertheless, very high temperature gradients establish across the residual vessel thickness
- The critical heat flux was not reached in the investigated basic flooding scenarios (without reduction of the emissivity), i.e. the external vessel wall temperatures lie in a small range between 373 K and 402 K despite the large variations of the local heat flux. For the cases

with reduction of the emissivity (very low emissivity value $\varepsilon = 0.01$), the peak heat flux exceeds the critical heat flux

- In most of the simulated cases for the critical thickness of the metal layer, the highest outer vessel wall temperatures (respectively the peak heat fluxes) are reached within the first 1.5 hours from the formation of a stable pool in the reactor pressure vessel lower head. Later on the heat fluxes to the surrounding water decrease with the decreasing of the decay heat in the pool
- Parameter studies on the critical thickness of the metal layer have shown that increasing the thickness of the metal layer, results in increasing heat fluxes to the water. The main reason is the heat radiated from the melt pool surface. The presented analyses are simulating an "empty" vessel after relocation of the molten core in the reactor pressure vessel lower plenum (the molten pool "sees" an empty inner vessel), and the external flooding is applied up to the top of the reactor pressure vessel
- With an external flooding the temperature of the outer reactor pressure vessel wall can be kept in the temperature range, which provides a sufficient mechanical strength for the IVR in the low pressure scenarios. However, it should be ensured that the critical heat flux is not exceeded in any position and that the generated steam can be released from the reactor pit
- Based on the simulations it can be stated that the crucial time point lies within the first 20 hours after melt relocation, because the decay heat is decreasing over time.

The capability of the vessel to withstand the melt attack depends on the amount of the relocated materials and the residual power, but it is strongly influenced by the configuration assumed for simulation of the corium pool. The differences to the results published in the literature are related to the applied initial parameters and conditions, as the initial melt pool temperature and the applied emissivity coefficients; weather the vessel is flooded up to the top, if there are remaining structures inside the vessel and if the computer models are applying 1D or 2D representation of the melt pool and lower reactor vessel head configurations. In the present research, a focusing effect has been observed in both homogeneous and segregated pool configurations. As in the case of segregated pool configuration the thermal attack of the vessel wall is in the area of the metal layer. The performed parameter studies on the thickness of the metal layer have shown that with increasing thickness of the metal above the oxide, the peak heat flux through the reactor pressure vessel wall is slightly increasing. The lower the metal layer thickness, the higher the upper melt surface temperature is. In that case more heat is released by radiation through the melt pool surface.

Main objective of this work was the in-depth investigation of a hypothetical severe accident scenario (station blackout) for a VVER-1000 reactor, considering all main phases and important phenomena from the early thermal-hydraulic phase up to the late in-vessel phase with core degradation and core melt. Different codes have been applied to account for the specific phenomena related to the different phases of the accident. It is an outcome of this work, that a proper modelling of the horizontal steam generators is necessary to predict the timings for steam

generators' depletion, for depletion of the primary side and finally for core heat-up with sufficient accuracy. Moreover, if different codes will be applied to simulate the different phases and to evaluate the effectiveness of severe accident management measures, an adequate and accurate modelling of the early thermal-hydraulic phase is an essential requirement. This includes an in-depth understanding of the phenomena occurring during the early thermal-hydraulic phase and a detailed evaluation of the calculated results. Therefore comparative simulations with ASTEC and ATHLET codes have been performed, to evaluate the capabilities of ASTEC in predicting the course of events up to core heat-up. After that the results from an ASTEC code simulation for the melt pool configuration have been applied as initial conditions for the ANSYS code simulations (Appendix D). This gives the possibility for a more detailed and more accurate modelling of the thermal and mechanical behaviour of the core melt and the reactor pressure vessel wall, additionally taking into consideration the heat transfer from the reactor pressure vessel outer wall to the surrounding water if external vessel cooling is applied.

With help of the presented method, by applying different codes for the different phases of the station blackout accident (Appendix D), a detailed evaluation of the course of events and the main thermal-hydraulic and severe accident phenomena, including an assessment of different severe accident management measures (e.g. secondary and primary side depressurization, external vessel cooling) has been provided.

Bibliography and credits

/AKS 2007/ N. Aksan: International Standard Problems and Small Break Loss-of-Coolant Accident (SBLOCA), Paul Scherrer Institut (PSI), 5232 Villigen PSI, Switzerland, December 2007

/ALL 2005/ H.-J. Allelein, K. Neu, J. P. Van Dorsselaere: European Validation of the Integral Code ASTEC (EVITA) First experience in validation and plant sequence calculations, Nuclear Engineering and Design, vol 235, pp 285-308, 2005

/ALS 1999/ Alsmeyer H., Adelheim C., Benz H., Cron T., Dillmann G., Tromm W., Schmidt Stiefel S., Schneider H., Schumacher G., Wenz T.: Corium cooling by bottom flooding: results of the COMET investigations, OECD Workshop on Ex-Vessel Debris Coolability Karlsruhe, Germany, 15-18 November 1999

/ALT 2005/ E. Altstadt, H.-G. Willschütz: Beitrag zur Modellierung der Schmelzerückhaltung im RDB nach Verlagerung von Corium in das untere Plenum: Berechnung des temperaturfeldes und der viskoplastischen Verformung der Behälterwand, Wissenschaftlich-Technische Berichte des Forschungszentrum Rossendorf, FZR-412, 2005

/ALT 2008/ E. Altstadt, M. Abendroth, H.-G. Willschütz: Thermo-mechanische Finite-Elemente-Modellierung zur Schmelzerückhaltung im RDB nach Verlagerung von Corium in das untere Plenum, Wissenschaftlich-Technische Berichte des Forschungszentrum Rossendorf; FZR-503 2008, ISSN 1437-322X, 2008

/ANS 2001/ ANSYS®, Programmer‘s Manual, ANSYS®, Inc., 2001

/ANS 2002/ ANSYS®, Theory Reference, ANSYS®, Inc., 2002

/ANS 2003/ ANSYS®, User‘s Manual, ANSYS®, Inc., 2003

/ASF 1996/ F.J. Asfia, V.K. Dhir: An experimental study of natural convection in a volumetrically heated spherical pool bounded on top with a rigid wall, Nuclear Engineering and Design, vol 163, pp 333-348, 1996

/AST 2006/ ASTEC Code: On-line User's Manual

/ATH 2001/ G. Lerchl, H. Austregesilo: ATHLET User's Manual, Gesellschaft für Anlagen- und Reaktorsicherheit (GRS) mbH, 2001, Cologne, Germany

/ATH 2003/ H. Austregesilo, C. Balls, A. Hora, G. Lerchl, P. Romstedt: ATHLET Model 2.0 Cycle A, Models and Methods, Gesellschaft für Anlagen- und Reaktorsicherheit (GRS) mbH, 2003, Cologne, Germany

/BAE 2006/ H. D. Baehr, K. Stephan: Heat and Mass Transfer, Springer, ISBN 3-540-63695-1, 2006

/BEC 2008/ S.V. Bechta, V.S. Granovsky, V.B. Khabensky, E.V. Krushinov, S.A. Vitol, V.F. Strizhov, D. Bottomley, M. Fischer, P. Piluso, A. Miassoedov, W. Tromm, E. Altstadt, H. G. Willschutz, F. Fichot, O. Kymalainen: VVER Steel Corrosion During In-vessel Retention of Corium Melt, European Review Meeting on Severe Accident Research (ERMSAR Meeting), 23-25 September 2008, 2008, Nessebar, Bulgaria

/BEL 1995/ J. Beljajew; W. Luther; S. Spolitak; N. Trunov; I. Tschekin: Modellierung von horizontalen Dampferzeugern in WWER-Reaktoranlagen mit ATHLET, Gesellschaft für Anlagen- und Reaktorsicherheit, TN-LUW-95-1,1995, Köln

/BER 1998/ L. Bernaz: Etude du transfert de chaleur à la frontière supèrieure d'un bain fluide avec dissipation volumique de puissance. Dissertation, L'Universite Joseph Fourier De Grenoble, 1998

/BON 1998/ J.M. Bonnet: BALI Test Reports for In-Vessel Configurations, MVI Project Contract FI4S-CT95-0007, Task 3-1, SETEX/LTEM/98-114, CEA/Grenoble, 1998

/BUI 1998/ V.A. Bui: Phenomenological and Mechanistic Modelling of Melt-Structure-Water Interactions in a Light Water Reactor Severe accident, Doctoral Thesis at Royal Institute of Technology, Stockholm, 1998

/CAC 2010/ Cacuci, D. G. (Editor) et al.: "Handbook of Nuclear Engineering", Vol. 4: Reactors of Generations III and IV; Springer, 2010

/CHE 1992/ F.B. Cheung, S.W. Shiah, D.H. Cho, M.J. Tan: Modeling of Heat Transfer in a Horizontal Heat-Generating Layer by an Effective Diffusivity Approach, OSTI ID: 10166428; Legacy ID: DE94014978, ANL/RE/CP--79355; CONF-920804—28, 1992

/CHE 2008/ M. Cherubini, N. Muellner, F. D'auria, G. Petrangeli : Application of an Optimized AM Procedure following a SBO in a VVER-1000, Nuclear Engineering and Design, vol 238, pp 74-80, 2008

/CHU 1975/ S.W. Churchill, H.S. Chu: Correlating Equations for Laminar and Turbulent Free Convection from a Vertical Plate, Int. J. Heat Mass Transfer, Vol.18, pp.1323-1329, 1975

/DIN 1997/ T.N. Dinh, R.R. Nourgaliev: Turbulence Modelling for Large Volumetrically Heated Liquid Pools, Nuclear Engineering and Design, vol 169, pp 131-150, 1997

/DOM 1998/ L. A. Dombrovskii, L. I. Zaichik, and Yu. A. Zeigarnik: Numerical Simulation of The Stratified-Corium Temperature Field and Melting of The Reactor Vessel for A Severe Accident in A Nuclear Power Station, Thermal Engineering, vol 45, No.9, pp 755-765, 1998

/DOR 2006/ J.P. Van Dorsselaere, B.Schwinges: Overview of the Integral Code ASTEC v1.3, Project reference ASTEC-V1/DOC/06-19, DPAM/ASTEC-2006-362, GRS ASTEC 06/02, IRSN, GRS, 2006

/ESM 2004/ H. Esmaili, M. Khatib-Rahbar: Analysis of In-Vessel Retention and Ex-Vessel Fuel Coolant Interaction for AP1000, NUREG/CR-6849, ERI/NRC-04-201, U.S. Nuclear Regulatory Commission Office of Nuclear Regulatory Research Washington, DC 20555-0001

/FOB 2005/ FoBaus Group: B. Kalchev, P. Tusheva, I. Mladenov, D. Dimov, P. Groudev, J. Georgieva, B. Atanasova, A. Stefanova, I. Ivanov, R. Passalacqua, ASTEC Engineering Handbook for Kozloduy NPP VVER1000/V320, Report SARNET-ASTEC-M01, 2005

/FRI 2008/ E. Fridman, E. Shwageraus, A. Galperin: Implementation of multi-group cross-section methodology in BGCore MC-depletion code, International Conference on the Physics of Reactors "Nuclear Power: A Sustainable Resource", Interlaken, Switzerland, September 14-19, 2008

/GEN 2005/ R. Gencheva, A. Stefanova, P. Groudev: RELAP5/MOD3.2 Investigation of Reactor Vessel YR Line Capabilities for Primary Side Depressurization during the TLFW in VVER1000/V320, Annals of Nuclear Energy, vol 32, pp 1407 – 1434, 2005

/GIL 2007a/ G. Guillard, F. Jacq, C. Seropian, W. Plumecocq: ASTEC-V1/DOC/07-21, SYSINT Module: Management of Events and Safety Systems Interactions, Technical Note SEMCA-2007-293, 2007, Cadarache, France

/GIL 2007b/ G. Guillard, F. Jacq, S. Pignet, P. Majumdar, A. Siméone: ASTEC-V1/DOC/07-19-rev1, DIVA Physical Modelling, IRSN/DPAM/SEMCA 2007/316, 2007, Cadarache, France

/GIO 2001/ P. Giordano, H. Larbi, D. Kadri: ASTEC-V1/DOC/01-15, ASTECV1 – CESAR: Two Phase Flow Thermal Hydraulic Module-Version 1.0 – Description of Physical and Numerical Modelling, Rev0, Technical Note 01/35, 2001, Cadarache, France

/GRS 2011/ Gesellschaft für Reaktorsicherheit mbH (GRS), Köln: Technische Daten Fukushima Nr. 1 im Normalbetrieb, http://fukushima.grs.de/sites/default/files/Technische_Daten_Reaktoren_Fukushima_Nr_1_0.pdf

/HEL 1997/ M. Helle, O. Kymäläinen, E. Pessa: COPO II-Lo Experiments, IVO Power Engineering, YDIN-GT1-43, 1997

/HEL 1998/ M. Helle, O. Kymäläinen: Crust Effect in the COPO II-Experiments. Report 2_EU-MVI(98)-FORTUM-35, IVO Power Engineering, Vantaa, Finnland, 1998

/HEU 2005/ R. Heuss: Thermisches Versagen von Reaktordruckbehältern bei extremen Störfällen in Druckwasserreaktoren – Analyse und Verbesserungsvorschläge, PhD Thesis, RWTH-Aachen, 2005

/IAEA: 23/ Accident Analysis for Nuclear Power Plants, Safety Reports Series No 23, International Atomic Energy Agency, Vienna, 2002

/IAEA: 32/ Implementation of Accident Management Programmes in Nuclear Power Plants, Safety Report Series No 32, International Atomic Energy Agency, Vienna, 2004

/IAEA: 56/ Approaches and Tools for Severe Accident Analysis for Nuclear Power Plants, Safety Report Series No 56, International Atomic Energy Agency, Vienna, 2008

/IAEA: INSAG-10/ Defence in depth in Nuclear Safety, INSAG-10, A Report by the International Nuclear Safety Advisory Group, International Atomic Energy Agency, Vienna, 1996

/IAEA: INSAG-12/ Basic Safety Principles for Nuclear Power Plants, 75-INSAG-3 Rev. 1, INSAG-12, A report by the International Nuclear Safety Advisory Group, International Atomic Energy Agency, Vienna, 1999

/IAEA: NS-R-1/ Safety of Nuclear Power Plants: Design, Requirements, No NS-R-1, International Atomic Energy Agency, Vienna, 2000

/IAEA: NS-G-2.15/ Severe Accident Management Programmes for Nuclear Power Plants, Safety Guide No NS-G-2.15, International Atomic Energy Agency, Vienna, 2009

/IAEA: SSG-2/ Deterministic Safety Analysis for Nuclear Power Plants, Specific safety guide, IAEA Safety Standards Series No SSG-2, Vienna, 2009

/IAEA: TECDOC-1200/ Application of Probabilistic Safety Assessment for Nuclear Power Plants, IAEA-TECDOC-1200, International Atomic Energy Agency, Vienna, 2001

/IKO 1999/ K. Ikonen: Creep Model Fitting Derived from REVISA Creep, Tensile and Relaxation Measurements, Technical Report MOSES-4/99, VTT-Energy, Espoo, Finland

/IRSN 2007/ A. Bentaïb, H. Bonneville, C. Caroli, B. Chaumont, B. Clément, M. Cranga, F. Fichot, J. Fleurot, R. Gonzalez, Vincent Koundy, Bruno Laurent, Jean-Claude Micaelli, R. Meignen, F. Pichereau, D. Plassart, E. Raimond, A. Tenaud, J. P. Van-Dorsselaere, G. Ducros, M. Durin, C. Journeau, D. Magallon, J-M. Seiler, E. Studer, B. Tourniaire, W. Ranval and EDF's Severe Accident Teams: Research and Development with Regard to Severe Accidents in Pressurised Water Reactors: Summary and Outlook, Rapport IRSN-2007/83, Rapport CEA-2007/351, 2007

/KOL 1996/ N.I. Kolev: External cooling of a pressurized water reactor vessel during a severe accident, Kerntechnik, vol 61, pp 67-76, 1996

/KOL 1999/ N.I. Kolev, I. Roloff-Bock: Potential for external cooling of boiling water reactors during postulated severe accidents with melt relocation, Tagungsbericht Jahrestagung Kerntechnik 1999, Karlsruhe, pp 287-295, 1999

/KRE 2008/ F. Kretzschmar, B. Fluhrer: Behavior of the Melt Pool in the Lower Plenum of the Reactor Pressure Vessel - Review of Experimental Programs and Background of the LIVE Program, Wissenschaftliche Berichte FZKA 7382, Forschungszentrum Karlsruhe FZK, April 2008, Karlsruhe, Germany

/KYM 1993/ O. Kymäläinen, O. Hongisto, E. Pessa: COPO- Experiments on Heat Transfer from a Volumetrically Heated Pool, DLVI-G380-0377, 1993

/KYM 1997/ O. Kymäläinen, H. Tuomisto, T.G. Theofanous: In-vessel Retention of Corium at the Loviisa Plant, Nuclear Engineering and Design, vol 169, pp 109-130, 1997

/MAG 2005/ D. Magallon, A. Mailliat, J.-M. Seiler, K. Atkhen, H. Sjövall, S. Dickinson, J. Jakab, L. Meyer, M. Buerger, K. Trambauer, L. Fickert, B. Raj Sehgal, Z. Hozer, J. Bagues, F. Martin-Fuentes, R. Zeyen, A. Annunziato, M. El-Shanawany, S. Guentay, C. Tinkler, B. Turland, L.E. Herranz Puebla: European Expert Network for the Reduction of Uncertainties in Severe Accident Safety Issues (EURSAFE), Nuclear Engineering and Design, vol 235, pp 309-346, 2005

/MON 1999/ Ph. Mongabure, M. Desmet: RUPTHER Test#14 – Rupture Test at 1000°C and Variable Pressure 8 then 6 bars, Report SEMT/LISN/RT/99-003/A, CEA, France, 1999

/MUE 2007/ N. Muellner, M. Cherubini, W. Kromp, F. D'Auria, G. Petrangeli: A procedure to Optimize the Timing of Operator Actions of Accident Management Procedures, Nuclear Engineering and Design, vol 237, pp 2151-2156, 2007

/NEA 1998/ Nuclear Energy Agency, Committee on the Safety of Nuclear Installations: VVER-Specific Features Regarding Core Degradation, Status Report, NEA/CSNI/R(98)20, 1998

/NIS 2011/ Nuclear and Industrial Safety Agency (NISA) Japan Nuclear Energy Safety Organization (JNES): The 2011 off the Pacific coast of Tohoku Pacific Earthquake and the seismic damage to the NPPs, 4th April, 2011, http://www.nisa.meti.go.jp/english/files/en20110406-1-1.pdf

/OVC 1992/ Ovchinnikov, F. Ia.; Voznesenskii, V. A.; Semenov, V.V. and others: "Эксплуатациоционные режимы АЭЦ с ВВЭР-1000; Энергоатомиздат, 1992

/PAV 2007/ M. P. Pavlova, M. Andreeva, P. P. Groudev: RELAP5/MOD3.2 Blackout Investigations for Validation of EOPs for KNPP VVER-1000/V320, Progress in Nuclear Energy, vol 49, pp 409-427, 2007

/PHE 2001/ Final Report FPT1, CD-ROM, PhebusPF, IPSN, 2001

/PHE 2004/ B. Clement and T. Haste: "ISP-46 PHEBUS FPT1: Integral Experiment on Reactor Severe Accidents", Comparison Report, NEA/CSNI/R(2004)18, 2004 ; http://www.oecd-nea.org/nsd/docs/2004/isp46/Homepage.pdf

/PHE 2007/ K. Mueller, B. Toth, M.S. Veshunov, K. Trambauer, C. Jamond, R. Dubourg, H. Manenc, N. Girault, M. Kissane, G. Repetto, W. Plumecocq, P. Taylor, T. Haste, J. Birchley, D. Bottomley, G. Schanz, J. Stuckert F. Lemoine, N. Davidovich, P. Mason: „Final Interpretation Report of the PHEBUS test FPT0 (Bundle Aspects)"; DG JRC, Institute for Energy, 2007

/PIG 2002/ S. Pignet: ASTEC-V1/DOC/02-04, Description of Thermal Hhydraulic Models of DIVA, Technical Note IRSN/DRS/SEMAR 02/31, 2002, Cadarache, France

/REM 1997/ J. L. Rempe, D. L. Knudson, C. M. Allison, G. L. Thinnes, C.L. Atwood, M.J. Cebull: Potential for AP600 In-Vessel Retention through Ex-Vessel Flooding, Technical Evaluation Report, Idaho National Engineering Laboratory, INEEUEXT-97-00779, 1997

/REM 2005/ J. L. Rempe, K. Y. Suh, F. B. Cheung, S. B. Kim: In-Vessel Retention Strategy for High Power Reactors, Final Report, Idaho National Engineering Laboratory, INEEL/EXT-04-02561, 2005

/ROU 1997/ Rougé, S., "SULTAN Test Facility for Large-Scale Vessel Coolability in Natural Convection at Low Pressure," Nuclear Engineering and Design, 169, pp. 185-195, 1997

/SARNET 2006/ Severe Accident Phenomenology Short Course, CEA Cadarache, France, January 9-13, 2006

/SARNET 2008/ B.R. Sehgal, P. Piluso, K. Trambauer, B. Adroguer, F. Fichot, C. Müller, L. Meyer, W. Breitung, D. Magallon, C. Journeau, H. Alsmeyer, C. Housiadas, B. Clement, M.L. Ang, B. Chaumont, I. Ivanov, S. Marguet, J-P. Van Dorsselaere, J. Fleurot, P. Giordano, M. Cranga: SARNET Lecture notes on Nuclear Reactor Severe Accident Phenomenology, CEA Cadarache, Rapport CEA-R-6194

/SCO 2003/ J.H. Scobel: The Potential for AP1000 Reactor Vessel Failure Induced by a Stratified Debris Bed with a Bottom Metal Layer during IVR, International Congress on Advances in Nuclear Power Plants (ICAPP 2003), Cordoba, Spain, May 13-17, 2003

/SEH 1999/ B.R. Sehgal, V.A. Bui, T.N. Dinh, R.R. Nourgaliev: Heat Transfer Processes in Reactor Vessel Lower Plenum during Late Phase of In-Vessel Core Melt Progressiont, Advances in Nuclear Science and Technology, vol 26, edited by Lewins and Becker; Kluwer Academic/Plenum Publishers, New York, 1999

/SEH 2000/ B.R. Sehgal, T.N. Dinh, R.R. Nourgaliev, V.A. Bui, J. Green, G. Kolb, A. Karbojian, S.A. Theerthan, A. Gubaidulline, M. Helle, O. Kymäläinen, H. Tuomisto, B.D. Turland, G.P. Dobson, K. Ikonen, N. Kolev, J.M. Bonnet, S. Rouge´, M. Narcoux, A. Lie`geois, A. Siccama, F. Parozzi, M. Caira: Final Report for the "Melt-Vessel Interactions (MVI)" Project, SKI Report 00:53, 2000

/SEH 2001/ B.R. Sehgal: Accomplishment and Challenges of the Severe Accident Research, Nuclear Engineering and Design, vol 210, pp 79-94, 2001

/SEH 2005/ B.R. Sehgal, A. Karbojian, A. Giri, O. Kymäläinen, J.M. Bonnet, K. Ikkonen, R. Sairanen, S. Bhandari, M. Buerger, J. Dienstbier, Z. Techy, T. Theofanous: Assessment of reactor vessel integrity (ARVI), Nuclear Engineering and Design, vol 235, pp 213-232, 2005

/TEPCO1 2011/ Tokyo Electric power Company, Inc.: The Great East Japan Earthquake and Current Status of nuclear power Stations, http://www.tepco.co.jp/en/index-e.html

/TEPCO2 2011/ Tokyo Electric power Company, Inc.: Reactor Core Status of Fukushima Daiichi Nuclear Power Station Unit 1, May 15th, 2011, http://www.tepco.co.jp/en/press/corp-com/release/betu11_e/images/110515e10.pdf

/THF 1996/ T.G. Theofanous, C. Liu, S. Additon, S. Angelini, O. Kymäläinen, T. Salmassi: In-Vessel Coolability and Retention of a Core Melt; DOE/ID-10460, Volume 2, 1996

/THF 1997a/ T.G. Theofanous, M. Maguire, S. Angelini, T. Salmassi: The first Results from the ACOPO Experiment, Nuclear Engineering and Design, vol 169, pp 49-57, 1997

/THF 1997b/ T.G. Theofanous, C. Liu, S. Additon, S. Angelini, O. Kymäläinen, T. Salmassi: In-vessel Coolability and Retention of a Core Melt, Nuclear Engineering and Design, vol 169, pp 1-48, 1997

/TUS 2007/ P. Tusheva, N. Reinke: Comparative Analyses of Thermal Hydraulic Behaviour of VVER-1000/V-320 for a Station Blackout Accident Scenario with ASTEC V1.2.1 and ATHLET 1.2a, Proceedings of Annual Meeting on Nuclear Technology 2007, Karlsruhe, Germany, 2007

/TUS 2008/ P. Tusheva, N. Reinke, F. Schäfer, A. Hurtado: Severe Accident Analysis for VVER-1000/V-320 for a Station Blackout Accident Scenario with ASTEC v1.3.0, Proceedings of Annual Meeting on Nuclear Technology 2008, Hamburg, Germany, 2008

/TUS 2009/ P. Tusheva, N. Reinke, E. Altstadt, F. Schäfer, F.-P. Weiß, A. Hurtado: Analysis of Severe Accidents in VVER-1000 Reactors Using the Integral Code ASTEC, Proceedings of the 17th International Conference on Nuclear Engineering ICONE17, Paper ICONE17-75563, Brussels, Belgium, 2009

/TUS 2010a/ P. Tusheva, E. Altstadt, F.-P. Weiss: Investigations on In-Vessel Melt Retention for VVER-1000 Reactors, Proceedings of Annual Meeting on Nuclear Technology 2010, Berlin, Germany, 2010

/TUS 2010b/ P. Tusheva, F. Schäfer, N. Reinke, F.-P. Weiß: Assessment of Early-Phase Accident Management Strategies in a Station Blackout

Scenario for VVER-1000 Reactors, Proceedings of the 18th International Conference on Nuclear Engineering ICONE18, Paper ICONE18-29954, Xi'an, China, 2010

/US NRC 2011/ United States Nuclear Regulatory Commission US NRC, Eric Leeds, Director Office of Nuclear Reactor Regulation: Presentation on Fukushima, April 2011

/VDI 2002/ VDI-Wärmeatlas, Berechnungsblätter für den Wärmeübergang, Neunte Auflage, Springer Verlag, Berlin, 2002

/WIL 2003/ H.-G. Willschütz, E. Altstadt, B. R. Sehgal, F.-P. Weiss: Simulation of Creep Tests with French or German RPV-Steel and Investigation of a RPV-Support against Failure, Annals of Nuclear Energy, vol 30, 10, pp 1033-1063

/WIL 2005/ H.-G. Willschütz: Thermomechanische Modellierung eines Reaktordruckbehälters in der Spätphase eines Kernschmelzunfalls, PhD Thesis, TUD, 2005

/WIL 2006/ H.-G. Willschütz, E. Altstadt, B.R. Sehgal, F.-P. Weiss: Recursively Coupled Thermal and Mechanical FEM-Analysis of Lower Plenum Creep Failure Experiments, Annals of Nuclear Energy, vol 33, pp 126-148, 2006

Internet Sources:

/IS 1/ http://nuklear-server.ka.fzk.de/lacomeco/Facilities/Quench/quench.htm
/IS 2/ http://nuklear-server.ka.fzk.de/lacomeco/Facilities/Disco/disco.htm
/IS 3/ http://www.oecd-nea.org/nsd/reports/rasplav_seminar2000.pdf
/IS 4/ http://www.oecd-nea.org/nsd/workshops/masca2004/oc/papers/FR_Seiler_MGapTH.pdf
/IS 5/ http://www.oecd-nea.org
/IS 6/ http://www.nsi.kiae.ru
/IS 7/ http://www.oecd-nea.org/jointproj/masca.html
/IS 8/ http://www.epri.com
/IS 9/ http://melcor.sandia.gov
/IS 10/ http://www.inl.gov
/IS 11/ http://www.irsn.fr

Publications and project work reports of the author

This thesis is in part based on the following publications and project work reports by the author:

Publications:

Roberto Passalacqua, Polina Tusheva, Ivan Mladenov, Dimitar Dimov, Jordanka Georgieva, Antoaneta Stefanova, Pavlin Groudev- ASTEC & MELCOR Comparison for a VVER-1000 / 60mm Small Break LOCA, Proceedings of the Energy Forum 2005, Varna, Bulgaria, 2005

Jordanka Georgieva, Antoaneta Stefanova, Boriana Atanasova, Pavlin Groudev, Polina Tusheva, Ivan Mladenov, Dimitar Dimov, Roberto Passalacqua- VVER-1000 Small-Medium Break LOCAs Predictions by ASTEC, Proceedings of the International Conference Nuclear Energy for New Europe 2005, Bled, Slovenia 2005

P. Tusheva, N. Reinke, Comparative Analyses of Thermal Hydraulic Behaviour of VVER-1000/V-320 for a Station Blackout Accident Scenario with ASTEC V1.2.1 and ATHLET 1.2a, Proceedings of Annual Meeting on Nuclear Technology 2007, Karlsruhe, Germany

P. Tusheva, N. Reinke, F. Schäfer, A. Hurtado, Severe Accident Analysis for VVER-1000/V-320 for a Station Blackout Accident Scenario with ASTEC V1.3.0, Proceedings of Annual Meeting on Nuclear Technology 2008, Hamburg, Germany

Tusheva, P., Reinke, N., Altstadt, E., Schäfer, F., Weiß, F.-P., Hurtado, A.: Analysis of Severe Accidents in VVER-1000 Reactors using the Integral Code ASTEC. Proceedings of the 17th International Conference on Nuclear Engineering, ICONE17, July 12-16, 2009, Brussels, Belgium

Tusheva, P., Schäfer, F., Reinke, N., Rohde, U.: Investigation on Accident Management Measures for VVER-1000 Reactors. 19th AER Symposium on VVER Reactor Physics and Reactor Safety, September 21–25, 2009, St. St. Constantine and Elena resort, Varna, Bulgaria

Tusheva, P., Schäfer, F., Reinke, N., Altstadt, E., Rohde, U., Weiss, F.-P., Hurtado, A.: Investigation on Primary Side Oriented Accident Management Measures in a Hypothetical Station Blackout Scenario for a VVER-1000 Pressurized Water Reactor, KERNTECHNIK 01/2010

Tusheva, P., Altstadt, E., Weiss, F.-P.: Investigations on in-vessel melt retention for VVER-1000 reactors, Proceedings of Annual Meeting on Nuclear Technology 2010, Berlin, Germany

Tusheva, P., Schäfer, F., Reinke, N., Altstadt, E., Rohde, U., Weiss, F.-P., Hurtado, A.: Assessment of Early-Phase Accident Management Strategies in a Station Blackout Scenario for VVER-1000 Reactors, Proceedings of the 18th International Conference on Nuclear Engineering, ICONE18, May 17-21, 2010, Xi'an, China

F.-P. Weiss, F. Schäfer, S. Kliem, P. Tusheva: "Analysis of Design Basis Accidents"; FJOHSS Frédéric Joliot/Otto Hahn Summer School on Nuclear Reactors, Aix-en-Provence, France, 2010

Work reports:

I. Ivanov, B. Kalchev, M. Marinov, R. Hristova, B. Neykov, P. Tusheva, D. Dimov, V. Hadjiev: RMPS-Project (Reliability Methods for Passive Systems): Approaches for applying the methodology to VVER reactor and assessment of the improvement of analyses of VVER reactor, Deliverable 10 and Deliverable 11, November 2003

B. Kalchev, P. Tusheva, D. Dimov, I. Mladenov, I.Ivanov: Validating of ASTEC v1.0 Computer Code against FPT1 test, PHEBEN2- Project; Validating Severe Accident Codes against Phebus FP for Plant Applications, June 2004

B. Kalchev, P. Tusheva, D. Dimov, I. Mladenov, I.Ivanov, S. Kisyoski, D. Ivanova: Validating of ASTEC v1.0 Computer Code against FPT2 test, PHEBEN2- Project; Validating Severe Accident Codes against Phebus FP for Plant Applications, July 2004

FoBAUs Group: Boris Kalchev, Polina Tusheva, Ivan Mladenov, Dimitar Dimov, Pavlin Groudev, Jordanka Georgieva, Boryana Atanasova, Antoaneta Stefanova, Ivan Ivanov, Roberto Passalacqua: ASTEC Engineering Handbook for Kozloduy NPP VVER-1000/V-320, SARNET-Project, September 2005

FoBAUs Group: VVER 1000 SBLOCA Calculations with ASTEC v1.1 and Comparison with MELCOR 1.8.5 and RELAP-SCDAP5, SARNET-Project WP4, June 2005

I. Ivanov, B. Kalchev, P. Tusheva, I. Mladenov, S. Kisyoski: Comparative analysis of the validations of ASTEC v1.1 and ASTEC v1.0 against PHEBUS FPT2 test, SARNET-Project WP3, August 2005

I. Ivanov, B. Kalchev, P. Tusheva, I. Mladenov, S. Kisyoski: TUS/EI-WP3 PHYMA Technical report on ASTEC v1.1 validation /Contribution to the Deliverable 30/, SARNET-Project WP3, September 2005

FoBAUs suggestions/requirements for ASTECv1.2 Development, SARNET-Project, September 2005

Kalchev, B., Tusheva, P., Mladenov, I., Dimov, D., Groudev, P., Georgieva, J., Stefanova, A., Atanasova, B., Ivanov, I.: VVER 1000 SBLOCA Calculations with ASTEC v1.2 and Comparison with ASTEC v1.1 and MELCOR 1.8.5, SARNET-Project, Sofia, November 2005

Kalchev, B., Tusheva, P., Dimov, D., Groudev, P., Georgieva, J., Stefanova, A., Atanasova, B., Ivanov, I., Passalacqua, R.: VVER 1000 SBO Calculations with ASTEC v1.2 and Comparison with MELCOR 1.8.5, SARNET-Project, Sofia, December 2005

FoBAUS Group: Progressing report for the JPA2 period: April 05 – July 05 with ASTEC v1.1 and September 05 – March 06 with ASTEC v1.2, SARNET-Project WP4, February 2006

P. Tusheva: COLIMA Experiment, Input Deck for ASTEC Code Validation, SARNET-Project, 2006

Severe Accident Management Guidelines (SAMGs) Review and Assessment in Compliance with International Requirements, SAMG, PHARE-Project, 2006

FoBAUs Group, Summary Report April 2007 – March 2008, Analyses with ASTEC v1.3 R0, SARNET-Project, March 2008

Tusheva, P.: Accident Analyses for a Reference German PWR Modelling with ATHLET 2.0A, Final Report, Forschungszentrum Dresden-Rossendorf, Internal Report, July 2008

Tusheva, P. Reinke, N.: Contribution Summary Report: Accident Analysis of SBO Sequence for VVER1000/V-320 ASTEC V1.3.2, SARNET-Project, October 2008

Tusheva, P., Schäfer, F.: CHF Experiment - Modelling with ATHLET - Blind Calculations, Forschungszentrum Dresden-Rossendorf, Internal Report, March 2009

Tusheva, P., Schäfer, F.: German Reference PWR- Investigation on CCFL and Reflux Condenser Mode/ ATHLET Code Simulation, Forschungszentrum Dresden-Rossendorf, Internal Report, May 2009

Figure credits

The permission to reproduce certain figures was obtained from the copyright holders. With hearty acknowledgments to the authors:

Dr. Marco Fulle – Stromboli Online, www.swisseduc.ch ; Photo: Erta Ale Volcano, with kind permission from the autor.

Dr. Hans-Georg Willschütz – Figure 7-4: ECCM principal scheme of a melt pool with internal heat sources

Figure 7-6: Temperature and velocity profile in the side boundary layer obtained from a CFD analysis

with kind permission from the author.

Appendix A: ATHLET nodalization schemes

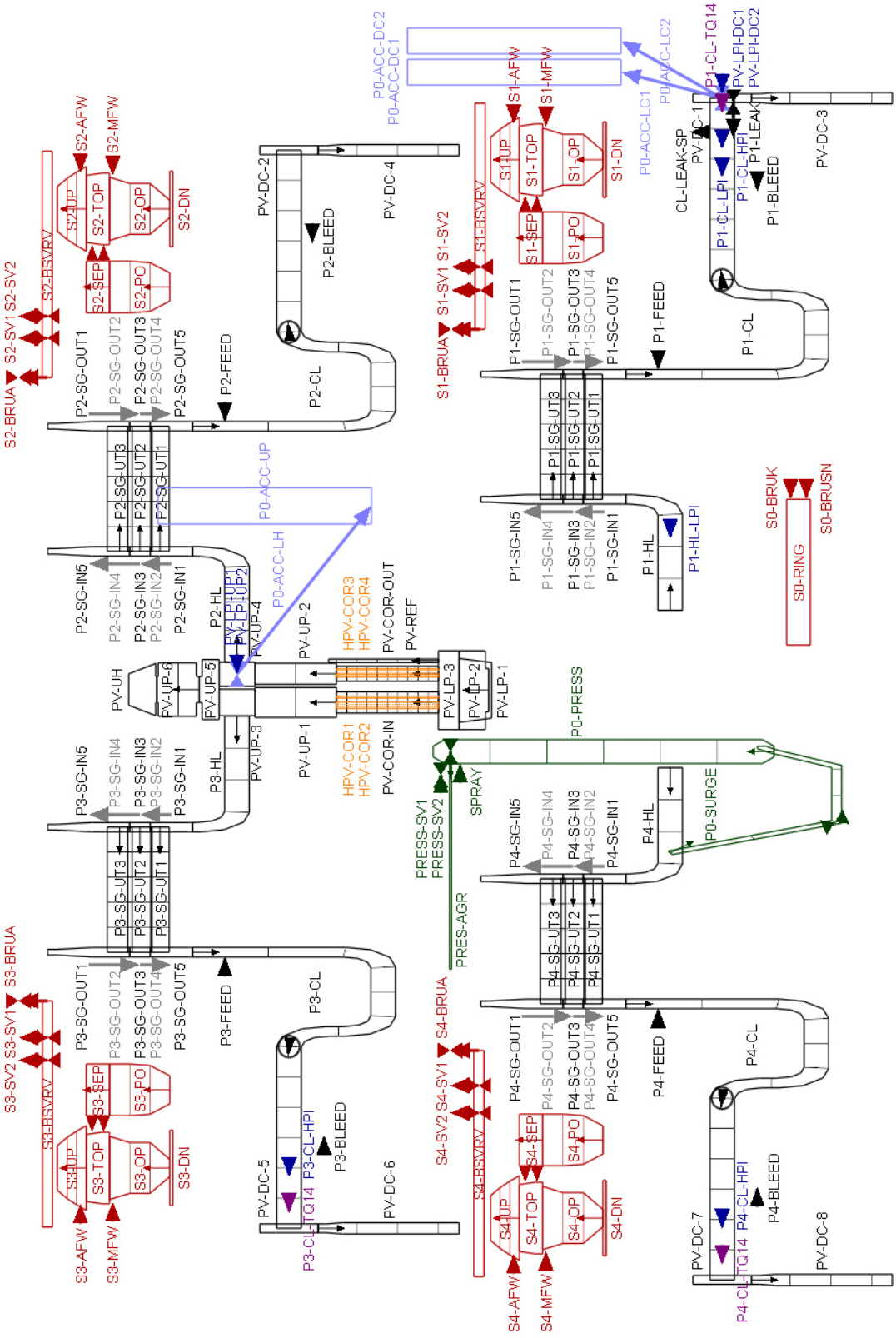

ATHLET nodalization scheme for primary loop 1–4, including reactor and steam generators

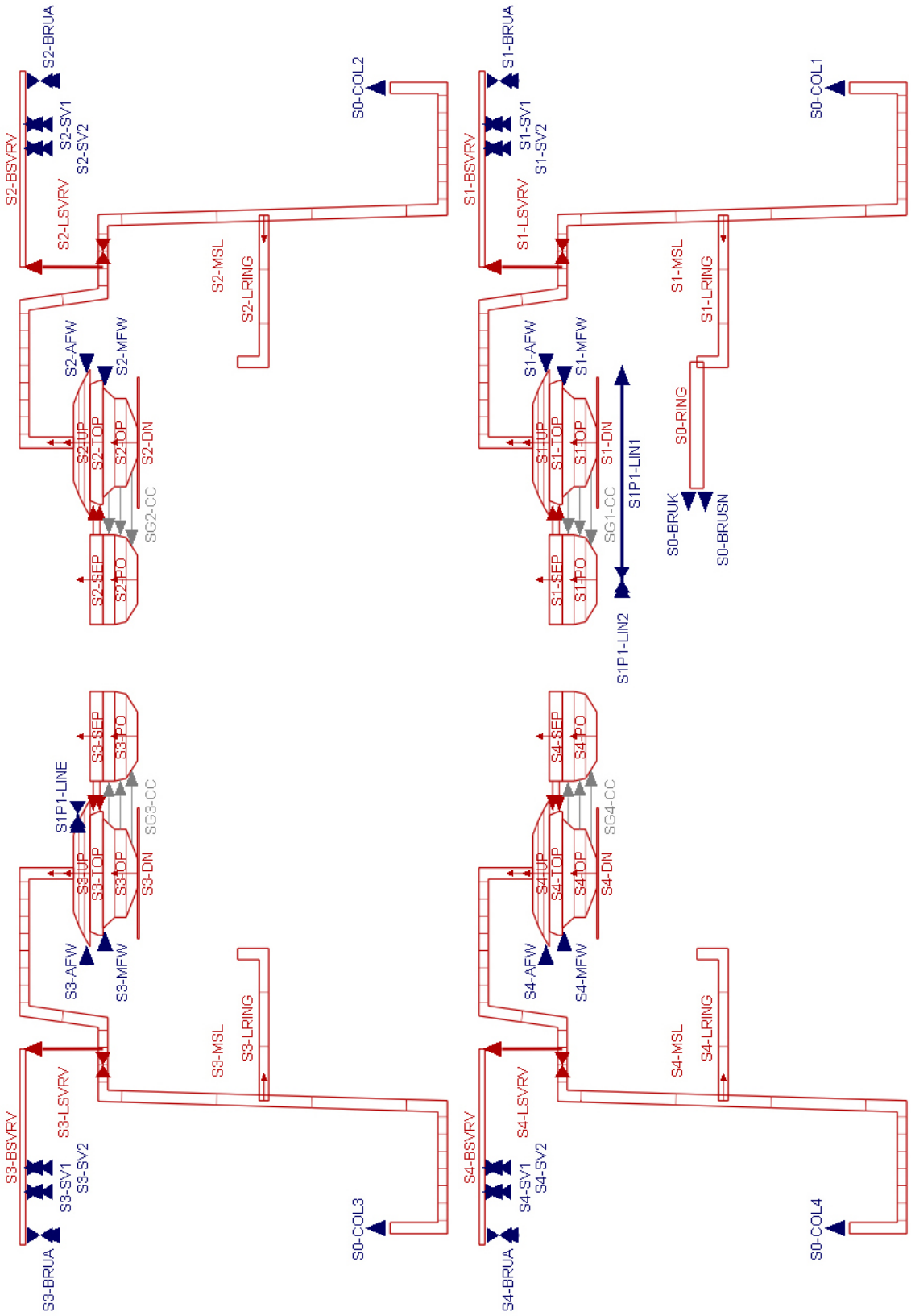

ATHLET nodalization scheme for secondary side, including steam lines for loop 1–4

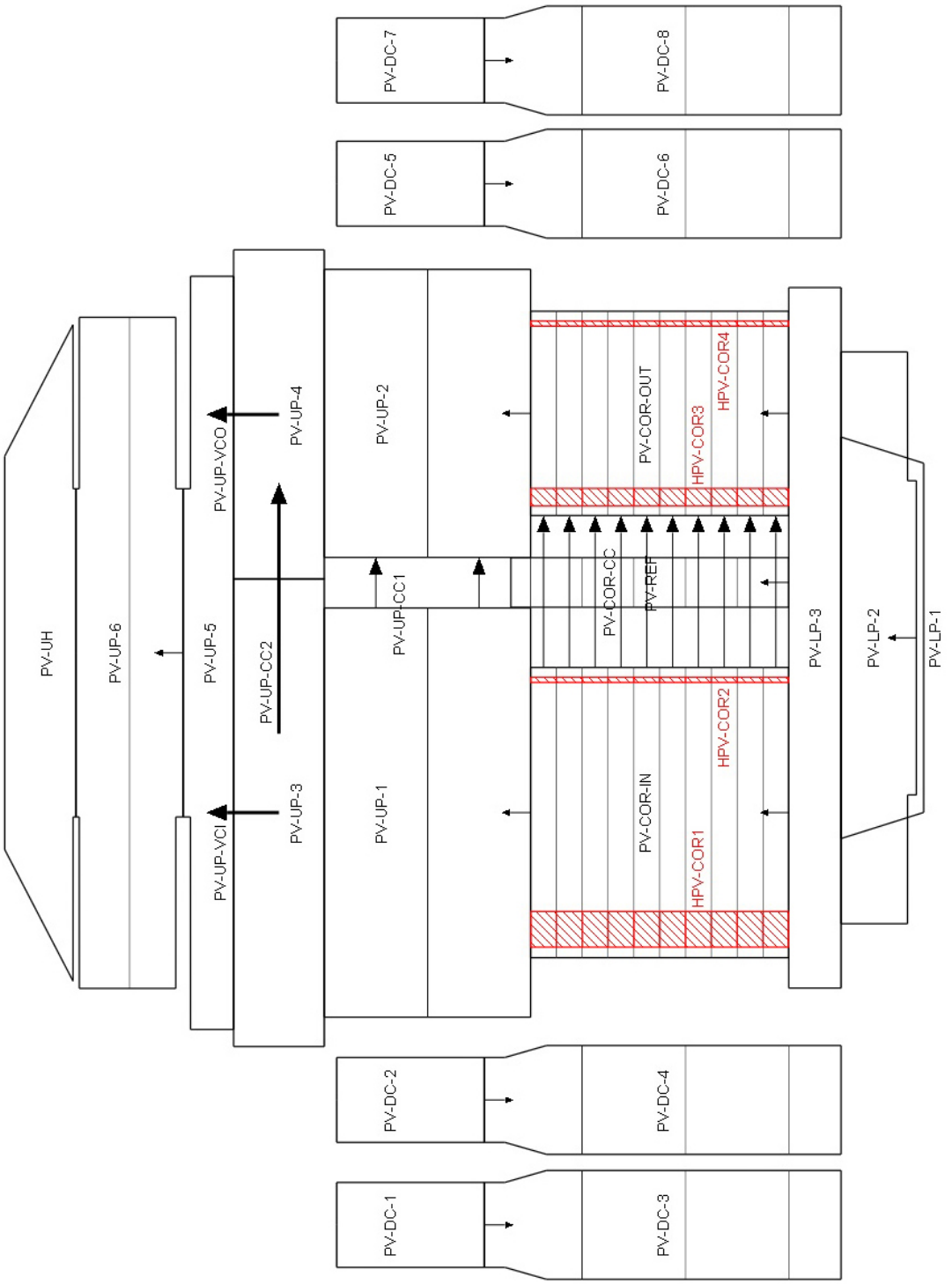

ATHLET nodalization scheme for reactor pressure vessel and downcomer section 1–4

Appendix B: ASTEC code abbreviations

CAND: Candling and relocation of molten mixtures along macros

CELL: Definition of a cell (a mesh) of an axial element

COND: Conduction between two macros

STRU EVENT: Structure indicating the events for the scenario

STRU COND: Condition for the event activation written in SIGAL analyzer syntax

STRU CONNECTI: Name of a connection

STRU CREE: Creep of the cladding

STRU JUNCTION: Name of the reactor coolant system junction involved in the connection, connection between grouped primary system volumes

STRU LOWE: Lower head mesh definition

STRU MACR: Definition of a macro-component

STRU MATE: Definition of a material

STRU PRIMARY: Primary Circuit description (Reactor Coolant System): definition of the primary side

STRU REGU: Regulation block: a parameter is adjusted in order to fit a computed response with an expected one. Used for instance during steady state calculation

STRU SYSTEMS: Definition of the systems

STRU VOLUME: Definition of a volume

STRU WALL: Definition of a wall

tstar_di: time for start of the core degradation module DIVA (option)

TYPG CYLINDER: Definition of a type

STRU VESSEL_D: Description of data for the reactor pressure vessel managed by DIVA

VOLUME: Definition of a volume

Appendix C: ANSYS code abbreviations

PLANE55: Element, used as a plane element or as an axisymmetric ring element with a 2-D thermal conduction capability. The element has four nodes with a single degree of freedom, temperature, at each node. The element is applicable to a 2-D, steady-state or transient thermal analysis. Calculation of the heat conduction in the area of the RPV.

CONTA171: Represents contact and sliding between 2-D "target" surfaces (TARGE169) and a deformable surface, defined by this element. The element is applicable to 2-D structural and coupled field contact analyses. Interface between the molten pool and the RPV wall.

TARGE169: Represents various 2-D "target" surfaces for the associated contact elements. The contact elements themselves overlay the solid elements describing the boundary of a deformable body and are potentially in contact with the target surface, defined by TARGE169. Interface between the molten pool and the RPV wall.

MATRIX50: A group of previously assembled ANSYS elements that is treated as a single element. The thermal radiation inside the RPV is modeled as a Superelement MATRIX50.

SURF151: Used for various load and surface effect applications. It may be overlaid onto a face of any 2-D thermal solid element. The element is applicable to 2-D thermal analyses. Since the thermal elements PLANE55 allow only one boundary condition at their free surface, the nodes at the outer surface are additionally meshed with “surface effect elements”.

A1…n: Different areas of the ANSYS model.

Appendix D: Code application for SA analysis

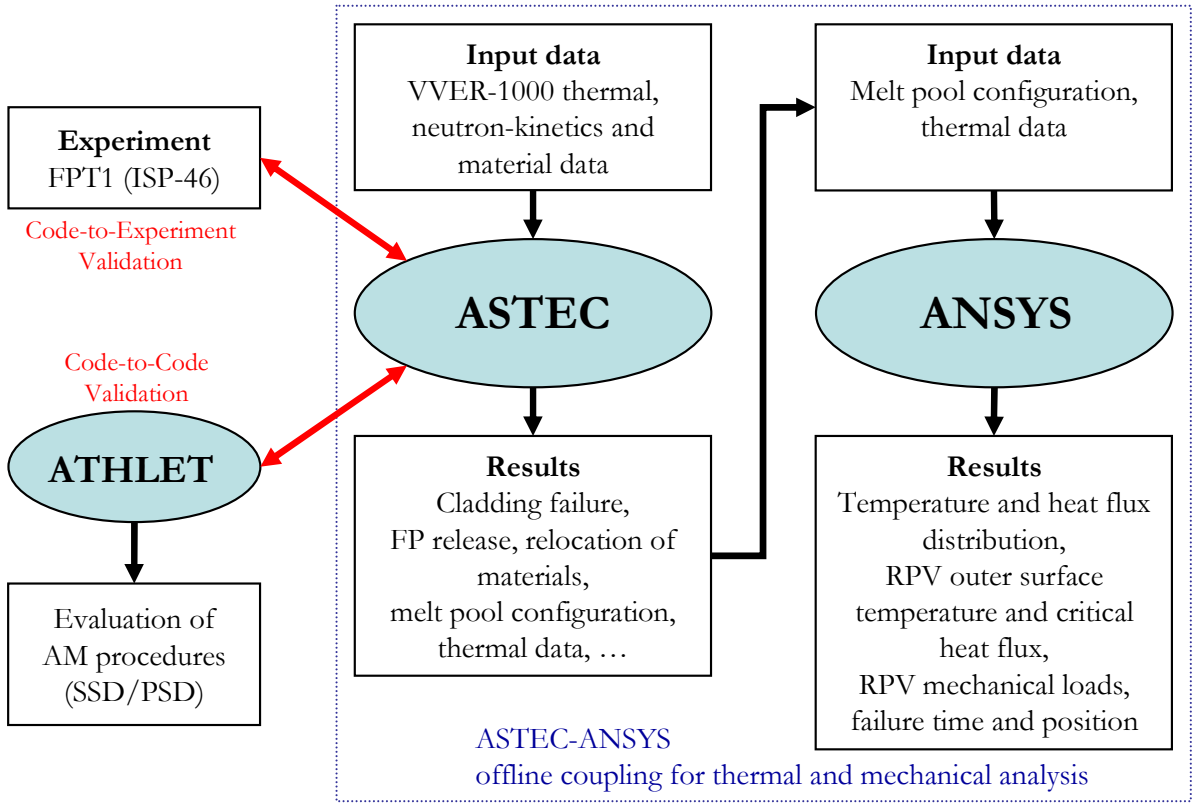

Applied codes for the early and late in-vessel phase investigations on a hypothetical station blackout scenario

Appendix E: Accident progression and AMM

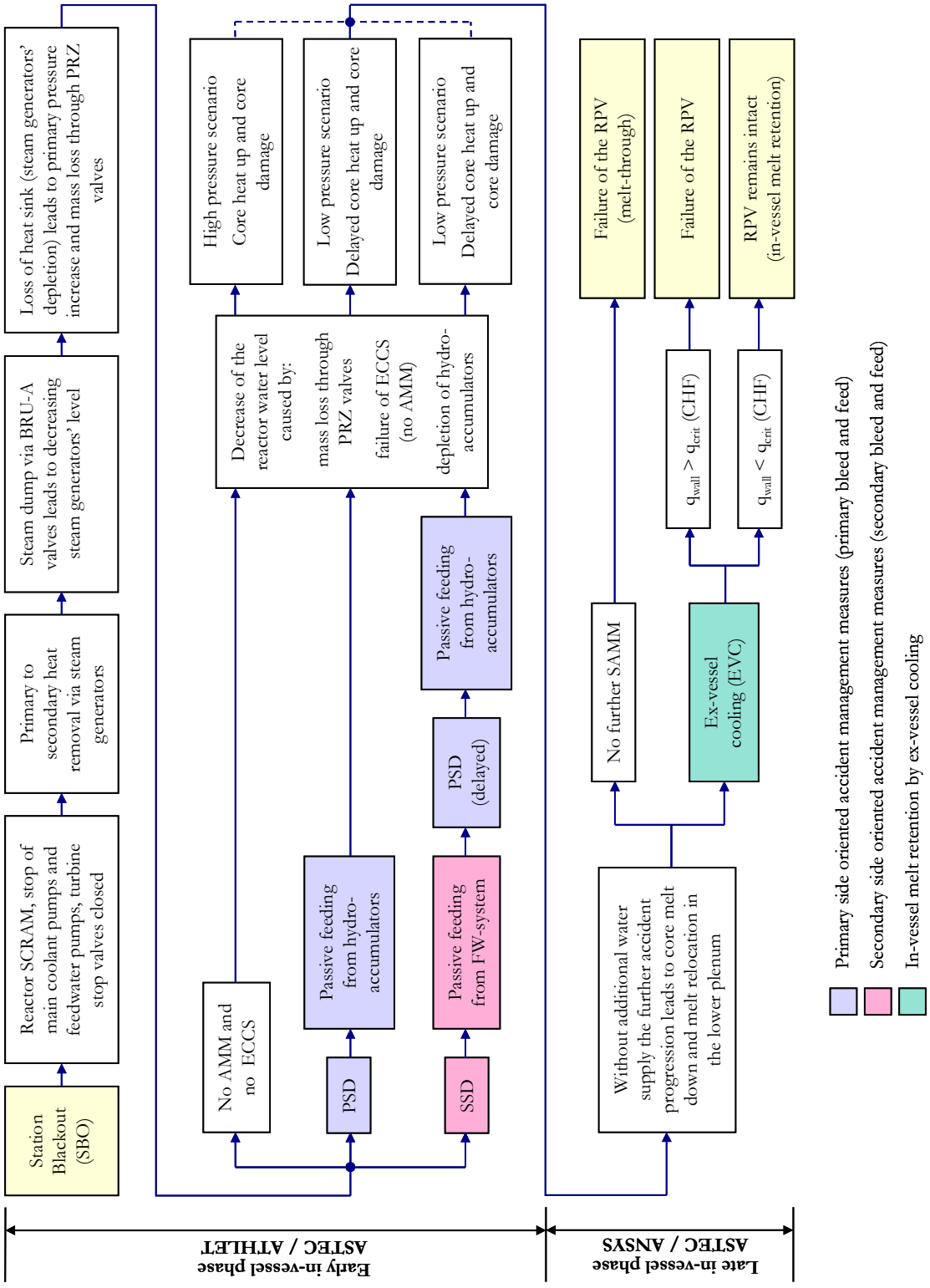

In-vessel phase accident progression of a hypothetical station blackout scenario

Appendix F: VVER-1000 and AMM basic scheme

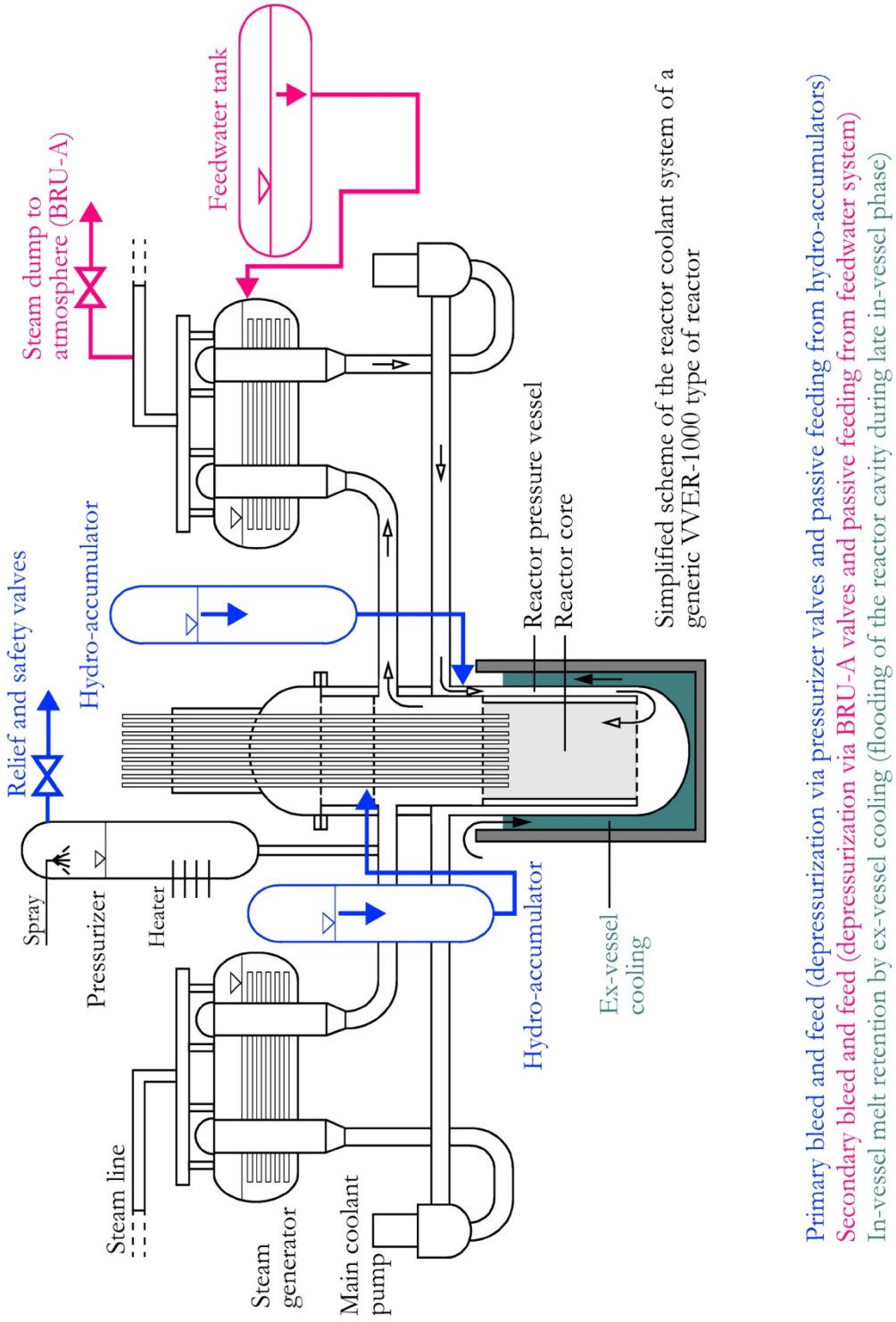

Accident management measures basic scheme

Appendix G: ATHLET visualization for SSD-Case 2

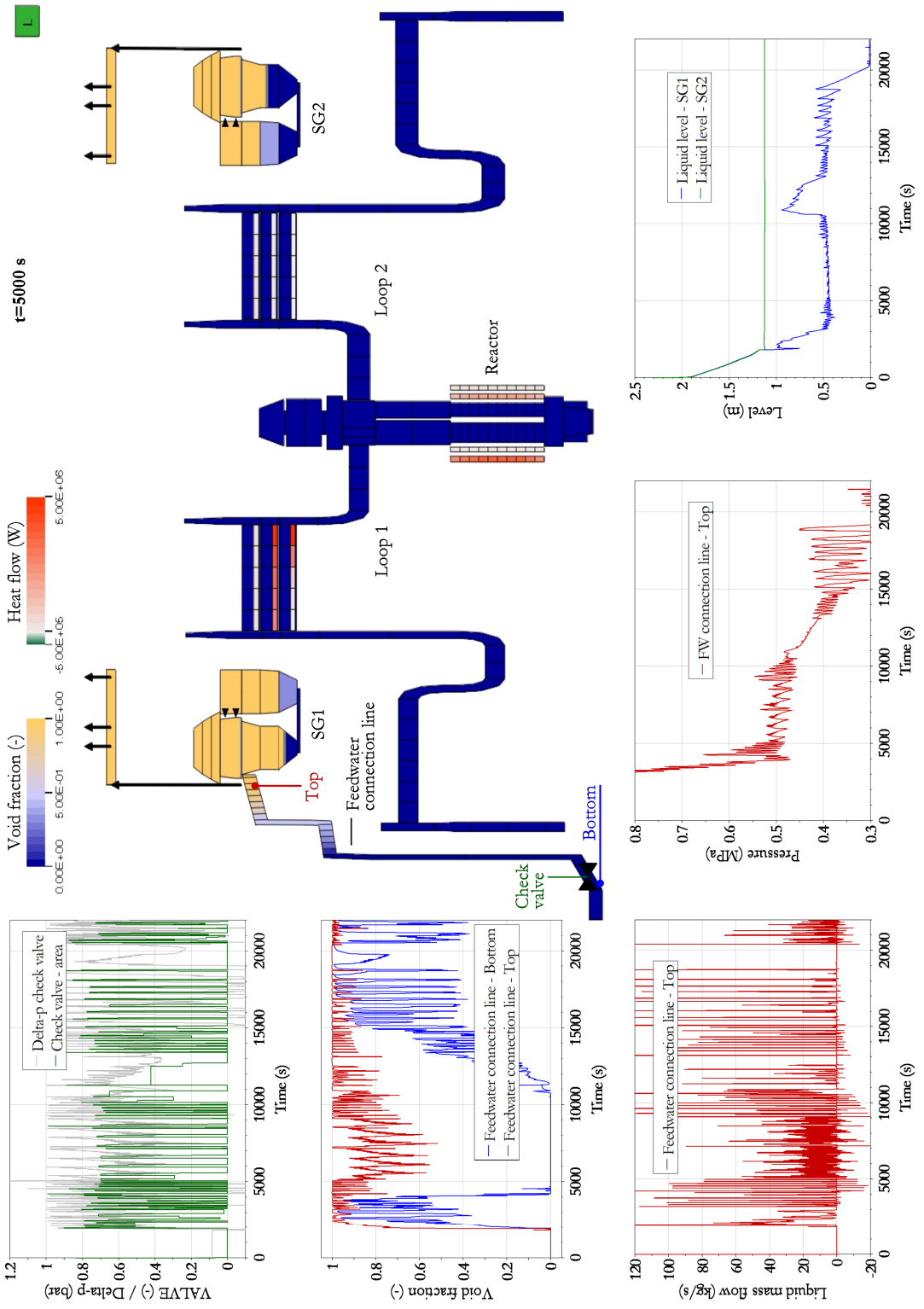

Distribution of the void fraction at 5000 s and results of the simulation till 22000 s

Appendix H: ATHLET visualization for SSD-Case 2

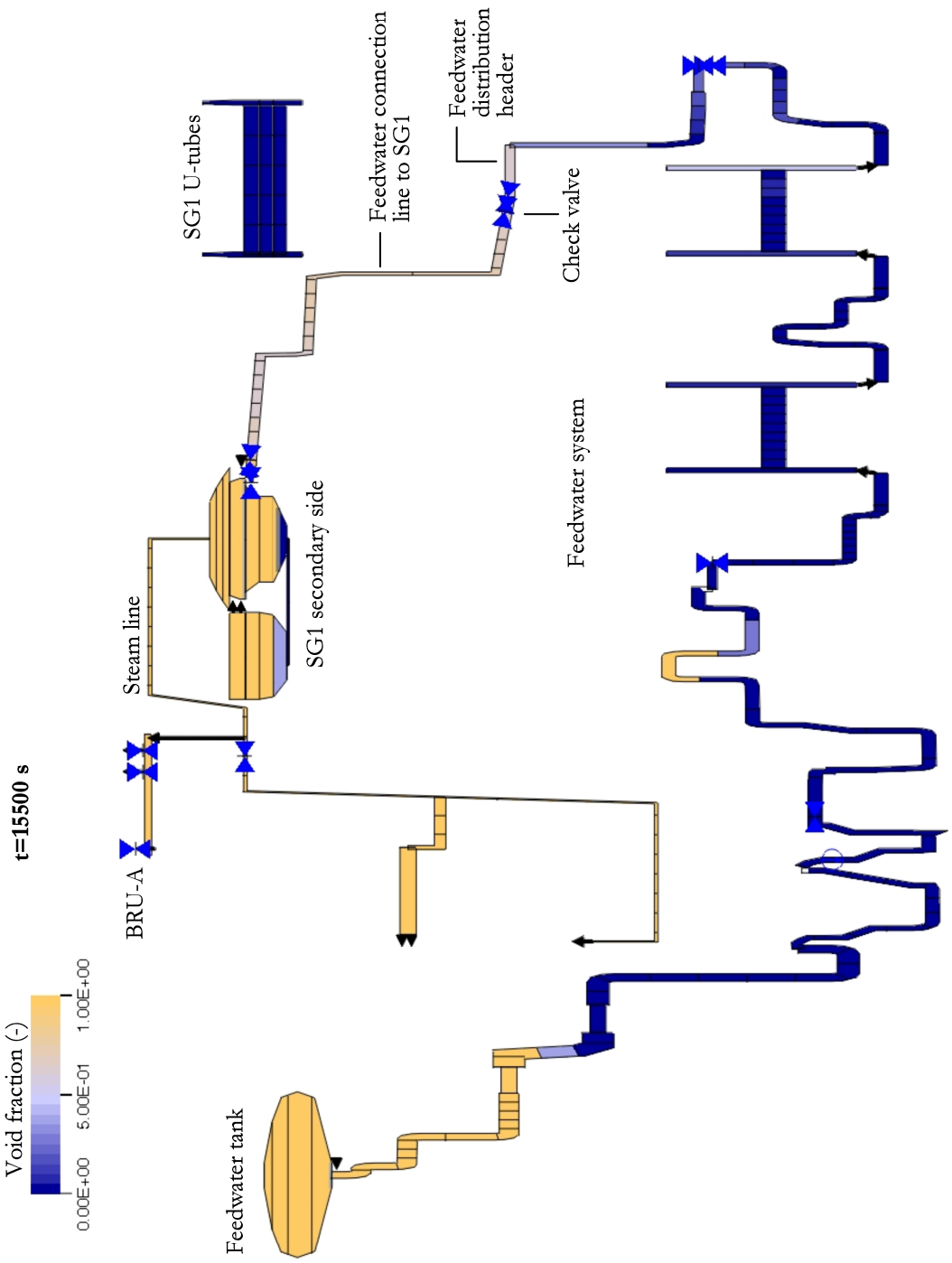

Distribution of the void fraction in the feedwater system at 15500 s

Acknowledgements

There are so many people I would like to say THANKS. Without you this work would not have existed.

This thesis is a result of my work performed at Technical University of Sofia (TUS), Bulgaria, Technische Universität Dresden (TUD), Germany and Helmholtz-Zentrum Dresden-Rossendorf (HZDR), Germany. A big part of it was carried out within the Severe Accident Research Network (SARNET) Project, EURATOM 6th framework programme. The stay at TUD was supported from the Herbert Quandt-Stiftung/ALTANA AG.

First of all I would like to thank Prof. Dr.-Ing. habil. M. Lakov for giving me the courage to start the PhD, for guiding me during the years of my studies and his advices. It happened that he could not see the finalization of this work, but he will stay forever in my thoughts.

Prof. Dr. rer. nat. F.-P. Weiß, to say only thanks to you is not enough. You invited me as a PhD student at HZDR and made my stay and writing the PhD thesis at your institute possible. I'm grateful for your sound guidance, strong advices from the very beginning and the way to find the most proper words when we were discussing. You opened many knowledge-doors for me. It is an honour to have you as a Professor.

I'm deeply thankful to Prof. Dr.-Ing. habil. A. Hurtado, for reviewing my thesis, his advices and lectures at TUD, and to Associate Prof. PhD. habil. B. Kalchev for the review, discussions and the great chance to work on the SARNET and SAMG projects. I would like to express my deep gratitude to the both direct supervisors of the thesis: Dr. E. Altstadt and Dr. F. Schäfer. The contact with you has guided me every single day. Thank you for the strong and fair words, for your efforts, scientific discussions and advices during the preparation of the thesis. I'm also especially grateful to Dr.-Ing. habil. W. Lippmann and Dr. N. Reinke for the courage during all these years and being on my side. The work and the conversations with you are always a pleasure for me.

Special thanks for the insights into the severe accidents, the valuable scientific discussions and support during my stays in France and Germany to all colleagues from IRSN and GRS. Especially Mr. J.-P. van Dorsselaere, Prof. H.-J. Allelein, Mr. B. Schwinges, Dr. M. Sonnenkalb, Mr. G. Lerchl, Dr. H. Austregesilo, Mr. W. Luther, Dr. K. Velkov, Mr. H. Wolff, Mr. J. Steinborn, Mr. I. Bakalov, Mr. P. Chatelard, Mr. C. Seropian, Dr. W. Plumecocq, Mr. G. Gilliard, Mr. F. Cousin. Special thanks to Prof. Sehgal, Mr. J.-P. van Dorsselaere, Dr. R. Passalacqua for the discussions during the Severe Accidents Course and for the organization of the educational trainings within the frames of the SARNET Project. This gave me a lot in understanding the phenomena, the severe accident analyses and the severe accident management. Dr. U. Rohde and Dr. S. Kliem – thank you for accepting me in your department, the discussions and the support from their side.

I'm very grateful to the colleagues from Kozloduy NPP for their help, advices and scientific discussions, everything around the VVER-1000 performance, thermal-hydraulics, accident management, particularly severe accident management measures and procedures etc., especially

Mr. K. Kamenov, Mr. R. Vaklev, Mr. A. Kamenov, Mr. I. Mladenov, the colleagues from the Bulgarian Nuclear Regulatory Agency, EI, INRNE and TUS: Prof. B. Bonev, Prof. V. Velev, Assoc. Prof. P. Grudev, Mr. K. Avdjiev, Mrs. E. Tsvetanova, Mr. N. Vlahov, Mrs. J. Georgieva, Mr. D. Karadzov. Also Dr. S. Nikonov (RRC "Kurchatov Institute"), Dr. N. Kolev (Siemens), Dr. A. Miassoedov (KIT) and Dr. W. Tromm (KIT) for the scientific discussions and advices. Thanks to all HZDR (Institute of Safety Research) and TUD (Professur für Wasserstoff- und Kernenergietechnik) colleagues for the excellent teams, especially Mrs. C. Hille, Dr. C. Lange, Dr. T. Wolf, Dr. C. Schuster, Prof. J. Knorr, Prof. W. Hansen, Mrs. S. Paufler, Mrs. M. Hermann, Mr. A. Andris, Mr. T. Langnickel, Dr. F.-D. Börner, the PhD students, Dr. E. Fridman, Dr. C. Vallée. Mr. S. Kehayov for the courage and the support. I'd like to thank very much also Dr. H.-G. Willschütz (E.ON) for the very fruitful scientific discussions and advices.

Thanks also to all friends who are always next to me!

Last-but-not-least, I'm very grateful to my family for the patience. You should have had definitely a lot from it. And personally, to you too.

Yours, Polina